# *STUDIES OF TRANSIENT FREE RADICALS IN SOLUTION BY FLASH PHOTOLYSIS E.S.R.*


A thesis presented in partial fulfillment of the examination of Doctor of Philosophy.

by

Nigel James Keiller Simpson.

Wolfson College, Oxford.

Trinity Term 1990

## Acknowledgements

If I were to be thorough in describing all the debts I owe this section would end up being the longest in the whole thesis (and include the names of most of the money lenders and pawn brokers in Oxford): I shall be short, which I am, and circumspect, which I haven't been . . . .

Firstly to Keith McLauchlan for his constant enthusiasm and helpful advice, very many thanks. Paul Smith has put untold effort into developing the software of the experiment and has, along with Dave, Clive and the unbelievably ancient Chris, made 372 a fun place to be. The staff of the P.C.L. have also been friendly and helpful, contributing to the smooth running of the lab.

Madeleine, Mike, Mary and Gregory have helped beyond the call of mere friendship, providing everything from champagne with oysters to a sleeping bag and gas fire! Perhaps the last word should go to – as indeed the last penny has come from – my family, whose tolerance and good sense never ceases to amaze me.

# STUDIES OF FREE RADICALS IN SOLUTION BY FLASH–PHOTOLYSIS E.S.R.

A thesis presented for the degree of Doctor of Philosophy

by

Nigel James Keiller Simpson

Wolfson College, Oxford. May, 1990.

Abstract:

An introduction is presented to the nature of polarized and non–polarized transient spin resonance signals, produced by flash–photolysis *e.s.r.*, followed by a description of the equipment used for experimental work. Theories of Chemically Induced Dynamic Electron Spin Polarization are reviewed and various models introduced to illustrate these concepts.

A description is given of the first thorough investigation into the effect of CIDEP polarization transfer down a free radical chain and expands upon the consequences of hyperfine–dependent relaxation and the relative signs of coupling constants in various radical species. It concludes with an account of two methods of kinetic analysis which are the first practical demonstrations of their kind, and employ extension of expressions developed in earlier chapters.

Studies are made of the CIDEP behaviour of radicals in high viscosity paraffins. A reassessment of previous published work is made: anomalous polarization behaviour was found to have been over–compensated for. A new method of extracting values for $T_1$ and $T_2$ is demonstrated for strong transient *e.s.r.* signals.

A collection of experimental data relating to the previously unexplained absorptive polarization observed in the spectrum of ketyl radicals and the longer–time phase inversion of hyperfine–dependent CIDEP is given. The operation of Triplet Mechanism CIDEP in the ketyl radical systems is ruled out and a division of radicals into geminately formed and free–encounter pairs is shown to be incapable of explaining the observed phase changes. In its place a cross–relaxational mechanism, drawing upon simultaneously generated nuclear spin polarization is advanced. Conclusions are drawn that this may account for both anomalies.

Lastly a photochemical application of CIDEP is demonstrated; two different reaction intermediates are identified upon photolysis of ortho–phthalaldehyde, depending upon the quenching conditions. A reaction scheme consistent with all experimental data is proposed. A brief comment upon the photo–chemistry of indan–2–one concludes this work.

# CHAPTER I : INTRODUCTION

# INTRODUCTION

## (1.1.1) The Free Radicals Hamiltonian

Flash–photolysis *e.s.r.* provides a method of studying radical–initiated reactions in the liquid phase. These fleeting free–radical species may be identified by analysis of their microwave absorption/emission spectra, which probe the energy differences between electron spin states, $\underline{S}$, and nuclear spin states, $\underline{I}$, in a magnetic field $\underline{B}$. These may be calculated from the Hamiltonian

$$\mathscr{H} = \beta_e \underline{S}.\underline{\underline{g}}_e.\underline{B} - \beta_n \underline{I}.\underline{\underline{g}}_n.\underline{B} - \sum_i \underline{I}.\underline{\underline{a}}_i.\underline{S} \qquad (1.1.1)$$

All terms have their usual significance, $g_e$ being the coupling tensor between electron spin and the field, $a_i$ being the coupling between electron's spin and that of the $_i$th nucleus.

In all but the most viscous solutions or in liquid crystals, and neither concern us in this work, the energies of the transitions represent a time–average of the interaction Hamiltonian (1.1.1) so that all tensors may be replaced by a scalar that is a third of their trace. Thus

$$g = (1/3)\mathrm{Tr}\{\underline{\underline{g}}\} \;\; ; \;\; a_i = (1/3)\mathrm{Tr}\{\underline{\underline{a}}_i\} \qquad (1.1.2)$$

and the Hamiltonian may be re–cast as

$$\mathscr{H} = g\beta_e S_z B_z - g_n \beta_n I_z B_z + \sum_i a_i \underline{I}.\underline{S} \qquad (1.1.3)$$

The eigenvalues consequent to this equation are written $|M_s,M_i\rangle$ where $M_s$ and $M_i$ refer to spin projections onto the axis of the static field, conventionally the z–axis of a Cartesian co–ordinate system.

(1.1.2) Free Radicals In Solution

Our investigations focus upon the curious appearances of *e.s.r.* signals at very short time after radicals are created in a short pulse of ultra–violet radiation. The formation of pairs of radicals and their subsequent pairwise encounter and reaction can both take place at rates far faster than those of processes attempting to establish equilibrium in the system. This results in a polarized signal (the word, whenever used hereafter, will refer to any system not at equilibrium, unless it is further qualified). The nature and size of that polarization is dependent on a number of parameters but should, in principle, be able to shed light on the intimate details of radical creation and destruction.

The field of Chemically Induced Dynamic Electron Polarization (CIDEP) is not easily approached. Its title itself is a misnomer for the polarization is only glancingly "chemical" in origin and it is not truly "dynamic" – for instance, as a consequence of cross–relaxation. The complex origins of polarization and the appearance of CIDEP spectra have contributed to its mis–use in assigning mechanisms in chemical reactions involving free–radical intermediates, and so an understanding of the phenomenon is essential if we are not to fall into the same trap. In order to put the experimental work into context, therefore, a considerable amount of theory must be explained.

What has been attempted has been to provide as classical an interpretation as possible of all phenomena, relegating as much of the mathematics as possible to the appendices. To be sure, the classical interpretation of the exchange interaction could be

attacked on the ground that there is no classical analogue to a phase–sensitive electrostatic interaction. In such cases we shall have to imagine that two classical and distinct forces are operating simultaneously.

The structure of this thesis is explained thus –

All presented work is derived from an experiment in which radicals are created in a static magnetic field and the second chapter addresses the behaviour of electron spins as they respond to this and to the probing microwave field. Development of equipment to monitor this behaviour is then dealt with, followed by an introduction to the actual polarization phenomena. In this way, applications of the CIDEP technique follow on naturally in chapters five to eight. This work is laid out so that we first see extension of theory to new chemical systems, in which chemical implications are subsidiary to the physical ones. Then a well documented photolysis reaction is analysed for its CIDEP content and, in contrast, two long–standing CIDEP enigmae are re–examined. The final chapter deals with a straight–forward photochemical problem that, by reference to the polarization observed, can be interpreted mechanistically. In many ways this is to be expected, for the majority of advances made over the years by the Oxford group have been demonstrations of how an interesting, polarized spectrum can be analysed "backwards" to derive information on electron exchange or internal motion, say, rather than by predicting and demonstrating how a physical or chemical process will affect the polarization and then trying to observe such an effect.

(1.2.1) Definitions

S.I. units have been used throughout this work. The following terms and symbols require definition:

$\wedge$ a cross product of two vectors

$\underline{X}$ a vector/spin function

$\underline{\underline{X}}$ a matrix/tensor

$\dot{x}$ first time derivative

$\ddot{x}$ second time derivative

$\otimes$ product of two matrices/irreducible representations

$\oplus$ convolution of two functions

$|x\rangle$ a wavefunction

$[x,y]$ a commutator

$\mathscr{H}$ a Hamiltonian operator

$|x|$ a determinant or modulus

# CHAPTER II : LINESHAPES

# LINESHAPES

## (2.1.1) A Forethought

All experiments recorded in this thesis arise from the generation and handling of time–resolved microwave signals resulting from the behaviour of electron spins in combined static and oscillating fields; a static magnetic field separates the energies of electron spin states (which are affected by the nature of the radical upon which the spin resides, and the coupling of that spin to neighbouring nuclear spins). A microwave field can be set up inside a suitable cavity such that the magnetic component of this oscillating field is concentrated at the sample. It is this field that effects transitions between the electron spin states with respect to the static field, and a transition is manifested by absorption or emission of microwave energy. An obvious point of departure for us, then, is the general analysis of these signals, irrespective of the presence or absence of spin polarization.

Such signals vary vastly from those observed under steady–state conditions (conventional *e.s.r.*) and further divergence occurs as a consequence of the need to achieve a high time resolution; a conventional *e.s.r.* spectrometer employs a field that is modulated at a particular frequency, and the signal will thus vary at this frequency, too, allowing all other frequency components to be rejected as experimental noise. No field modulation is employed in this experiment so a direct, rather than a derivative lineshape results. Two types of spectrum will be displayed in this thesis, one of which monitors the absorption/emission of microwaves with time, at one static field position. The second type takes a reading of this signal from a region of the time decay and outputs it to a recording device, after which the static field is advanced to a new position. In this way either a time– or a field–swept spectrum results. The treatment is

phenomenological, beginning with a solution of the appropriately modified Bloch equations (a brief review of the density matrix description is given in Appendix B). An expression for the time dependence of the signal is derived in which we posit polarization terms, and this is then extended to deal with the field–swept spectrum. Supplementary information of the method of simulation is given in Appendix A. The influence of various relaxation processes upon the signal's time dependence will be returned to later in the thesis so an overview of relaxation is given here.

(2.2.1) Relaxation

The mechanisms that serve to restore a perturbed system to its equilibrium state are termed collectively as relaxation processes. For most work in flash–photolysis *e.s.r.* it has been possible to ignore the origins of this relaxation and to adjust the appropriate relaxation parameters empirically when simulating a spectrum. However, an unusual type of relaxation is observed in some of the work presented and a cross–relaxational theory is discussed in the light of some experimental observations. It will prove worthwhile, therefore, to examine the phenomenon in greater detail. Various reviews exist, covering this field [1] and several thorough analyses have been made [2 – 4].

In this experiment we observe an ensemble of spins which is subject to one static and relatively intense field, and one perturbing field which is rotating and relatively weak. Under these conditions the spins will precess around the static field direction, which is conventionally written as the z–axis in our co–ordinate system. For a system in thermal equilibrium with its surroundings there will be a net excess of electron spins whose angular momenta are aligned parallel to this field. This fractional excess is the equilibrium polarization. If the parallel state is defined as $\beta$ and the antiparallel one as

$\alpha$ then the equilibrium polarization may be written as

$$P_{eq} = (n_\beta - n_\alpha)/(n_\beta + n_\alpha) \qquad (2.2.1)$$

No resultant perpendicular component of magnetization exists in an ensemble of spins until the secondary field is applied, as no factor exists to discriminate between x– and y–directions. When such a field is applied then, if it is of the right frequency to match an energy difference between $\alpha$ and $\beta$ states of an electron on a radical, a transition may take place, provided nuclear spin states remain unchanged. This is depicted in Fig.(2.2.1) for an ensemble of spins, in a co–ordinate system that is rotating at the same frequency as the Larmor precession frequency of the spin ensemble. If populations of $\alpha$ and $\beta$ states differ then a net motion of the ensemble will result. The $\beta \leftrightarrow \alpha$ transition can only occur in a plane perpendicular to the perturbing field so components of magnetization are developed in the y–direction by a field aligned with the x–axis, as the system is disturbed from its equilibrium position.

(2.2.2) Parallel And Perpendicular Relaxation Times

It is the rôle of relaxation to attempt to restore the system to its equilibrium state and clearly there will be two forms: one tends to restore the magnetization in the z–direction to its equilibrium value and it may be considered, since this represents a net energy change to or from system to surroundings, as a classical relaxation process; the other tends to return the perpendicular components of magnetization to zero, though with respect to the energies of the spins in the static field there is no energy change.

The first of these we call spin–lattice or longitudinal relaxation and, for an ensemble of spins, it may be characterised by a parameter $T_1$, reflecting the rate at

Fig.(2.2.1)

The Motion Of The Magnetization Vector Upon Undergoing A Transition

Motion of magnetization vector as spins are flipped from $\beta$ to $\alpha$ states by a probing microwave field, along the x–axis. Motion is in a plane $\perp$ to the $\omega_1$ field.

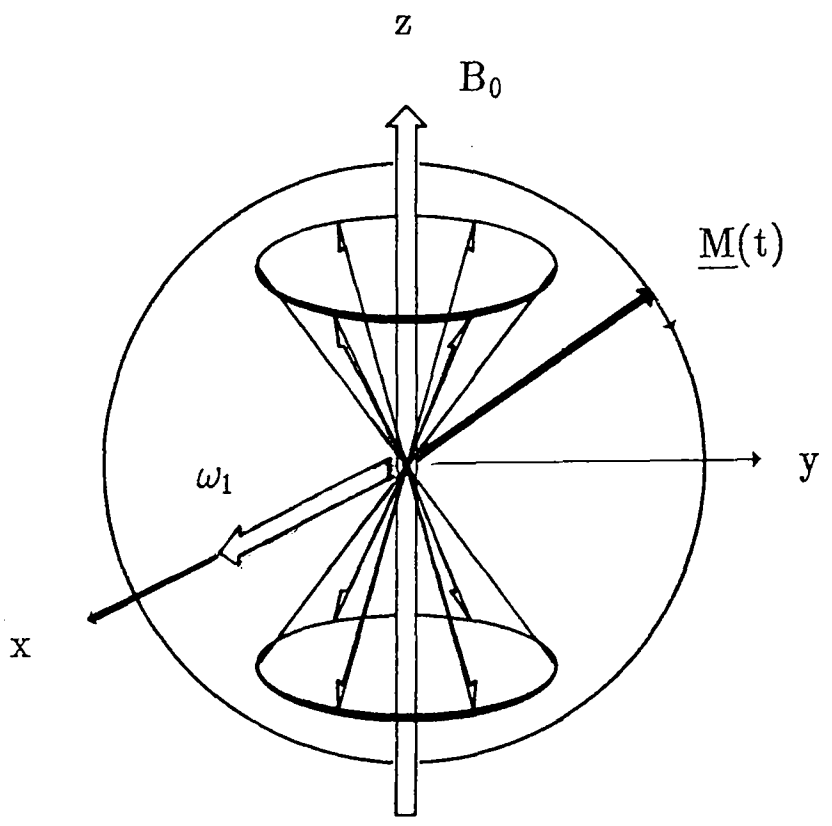


(Frame is rotating at the Larmor frequency of the spin under observation)

which transitions are induced between $\alpha$ or $\beta$ states by processes other than the effect of a resonant microwave field. The second type is the spin–spin or transverse relaxation. Again, we may characterize it by a time constant $T_2$, which represents the rate at which a component of magnetization, initially in the y–direction, diminishes with time (in terms of the spins themselves, the time after which an initially coherent ensemble of spins, precessing together, loses that coherence).

$T_1$ defines the lifetime of a state and will therefore affect the energy of that state by the Uncertainty Principle. The major contributor to the width of a spectral line, however, comes from any interaction that serves to change the magnetic field experienced by a spin and hence to change its precession frequency, and $T_2$ is a measure of the range of precession frequencies – the larger the range, the faster an initially coherent set of spins will "fan out" away from the y–axis. $T_1$ and $T_2$ are therefore different in another respect, too: in order to induce a transition between states an *oscillating* magnetic perturbation, fluctuating at the Larmor precession frequency, must affect the spin just as the microwave field is doing; to cause a loss of coherency in a spin ensemble a *static* magnetic interaction must be present to augment or reduce the effective field experienced by each spin and, *ipso facto*, augment or reduce the Larmor precession frequency.

Two classes of interactions may be identified. The first arises through the quantisation of energy in a frame defined by the axes of the molecule that the electron resides upon (yet that frame will undergo continual re–orientation by the random buffeting of surrounding molecules with respect to that of the static magnetic field, which determines the spin's energy – any molecular motion will modulate this energy, therefore). The second class includes internal motion such as conformational exchange,

degenerate exchange such as electron transfer and chemical reaction. They are dealt with in detail below.

(2.2.3) Relaxation By Motion In A Fixed Frame

In isotropic solution the frequency or field at which a transition will appear is determined by the isotropic parts of the tensors which describe the interaction of spin and magnetic field. All anisotropic terms average to zero over any realistic coupling period and therefore do not give rise to a range of spectral transitions directly. However, these are precisely those terms which will relax the spin system and thence affect the spectrum.

In solution orbital angular momentum is normally quenched by the solvent molecules surrounding the radical. However, an unpaired electron in a molecular orbital may acquire orbital angular momentum via the spin–orbit interaction and this acquired momentum will be greater in some directions in the molecular frame than in others, depending on the anisotropy of the spin–orbit interaction. This spin anisotropy is reflected in the g–tensor. Collision with neighbouring molecules will rapidly re–orient the molecular axes, modulating the interactions with the external field and inducing relaxation. The contributions to the total effective relaxation times from this source are [5,6]

$$1/T_1^g = (1/5)\sum_i (g_i - g)^2 . \frac{{\omega_0}^2}{g^2} . \left[ \frac{\tau_r}{1 + {\omega_0}^2 {\tau_r}^2} \right] \qquad (2.2.2)$$

$$1/T_2^g = (1/30)\sum_i (g_i - g)^2 . \frac{{\omega_0}^2}{g^2} . \left[ 4\tau_r + \frac{\tau_r}{1 + {\omega_0}^2 {\tau_r}^2} \right] \qquad (2.2.3)$$

The sum over i represents the sum over the three principal components of the g–tensor, g is the isotropic g–value, $\tau_r$ is the rotational correlation time and $\omega_0$ is the frequency of the transition. This summation is sometimes written (g′:g′), denoting the inner product of the traceless part of the g–tensor with itself. Interpreting this contribution we see that as $\tau_r$ increases as when, for example, the viscosity of a solution increases, $T_1$ will pass through a minimum and $T_2$ will decrease continuously.

That contribution to relaxation from molecular rotation/spin coupling relies upon the validity of the Hubbard Relationship [8]

$$\tau_j \tau_r = I/6kT \qquad (2.2.4)$$

where I is the molecular moment of momentum. However, the quantitative expressions [6,9]

$$1/T_1^{sr} = 1/T_2^{sr} = \frac{1}{9\tau_r}\sum_i (g_i - g_e)^2 \qquad (2.2.5)$$

do correspond to observed behaviour [10]. $g_e$ is the free–electron g–value.

When the anisotropy of the coupling between electron and nuclear spins is small and when no quadrupolar nuclei are coupled to the spin these two effects dominate relaxation and we may then write

$$1/T_1 = 1/T_1^{sr} + 1/T_1^{g} \qquad (2.2.6)$$

$$1/T_2 = 1/T_2^{sr} + 1/T_2^{g}$$

Fig.(2.2.2)

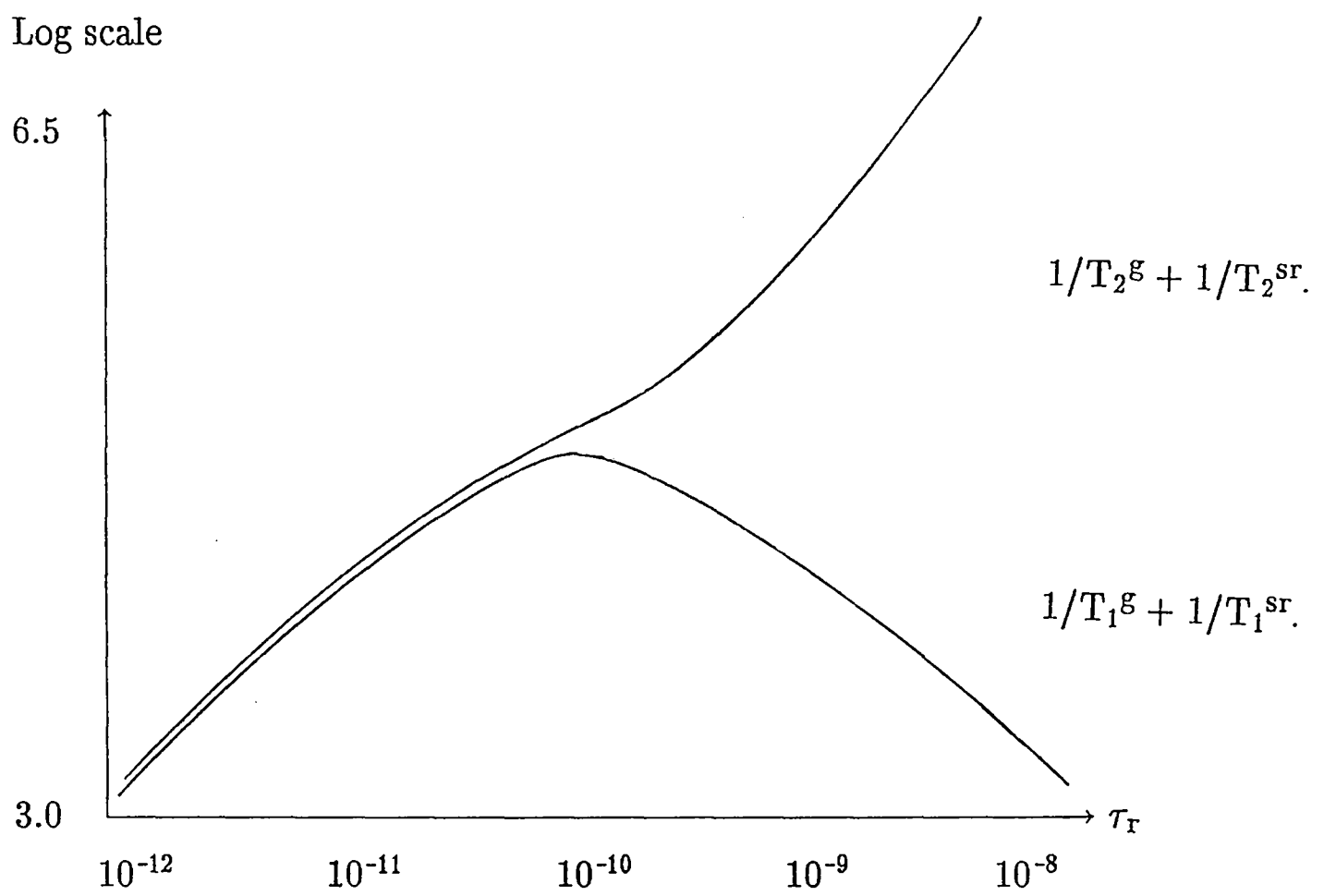


Contributions to relaxation parameters from g–anisotropy and spin–rotation sources [7].

Whilst the second constraint holds for all species examined in this work the anisotropy of the hyperfine coupling cannot always be neglected.

The Electron–Nuclear Dipolar Interaction arises, as with the two effects already mentioned, from a non–isotropic coupling between the electron and some molecular property, in this case the spins of nuclei in the vicinity of the electron spin. The consequence is simultaneous electron, nuclear and electron/nuclear cross–relaxation [5]. Two forms of coupling of electron and nuclear spin interaction may be identified: the Fermi, or contact interaction arises only when the electron under consideration possesses a non–zero spin density at the magnetic nucleus, and is an isotropic interaction; the dipolar interaction arises by the coupling of two dipoles through space, and is thus dependent upon orientation. When a hyperfine coupling contains a large dipolar component once again this coupling will be strongly modulated by molecular tumbling. The important difference here is that, as this is due to the effects of different nuclear spin states upon relaxation, this relaxation must be hyperfine dependent. For the nuclear quantum number $M_i$ the total linewidth is

$$1/T_2(M_i) = A + BM_i + CM_i^2 \qquad (2.2.7)$$

$$1/T_1(M_i) = A' + B'M_i + C'M_i^2$$

where A and A′ contain spin–rotation and g–anisotropy terms, provided that the END term is small compared to the sum of hyperfine–independent relaxations. This requirement arises because the END mechanism generates compound lineshapes and the relaxation of each line becomes multi–exponential, each exponential corresponding to each element of the lineshape [11], so $T_1$ and $T_2$ cease to have meaning.

Values of the coefficients in (2.2.7) have been estimated from several studies [7,12,13] and, provided assumptions about the nature of the coupling tensors can be made, the sign of the anisotropic coupling constants may be extracted from analysis of the $BM_i$ term. Work presented in chapter five shows that analysis is not always simple.

Coefficients B and C are given for rapid molecular re–orientation as

$$B = \frac{7\omega_0\tau_r}{15\hbar^2}\sum_i (g_i - g).(a_i - a) \qquad (2.2.8)$$

$$C = \frac{\tau_r}{15\hbar^2}\sum_i (a_i - a)^2$$

Equation (2.2.7) is derived from an invalid approximation – that those very terms leading to nuclear relaxation may be ignored.[1]

(2.2.4) Relaxation By Chemical Reaction

Provided that a chemical reaction, and the term is used loosely to cover exchange processes, occurs sufficiently fast then it may also contribute to relaxation. This requirement limits the range of effects to internal motions and electron and proton exchange. Anticipating the contents of Chapter 4 somewhat, three important regimes may be set up, rather than the two commonly encountered in steady–state *e.s.r.* or *n.m.r.*

---

[1] It is my belief that the occurrence of hyperfine–dependent relaxation, though familiar in the *e.s.r.* of transition metal ions, has been underestimated for carbon–centred radicals mainly because much of the work carried out in our laboratory has been on systems in which chemical and physical exchange has annihilated any such effect.

When the frequency of exchange is so slow that it is considerably less than the smallest frequency separation between hyperfine lines in a spectrum then, while it will provide a component of the relaxation parameters of each line, it will not shift their relative positions. As the exchange frequency increases up to and beyond the smallest separation the spin is no longer defined by a particular set of magnetic interactions and the positions of the lines shift towards a weighted average of each set of lines affected by this exchange.

When polarization of hyperfine lines takes place in a radical creation step or by subsequent reaction then an intermediate regime may be identified. This is where the relaxation rate induced by exchange is not a major component of overall relaxation but the rate of exchange is sufficiently fast to interchange hyperfine lines before relaxation can destroy incipient polarization [14,15]. The ring–flipping of the cyclohexanolyl radical is an exemplary system in this respect [16].

Another form of internal motion is the rotation of methyl groups and several radicals treated in this thesis possess coupled methyl groups. They have been shown to produce alternating linewidths when their rotation is restricted [17] though in none of our studies is there reason to consider such an effect; an estimation of the lifetime of an aromatic methyl group in one orientation at 313K is approximately $10^{-12}$s [18]. This results in a negligible contribution to relaxation, even in solutions of very high viscosity at room temperature.

The specific effect of proton and electron exchange on non–polarized *e.s.r.* signals [19,20] has been treated elsewhere and is not considered in relation to the experimental work (this may be an oversight with respect to radicals created in alcoholic solution).

Electron exchange may be either of the form

$$R^{\cdot -} + R \rightleftharpoons R + R^{\cdot -} \tag{2.2.9}$$

which is a true chemical reaction, albeit with identical initial and final species, or

$$R_1^{\cdot -} + R_2^{\cdot -} \rightleftharpoons R_2^{\cdot -} + R_1^{\cdot -} \tag{2.2.10}$$

which is classified as Heisenberg Spin exchange. The former, at typical concentrations of radical anion, normally outweighs the latter and reaction (2.2.10) is often ignored though both have the same functional effect on the relaxation parameters [21].

Provided that exchange falls under the slow motion regime it may give rise to differential hyperfine relaxation since each $\alpha \leftrightarrow \beta$ electron transition for one particular nuclear hyperfine state is independent of all the others yet the exchange process randomises the population of hyperfine states that it connects. The population of one hyperfine state is affected then by the rate of $\alpha \leftrightarrow \beta$ transitions and the rate of population/de–population by the exchange process. This competitive cycle is shown in Fig.(2.2.3). Exchange can be seen to have the following effect; the higher the degeneracy of the line under observation the smaller the reservoir of spins in other states capable of re–populating that line. This implies that the higher degeneracy lines will appear to have faster relaxation times than the lower degeneracy lines [22]. Under such conditions and at slow exchange, effective relaxation times, for line $_i$ of degeneracy $D_i$, are

Fig.(2.2.3)

The effect of exchange upon an emissively polarized radical ensemble.

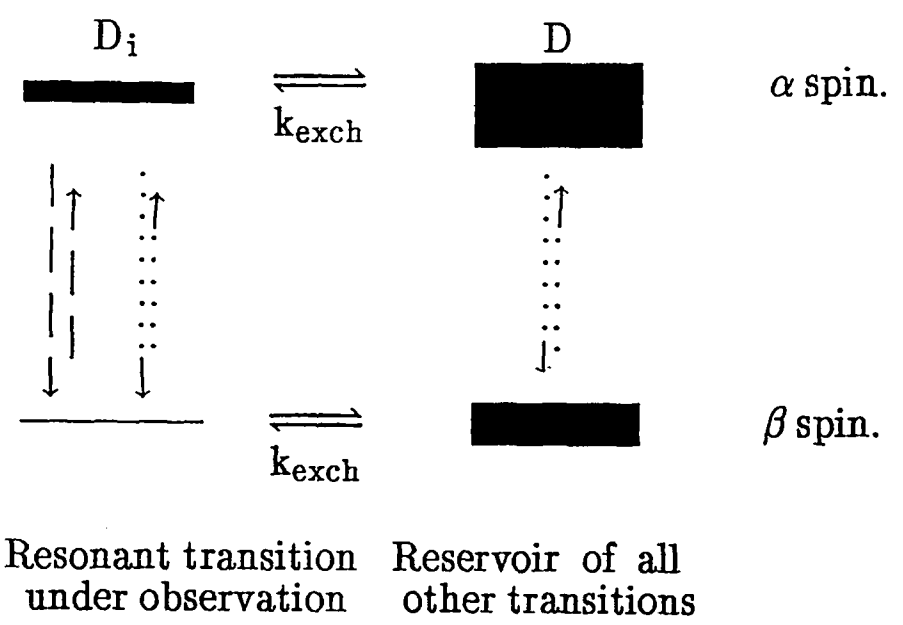


.....→ Relaxation ($T_1^{-1}$); ----→Stimulated transitions ($\omega_1$)

$$1/T_{2i} = 1/T_2 + \frac{(D - D_i)}{D}.k_{ex}[A] \qquad (2.2.11)$$

$$1/T_{1i} = 1/T_1 + \omega_1^2/(T_{2i}^{-1} - T_1^{-1}) \qquad (2.2.12)$$

D is the total degeneracy of the radical. These formulae must be applied with care since they assume that no hyperfine–dependent polarization is present. Yet radical anions do not show any hyperfine dependency precisely because of this exchange process. A resolution of this cyclic argument, or an apology at least, can be found in the original and erroneous explanation for the lack of observed hyperfine–dependent polarization in radical anions, namely their small spectral spread and large hyperfine–independent polarizations. The slow exchange limit has been analysed experimentally [23]. The fast exchange limit has also been investigated though the problem is far more complex as the simple separation into population and depletion of a resonance line is no longer appropriate (the relative populations of a set of n coupled lines is determined by the solution of 3n coupled differential equations), but these systems still yield to analysis [24] and the solutions approximate to equations (2.2.11) and (2.2.12) as the rate of exchange decreases.

### (2.2.5) The Exponentiality Of A Polarized Signal Decay

All the foregoing expressions have relied upon the system under observation lying close to the equilibrium position – evidently true if the system was initially at equilibrium with a static field, as the microwave field is very small in comparison. We must look at systems that are polarized perhaps by as much as $200P_{eq}$. Are we still justified in talking of $T_1$ and $T_2$? We may assume that the effect of an initial polarization may be substituted by a static field in the z–direction that is vastly greater

than that present when the microwave field acts. This is valid since $M_z > M_{eq}$ at $t \geq 0$ and $M_x = M_y = 0$, so the conditions for $t \leq 0$ have been supplied. Re–writing equation (2.2.1) in terms of the Boltzmann factors gives

$$P = \left[ \frac{1 - e^{-g\mu_B B_z/kT}}{1 + e^{-g\mu_B B_z/kT}} \right] \qquad (2.2.13)$$

where $B_z$ represents the imaginary field at $t < 0$. This may be expanded into

$$P \approx -\tfrac{1}{2}(g\mu_B B_z/kT) + (1/12)(g\mu_B B_z/kT)^3 \qquad (2.2.14)$$

if we ignore quartic and higher terms. P is then linear in $B_z$ provided that $(g\mu_B B_z/kT)^3 \ll 1/6$. This value is not exceeded until a $B_z$ equivalent to a polarization of around $600P_{eq}$ is reached [25]. Attempts to measure polarization ratios have not been very successful but it is clear that they never approach such a large figure.

(2.3.1) Composing The Lineshape

Let us, without explaining why just yet (justification is given in chapter 4), impose some *a priori* constraints: i) polarization may be introduced without affecting interaction of spin with static and rotating fields; ii) relaxation may be introduced in all cases as a first–order phenomenon; iii) our observed signal is recorded directly, without modulation or phase–sensitive detection, contrary to the norm in steady–state *e.s.r.*, and is not damped by a slow response of the spectrometer to changes in the magnetization of the sample; iv) reaction, if slow, may be introduced at a later stage (examples where this cannot be said to hold are treated in chapter 5); v) radical creation

is instantaneous[2]. Comparison of experiment with simulation should then, in principle, allow us to extract information about relaxation and polarization effects [26].

The starting point will be the Bloch equations [27], modified to take into account sudden creation of spin in a magnetic field [28]. Thus, magnetization created in the z–direction is tipped over into the y–axis by a resonant field along the x–axis and it is this y–component to which the observed signal is proportional.

(2.3.2) Modifying The Bloch Equations

Let us begin by stating the Bloch equations in the static frame,

$$\dot{M}_x = \gamma(M \otimes \mathrm{B})_x - M_x/\mathrm{T}_2$$

$$\dot{M}_y = \gamma(M \otimes \mathrm{B})_y - M_y/\mathrm{T}_2 \qquad (2.3.1)$$

$$\dot{M}_z = \gamma(M \otimes \mathrm{B})_z - M_z/\mathrm{T}_1 + M_{eq}/\mathrm{T}_1$$

where $M_{eq} = \mathrm{nP}_{eq}$ and $\gamma$ is the magnetogyric ratio. Since we are observing a magnetization generated in a frame rotating at the frequency of the microwave field it is expedient to convert these equations into ones operating in the rotating frame. If we define $\omega_1$ as the incident perturbing field strength in angular frequency units, and $\Delta\omega$ as

---

[2] Refined theoretical work has been published that includes the profile of the exciting radiation that initiates reaction [29], but for our work this may be comfortably ignored; our time–resolution, though good, is insensitive to the sub–$10^{-8}$s timescale.

the offset between $\omega_1$ and the Larmor frequency for the line under consideration $\omega_0$, then in the rotating frame

$$\dot{M}_x = \Delta\omega M_y - M_x/T_2$$

$$\dot{M}_y = (\omega_1 M_z - \Delta\omega M_x) - M_y/T_2 \qquad (2.3.2)$$

$$\dot{M}_z = -\omega_1 M_y - M_z/T_1 + M_{eq}/T_1$$

This is conveniently written in matrix form as

$$\dot{\underline{M}}(t) = \underline{\underline{L}}.\underline{M}(t) + T_1^{-1}\underline{M}_{eq} \qquad (2.3.3)$$

where $\underline{\underline{L}} = \begin{pmatrix} -T_2^{-1} & \Delta\omega & 0 \\ -\Delta\omega & -T_2^{-1} & \omega_1 \\ 0 & -\omega_1 & -T_1^{-1} \end{pmatrix}$ and $\underline{M}_{eq} = nP_{eq}\begin{pmatrix} 0 \\ 0 \\ 1 \end{pmatrix}$

and it is often referred to as a transport equation as it shows how magnetization is shipped from one direction to another by the combined action of relaxation and the perturbing field. Now we may introduce radical reaction [30] and initial spin polarization as phenomenological terms [31].

Neglecting for the moment any polarization process that operates after radicals have been formed we incorporate polarization as an initial condition (a valid operation as radical creation is largely complete in under ten nanoseconds whilst observation is

over the microsecond timescale). To equation (2.3.3) we can then add the term

$$\underline{M}(0) = n(0)P_i \begin{pmatrix} 0 \\ 0 \\ 1 \end{pmatrix} \qquad (2.3.4)$$

Radical reaction can be included by replacing a time–independent radical population n(0) by a time–dependent one n(t), which may include both bimolecular recombinations or pseudo–unimolecular scavenging reactions. $M_z(t)$ will tend towards $n(t)P_{eq}$ as relaxation restores the system to a non–polarized state.

$$\dot{\underline{M}}(t) = \{\underline{\underline{L}} - \dot{n}(t)\underline{\underline{1}}/n(t)\}.\underline{M}(t) + T_1^{-1}\underline{M}_{eq} \qquad (2.3.5)$$

This equation has exact analytical solutions only under certain limits [32,33]. A general solution by numerical techniques is employed later, when we consider polarization generated at long times after radical creation. Here we attempt an analytical solution by employing an eigenvalue approach [34,35], but (2.3.5) may also be solved by Laplace transform methods [28,36].

Equation (2.3.5) is of the form

$$\dot{\underline{S}}(t) = \underline{\underline{R}}(t).\underline{S}(t) + \underline{Q}(t) \qquad (2.3.6)$$

where $\underline{\underline{R}}(t) = \{\underline{\underline{L}} - \dot{n}(t)\underline{\underline{1}}/n(t)\}$ and $\underline{Q}(t) = T_1^{-1}\underline{M}_{eq}$. Its solution is

$$\underline{S}(t) = e^{\int_0^t \underline{\underline{R}}(t)dt} . \left\{ \underline{S}(0) + \int_0^t e^{-\int_0^t \underline{\underline{R}}(t)dt} . \underline{Q}(t)\, dt \right\} \qquad (2.3.7)$$

When the limiting conditions are met (2.3.7) may be solved to give, for the y–component of magnetization

$$M_y(t) = \{P_i . g_y(t) + P_{eq} . G_y(t)/T_1\} . n(t) \qquad (2.3.8)$$

where $G_y(t) = \int_0^t g_y(t)dt$ and $g_y(t)$ is itself the y–component of $e^{\underline{\underline{\varrho}}(t)}$ where $\underline{\underline{\varrho}}(t)$ is the diagonalised form of $\int_0^t \underline{\underline{R}}(t)dt$. These two parameters are given by

$$g_y(t) = \frac{\omega_1 e^{at}}{b} . \sin bt \qquad (2.3.9)$$

and

$$G_y(t) = \frac{\omega_1}{(a^2 + b^2)T_1} \left\{ [(a/b)\sin(bt) - \cos(bt)] . e^{at} + 1 \right\} \qquad (2.3.10)$$

The limiting conditions are reflected in the definitions of a and b: one of the following requirements must be met;

i) if $\Delta\omega = 0$ then $a = -\frac{1}{2}(T_1^{-1} + T_2^{-1})$ ; $b = [\omega_1^2 - \frac{1}{4}(T_2^{-1} - T_1^{-1})^2]^{\frac{1}{2}}$

(an easily achievable condition)

ii) if $T_1 = T_2$ then $a = -T_1^{-1}$ ; $b = (\omega_1^2 - \Delta\omega^2)^{\frac{1}{2}}$

(an unrealistic situation)

iii) if $T_1 \gg T_2$ and $\omega_1^2 T_1^2 \ll 1$.

In this last case the three components of $\underline{M}(t)$ are

$$M_z(t) = n(t)\{(P_i - P_{eq}T_{1eff}/T_1).e^{-t/T_{1eff}} + P_{eq}T_{1eff}/T_1\}$$

$$M_y(t) = \{\omega_1 T_2/(1+\Delta\omega^2 T_2^2)\}.M_z(t) \qquad (2.3.11)$$

$$M_x(t) = \Delta\omega.T_2.M_y(t)$$

$$T_{1eff} = \{T_1^{-1}+\omega_1^2 T_2/(1+\Delta\omega^2 T_2^2)\}^{-1} \qquad (2.3.12)$$

In the first two cases it is clear that we observe transient nutations both in the time domain and (as $\Delta\omega$ increases so does the frequency of the time–domain oscillations) in the field or frequency domain. These nutations may even be observed exactly on resonance provided that $\omega_1 > \frac{1}{2}(T_1^{-1} - T_2^{-1})$, and are called Torrey Oscillations. They have long been observed in *n.m.r.* spectra [28] but only recently in transient *e.s.r.* [37].

To see how these nutations arise we examine the motion of the bulk magnetization vector M(t) as it precesses about the main field, $\omega_0$ (Fig.2.3.1). To this an exactly resonant microwave field is applied along the x–axis. In this rotating frame the only field apparent to the spin ensemble is this $\omega_1$ field and precession of the magnetization about the x–axis results, tipping the magnetization vector into the y–direction. If the $\omega_1$ field exceeds $\frac{1}{2}(T_1^{-1} - T_2^{-1})$ then, before relaxation can scramble this initially coherent motion the vector will have completed a half revolution and $M_y(t)$ will begin to become negative. This represents the condition for observations of nutations made exactly on resonance.

Fig.(2.3.1)

The creation of transient nutations

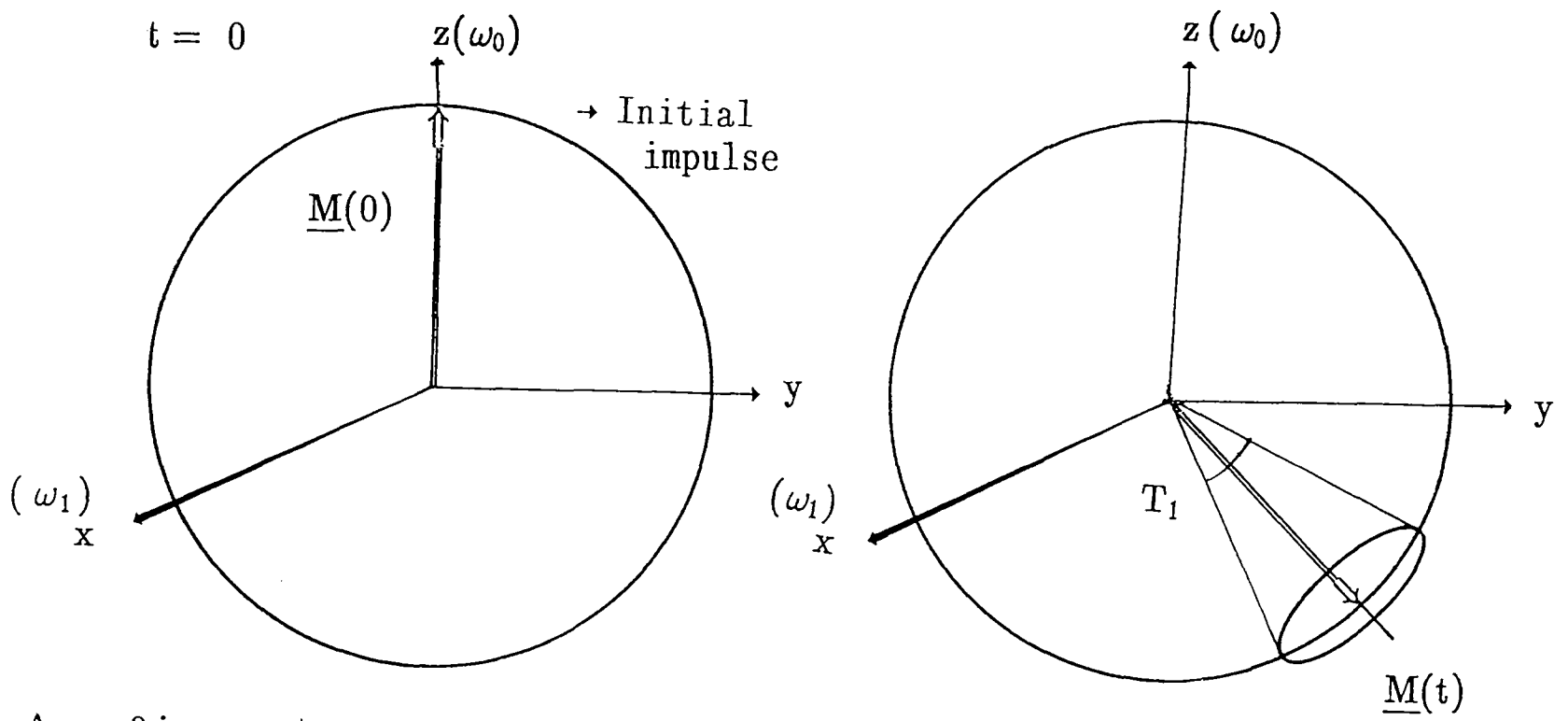


$\Delta\omega = 0$ i.e. exact resonance.

Frames are rotating at the Larmor frequency of that resonant transition under observation. The initial impulse to $\underline{M}(t)$ by the $\omega_1$ field pushes it into the y–direction, where it undergoes diffusion into the X–direction by $T_2$ processes and loses its z–y coherence through the action of $T_1$. If the torque imparted by $\omega_1$ is strong then $\underline{M}(t)$ may complete a half–revolution before $T_1$ can scramble this coherence, and the y–component of magnetization is then observed to reverse its sign – the condition for the onset of Torrey oscillations.

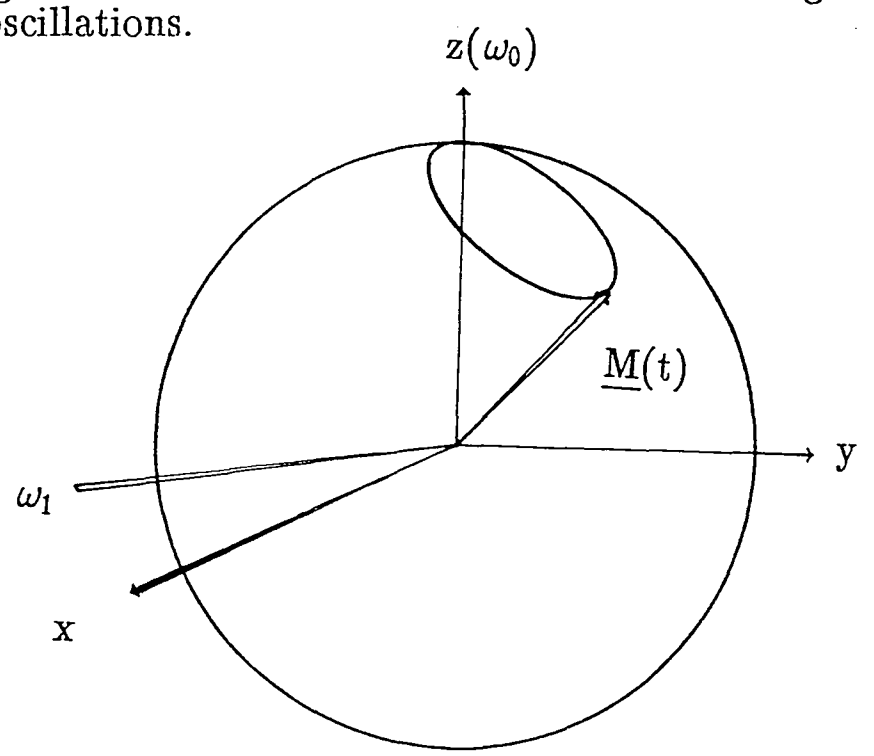


$\Delta\omega \neq 0$ i.e. off–resonance $\omega_1$ field.

The difference in precession frequencies ensures that, although initially the spins develop a y–component of magnetization, this has been lost by the time $\Delta\omega t = \pi/2$.

When the microwave field is not exactly resonant the bulk magnetization vector experiences varying proportions of $\omega_1$ and $\omega_0$ fields and precession occurs about their resultant. The frequency of precession relative to that of the microwave field is a function of $\omega_1$ and $\Delta\omega$, giving nutations provided, once again, this precession difference is faster than relaxation. Early time line broadening is simply accounted for; on or off resonance, the instantaneous application of an $\omega_1$ field or the creation of a spin system within a static field yields a bulk magnetization along the z–axis alone; whatever the frequency of the secondary field the torque exerted on $M_z$ always shifts it into the y–direction and only thereafter will a phase lag between $\omega_1$ and M(t) occur, to be damped by $T_1$, $T_2$ and reaction.

Returning to the lineshape function (2.3.8), one aspect was left unfinished and that was the evaluation of $e^{\underline{\underline{\varrho}}(t)}$. Assuming slow radical decay, so that $\int_0^t \underline{\underline{\varrho}}(t)dt \approx t\underline{\underline{\varrho}}(t)$, $e^{\underline{\underline{R}}(t)}$ may be diagonalised by finding its matrix of eigenvectors, $\underline{\lambda}_i$, and defining a diagonal matrix $\underline{\underline{Q}}$ whose elements are the eigenvalues of $\underline{\underline{R}}(t)$, $\lambda_i$. Thus,

$$Q_{ii}(t) = \lambda_i\,; \quad Q_{\substack{ij \\ i\neq j}} = 0 \tag{2.3.13}$$

the exponential matrix we require is then given by

$$e^{\underline{\underline{R}}(t)} = \underline{\underline{X}}.e^{\underline{\underline{Q}}(t)}.\underline{\underline{X}}^{-1} \tag{2.3.14}$$

Provided that the eigenvalues are not perfectly degenerate (and this is not a realistic possibility) we shall only have solutions of the form $e^{\lambda_i t}$. The eigenvalues are the roots of $|\underline{\underline{R}}|$,

$$\lambda^3 + (T_1^{-1}+2T_2^{-1})\lambda^2 + (T_2^{-2}+2T_1^{-1}T_2^{-1}+\omega_1^2+\Delta\omega^2)\lambda$$
$$+ (T_1^{-1}T_2^{-1}+\omega_1^2T_2^{-1}+\Delta\omega^2T_1^{-1}) = 0 \qquad (2.3.15)$$

To simplify their forms we introduce two groups of combinations of parameters:

$$\delta = (T_2^{-1} - T_1^{-1})$$
$$p = -\delta^2/3 + \omega_1^2 + \Delta\omega^2 \qquad (2.3.16)$$
$$q = -(2/27)\delta^3 + (1/3)\omega_1^2\delta - (2/3)\Delta\omega^2\delta$$

$$\alpha_\pm = \left[ \frac{q \pm (q^2+(4/27)p^3)^{\frac{1}{2}}}{2} \right]^{\frac{1}{3}}$$
$$\beta_\pm = -\tfrac{1}{2} \pm (\sqrt{3}/2)i \qquad (2.3.17)$$
$$\Theta = (1/3)(T_1^{-1} + 2T_2^{-1})$$

The roots are then simply

$$\lambda_1 = \alpha_+ + \alpha_- - \Theta \qquad (2.3.18)$$

$$\lambda_2 = \beta_+\alpha_+ + \beta_-\alpha_- - \Theta \qquad (2.3.19)$$

$$\lambda_3 = \beta_-\alpha_+ + \beta_+\alpha_- - \Theta \qquad (2.3.20)$$

The $_i$th column vector of $\underline{\underline{X}}$ is

$$\begin{pmatrix} \Delta\omega/(\lambda_i + T_2^{-1}) \\ 1 \\ -\omega_1/(\lambda_i + T_1^{-1}) \end{pmatrix} \qquad (2.3.21)$$

Combining all these elements yields a solution of the form

$$e^{\underline{\underline{R}}t} = S.e^{\underline{Q}t} \tag{2.3.22}$$

We are interested in the y component of $Se^{\underline{Q}t}$,

$$g_y(t) = \sum_{i=1}^{3} S_{iy}.e^{\lambda_i t} \tag{2.3.23}$$

where $S_{1y} = \omega_1(\lambda_1 + T_2^{-1})/(\lambda_1 - \lambda_2)(\lambda_1 - \lambda_3)$ (2.2.24)

Cyclic permutation of the eigenvalues yields $S_{2y}$ and $S_{3y}$. Equation (2.3.23) is an exact solution for a general case: specific conditions, such as were dealt with earlier will generate appropriately simple solutions. Examples of how these equations perform under a range of $T_1$, $T_2$, $\omega_1$ and $\Delta\omega$ values are shown in Fig.(2.3.2).

(2.3.3) A General Numerical Solution To The Bloch Equations

The exact solutions presented in the previous section are valid provided polarization can be treated as an initial condition. When this is not the case, and one of the principal origins of polarization will be found to arise as a consequence of radical pair encounters a long time after the radicals have been created, an analytical solution is no longer possible and we must instead seek a numerical approach.

If each encounter between pairs of radicals creates a polarization $P_f$, of an as yet unspecified nature, then this source can be included in the transport equation [31]

Fig.(2.3.2)

The time–decays for a series of offsets from resonance, $\Delta\omega$, and microwave field strengths $\omega_1$. Time span is 20.5$\mu$s.

a) $\Delta\omega = 0.0$; $\omega_1 = 0.5$radMHz; $T_1 = 5.0\mu$s; $T_2 = 0.8\mu$s

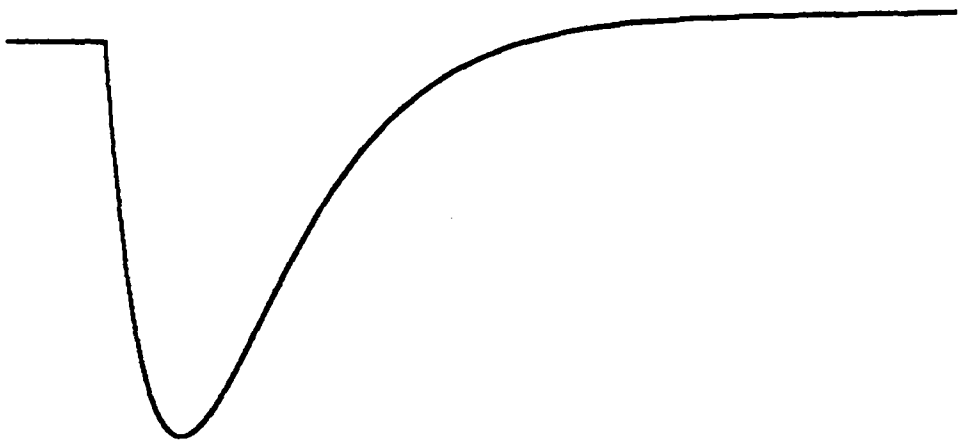

b) $\Delta\omega = 0.1$; $\omega_1 = 0.5$radMHz; $T_1 = 5.0\mu$s; $T_2 = 0.8\mu$s

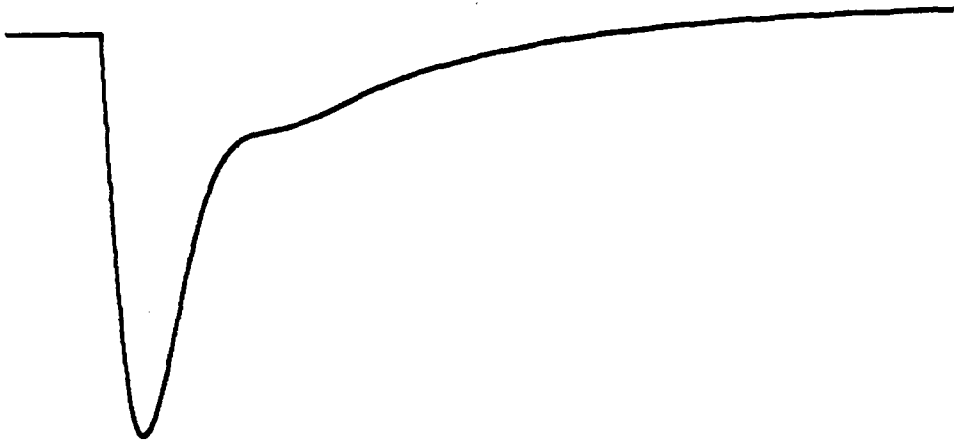

c) $\Delta\omega = 0.2$; $\omega_1 = 0.5$radMHz; $T_1 = 5.0\mu$s; $T_2 = 0.8\mu$s

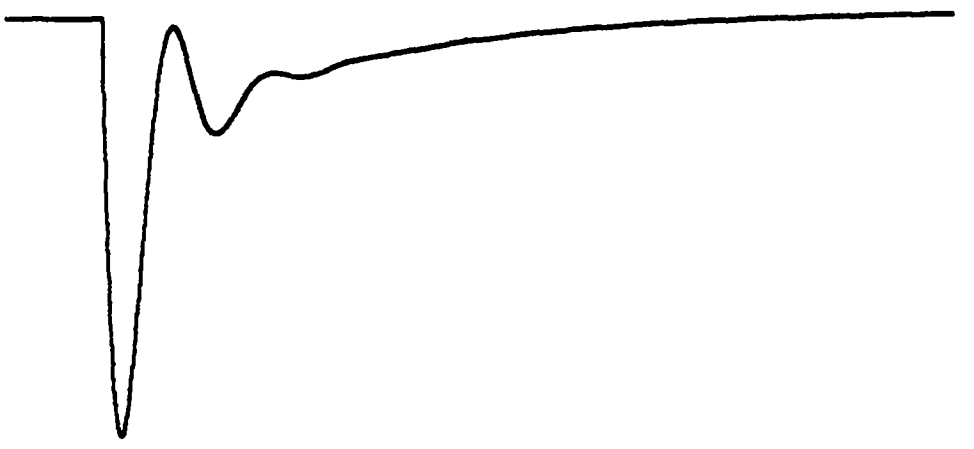

d) $\Delta\omega = 0.0$; $\omega_1 = 1.0$radMHz; $T_1 = 5.0\mu$s; $T_2 = 0.8\mu$s

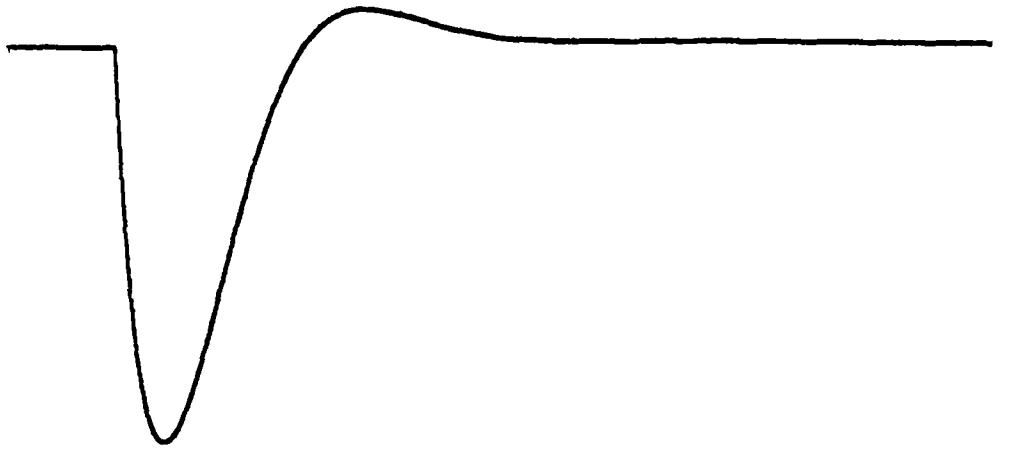

Surfaces using the parameters in Fig(2.3.2) over a field range of 0.1mT

$P_i/P_{eq} = +10.0$ and $-5.0$ respectively. Both surfaces cover an eight $\mu$s window.

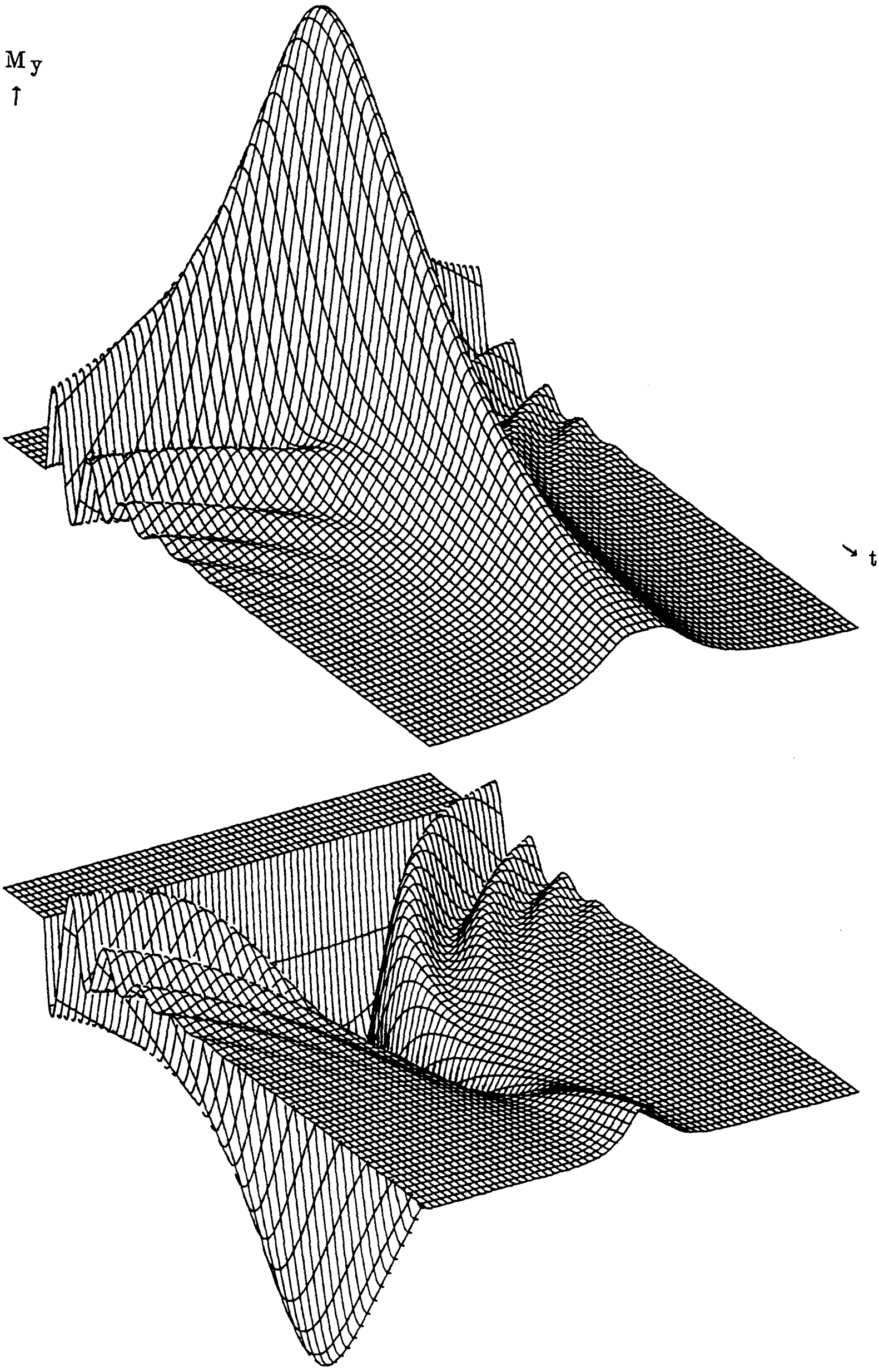

Fig.(2.3.3)

The contribution from G–pair polarization for the initial conditions

Radical conc. $n(0) = 10^{-5}mol.dm^{-3}$.
Second order reaction rate $k_1 = 10^9 dm^3 mol^{-1} s^{-1}$.
$P_f{:}P_i{:}P_{eq} = 0{:}-10{:}1$
($\omega_1 = 0.5$radMHz, $T_1 = 5.0\mu s$, $T_2 = 0.8\mu s$ and $\Delta\omega = 0.0$).

a)

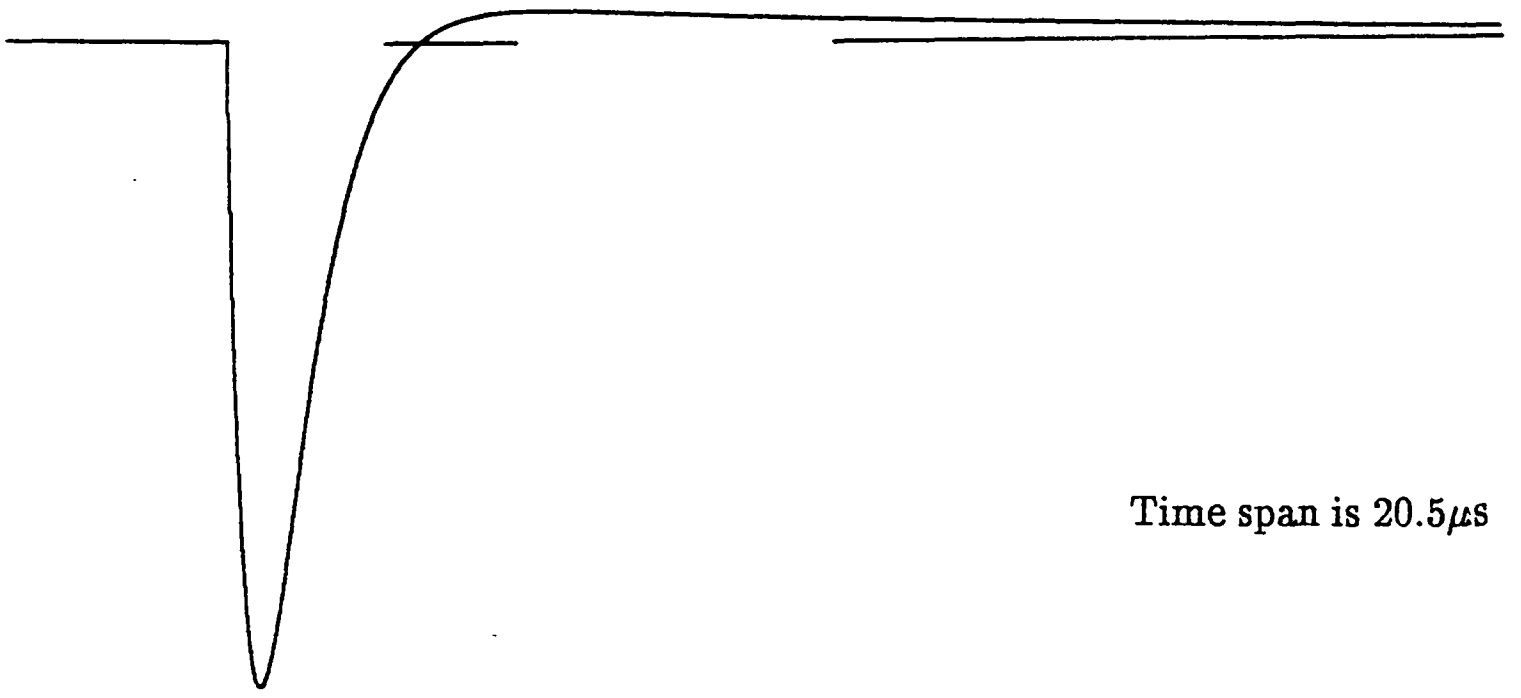

Time span is $20.5\mu s$

The G–pair polarization, $P_i$ (for a single decay line it is indistinguishable from the TM).

b)

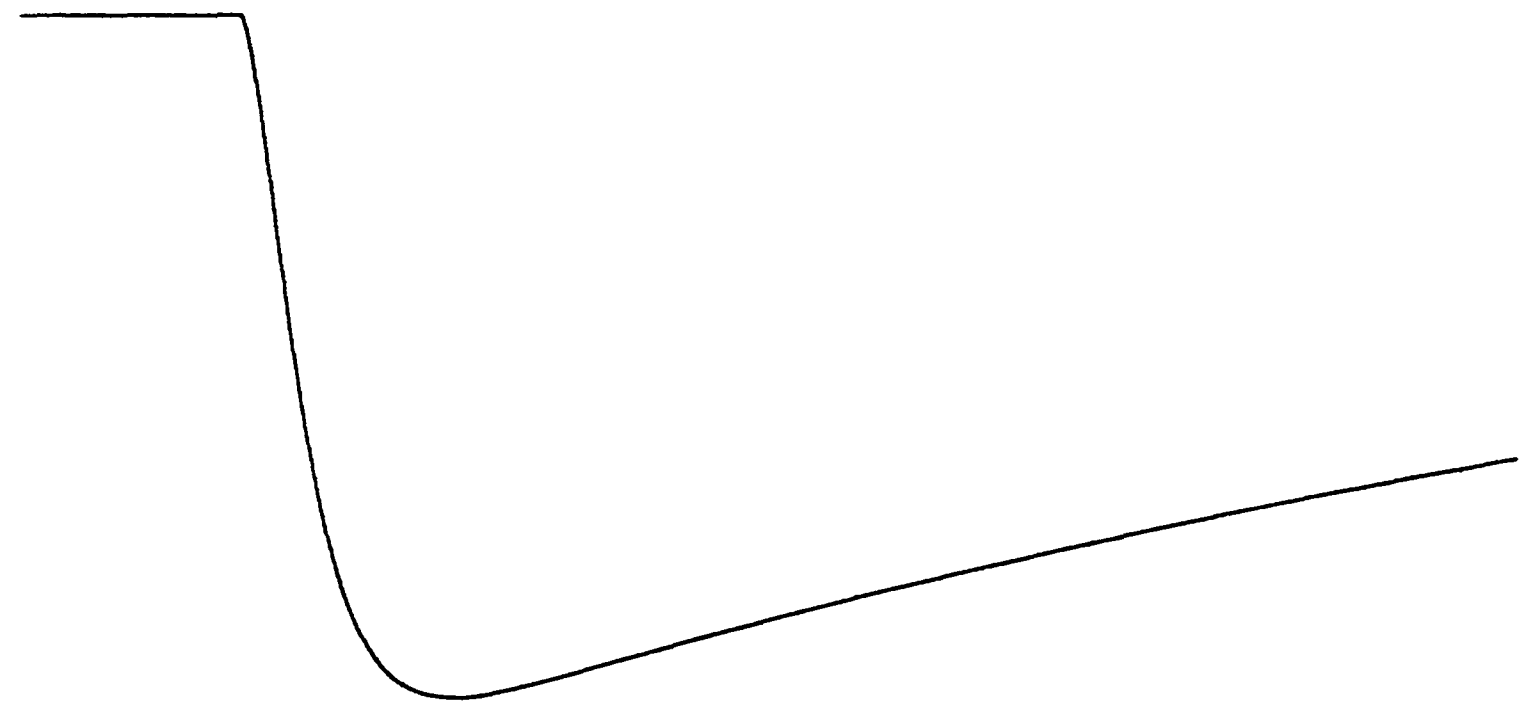

and the F–pair term, $P_f$, which can be seen to maximise at a later time than $P_i$ (but not very much later).

For identical conditions except that the initial concentration is now $10^{-3}$mol.dm$^{-3}$. these become

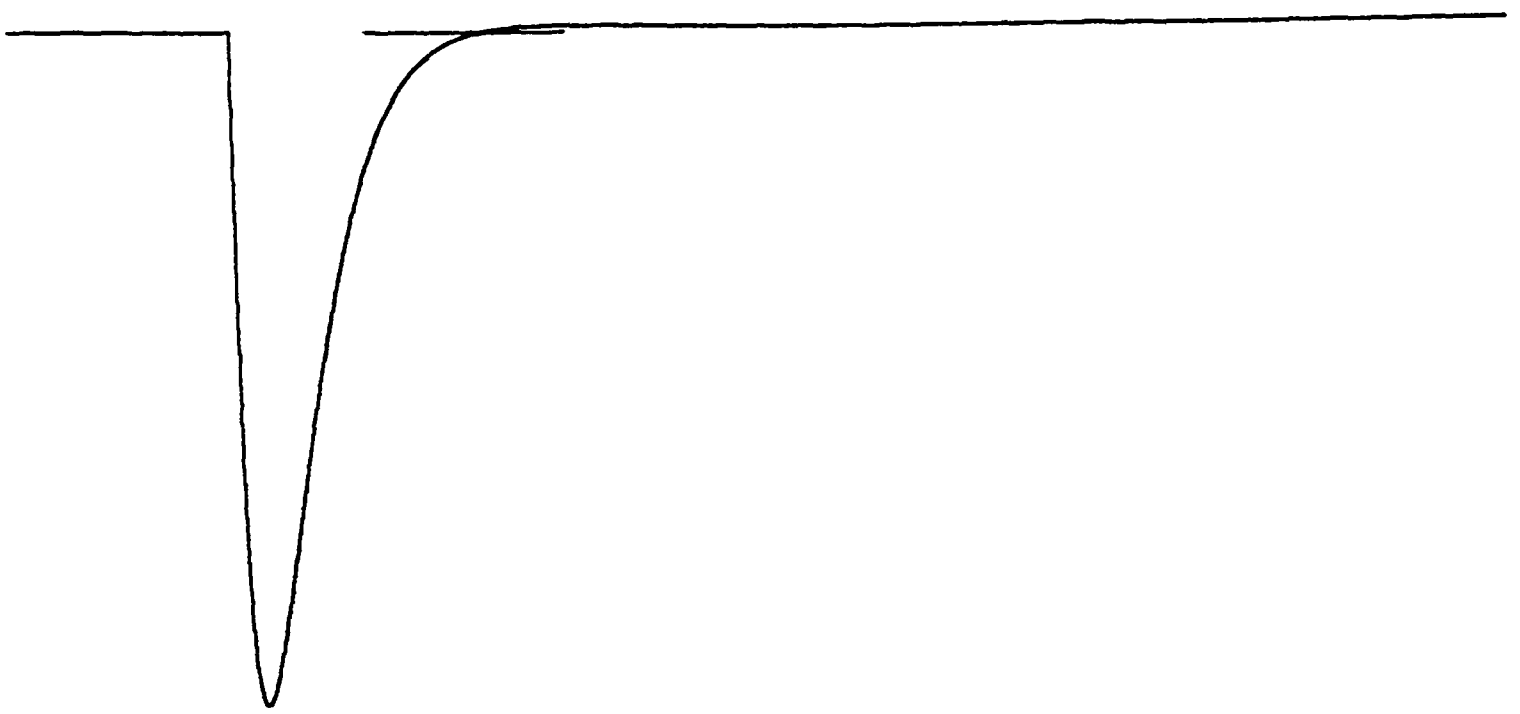

Under these conditions F–pair effects maximise within 1$\mu$s of G–pair signals and persist for far longer.

$$\dot{\underline{M}}(t) = \underline{\underline{L}}.\underline{M}(t) + T_1^{-1}n(t)P_{eq}.\begin{pmatrix}0\\0\\1\end{pmatrix} + k_2n(t)^2P_f.\begin{pmatrix}0\\0\\1\end{pmatrix} + \frac{\dot{n}(t)}{n(t)}.\underline{M}(t) \qquad (2.3.25)$$

(the random orientation of radicals in solution ensures that polarization is only generated in the z– direction), where $k_2$ is the rate of the bimolecular, polarization–generating reaction, and n(t) is given by

$$\dot{n}(t) = -k_1n(t) - k_2n(t)^2 \qquad (2.3.26)$$

$k_1$ is a pseudo–first–order scavenging rate constant. Equation (2.3.25) is also of the form (2.3.6) but its solution will be a combination of the solution (2.3.22) and a convolution of the polarization–generating term $(k_2n(t)^2P_f)_z$ with the matrix $\underline{\underline{L}}$. This contribution, at time t, is

$$\underline{\underline{M}}_f(t) = k_2n(t)P_f.\int_0^t \underline{\underline{L}}(t-t').n(t')^2\begin{pmatrix}0\\0\\1\end{pmatrix}dt' \qquad (2.3.27)$$

Such a convolution is easily programmable, by calculating $n(t')$ at each point in time and returning it to (2.3.27). Examples are shown in Figure (2.3.3), demonstrating how signals with recombinant polarization differ from those without.

(2.4.1) Creation Of The Integrated Lineshape

The experiment that provides the majority of the spectra in this thesis involves a summation of the signal from of a series of time points after radical creation, at a series of field settings. We are not concerned with the practicalities of the experiment here but

now is the best time to address the implications of this form of signal sampling [38]. The acronym TIS (Time Integration Spectroscopy) is slightly misleading since what is observed is actually a summation but, since the simulations are created in the same way as the spectra are recorded this is not an important point. In any case, provided that sampling time is smaller than the rate of change of the signal (including response time of the spectrometer) the integration and summation are essentially equivalent.

Neglecting radical reaction, once again we take equation (2.3.3) which, by writing $\underline{M}(t) = n(t)\underline{P}(t)$, becomes

$$\dot{\underline{P}}(t) = \underline{\underline{L}}.\underline{P}(t) + \underline{P}_{eq}/T_1 \qquad (2.4.1)$$

and its solution, as for (2.3.5) is

$$\underline{P}(t) = \left\{ e^{\underline{\underline{L}}t}.\underline{P}_i + [e^{\underline{\underline{L}}t} - \underline{\underline{1}}].\underline{\underline{L}}^{-1}.\underline{P}_{eq}/T_1 \right\} \qquad (2.4.2)$$

We wish to find

$$\sum_{t}^{t+nt'} \underline{P}(t) \approx \int_{t}^{t+n\,t'} \underline{P}(t)dt \equiv \underline{I}(t_1,t_2) \qquad (2.4.3)$$

where $t'$ is our sampling rate and n is the number of samples taken. Thus, from (2.4.1)

$$I(t_1,t_2) = \int_{t}^{t+n\,t'} \underline{\underline{L}}^{-1}(\dot{\underline{P}}(t) - \underline{P}_{eq}/T_1)dt$$

$$I(t_1,t_2) = \underline{\underline{L}}^{-1}[\underline{P}(t) - (\underline{P}_{eq}/T_1)t]_{t}^{t+nt'} \qquad (2.4.5)$$

Substituting a value of $\underline{P}(t)$ from (2.4.2) then gives

$$\underline{I}(t_1,t_2) = (\underline{P}_{eq}/T_1)\underline{\underline{L}}^{-1}\left[ [\gamma\, T_1 e^{\underline{\underline{L}}t} - t\underline{\underline{1}}] + [e^{\underline{\underline{L}}t} - \underline{\underline{1}}].\underline{\underline{L}}^{-1} \right]_{t_1}^{t_2} \qquad (2.4.6)$$

where $\gamma$ ($= P_i/P_{eq}$) is called the Polarization Ratio. The term containing $\gamma$ represents the contribution from initially polarized signals and $t\underline{\underline{1}}$ is that from the equilibrated radicals. Both these terms give Lorentzians; the last two, being operated on by $\underline{\underline{L}}^{-1}$ twice give squared Lorentzians.

The effects of this integration are shown in Fig.(2.4.1) for various integration widths and relaxation/polarization parameters. Radical reaction, if modelled, would have to be included before equation (2.4.5) is solved and would render the solutions far more complex. As a result it is not considered in any of the simulations given in this work. Intuitively, however, it may be seen to enhance the polarized with respect to the equilibrium signal, as long–time contributions to the lineshape would be damped. Equation (2.4.6) is separable into polarized and equilibrium terms so a closer approximation to the true signal could be manufactured by juggling with $\gamma$. The two halves of (2.4.6) can combine to give some interesting lineshapes, as shown in fig (2.4.2) which may allow $\gamma$ to be extracted if assumptions are made about negligible reaction [39].

Advantages in recording spectra by the TIS technique are that signal–to–noise ratios are improved over and above those from single point sampling methods, without introducing the arbitrariness of box–car integration, and spurious off–resonance

Fig.(2.4.1)

An illustration of the effect of increasing the integration period for one line.

$T_1 = 5.0\mu s$; $T_2 = 0.8\mu s$; $P_i = 10P_{eq}$ ; $\omega_1 = 0.5$radMHz; range of spectrum = 0.5mT.

$t_1 = 0.50\mu s$
$t_2 = 0.51\mu s$

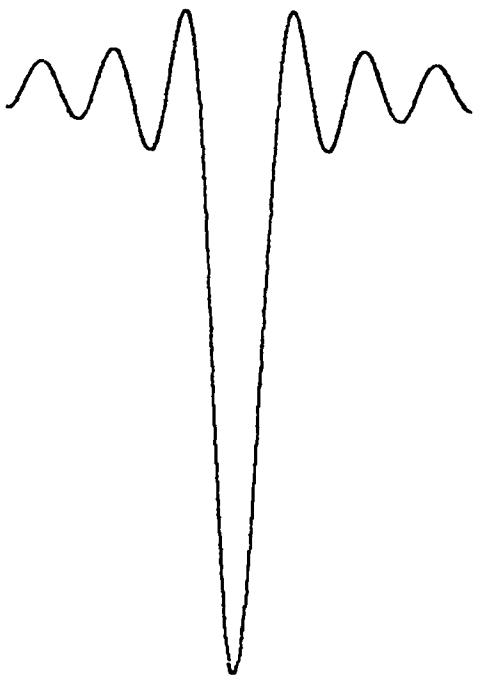

A single point sample

$t_1 = 0.50\mu S$
$t_2 = 0.75\mu S$

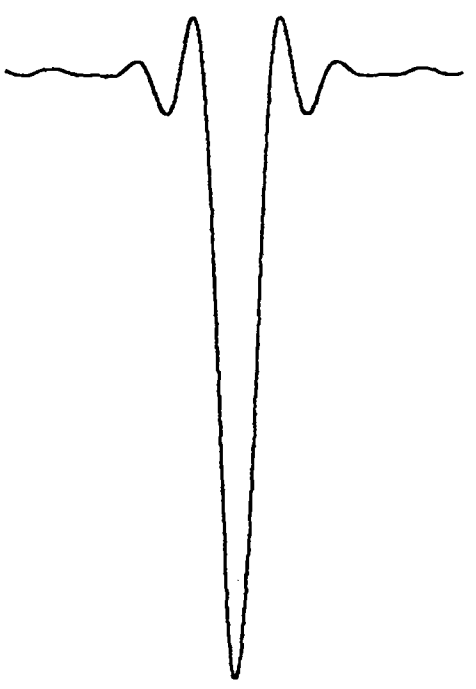

25 point sample

$t_1 = 0.50\mu S$
$t_2 = 1.50\mu S$

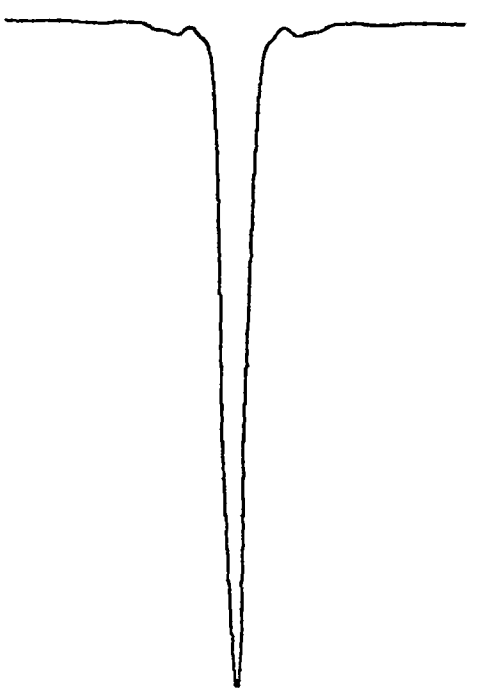

100 point sample

Fig.(2.4.2)

The effect of polarization ratios upon the "crossover" lineshape.

A combination of Equilibrium and polarized lineshapes is most easily resolved when the magnitude of residual polarization is of the same order of magnitude as that of the equilibrium contribution. This is illustrated for a range of $\gamma$ for a line with the following parameters:

$T_1 = 5.0\mu s$; $T_2 = 0.8\mu s$; $\omega_1 = 0.5$ radMHz

Period of sampling – 8.0 to 9.0 $\mu s$ post–flash; field sweep = 0.1mT.

$\gamma = -12$

$\gamma = -24$

$\gamma = -72$

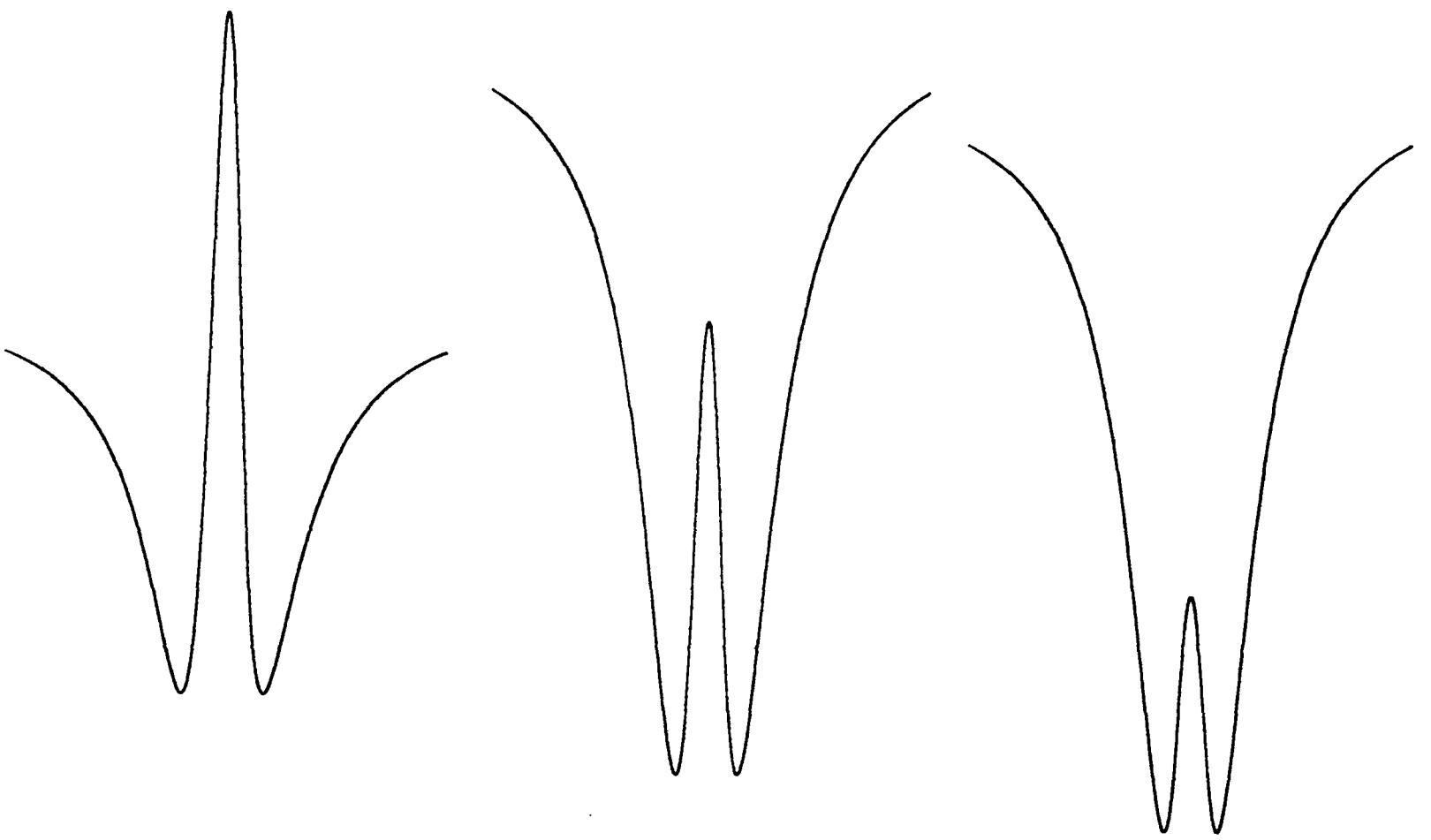

nutations may be averaged out to facilitate interpretation of spectra. On the other hand, the precision of the time measurement is lowered in comparison with single time–point sampled spectra.

(2.4.2) The Uses Of A Lineshape Function

Reference to equation (2.4.6) and the simulations in Figs.(2.4.1) and (2.4.2) indicates how sensitive the lineshape is to the various parameters affecting it. We select the integration limits for each experiment but must attempt to fit $P_i$, $P_{eq}$, $T_1$, $T_2$ and $\omega_1$ to the observed spectral line. It is often assumed that we already know $\omega_1$ and, to be sure, microwave field strength can be controlled very accurately. What is less clear is the actual field strength at the sample, which will be modified by the susceptibility of the sample and the disrupting effect of the sample cell upon the field within the cavity. We shall encounter this problem again in chapter 5.

The majority of radicals investigated by the Oxford group seem to fall into the region for which $T_1 \gg T_2$ (as a result of electron exchange shortening the effective $T_2$), whence we may use equations (2.3.11) and (2.3.12) to determine $T_1$ more accurately; fitting of $T_2$ to the lineshape in the frequency domain, followed by fitting of the long–time decay curve exactly on resonance at various low microwave powers, gives an approximate $T_1$ from

$$M_y(t) \approx \omega_1 T_2 n(t) P_{eq} / (1+\omega_1^2 T_1 T_2) \qquad (2.4.7)$$

This method is riddled with assumptions and does not take advantage of the strong early–time signal. A better approach is to switch the microwave field on at varying times after radical creation [40]. If $\tau$ is the delay between creating radicals and

switching the field on then, from (2.3.11) and (2.3.12)

$$M_z(\tau) = n(0)\left\{(P_i - P_{eq}).e^{-\tau/T_1} + P_{eq}\right\} \qquad (2.4.8)$$
$$M_y(\tau) = 0$$

At a subsequent time $(\tau + t)$

$$M_y(\tau+t) = n(0)\left\{[(P_i - P_{eq}).e^{-\tau/T_1} + P_{eq}].g_y(t) + P_{eq}.G_y(t)/T_1\right\} \qquad (2.4.9)$$

By holding all other parameters constant and varying just the delay time $\tau$, $M_y(\tau+t)$ can be seen to decay as a monoexponential dependent only on $T_1$. The integrated expression for $M_y$ is similarly dependent only on $T_1$ so higher microwave fields and longer integration periods may be used. However, problems of switching circuitry designed for continuous wave use causes considerable problems. To date only one attempt to measure $T_1$ this way has been published [41]. This method may also be used to measure $\gamma$ but is imprecise. Our best hope is in determining all other spectral parameters and then fitting a value of $\gamma$ to the "crossover point" of the spectrum, at which point both polarized and equilibrium terms can be seen (most easily distinguishable when $P_i$ and $P_{eq}$ are of opposite sign) [39].

## REFERENCES – CHAPTER 2


1 Atkins P.W. *International Review Of Science Series 2. Phys.Chem.*(1975) 4, 1.

2 Rengan S.K., Khakhar M.P., Prabhananda B.S., Venkataraman B. *Pure and Applied Chem.* (1972) 32, 287.

3 Wilson R., Kivelson D. *J.Chem.Phys.* (1966) 44, 154.

4 McLauchlan K.A., Sealy R.C., Wittmann J.M. *Mol.Phys.* (1978) 35, 51.

5 Kivelson D. *J.Chem. Phys.* (1960) 33, 1094.

6 Nyberg G. *Mol.Phys.* (1967) 12, 69.

7 Leniart D.S., Connor H.D., Freed J.H. *J.Chem.Phys.* (1975) 63, 165.

8 Hubbard P.S. *Phys.Rev.* (1963) 131, 1155.

9 Nyberg G. *Mol.Phys.* (1969) 17, 87.

10 Atkins P.W., Horsfield A., Symons M.C.R. *J.Chem.Soc.* (1964) 5220.

11 Freed J.H. *J.Chem.Phys.* (1965) 43, 2312.

12 Carrington A., Longuet–Higgins H.C. *Mol.Phys.* (1962) 5, 447.

13 de Boer E., Mackor E.L. *Mol.Phys.* (1962) 5, 493.

14 Hore P.J., McLauchlan K.A. *Chem.Phys.Lett.* (1980) 75, 582.

15 Stevens D.G. *D.Phil Thesis, Oxford* (1986) Chapter 6.

16 McLauchlan K.A., Stevens D.G. *J.Chem.Phys* (1987) 87, 4399.

17 Sullivan P.D., Boulton J.R. *Adv.Magn.Reson.* (1970) 4, 39.

18 Kuhlmann K.F., Grant D.M. *J.Chem.Phys.* (1971) 55, 2998.

19 McLauchlan K.A., Ritchie A.J.D. *Mol.Phys.* (1985) 56, 141.

20 Kreilick R.W., Weissman S.I. *J.Am.Chem.Soc.* (1966) 88, 2645.

21 Freed J.H. *J.Phys.Chem.* (1967) 71, 38.

22 Hore P.J., McLauchlan K.A. *Mol.Phys.* (1981) 42, 1009.

23 Smith I.C.P., Carrington A. *Mol.Phys.* (1967) 12, 439.

24 McLauchlan K.A., Ritchie A.J.D. *Mol.Phys.* (1985) 56, 1357.

25 Hore P.J., McLauchlan K.A. *Mol.Phys.* (1981) 42, 533.

26 Hore P.J., Joslin C.G., McLauchlan K.A.
*J.Chem.Soc. Specialist Periodical Report – e.s.r.* (1979) 5, 1.

27 Bloch F. *Phys.Rev.* (1946) 70, 460.

28 Torrey H.C. *Phys.Rev.* (1949) 76, 1059.

29 Pedersen J.B., "*Chemically Induced Magnetic Polarization*",
(Ed. Muus L.T. et al.) Chapter 9. (Pub. D.Reidel, 1977).

30 Verma N.C., Fessenden R.W. *Farad.Disc.Chem.Soc.* (1977) 63, 104.

31 Pedersen J.B. *J.Chem.Phys.* (1973) 59, 2656.

32 Hore P.J., McLauchlan K.A. *Rev.Chem.Int.* (1979) 3, 89.

33 Hore P.J., McLauchlan K.A. *J.Magn.Reson.* (1979) 36, 129.

34 Eyes H. "*Elementary Matrix Theory*" (Pub. Dover 1966).

35 Basu S. *D.Phil. Thesis, Oxford* (1983) Chapter 3.

36 Atkins P.W., McLauchlan K.A., Percival P.W. *Mol.Phys.* (1973) 25, 281.

37 Atkins P.W., Dobbs A.J., McLauchlan K.A. *Chem.Phys.Lett.* (1973) 25, 105.

38 Basu S., McLauchlan K.A., Sealy G.R. *Mol.Phys.* (1984) 52, 431.

39 McLauchlan K.A., Stevens D.G. *Mol.Phys.* (1987) 60, 1159.

40 Furrer R., Fujara F., Lange C., Stehlik D., Vieth H.M., Vollmann W. *Chem.Phys.Lett.* (1980) 75, 332.

41 McLauchlan K.A., Sealy G.R. *Mol.Phys.* (1984) 52, 783.

# CHAPTER III : AN EXPERIMENTAL REVIEW

# AN EXPERIMENTAL REVIEW

## (3.1.1) Response Time And Sensitivity

To understand why the spectra featured in this thesis are of an unusual nature for *e.s.r.* work we must look at what our aims are. Conventionally, *e.s.r.* spectrometers employ field modulation to gain highest sensitivity, allowing just one frequency to be selected from a range pouring out of the microwave cavity in which the sample resides. Further, a very high Q factor [1], defined as

$$Q = 2\pi \frac{(\text{energy stored per cycle})}{(\text{energy lost per cycle})} \qquad (3.1.1)$$

is chosen to enhance the signal further. If we wish to examine phenomena that are observable only in the first few microseconds after radical generation (and here we may equate "radical" with "signal") we encounter an age–old problem; sensitivity and reaction to a stimulus are inversely related.

Specifically we see that if Q is high, a rapid change in the energy stored in the cavity will only leak out slowly. A low energy loss per second is equivalent to a filter on high–frequency changes and may be represented by a band width. An approximate relationship exists between bandwidth $\Delta\nu_s$ and response time $t_s$, such that

$$t_s \, \alpha \, (3\Delta\nu_s)^{-1} \qquad (3.1.2)$$

One consideration, therefore, must be to find a healthy balance between these two values. This is discussed further when actual timescales are imposed. The problem of field modulation is more simply solved; we simply dispense with it: not only would we

introduce complex and poorly characterized functions upon the resultant signals but, with normal modulation (e.g.100KHz) the greatest time–resolution we could obtain would be $\approx 30\mu s$. As seen in the previous chapter the signals detected directly are comparatively straightforward and, more importantly, are immediately applicable. Again the trade–off is with signal–to–noise ratios and an alternative enhancement of signal strength is therefore highly desirable.

(3.1.2) Comparisons Of Alternatives And Spectrometer History

With the benefit of hindsight and plenty of published material it is possible to draw conclusions about how best to circumvent the problems discussed above. This is left until after a review of the development of the spectrometer used in this study. Our equipment has been developed around some novel methods used to study radical signal decays [2] that used 2MHz modulation for field–swept spectra of radicals generated by a triggered laser pulse, recording a value for the signal at a specific field, and repeating the process over a series of new fields. Some on–resonance decays of signals with time were recorded from strong radical signals without the need for modulation, by employing extensive signal averaging. Along the way a new form of CIDEP, now referred to as the Triplet Mechanism was chanced upon [3]. These methods all employed continuous microwave fields.

Concurrently a spin–echo technique was being developed for transient *e.s.r.* that gave high signal–to–noise ratios and good time resolution [4]. However, it is not clear in such methods what the signal actually represents; resolution of field domain spectra often show linewidths of a few Gauss as a consequence of the frequency uncertainty inherent in very short and powerful microwave pulses. In addition, the echo is the resultant of two free–induction decays so its width is limited and a choice of a wider

sampling time will not enhance its magnitude. In its favour it can provide a good value for $T_1$ of radicals in solution, it does utilise the entire magnetization, $M_z$, rather than a small part of it, and it is eminently suitable for pulse–radiolysis experiments [5] since the delicate microwave circuitry can be completely isolated from the sample when an electron pulse is supplied.

A second method of operation is to use a box–car to accept and store a signal for a fixed period of time after each photolysis flash [6]. Long time intervals can be sampled by this method but there is a problem associated with the box–car integrator and the analogue field sweep – that the box–car must be gated open for a period of time in order to allow a charging capacitor to develop a steady potential, and to do this ~~the~~ and yet retain acceptable signal–to–noise levels requires that the open period tends to be larger than the periods of earliest–time oscillations. It is worth noting, for instance, that no transient nutations have been recorded on box–car spectrometers.

These problems all suggest themselves to the development of an entirely different method of detection. This method follows on from the use of digitally recorded time–decays of radical signals and in essence, though not necessarily in practice, it is very simple. Neglecting the practicalities of triggering the respective components of the spectrometer for the moment, we consider a sample flowing through a microwave cavity and bathed simultaneously in a continuous microwave field and static magnetic field. A digital transient recorder begins to sample the output from the cavity, then a radiation pulse strikes the sample, generating radicals (and, invariably, spurious noise arising from sample heating and photo–electron emission from the cavity walls). The transient recorder completes its time scan and stores the signal in a data buffer, clears its recording buffer and indicates that it is ready to store another transient. After each cycle the recorded signal is added to the previous signal store, scaling taking place if

necessary. This will give a profile with time with increased signal–to–noise ratios, of a signal that will include an *e.s.r.* transition if the static field is a resonant one. If a second field position is then selected and the signal from this position is subtracted (added anti–phase) from the first then the result should be a flat line for two off–resonance field positions and a pure radical signal decay for one on– and one off–resonance position. This cycle is at the heart of all the experiments reported in this work. We may note the following advantages inherent in this method: i) the quantity $M_y(t)$ is precisely defined as demonstrated in chapter 2; ii) the signals are in digitised form and are therefore amenable to off–line handling [7] and enhancement [8]; iii) signal averaging and the concomittant improvement of signal–to–noise is determined only by the operator's patience; iv) the signal may be further improved by adding together consecutive time points on the decay curve. This last observation has led to the method whereby field–swept spectra are usually obtained.

There is one technique that has not been mentioned. This employs a Fast Fourier Transform carried out on the signal derived from a pulsed *e.s.r.* experiment [9]. Only a couple of spectra of transient species have been published so far, but the first flush indicates that, though it may not offer the flexibility of the continuous–wave spectrometer, its signal–to–noise and resolution are exceptional, especially in the sub–microsecond range, in which continuous–wave experiments display poor signal–to–noise ratios.

### (3.2.1) An Overview Of The Experiment

In opting for the experiment described above we must make choices of photolysis source, magnetic field and so on. Whilst a great deal of the software has been developed since its inception the core of the spectrometer has remained the same [10].

A microwave cavity ($TE_{102}$ or $TE_{103}$) with a port cut in its front block to admit laser radiation, resides between the poles of a water–cooled, 9" electromagnet, composed of a stable field of $\approx$ 0.35 Tesla, and with scanning coils mounted on the pole faces. The field is controlled by a Bruker ER031M 12 bit digital field controller, informed by a Hall effect probe of the field strength between the pole faces. This set–up is stable to 100 p.p.m. Samples flow through the irradiation region in a flat silica cell of internal width 0.1mm, aligned such that the sample is maintained at the region of maximum magnetic and minimum electric microwave field strength. When solvents of low dielectric constant are employed a thin–walled silica tube of internal diameter 2mm may be substituted if required (for example when the sample has a low extinction coefficient at the radiation wavelength).

Viscous samples require pumping through the sample cell by a peristaltic device but the flow rate for the majority of experiments is most easily controlled by capillary flow under pressure from a constant head of solution, maintained by a peristaltic pump feeding solution from a reservoir. Careful work requires the sample to be de–oxygenated and this is most conveniently achieved by bubbling $O_2$–free nitrogen through for several minutes prior to, and during the course of the experiment.

The light source employed is a Lambda Physik MSC 103 laser. Various gas fills are available but it has been found that the 308 nm radiation produced from a XeCl exciplex is of a short duration ($\approx$ 20 ns), reproducible, fairly intense (up to 100 $mJPulse^{-1}$) and is absorbed strongly by a lot of species of interest to us such as carbonyls or heterocycles, whilst the majority of solvents and chemical quenchers we use, such as alkanes, alcohols and amines, are transparent to it. At most about a third of the laser radiation strikes the sample, and a simple calculation yields an upper bound on radical concentration of $\approx 10^{-3}$ $mol.dm^{-3}$ for a quantum yield of unity. Each sample can therefore be photolysed

at least ten times before a 1% change in molarity of photo–active species at 1 Molar concentration has taken place.

The laser is typically run at a 20Hz repetition rate; a second crude calculation shows that a flow rate of one drop every five seconds will keep concentrations of photoactive species constant to within 1% and prevent build–up of unwanted photolysis products. Most experimental flow rates used were about twice this velocity. The laser is monitored by a control device which samples a small percentage of the beam and responds by increasing or decreasing the voltage discharged across the laser cavity. In this way long–term stability of a pre–selected laser output is possible.

(3.2.2) A Fast Response Detection System

In order to respond to a sub–microsecond signal various modifications have been made to an otherwise conventional microwave bridge (Bruker ER200D). A schematic is shown in Fig.(3.2.1), which includes all the main features.

Microwaves are generated by a water–cooled klystron that is tuned over a 100MHz range by an AFC circuit. This frequency control unit monitors an error signal generated by the 79KHz–modulated output of the klystron. At its limit the klystron can produce over 1000mW but this is not stable so a leveller, cutting out all but 195mW, is introduced. There is then no problem with consistency of output. The circuit is tuned by hand for each cavity, over an operating range of 9.2 to 10.2 GHz. It may then be impedance–matched so that with no signal being generated, no microwaves are reflected back out of the cavity (a method akin to the dual beam technique in *i.r.* spectroscopy). When signal is generated it is pre–amplified by a GaAs field effect transistor, selected for its low noise characteristics, and fed onto a detector crystal which is biased to keep it in the linear response region. A broad–banded amplifier further increases the signal

Fig.(3.2.1)

THE MICROWAVE BRIDGE.

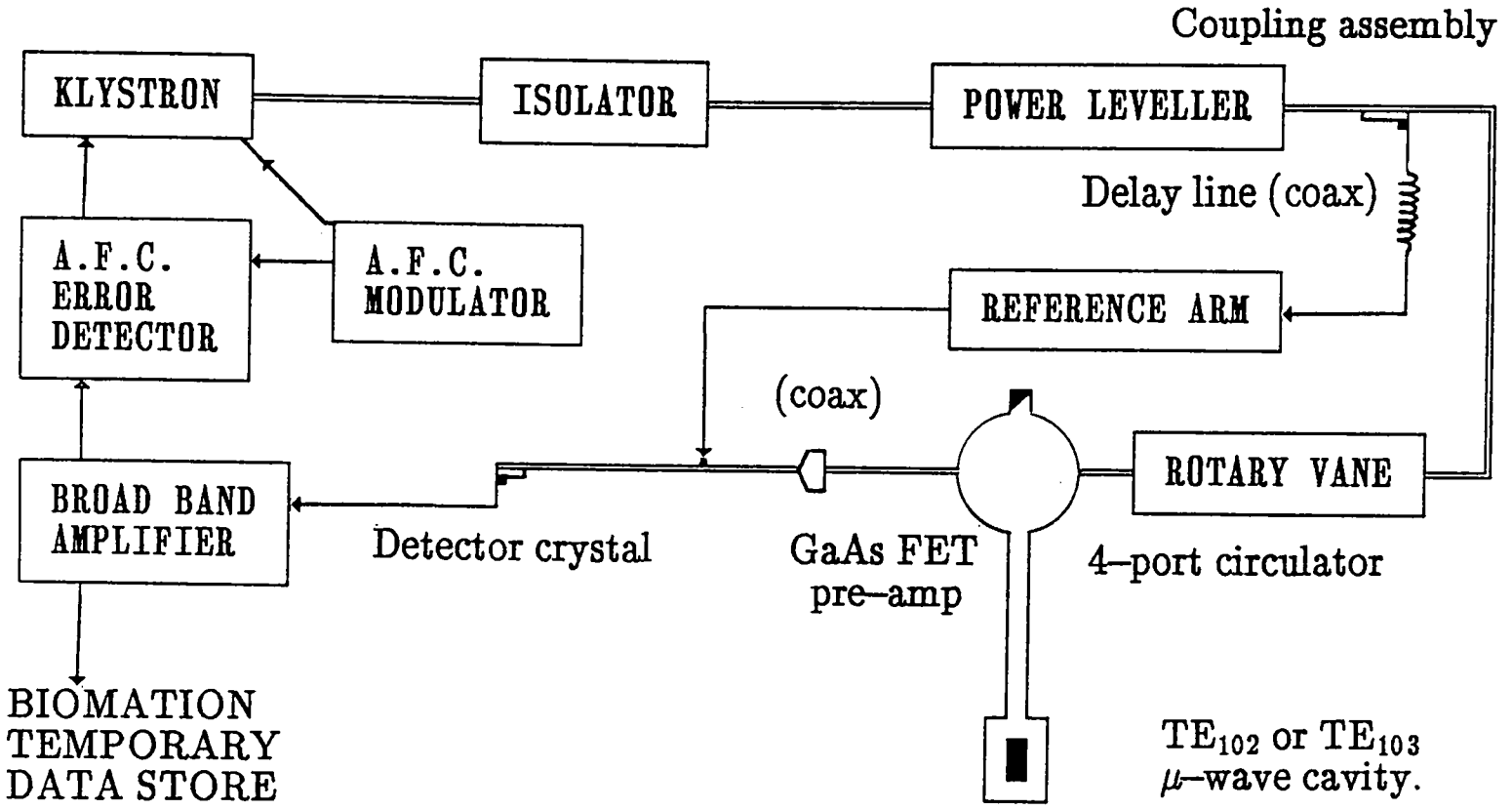

before passing it on to a transient recorder (Gould Biomation 3100) where it is digitised and stored prior to manipulation by a dedicated fast adder and desktop microcomputer.

All components were selected for their fast response characteristics and low noise; ultimately it is the cavity that sets a limit on response time and a value for its Q factor of around 1000 has been chosen as an optimum [7] (A Q factor of 600 gives a response time of $\approx$ 1ns but since the laser pulse may lag behind or pre–empt the mean by up to 100ns such a speed of response would be worthless). At the Q value chosen there is no need to deconvolute the signal from a spectrometer response function in order to compare spectra with simulations. Measurement of the cavity Q is done by firing a pulse into the matched cavity and comparing the response of the output to the input [11].

The microwave field strength, $\omega_1$, is given approximately by [12]

$$\omega_1 = \omega_0.10^{-\mathrm{dB}/20} \qquad (3.2.1)$$

where dB is the attenuation in decibels and $\omega_0$ is the unattenuated field strength ($\approx$ 5.3radMHz). It must be stressed that this is approximate, however; it will be increased or reduced at the sample depending upon the sample's dielectric susceptibility and positioning within the cavity.

(3.2.3) Peripheral Devices

A block diagram is provided in Fig.(3.2.2) of the whole experiment. Following the signal path through this scheme we see that, after it has been digitised by the Biomation recorder, it may be temporarily displayed on a transient scope. This is useful for ensuring that none of the amplifiers in the signal channel are saturating over the course

Fig.(3.2.2)

AN EXPERIMENTAL SCHEME

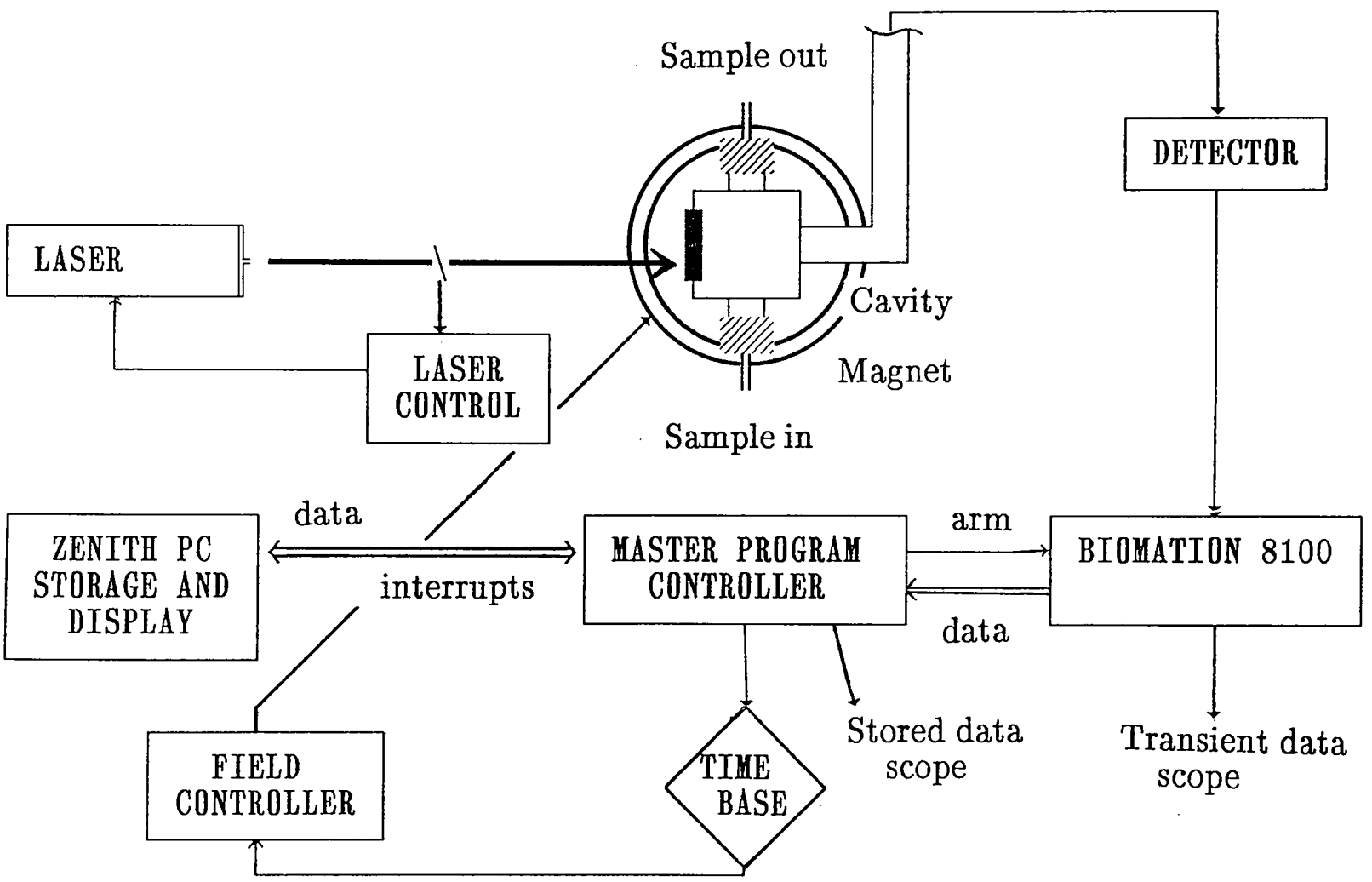

of a single experimental run. At the same time, however, we may wish to increase amplification to minimise digitisation errors.

Transfer of data from the transient recorder to a dedicated storage and handling device is controlled by a master clock, locked into the timebase of the Bruker ER001 console, which also advances the field controller and manages the necessary trigger sequence for laser, Biomation and display on the transient scope[1]. The spectrum is displayed, as it is being generated, on a Tektronix 2225 oscilloscope, to allow the operator to determine whether to complete a scan or abort it before completion.

As mentioned earlier, a signal, caused by the heating of the sample and photoelectron processes, will always be present at any field position. This underlying signal, invariant with field position, may be removed by integrating a current pulse unit, geared to the dedicated storage device, which supplies a current to the fast sweep coils on the pole faces. For such work, especially on radicals with narrow lines, a field/frequency lock (Bruker ER033) is necessary. This uses the relationship between $B_z$ and $\nu$ at resonance to ensure that exact resonance is achieved whenever the current pulser is inactive. It monitors the error signal generated by $\alpha\alpha$'–diphenyl $\beta$–picrylhydrazyl radical, held in a probe between the pole faces. The degree of stability of field and frequency achievable in this way is 1 p.p.m.

Temperature of the sample is conveniently controlled by a Bruker 4111VT variable temperature unit, which bathes the sample cell, held in a Dewar jacket inside the cavity, in pre–heated nitrogen vapour. An evaporator and heater for the $N_2$ vapour are controlled by a servo system which feeds back from thermocouples in the vapour stream and in the sample itself. When carefully prepared a temperature stable to within $0.2^0$C

---

[1] It would be easier to run the whole experiment from the trigger on the laser power supply, but this would reduce its flexibility.

at room temperature is possible. Care must be taken at lower temperatures to ensure that water vapour and other volatile substances do not condense in the cavity.

(3.3.1) Data Handling

The signal from each photolysis flash is accepted by the Biomation 8100 Transient Recorder, which has been prepared to begin recording for a period before the laser fires, so that a pre–trigger baseline may be established. A maximum time resolution of 10ns per point is possible and is the most commonly used sampling rate. The contents of the Biomation are then fed to a purpose–built temporary memory store and fast adder for handling. If there is time the signal is also returned to the oscilloscope in the main console, to allow the operator to modify machine settings if necessary.

If this dedicated device has been programmed to record in what is hereinafter referred to as Mode I then the contents of the Biomation are simply added to the contents of a data buffer with an appropriate scaling factor, and the Biomation is re–armed for further data collection. A refinement on this mode is to use off–resonance subtraction, in which a counter records the number of flashes at a field setting chosen to lie on a resonance line. The current pulser is then activated and an equal number of flashes is recorded in counterphase.

To create a Mode II or field–swept spectrum a different approach is used. A Mode I decay is recorded to allow the operator to determine when the laser strikes the sample and appropriate limits are set relative to this point, between which the digitised spectrum is summed (time–integrated) using as the baseline the average of the first 256 points recorded before the laser fires. Both values are determined by the fast adder device and the integrand is passed on to a temporary add–buffer where the values from sixteen such steps are stored. The sum of these values is output to a specific address in a

data buffer, corresponding to one field position. The field is then advanced and the cycle repeated for the next field point.

Field sweep–width and centre–field for each scan are entered via the Bruker ER031M field controller . All other commands are entered from a Zenith PC via a menu–driven suite of control programs. These are sent to a program buffer in the dedicated device and include number of field points (field resolution) per scan, the number of averages to be taken and the periods of integration if Mode II has been selected. Figs.(3.3.1) and (3.3.2) explain the interconnections between the hardware and the two most commonly used operating cycles respectively.

(3.3.2) Refinements To The Technique And An Acknowledgement

It can be easily appreciated that Mode II, in which the majority of data collected is subsequently thrown away, is an inefficient method of operation. It was originally developed as a means of circumventing limited memory storage (an *e.s.r.* surface built up from a collection of 2048 field points, each with 2048 point time–decays, would occupy 8MB of storage space). With the introduction of a hard disk this is no longer a problem and several two–dimensional *e.s.r.* spectra have now been published (The principle is simply to record an entire Mode I at each field point and stack–plot or handle off–line the entire family of decay curves so produced) [7,13]. The quality of each surface is improved considerably by regulating the laser power; provided the laser power is kept constant these surfaces show how reproducible the off–resonance background signal is. A prediction that this will become the normal mode of operation [13] is only now being bourne out because of problems associated with the transfer of such large volumes of data between laboratory computers.

Fig(3.3.1)

Data Handling Hardware

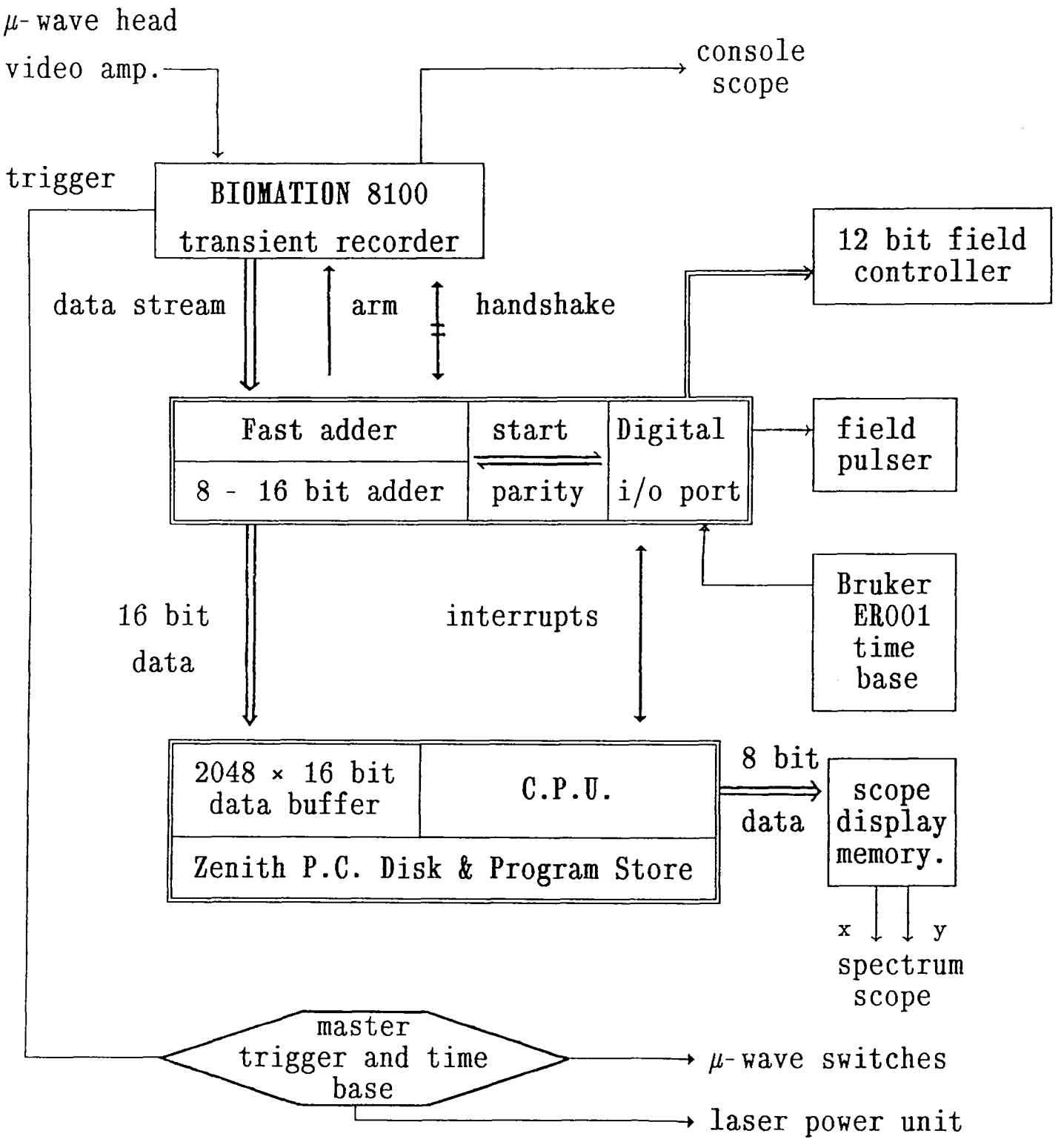

Fig.(3.3.2)

TWO OPERATING CYCLES.

Mode I (on/off resonance)

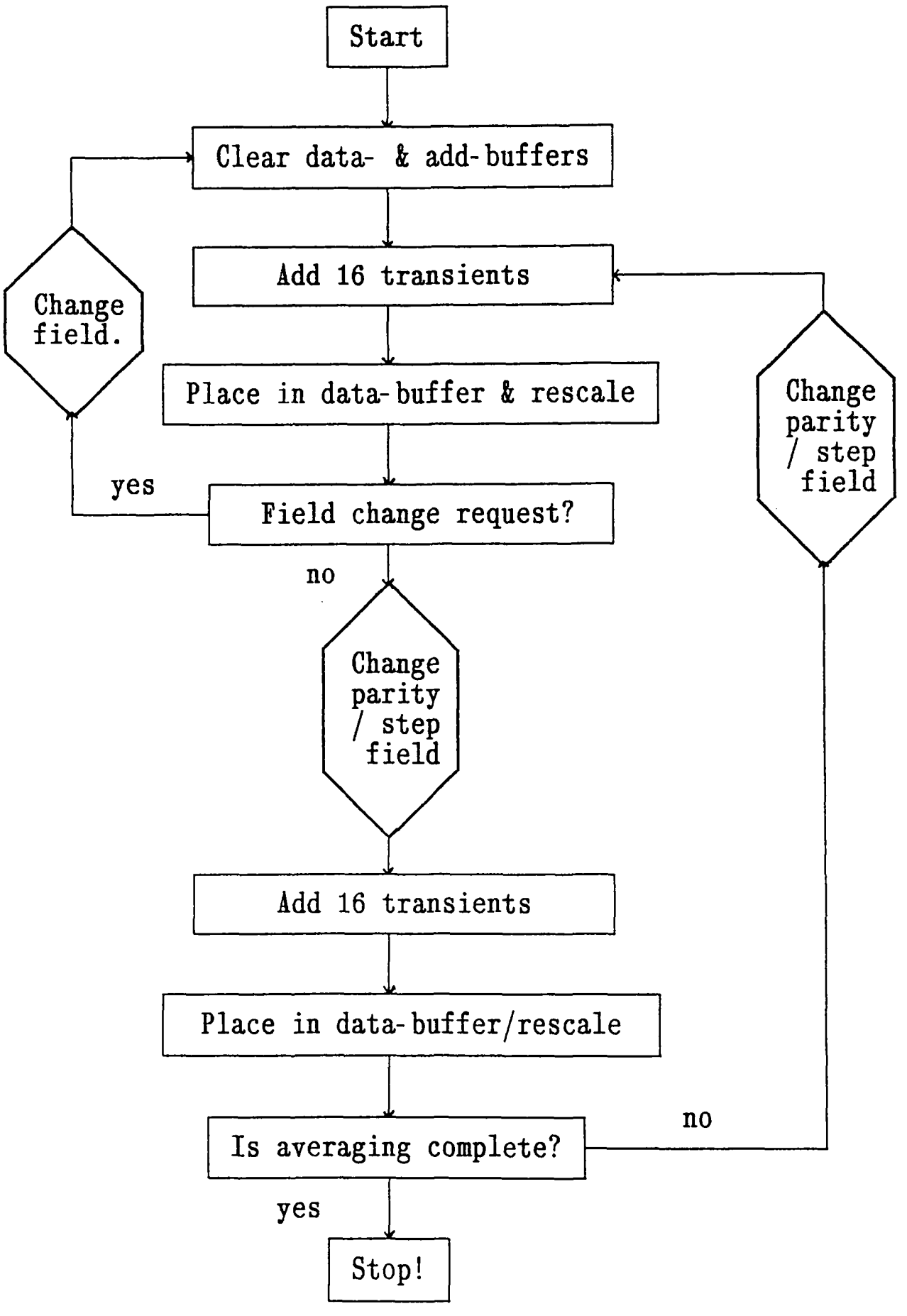

Mode II (field–swept spectrum)

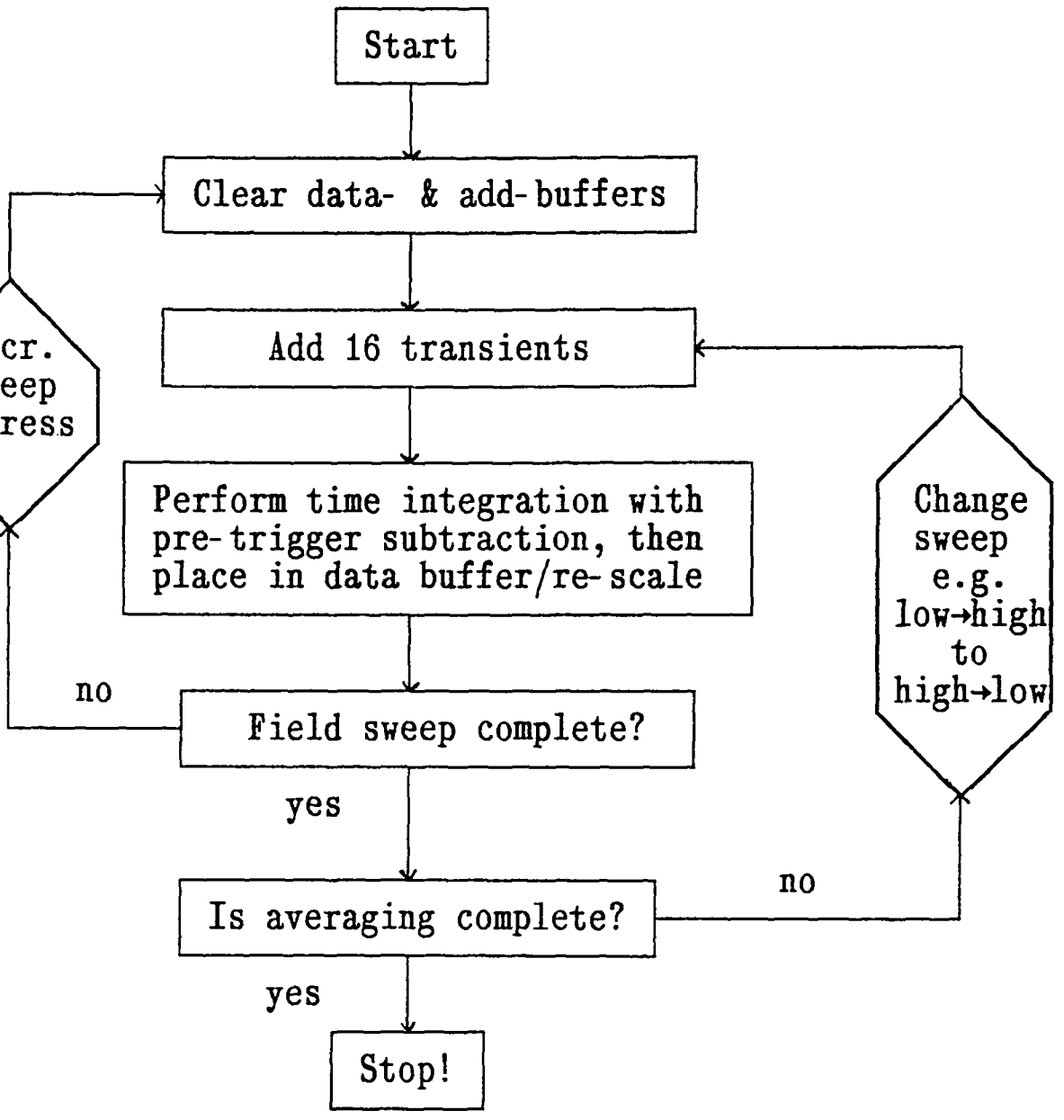

A second development is the insertion of a microwave attenuation switch into the microwave bridge, allowing the microwaves to be toggled on or off. This technique (MIcrowave Switched Time Integration) has been advanced as a means of determining $T_1$ and $\gamma$ [14] but problems with microwave stability have been encountered and, to date, no satisfactory experiments have been published, attractive though the technique is.

Over the last two years an earlier, purpose–built computer has been replaced in part by a Zenith PC–compatible, thereby vastly increasing ease of operation and flexibility. I could not leave this section without a word of gratitude to Paul Smith who has spent months writing and re–writing the software and dealing with the problems of interlacing and synchronization, as well as taking on the rôle of "computer hygenist" for the group. May his programs run and run... .

(3.3.3) Thoughts On the Final Spectra And Their Simulation

TIS lends itself to signal–averaging – a process that the foregoing discussion on spectrometer sensitivity would suggest was inevitable. We have three factors in our favour, one of which is the trivial observation that our experiment is pulse–correlated, with pre–trigger subtraction wheedling out all bar the most recently created radicals, and hence we are only observing radical signals over times at which populations of radicals are high. The second is that we may simply repeat the experiment many times (each field point is averaged sixteen times in each field sweep and the whole field sweep may be repeated any number of times). In this case, whilst the signal increases by a factor of n for n averages, the noise increases by a factor of $\sqrt{n}$: an overall signal enhancement of $\sqrt{n}$ is obtained.

Then we may choose a range of integration periods, the increase in signal being offset by a loss in time information but, in contrast to other methods, a definable loss giving a quantifiable spectrum still. For a summation of n time points an approximate improvement in signal–to–noise of between $\sqrt{n}$ and $\frac{1}{2}\sqrt{n}$ is expected over the maximum signal existing during the period of integration. Unlike box–car or spin–echo methods we may assess how crucial a knowledge of the time–content of each experiment is and adjust the sampling times to maximise signal accordingly.

One final and pertinent point is that all our spectra are digital so we can achieve exact correspondence between experimental and digitally simulated spectra. A discourse on how Mode II spectra are simulated is left to appendix 1.

## REFERENCES – CHAPTER 3


1 Poole C.P. "*e.s.r. – A Comprehensive Treatise On Experimental Technique*" (Pub. Wiley Interscience, 1983).

2 Atkins P.W., McLauchlan K.A., Simpson A.F. *Chem.Commun.* (1968) 4, 179.

3 Atkins P.W., McLauchlan K.A., Simpson A.F. *J.Phys.Suppl.E* (*Sci.Instrum.*). (1970) 3, 547.

4 Trifunac A.D., Norris J.R. *Chem.Phys.Lett.* (1978) 59, 140.

5 Trifunac A.D., Norris J.R. *J.Chem.Phys.* (1979) 71, 4380.

6 Terazima M., Yamauchi S., Hirota N. *J.Phys.Chem.* (1985) 89, 1220.

7 McLauchlan K.A., Stevens D.G. *Mol.Phys.* (1986) 57, 223.

8 Basu S., McLauchlan K.A., Sealy G.R. *Mol.Phys.* (1984) 52, 431.

9 Prisner T., Dobbert O., Dinse K.P., van Willigen H. *J.Am.Chem.Soc.* (1988) 110, 1622.

10 Basu S., McLauchlan K.A., Sealy G.R. *J.Phys.Suppl.E* (*Sci.Instrum.*). (1983) 16, 767.

11 Sealy G.R. *D.Phil.Thesis, Oxford* (1983) Chapter 6.

12 Bruker ER Series User Manual (1983).

13 McLauchlan K.A., Stevens D.G. *J.Chem.Soc. Faraday Trans.I.* (1987) 83, 29.

14 McLauchlan K.A., Sealy G.R. *Mol.Phys.* (1984) 52, 783.

# CHAPTER IV : THE BIRTH OF POLARIZATION

# THE BIRTH OF POLARIZATION

## (4.1.1) Introduction

This chapter addresses that matter central to all new work presented in this thesis: what is polarization, do we understand it fully and how can we use it as an investigative tool?

CIDEP was first observed when pulse radiolysis of methane generated hydrogen atoms in which the low–field resonance line appeared in emission [1], but this was a once–off experiment and it was only really when *n.m.r.* spectra of irradiated systems were found to show considerable deviations from equilibria [2,3] that theories could be advanced. Two have gained current acceptance and can account for the majority of observations of electron polarization. The Triplet Mechanism is a consequence of anisotropic spin state population during radical pair generation, and the Radical Pair Mechanism arises from the separation and re–encounter of pairs of radicals undergoing diffusion in solution (a sub–effect of diffusion of radical pairs, $ST_-$ mixing, requires only that the radicals separate). Much information has been accumulated, and these models and the predictions therefrom have been comprehensively examined and often arbitrarily applied. There are, however, several caveats that must be added: i) we do not yet have a single conclusive, quantitative test for TM though much qualitative evidence [4–6] rests in its favour; ii) there are cases where the TM cannot be invoked to explain qualitatively similar polarizations [7]; iii) certain aspects of RPM polarizations [7,8] are not fully understood or are wholly mystifying; iv) care must be taken in applying the CIDEP sign rules without consideration of kinetics, as is demonstrated in chapter 5. Despite these reservations CIDEP, if applied thoughtfully, will be shown to be a very enlightening phenomenon.

(4.2.1) The Triplet Mechanism

A process that generates polarization on formation of radicals, a polarization that is rapidly destroyed by relaxation, requires a very fast detection system to be observed, and it was thus ten years after the first RPM observation that the TM was conclusively established [10]. It is curious to note that the first mechanism proposed bore a resemblance to the TM, but was rejected initially in favour of explanations based on RPM–like processes [11], because of concerns over rates of reactions and magnitudes of perturbations acting on a rotating triplet. It was known, however, that photo–generated triplets were found to be very strongly polarised in glasses in which a degree of orientation is possible [12].

Rate constants and a reaction pathway for a photolytic reaction are displayed in Fig.(4.2.1). We shall look at each step in turn, to follow the generation and evolution of nascent polarization. The essential feature is that polarization is first produced in the molecular triplet sub–levels, so it is necessary to establish why a triplet, even in the absence of an external field, must have non–degenerate sub–levels.

(4.2.2) The Molecular Triplet State

The dipolar interaction between two electrons, separated by a distance vector $\underline{r}$ and assuming an isotropic g–value, is

$$\mathcal{H}_{dip} = (g\mu_B)^2.\left[\frac{\underline{S}_1.\underline{S}_2}{\underline{r}^3} - \frac{3(\underline{S}_1.\underline{r})(\underline{S}_2.\underline{r})}{\underline{r}^5}\right] \qquad (4.2.1)$$

The total spin, $\underline{S} = (S_{1x}+S_{2x})\underline{i} + (S_{1y}+S_{2y})\underline{j} + (S_{1z}+S_{2z})\underline{k}$, can be substituted into

Fig.(4.2.1)

A RADICAL–CREATING PHOTOLYTIC PATHWAY

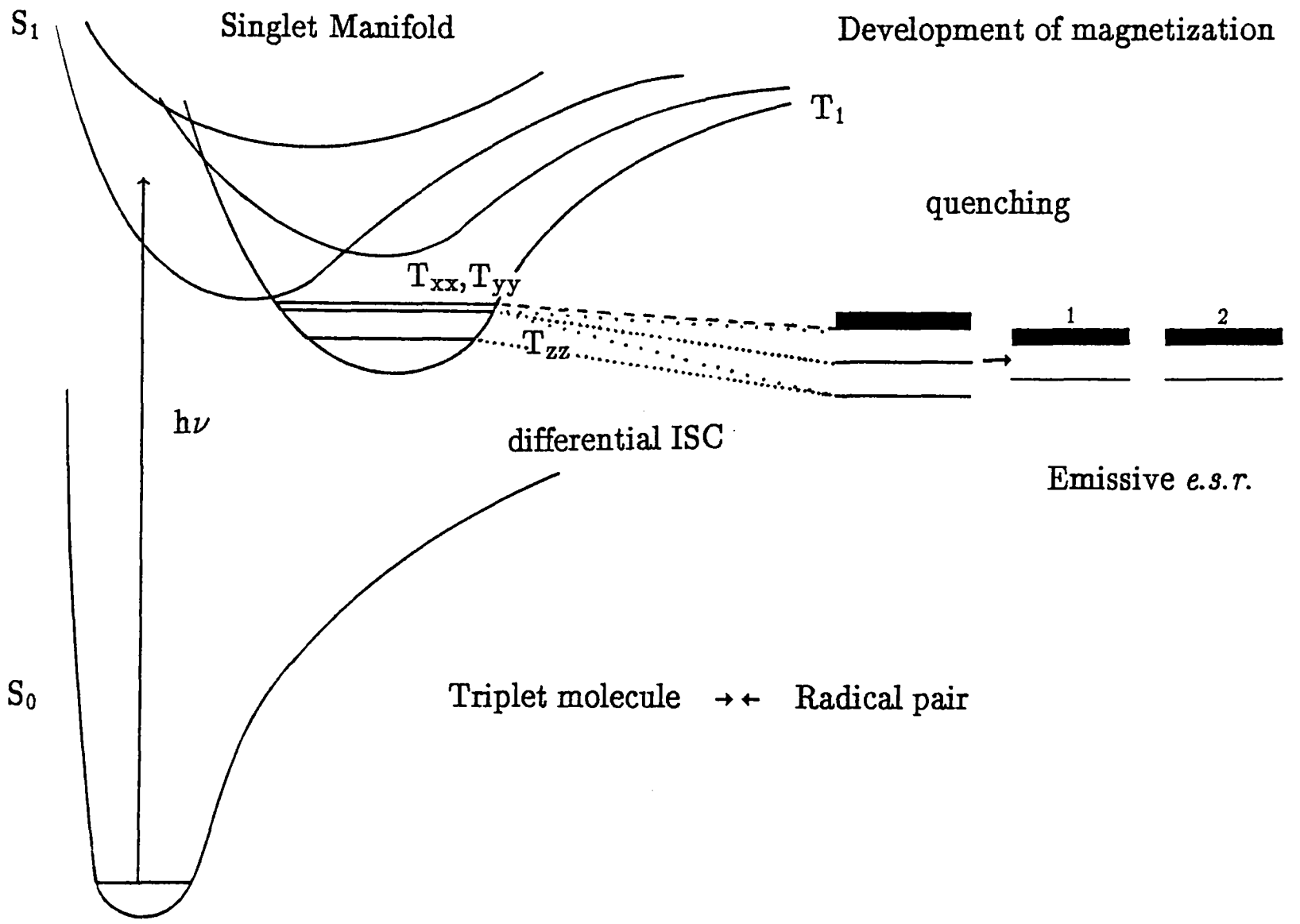


Typical rate constants for these processes are: molecular re–orientation $\leq 10^{-12}$s; Triplet relaxation rate, $^3T_1 \approx 10^{-9}$s; ISC rate $= 10^{-10} - 10^{-11}$s; quenching rate necessary to trap polarization $\geq 10^9 s^{-1}$; radical relaxation $^2T_1 \approx 10^{-6}$s.

(4.2.1) and the equation re–cast in tensor notation

$$\mathscr{H}_{dip} = \underline{S}.\underline{\underline{D}}.\underline{S} \qquad (4.2.2)$$

where $\underline{\underline{D}}$ is the zero–field splitting tensor [13] and comprises two types of term – the diagonal elements,

$$D_{ii} = (g^2\mu_B{}^2/2).\{\underline{r}_{12}{}^2 - 3\underline{i}_{12}{}^2\}/\underline{r}_{12}{}^5 \qquad (4.2.3)$$

and the off–diagonal elements

$$D_{\substack{ij \\ i\neq j}} = (g^2\mu_B{}^2/2).\{-3\underline{i}_{12}\underline{j}_{12}\}/\underline{r}_{12}{}^5 \qquad (4.2.4)$$

where i,j = x,y,z. By choosing a suitable set of axes [14] $\underline{\underline{D}}$ may be diagonalised (these axes are, in fact, the principal axes of the molecular point group) and (4.2.2) is then

$$\mathscr{H}_{dip} = -XS_x{}^2 - YS_y{}^2 - ZS_z{}^2 \qquad (4.2.5)$$

$\underline{\underline{D}}$ must be traceless as a dipolar interaction averages to zero over all orientations, so only the two parameters D and E are required to define its components exactly.

$$D = (X+Y)/2 - Z = -3Z/2\,; \quad E = (X-Y)/2 \qquad (4.2.6)$$

X, Y and Z are the eigenenergies of the triplet spin functions $T_i$

$$T_x = (1/\sqrt{2}).|\beta_1\beta_2 - \alpha_1\alpha_2\rangle$$
$$T_y = (i/\sqrt{2}).|\beta_1\beta_2 + \alpha_1\alpha_2\rangle \qquad (4.2.7)$$
$$T_z = (1/\sqrt{2}).|\alpha_1\beta_2 + \beta_1\alpha_2\rangle$$

and the usual properties of angular momentum apply – namely,

$$S_iT_i = 0\,; \quad S_iT_j = iT_k\,; \quad S_iT_k = -iT_j\ (i \neq j \neq k) \qquad (4.2.8)$$

Physically, the size of X, Y or Z depends on the distribution of electrons perpendicular to the spin axes x, y or z. If axes of symmetry exist for a triplet moiety in a molecule, then the squares of the spin functions, and hence the spin functions themselves, must be zero, as the energy of that moiety must remain invariant under a symmetry operation. We can see now why $\underline{\underline{D}}$ is diagonalised by these axes.

(4.2.3) Molecular Spin State Interconversion

Absorption of energy and subsequent excitation to a higher singlet state, followed by cascade down vibrational levels in the singlet manifold is rapid. From the lowest level in the excited singlet the chromophore may either be internally converted or fluoresce to return it to the ground state singlet, it may react with a neighbouring molecule, or it may inter–system cross to a triplet sublevel. This is a formally forbidden process but for most chromophores, especially if a hetero–atom is present, ISC may take place through the intervention of spin–orbit coupling [15]. It is allowed because no net angular momentum is created or destroyed. Rather, spin angular momentum is generated at the expense of an equal and opposite amount of orbital angular momentum. We may regard the effect as a trade–off between the internal degrees of freedom of the

molecule. This is illustrated in Fig.(4.2.2) for the propan–2–one molecule.

The spin–orbit Hamiltonian is approximated by

$$\mathscr{H}_{so} = \zeta\, \underline{l}.\underline{s} \approx \zeta(\underline{l}_1.\underline{s}_1+\underline{l}_2.\underline{s}_2) \qquad (4.2.9)$$

provided $\mathscr{H}_{so}$ is small compared to the zero–field splitting of the triplet. $\zeta$ is the spin–orbit coupling constant. (4.2.9) can be further decomposed into a combination of symmetric and anti–symmetric parts,

$$\mathscr{H}_{so} = (\zeta/2)\{(\underline{l}_1+\underline{l}_2)(\underline{s}_1+\underline{s}_2) + (\underline{l}_1-\underline{l}_2)(\underline{s}_1-\underline{s}_2)\} \qquad (4.2.10)$$

in which the first term can be viewed as removing the degeneracy of triplet and singlet levels as the second term mixes them together:

$$\langle S|\, \zeta(s_1-s_2)|\, T\rangle = \langle\, \alpha\beta-\beta\alpha|\, \zeta(s_1-s_2)|\, \alpha\beta+\beta\alpha\rangle = \zeta\langle\, \alpha\beta-\beta\alpha|\, \alpha\beta-\beta\alpha\rangle = \zeta$$

As an aside, the total angular momentum J is unchanged by $\mathscr{H}_{so}$ since $J^2$ commutes with $\mathscr{H}_{so}$. So do all the nuclear spin operators: the differential ISC is clearly hyperfine–independent.

As shown above, the $T_x$, $T_y$ and $T_z$ sub–levels may be described in terms of components along the axes of symmetry of a molecule. They are conveniently defined by the representations of the molecular point group. While we may have difficulty calculating a magnitude for $\zeta$ it is a simple matter to determine whether it will be zero between the singlet and any one of $T_x$, $T_y$, $T_z$ sub–levels; the quantity $\langle S|\, \mathscr{H}_{so}|\, T_q\rangle$ is a physical property of the molecule and must therefore be invariant under all the symmetry operations of that molecule, as was the case for the dipolar splitting: $\langle S|\, \mathscr{H}_{so}|\, T_q\rangle$ must possess $A_1$ symmetry. To determine whether it has or not we

Fig (4.2.2)

Photophysics Of The 2–propanone Molecule.

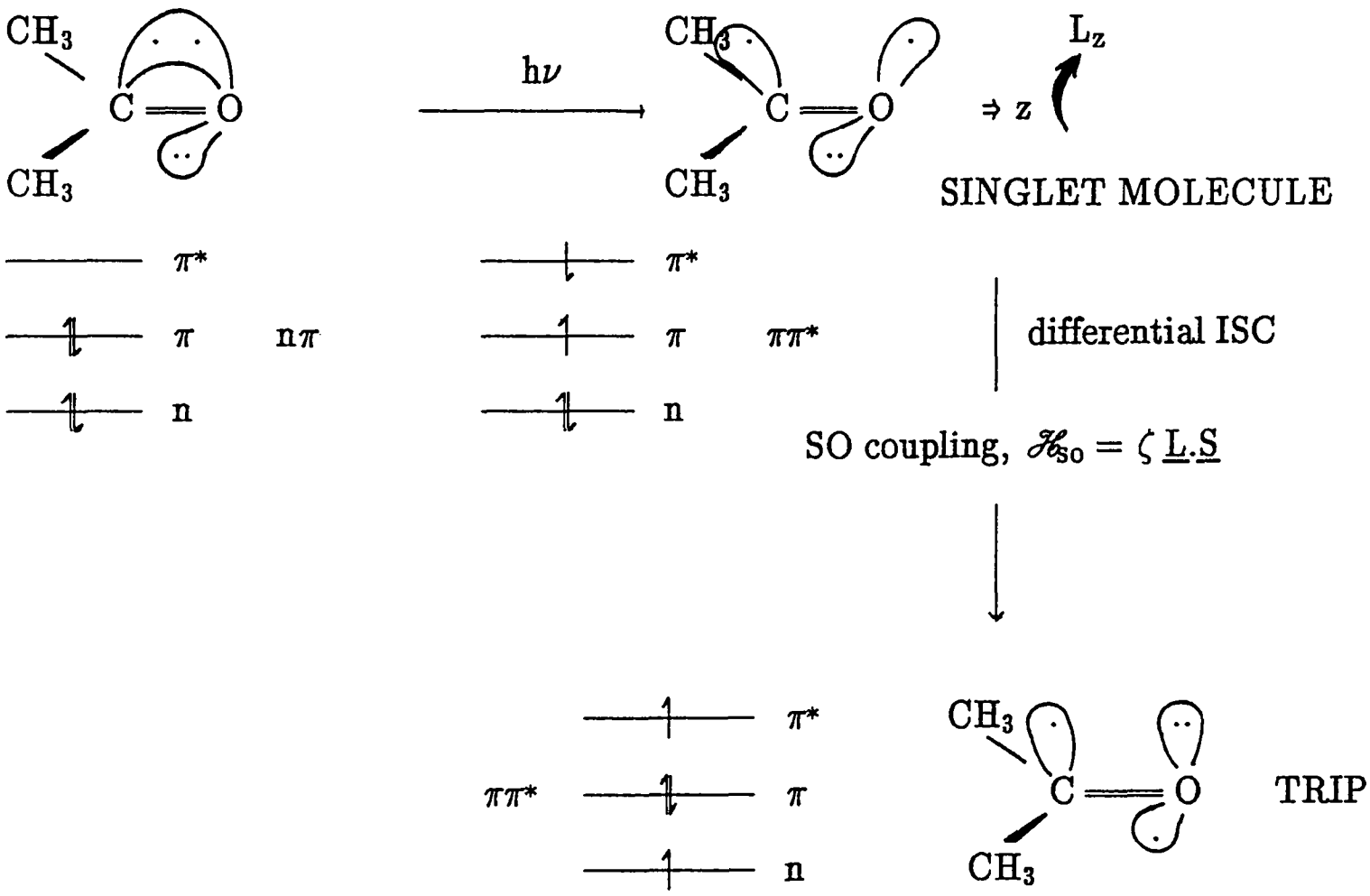


Illustration of the effect of spin–orbit coupling upon the ISC step from $^1[\pi\pi^*]$ to $^3[n\pi^*]$. The corresponding electron spin–operator will determine what molecular spin state will be populated.

consider all the representations of the spin and orbital functions.

$$\{\Gamma_{orb}(S) \otimes \Gamma_{spin}(S)\} \otimes \Gamma_{so} \otimes \{\Gamma_{orb}(T_q) \otimes \Gamma_{spin}(T_q)\} \equiv A_1 \qquad (4.2.11)$$

This may be simplified, since $\mathscr{H}_{so}$ is a scalar and transforms as $A_1$ under any point group, as does the singlet spin function (it is totally symmetric). (4.2.11) reduces to

$$\Gamma_{orb}(S) \otimes \Gamma_{orb}(T_q) \otimes \Gamma_{so}(T_q) \equiv A_1 \text{ or}$$

$$\Gamma_{orb}(T_q) \otimes \Gamma_{so}(T_q) \supset \Gamma_{orb}(S) \qquad (4.2.12)$$

To return to propan–2–one, which possesses $C_{2v}$ symmetry, we could propose that, according to (4.2.12), the $T_z$ state would be filled and that, as D is inferred to be positive from calculations on similar molecules, the radical pair created from the triplet would have an excess of $\beta$ spin. That is, to jump a couple of steps, we should observe an absorptive TM. Alas, things are not that simple for, to anticipate some of the problems we shall encounter, the reaction rate of propan–2–one with quenchers that give an absorptive polarization is far too slow to generate TM [7]. In addition, considerable out–of–plane distortion is expected in the excited states [15,16], complicating the designation of symmetry point groups and representations of spin and orbital functions that result.

Instead we examine a nitrogen heterocyclic molecule to illustrate the creation of polarization, in Fig.(4.2.3). As with the carbonyl group we find that it is the $T_z$ state that is populated, according to (4.2.12) and a product table for a $C_{2v}$ molecule, since

$$B_1 \otimes B_2 \otimes A_2 = A_1$$

Fig (4.2.3)

A Jablonski Diagram For The Relevant States Of Quinoxaline

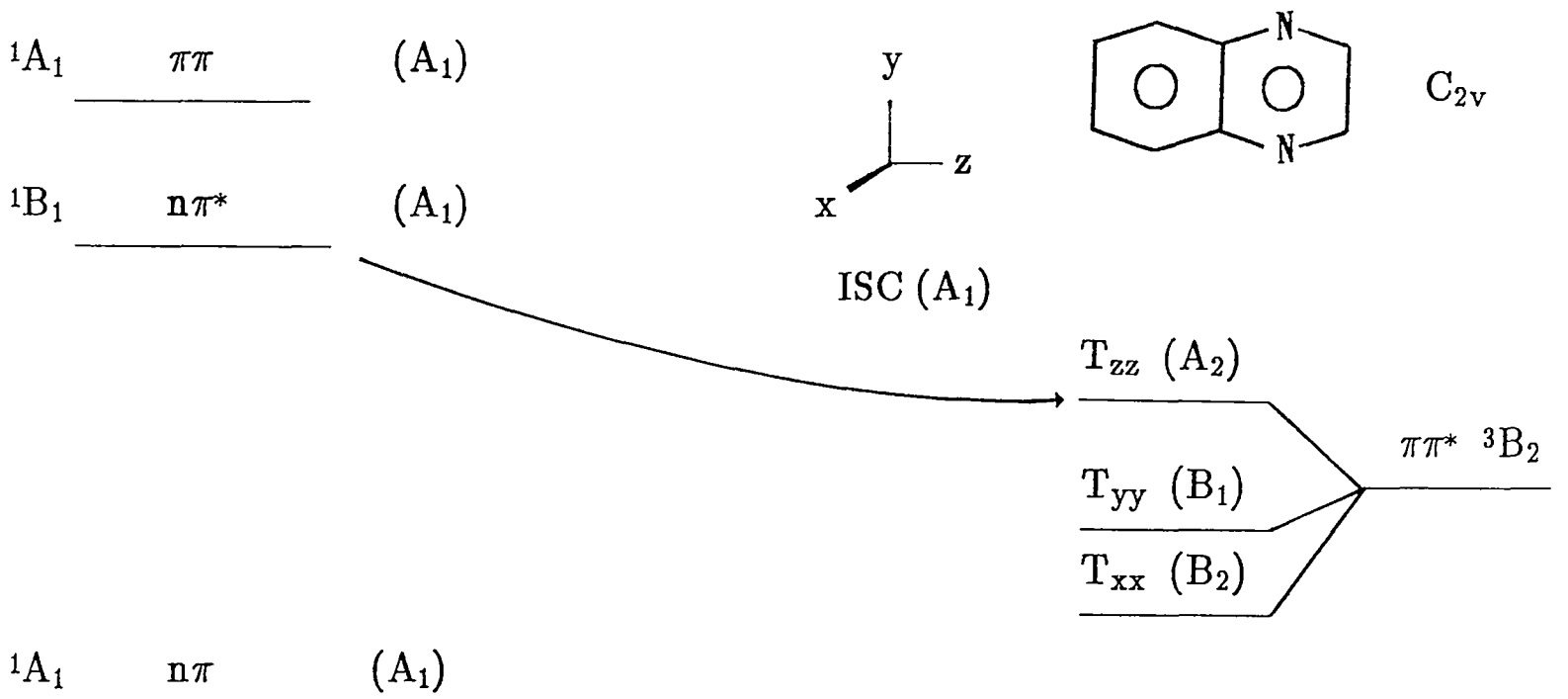


Orbital symmetries are represented by superscripts. Spin symmetries are placed in parentheses.

CHARACTER TABLE

| $C_{2v}$ | E | $C_2$ | $\sigma_v^{xz}$ | $\sigma_v^{yz}$ | correspondence |
|---|---|---|---|---|---|
| $A_1$ | 1 | 1 | 1 | 1 | z |
| $A_2$ | 1 | 1 | -1 | -1 | $R_z$ |
| $B_1$ | 1 | -1 | 1 | -1 | x, $R_y$ |
| $B_2$ | 1 | -1 | -1 | 1 | y, $R_x$ |

PRODUCT GROUP

| ⊗ | $A_1$ | $A_2$ | $B_1$ | $B_2$ |
|---|---|---|---|---|
| $A_1$ | $A_1$ | $A_2$ | $B_1$ | $B_2$ |
| $A_2$ | $A_2$ | $A_1$ | $B_2$ | $B_1$ |
| $B_1$ | $B_1$ | $B_2$ | $A_1$ | $A_2$ |
| $B_2$ | $B_2$ | $B_1$ | $A_2$ | $A_1$ |

It is found that the important symmetry property of a molecule is the symmetry of the chromophore so that, although methylphenyl ketone does not possess $C_{2v}$ symmetry, the carbonyl function does and the polarization observed is correspondingly emissive. When dealing with nitrogen heterocycles the whole molecule is the chromophore and symmetry requirements are more stringent. In the solid state the local environment may modify the molecular symmetry, as may vibronic coupling in any phase, but these effects do not change the essential condition that equation (4.2.12) must be satisfied for spin and orbital functions.

One of the great successes of TM CIDEP has been in confirming the level–ordering of triplet levels and sub–levels in the liquid phase. In particular it has been employed in a case–study on pyrazine and its methyl derivatives [17], in demonstrating triplet reactivity [18], and in confirming that when ISC is forbidden then singlet reactivity dominates [19,6]. A system in which no TM is observed is the 2,3–diazanaphthalene triplet, in which $n\pi^*$ and $\pi\pi^*$ states are so close together as to be poorly defined in terms of orbital and spin symmetries, so the ISC populates all levels equally.

### (4.2.4) From The Molecular To The Laboratory Frame

A molecule experiencing differential ISC into its triplet sub–levels is polarized in its own frame of reference but in a non–oriented system (e.g. isotropic excitation in solution) this is still only a virtual polarization. Some degree of orientation of the spins, without tearing them away from the molecular axes to which they are coupled and within which they are polarized, must be developed. Instinctively this will be that point at which the interaction of the external field is comparable to the zero–field splitting, which we simplify to just D by assuming an axially symmetric molecule. Competing against this development of laboratory–frame polarization will be re–orientation of the

triplet and relaxation (rapid because of the dipolar interaction itself). The problem was first treated for a static array of triplets [20] and extended to include tumbling in isotropic solution [21].

In a magnetic field of 300mTesla the Zeeman interaction is of the same magnitude as the dipolar splitting in a large number of organic triplets (in frequency units this is about $5 \times 10^{10}s^{-1}$), and within the range of rotational correlation times in solution. The magnetic field states in such a field do not correspond either to the molecular spin states $|T_Q\rangle$ as stated in equation (4.2.7), nor with the high–field states given by

$$\begin{aligned} |T_+\rangle &= |\alpha_1\alpha_2\rangle \\ |T_0\rangle &= (1/\sqrt{2})|\alpha_1\beta_2 + \alpha_2\beta_1\rangle \\ |T_-\rangle &= |\beta_1\beta_2\rangle \end{aligned} \qquad (4.2.13)$$

but with a complex admixture of the two. As measurements are made on radicals in a high–field limit it is usual to represent the intermediate state with respect to a basis set from equations (4.2.13), transformed into the axes of the molecular spin functions. The Zeeman interaction can then be considered as a perturbation on the molecular frame states. Writing molecular states as combinations of the high field states, $|T_\perp^{\pm}\rangle = (1/\sqrt{2})(|T_x\rangle \pm |T_y\rangle)$,

$$\begin{aligned} |T_z\rangle &= |T_=\rangle = (1/\sqrt{2})\{\sin\Theta|1\rangle + \sqrt{2}\cos\Theta|0\rangle - \sin\Theta|-1\rangle\} \\ |T_\perp{}^+\rangle &= \tfrac{1}{2}e^{i\phi}\{(1+\cos\Theta)|1\rangle - \sqrt{2}\sin\Theta|0\rangle + (1-\cos\Theta)|-1\rangle\} \\ |T_\perp{}^-\rangle &= \tfrac{1}{2}e^{i\phi}\{(1-\cos\Theta)|1\rangle - \sqrt{2}\sin\Theta|0\rangle + (1+\cos\Theta)|-1\rangle\} \end{aligned} \qquad (4.2.14)$$

where $\Theta$ represents that angle between the field axis and the principal axis of the $\underline{\underline{D}}$

Fig.(4.2.4)

Transfer Of Polarization From Molecular To Laboratory Frame

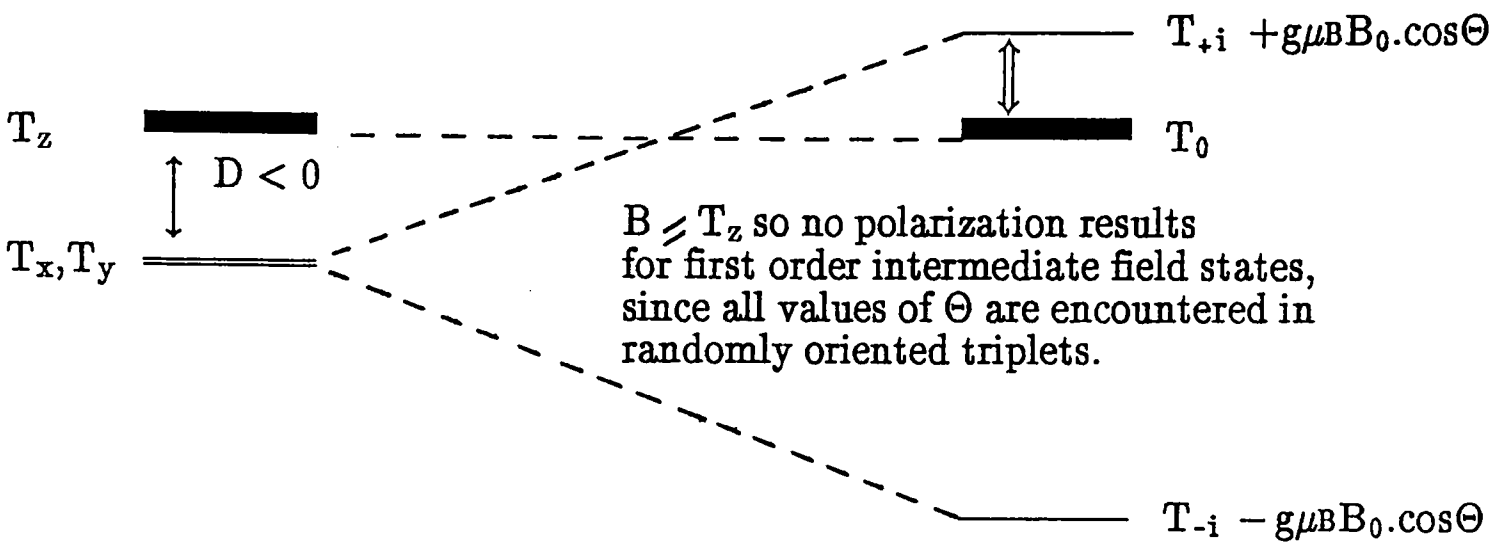


To second order, however, those states which are closest in energy will be mixed most strongly (represented by the double–headed arrow), selectively populating those states for which the product of spin and orientation give a net emission.

tensor, and $\phi$ is that angle between field and minor axes. It is clear that to first order when the Zeeman perturbation is applied $|T_{=}\rangle$ does not acquire an excess of either $\alpha$ or $\beta$ spin and $|T_{\perp}^{\pm}\rangle$ states develop an equal and opposite amount of $\alpha$ and $\beta$ spin. It is only in the second–order effect, in which $|T_{\perp}^{\pm}\rangle$ mix to a different extent with $|T_{=}\rangle$ that laboratory frame polarization is developed, by the mixing in of $\alpha$ spin from $|T_{\perp}^{+}\rangle$ to $|T_{=}\rangle$. This occurs more readily from $|T_{\perp}^{+}\rangle$ as these two levels lie closer in energy for $-90^{o} < \Theta < +90^{o}$ as shown. The corollary of this is that in the low or high field limits there is little relative difference in energy between all these states and so all states would be equally mixed by the second–order process; this is the reason why the D and Zeeman splitting need to be comparable for TM to be maximised.

(4.2.5) Preservation Of Polarization Into The Radical Pair

Before this polarization can be observed the triplet must react to form a radical pair. To date no triplet *e.s.r.* spectrum has been recorded in the liquid state, both reaction and relaxation rates being too fast. The essential requirement is that reaction rate must compete with relaxation rates (typically $< 10^{-9}$s [22]) and proton abstraction, electron transfer and bond scission are therefore liable to dominate the quenching reactions under consideration. If reaction is too slow then the polarized triplet will relax through to a thermally equilibrated triplet, though this can still give a small absorptive polarization to the doublet radicals of $\approx 1.3P_{eq}$. This has been invoked to account for the equilibrium polarization observed in aliphatic carbonyl–derived radicals, though the observed magnitude of polarization would appear to be too large [4].

On the other hand, if quenching is too fast then the lifetime of a triplet state is so short as to introduce uncertainty into its energy. Specifically, if the lifetime of the triplet, $(1/k_q)$ where $k_q$ is the quenching rate, is smaller than $\omega_0$ where $\omega_0 = g\mu_B B_0/h$,

then polarization will be destroyed. Similarly, the rotational correlation time, $\tau_r$ (the energies of the intermediate field states are affected by molecular orientation) must be less than $\omega_0^{-1}$. This dependence of polarization upon these two parameters has been dealt with quantitatively [21] and is demonstrated in Fig.(4.2.5).

We now turn to the results of the full analysis [21,23]. Introducing the spin density matrix, $\rho(t)$ the equation of motion may be written in terms of a static Zeeman interaction, $\mathscr{H}_0$, and an orientation–dependent dipolar interaction, $\mathscr{H}_{dip}(\Omega)$.

$$\frac{\partial\rho(t)}{\partial t} = (i/\hbar)[\rho(t),\ \mathscr{H}_0 + \mathscr{H}_{dip}(\Omega)] \qquad (4.2.15)$$

An anisotropic ISC from the excited singlet state may be introduced as a formation function, $\underline{k}P_s$ where $P_s$ is the singlet population and $\underline{k}$ is a diagonal matrix in the molecular frame whose elements contain the respective sub–level population rates. A "sink", $-k_r$, is also included to account for the disappearance of triplets by reaction.

$$\frac{\partial\rho(t)^T}{\partial t} = (i/\hbar)[\rho^T(t),\ \mathscr{H}_0+\mathscr{H}_{dip}(\Omega)] + \underline{\underline{k}}P_s(\Omega,t) - k_r\rho^T(t) \qquad (4.2.16)$$

The polarization effectively frozen, on the triplet timescale, into the doublet radicals is

$$Pol_{TM} = k_r.\int_0^\infty (\rho^T{}_{t\text{-}t\text{-}} - \rho^T{}_{t_+t_+})dt \qquad (4.2.17)$$

This results in a complex expression that can be simplified if $k_r \ll \tau_r^{-1}$ and $D \ll (\omega_z^2 + \tau_r^2)$, in which case polarization becomes

Fig.(4.2.5)

The dependence of polarization transferred to radicals upon quenching rate, $k_q$, and rotational correlation time $\tau_r$.

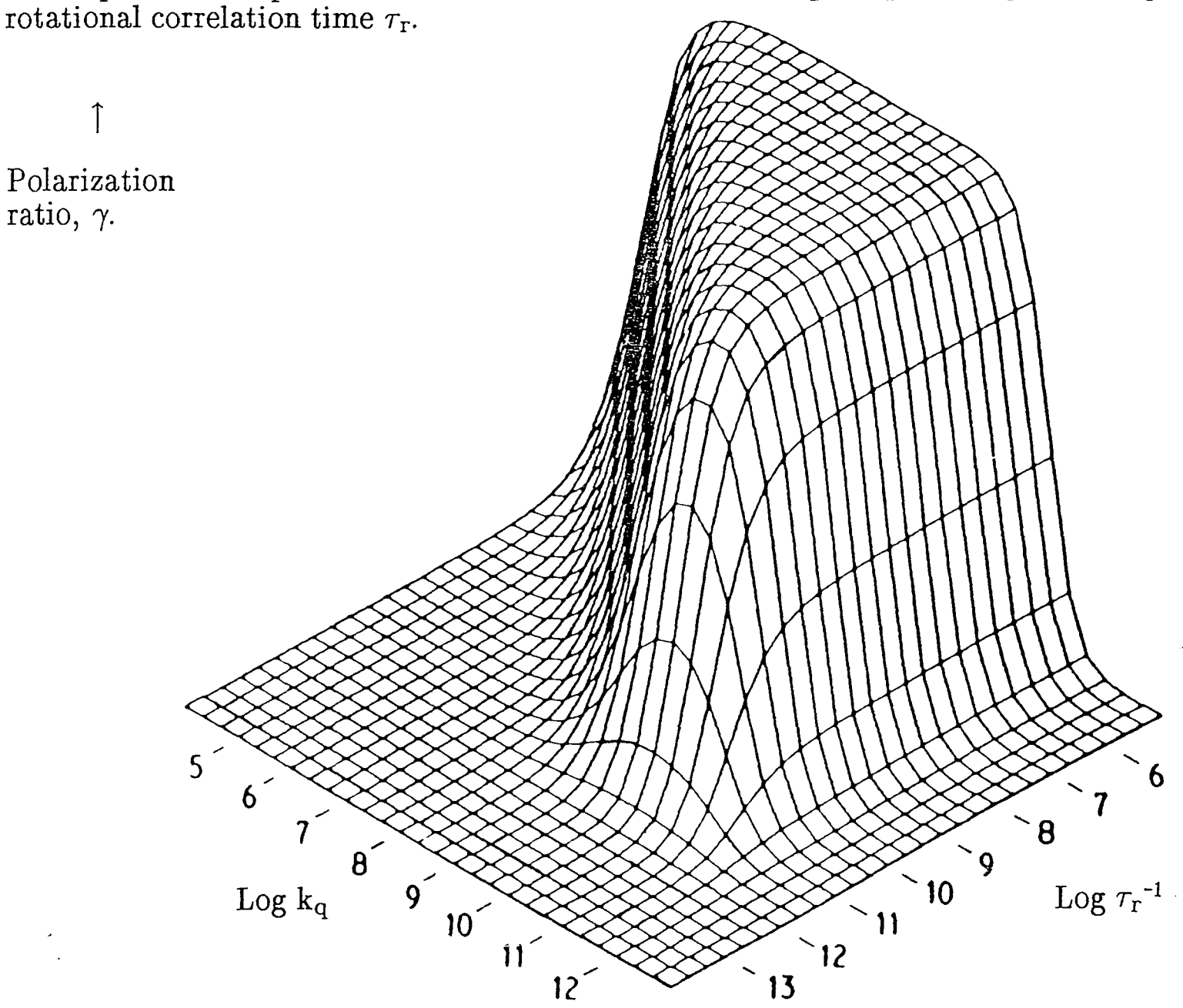


This has been calculated for an axially symmetric molecule (E = 0); D = 100mT, $\omega_e = 6 \times 10^{10} s^{-1}$. Population is initially entirely in the $T_z$ spin sub–level.

$$Pol_{TM} = (P^T k_r + P_{eq}.{}^3T_1^{-1})/(k_r + {}^3T_1^{-1}) \qquad (4.2.18)$$

where $P^T$, the triplet polarization, is given by

$$P^T = -\frac{4 D k g \mu_B B_0}{15 h}.\left[\frac{4}{4\omega_0^2 + (k_t+\tau_r)^2} + \frac{1}{\omega_0^2 + (k_t+\tau_r)^2}\right]$$

$P_{eq}$ refers to the triplet equilibrium polarization, and the other terms are

$$k = \tfrac{1}{2}(k_{xx} + k_{yy}) - k_{zz}$$

$$D = \tfrac{1}{2}(D_{xx} + D_{yy}) - D_{zz}$$

Equation (4.2.18) predicts a maximum polarization ratio, $\gamma$, of about 250 for optimum values of D, $\omega_0$, $k_r$ and $\tau_r^{-1}$, a realistic value of ${}^3T_1$ and for a perfectly anisotropic ISC step.

(4.2.6) A Few Thoughts

A molecule has a probability of excitation by an electric field of strength E that is proportional to $(\underline{\mu}.\underline{E})^2$ if $\underline{\mu}$ is its transition dipole moment. If plane–polarized light is used to excite a molecule and ISC occurs faster than molecular re–orientation then the polarization given in equation (4.2.17) will be a function of the angle of the plane of polarization to the magnetic field [24], with a predicted maximum variation of polarization with orientation of this plane of up to 10% in the liquid phase. Workers have claimed to observe this effect [25,26] but it is likely, considering the signal–to–noise ratios achieved, that what they were observing was a spurious effect. It has since been conclusively proved that even in species exhibiting strong TM no

discernible change in signal arose as a result of changing the orientation of the plane of polarized exciting radiation [27].

This leaves us with no quantifiable test that definitely indicates that the Triplet Mechanism is operative in a system, since direct measurements of $\gamma$ are, at best, approximate. What we do have, however, is a large body of corroborative evidence [4–6,17–19] in terms of the sign of – or absence of – net polarization, and the observation that both components of the radical pair produced from an excited triplet are identically polarized, thereby ruling out any variant on the accepted Radical Pair Mechanism [28,29]. A correspondence between $\gamma$ and $k_q$ has been shown for a limited range of quenching rates, too [30]. Encouraged by this, the optimistic have applied the TM to calculating $^3T_1$ in solution [31] and to predicting the sign of the D splitting of triplets in the liquid phase [32] with wholly believable results.

(4.3.1) The Radical Pair Mechanism

In our flash–photolysis experiments we always observe the consequences of interaction between radicals that have been generated together. We shall also observe interaction between pairs that encounter each other during free diffusion. Interaction here may mean reaction, rephasing of randomly oriented spins into combined wavefunctions or modification of relative diffusion. Let us first assume that the interactions of spins with their surroundings are random processes. After all, these are just the relaxation phenomena dealt with in chapter 2. Putting the cart well before the horse, a scheme whereby polarization may be generated by these pairwise encounters is given in Fig.(4.3.1); it will be clarified later. We should also remind ourselves that we define polarization as an ensemble phenomenon.

There are two possible initial states that describe the radical pair: it may be

Fig.(4.3.1)

THE LIFE CYCLE OF A RADICAL PAIR

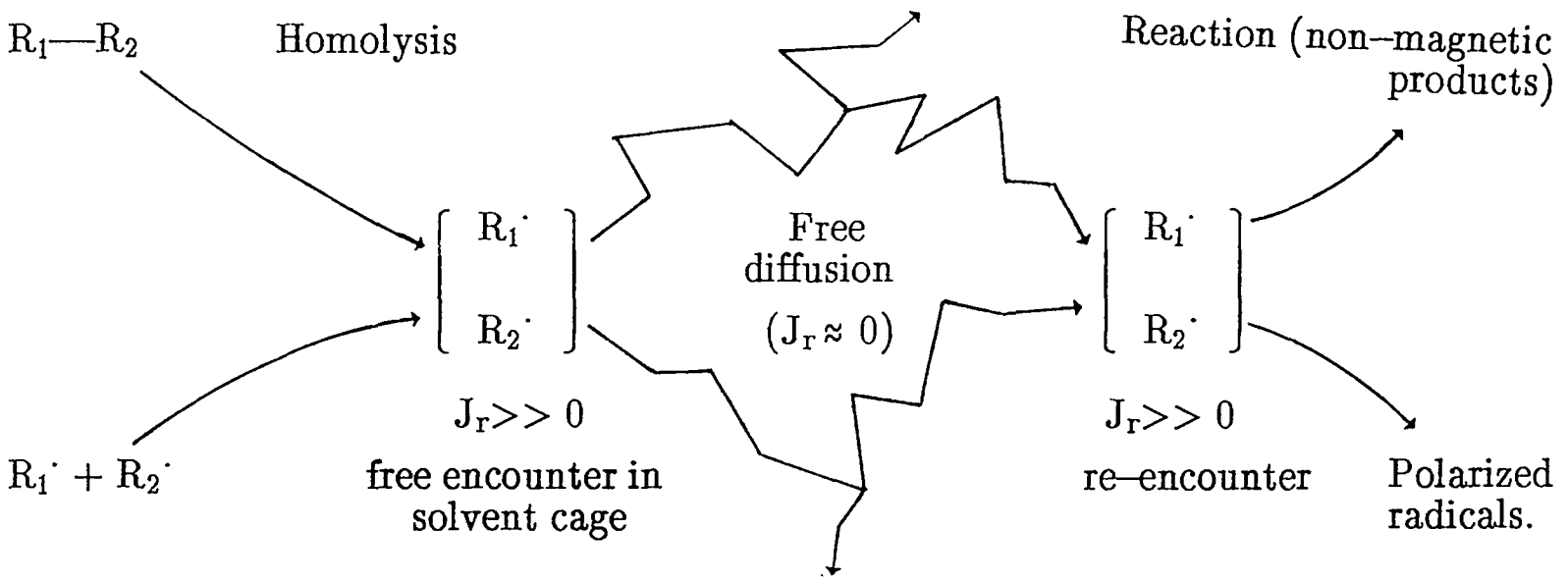


Mean time between diffusive jumps $\tau_d \approx 10^{-11}$s. Approximately 31% of radicals re–encounter.

created via reaction of either an excited singlet or triplet molecule (referred to as geminate or G–pairs); it may arise as the result of chance encounters in which one spin state, usually but not always the singlet state [33], reacts, leaving the remainder of radical pairs to separate (referred to as free–encounter or F–pairs). If this is indeed the origin of the RPM then it should be far more common than the TM which required such strict pre–conditions.

The first theories [34,35] put forward were concerned with the nuclear spin analogue CIDNP and were very basic models. They showed how, with nuclear spin–dependent mixing of singlet and triplet states from an initially defined electron spin state, an excess of $\alpha$ or $\beta$ nuclear spins would accrue in the products of re–encounter (cage) or scavenging (escape) reactions, if either of the two reactions was spin–selective. CIDEP is more subtle as it requires the gentle re–phasing of spins upon re–encounter, and it did not receive a reasonable treatment until a more complete CIDNP model had been developed [36,37]. This did, indeed, propose the cycle of creation/encounter when the exchange interaction is large, followed by free diffusion and then a re–encounter at a later time. The radicals emerging from this sequence were electron spin–polarized.

Any pair of radicals separating from close proximity to each other (defined as that period for which the exchange interaction $J_r \gg kT$) will either be in a triplet or a singlet state. As they separate the exchange interaction decreases through a region where, in a magnetic field, the S and $T_-$ states become degenerate and then, when $J_r \approx 0$, the S and $T_0$ states are degenerate. For most solutions of normal viscosity (and this itself is a valid and worthwhile finding of CIDEP) the region for which S and $T_-$ states are close together is such that radicals pass through it very fast[1]. As a consequence the weak

---

[1] When $\underline{r}$ is one to two Van der Waals diameters $J_r \approx g\mu_B B_0$. Three terms could cause $ST_-$ mixing: spin–rotation, spin–orbit coupling – very small for a triplet at this

Fig.(4.3.2)

Variation In Energy Between Triplet And Singlet Levels With Separation, r.

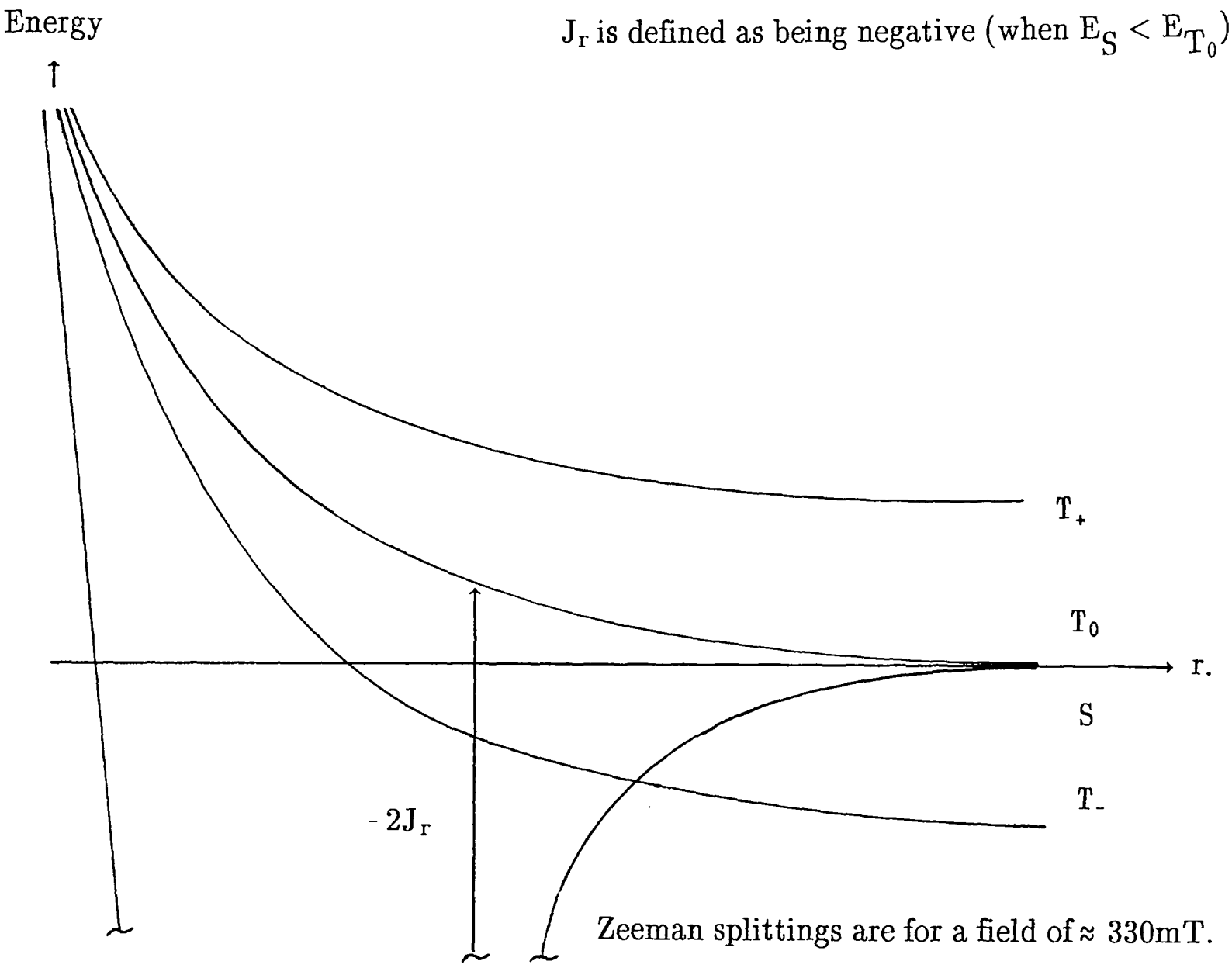

perturbations that could mix these states cannot normally operate in solutions of low to medium viscosity, though cases where they can will be discussed later. We are left, then, with a two–level problem, involving just S and $T_0$ states.

(4.3.2) The Radical Pair

A convenient description of the behaviour of an ensemble of electron spins is the density matrix. For our purposes it will include just the two states

$$|T_0\rangle = (1/\sqrt{2})|\alpha\beta + \beta\alpha\rangle \; ; \quad |S\rangle = (1/\sqrt{2})|\alpha\beta - \beta\alpha\rangle \qquad (4.3.1)$$

The complete description of our wave function is

$$\Psi(t) = C_s(t)|S\rangle + C_t(t)|T_0\rangle \qquad (4.3.2)$$

and the density matrix is built up from the time–dependent coefficients

$$\underline{\underline{\rho}}(t) = \begin{pmatrix} \rho_{ss} & \rho_{st} \\ \rho_{ts} & \rho_{tt} \end{pmatrix} = \begin{pmatrix} C_sC_s^* & C_sC_t^* \\ C_tC_s^* & C_tC_t^* \end{pmatrix} \qquad (4.3.3)$$

These equations assume that the nuclear spin states do not change over the timescale of observation. The Hamiltonian for this system is

---

separation – and the hyperfine interaction [39]. Initially, we ignore spin–rotation (see chapter 7) and take a typical hyperfine coupling constant of $a_i = 2 \times 10^{-3}$ Tesla. To induce an $ST_-$ mixing greater than $P_{eq}$ the residence time in the region of degenerate S and $T_-$ states must be greater than $10^{-9}$s. For solutions of low viscosity the residence time is around $10^{-11}$s.

$$\mathscr{H}_{rp} = -J_r(2\underline{S}_1.\underline{S}_2+\tfrac{1}{2}) + \mu_B(g_1\underline{S}_1+g_2\underline{S}_2).B_0 + \sum_n a_{1n}\underline{I}_n.\underline{S}_1 + \sum_m a_{1m}\underline{I}_m.\underline{S}_2 \qquad (4.3.4)$$

where the subscripts $_m$ and $_n$ refer to nuclear spin states, and $_1$ and $_2$ refer to the two radicals that comprise the pair.

Since that point for which exchange and hyperfine terms are of comparable size is very narrow in normal solution, we do not consider the combined action of Zeeman and exchange terms but instead divide the spin evolution into two regions that are separated in time – called the Exchange Impulse Model. The period between separation and re–encounter is typically very much greater than $\tau_c$ [38] so the isotropic g–values may be used in this model.

Setting $\hbar = 1$ so that all energies are expressed in frequency units, the evolution of the spin system is described by [40]

$$i\frac{\partial\rho}{\partial t}(t) = [\mathscr{H}_{rp}\,,\,\rho(t)] \qquad (4.3.5)$$

where $\mathscr{H}_{rp} = \begin{pmatrix} J_r & Q_{ab} \\ Q_{ab} & -J_r \end{pmatrix}$ and $Q_{ab} = \frac{1}{2}\mu_B B_0 \Delta g + \frac{1}{2}\sum_n a_{1n}M_{1n} - \frac{1}{2}\sum_m a_{2m}M_{2m}$.

Expanding (4.3.5) gives us four terms:

• $(\rho_{ss} + \rho_{tt})$ is the total number of spins in a system and will remain constant in the absence of reaction. This disappears when the time derivative in equation (4.3.5) is evaluated.

• $(\rho_{ss} - \rho_{tt})$ is that difference in singlet and triplet populations originating from the first encounter of spin pairs and is therefore a real physical property of the system.

Fig.(4.3.3)

A Depiction Of The Effect Of Differential Precession Of Spins Upon The Wavefunction.

$B_0$

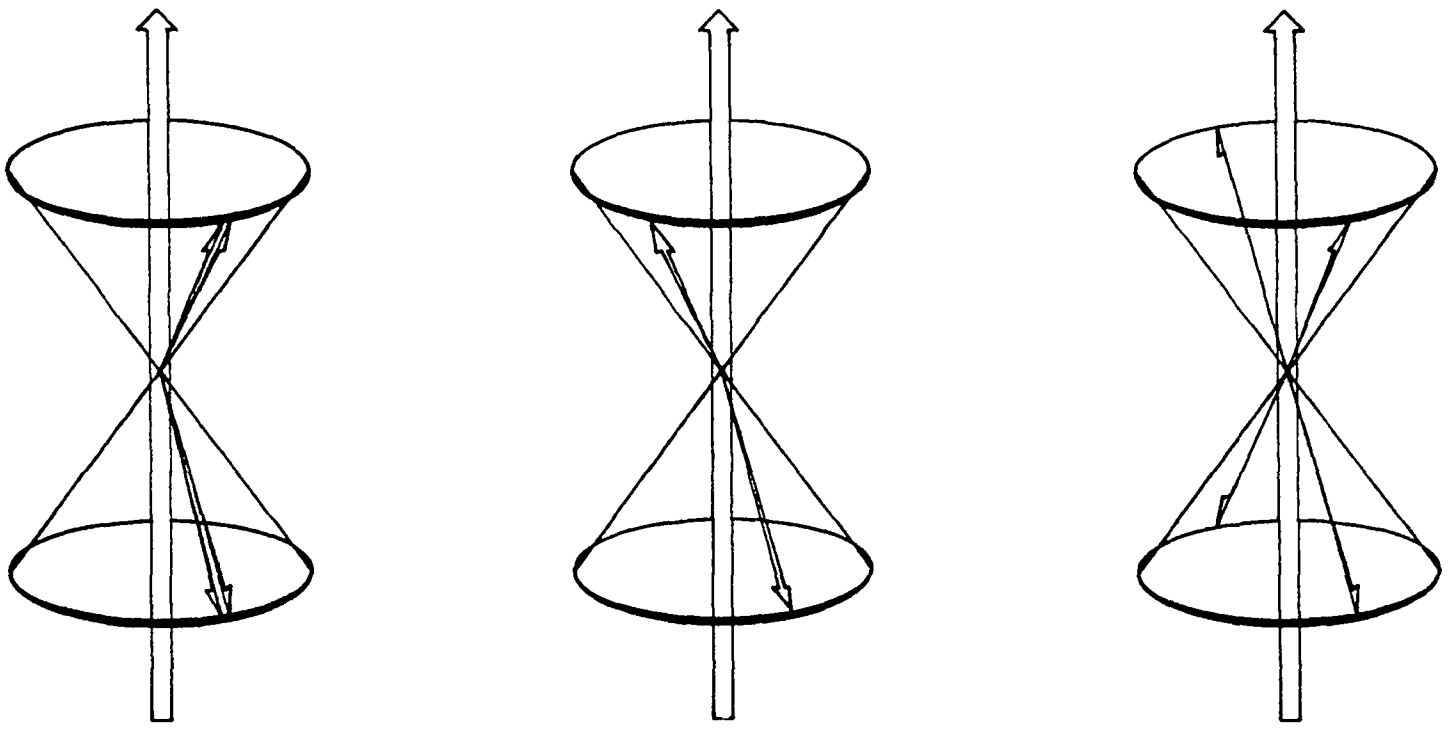

$|T_0\rangle = (1/\sqrt{2})(\alpha\beta + \beta\alpha)$ virtual state $|S\rangle = (1/\sqrt{2})(\alpha\beta - \beta\alpha)$

$J_r \gg kT$ $J_r \approx 0$ $J_r \gg kT$

$t = 0 \longrightarrow t = \pi/(2|Q_{ab}|)$

where $Q_{ab}$ is the difference in Zeeman and hyperfine energies between the two radicals. The effect of strong exchange is to re–phase spins, destroying in the process any off–diagonal terms of the density matrix (phase angles between spins). This is shown below.

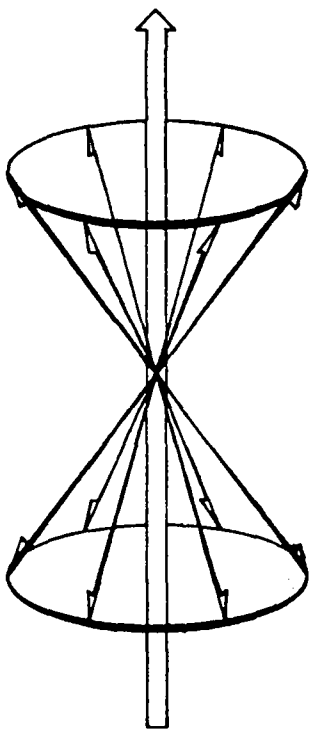

• $(\rho_{ts} - \rho_{st}) = 2\,\Im(\rho_{ts})$ represents the phase angle between the two initially correlated spins and it is caused by the differential precession that $Q_{ab}$ induces.

• $(\rho_{ts} + \rho_{st}) = 2\Re(\rho_{ts})$ is a measure of the extent to which the exchange interaction re–phases the spins upon radical re–encounter. In this step more $\alpha$ spin accumulates on one radical and more $\beta$ spin is collected upon the other. Put crudely, the exchange interaction separates the mixed state into a combination of $|\alpha\beta + \beta\alpha\rangle$ and $|\alpha\beta - \beta\alpha\rangle$ states, which are superimposed upon the whole spin ensemble; in other words a net excess of $\alpha$ spin on radical one and a net excess of $\beta$ spin on radical two is created. The size of that difference is dependent upon how effectively the exchange interaction operates and how much the differential precession of spins can mix $|S\rangle$ and $|T_0\rangle$ states.

These three terms can be conveniently rearranged to give a model of a vector, representing spin–evolution with time [40,41]

$$\frac{\partial \underline{\rho}(r,t)}{\partial t} = \underline{\Omega}(r) \wedge \underline{\Pi}(r,t) \qquad (4.3.6)$$

where $\underline{\Omega}(r) = \begin{pmatrix} -2Q_{ab} \\ 0 \\ -2J_r \end{pmatrix}$; $\quad \underline{\Pi}(r,t) = \begin{pmatrix} \rho_{st} + \rho_{ts} \\ -i(\rho_{st} - \rho_{ts}) \\ \rho_{ss} - \rho_{tt} \end{pmatrix}$

This is depicted in Fig.(4.3.4): the sequential action of $Q_{ab}$ and $J_r$ is easily quantified by this model; thus, for radicals that separate for a time $t_q$ and then experience an average exchange upon re–encounter of $J_r$ for a time $t_j$, $\underline{\Pi}(r,t)$ will have developed a component in the x–direction of

$$\Pi_x(t_q+t_j) = \Pi_x(0)\{\cos(2J_r t_j) + 2Q_{ab}{}^2\sin^2 t_q\} + \Pi_y(0)\{\cos(2Q_{ab}t_q).\sin(2J_r t_j)\}$$
$$+ \Pi_z(0)\{\sin(2Q_{ab}t_q).\sin(2J_r t_j)\} \qquad (4.3.7)$$

Fig.(4.3.4)

A Vector Model Of Polarization Development

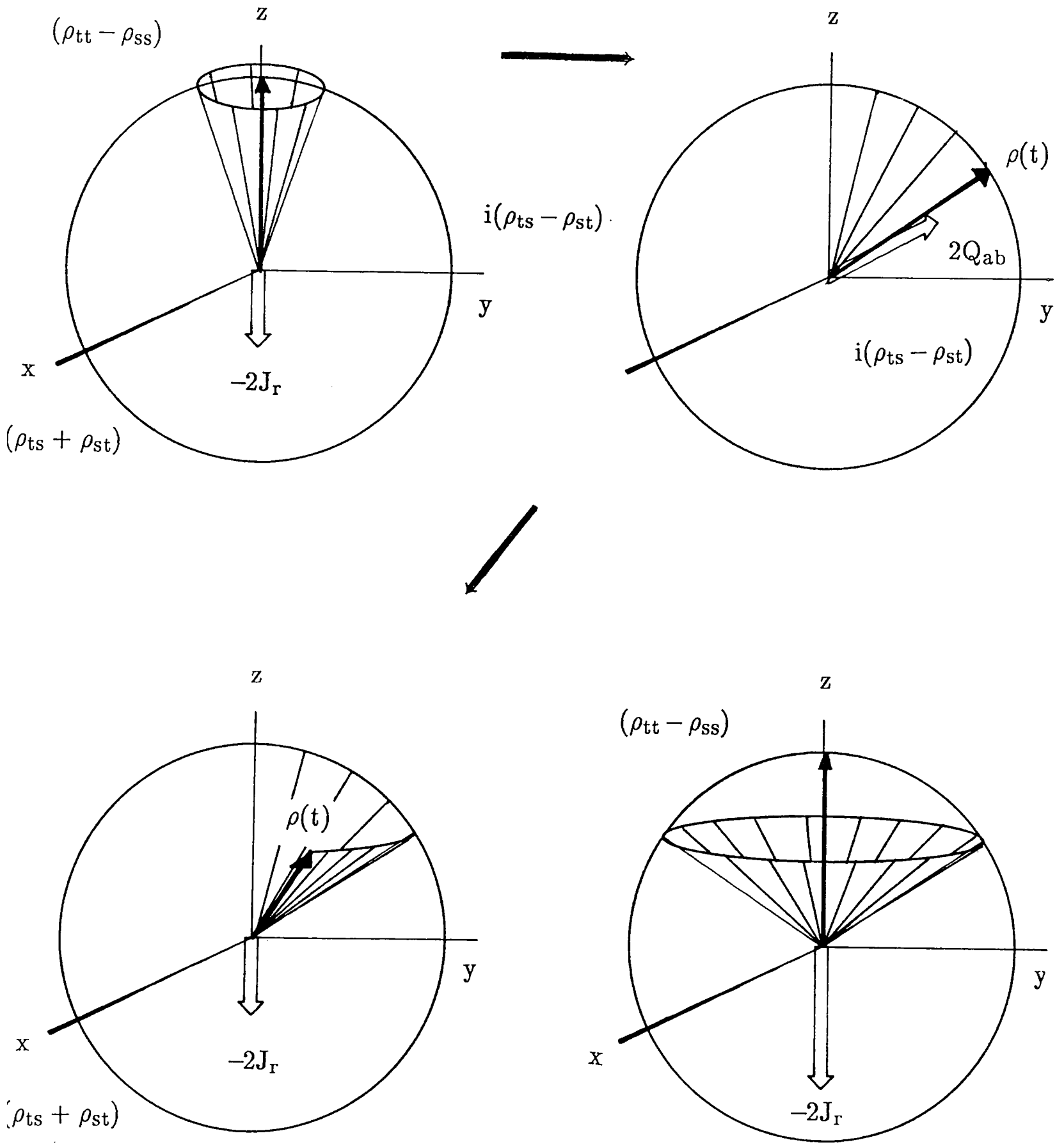


Large $J_r t_j$ gives no polarization

We may also pick out limiting cases from this solution: i) when $J_r$ is large the emerging polarization is scrambled as a consequence of the physical exchange of electrons ( i.e. when $J_r \gg t_j^{-1}$); ii) when the degree of $ST_0$ mixing is small then the polarization is proportional to $\sqrt{Q_{ab}}$ ($|Q_{ab}| \approx 10^8 rads^{-1}$ for most organic radicals in solution whilst re–encounter times $t_q$ are usually around $10^{-9}s$ so this is a reasonable assumption, though in micellar or high–viscosity solutions this is not necessarily true [42,43]. Returning to the trivial picture of the action of $J_r$ it is, of course, not tenable to maintain a coupled wavefunction for a pair of spins when $J_r$ is zero. However, the two spins after encounter do keep a "memory" of the relative phase at encounter – a memory which is modified by the action of $Q_{ab}$ and erased by relaxation. The component $\Pi_y(r,t)$ is not therefore a real or physical state but a combination of the two off–diagonal elements of the density matrix, which contain this phase information.

(4.3.3) Sign Rules For Polarization

It is easily seen that the polarization developed on radical 1 will be equal and opposite to that on radical 2. This is to be expected since only S and $T_0$ states are involved and neither possess an excess of $\alpha$ or $\beta$ spins, and no "spin–flips" $\alpha \leftrightarrow \beta$ occur. The net polarization over the pair must be zero, therefore. Alternatively, from (4.3.7) $Q_{ab}$ is equal and opposite to $Q_{ba}$ so, again, the polarization should be equal and opposite in sign. Inspection of the vector diagram shows that the sign of polarization for both radicals is reversed if $J_r$ changes sign (becomes positive), as is found in triplet exciplexes. Secondly, if $Q_{ab}$ reverses sign then the sign of the polarization for each radical also reverses. Finally, if the radical pair emerges from a singlet–geminate state

so that $(\rho_{tt} - \rho_{ss})$ is negative, then we should expect the sign of polarization for a given line to be opposite to that from triplet–geminate pairs.

There are also limits of $Q_{ab}$ between which all real systems fall. One is where the $Q_{ab}$ term is dominated by the $\Delta g$ term, which corresponds to a case for two very dissimilar radicals whose spectra do not overlap at all. For this system $Q_{ab}$ will be negative for all lines in one radical spectrum and positive for all lines in the other. The result is termed a net effect and is shown in Fig.(4.3.5a). Where $Q_{ab}$ is dominated by the hyperfine splittings (almost exclusively the case for organic free radicals[2]), then for any radical the polarization is equal and opposite in sign to the weighted average of the polarizations developed in all the possible nuclear spin states of the counter radical. This hyperfine multiplet effect is shown in Fig.(4.3.5d). These two extremes are embodied in the Kaptein Rules [44] which state that

$$\begin{aligned} \mathrm{Sign_{net}} &= \mu.\mathrm{J_r}.\Delta g \\ \mathrm{Sign_{multiplet}} &= \mu.\mathrm{J_r} \end{aligned} \qquad (4.3.8)$$

All terms are negative except where $\mu$ is positive (for a triplet G– or F– pair), or when $J_r$ is positive, in which case $E_s > E_t$. If $\mathrm{Sign_{net}}$ is positive for a radical then the net effect for that radical will be absorptive; if negative then the net effect will give an emissive contribution. For the multiplet effect a positive sign implies a phase from low to high field of absorption/emission or A/E, and if negative then emission/absorption or E/A.

From consideration of the ensemble nature of the RPM we may draw a simple conclusion – that the RPM polarization envelope of one radical passes through zero at

---

[2] As an example, $\Delta g$ for $(CH_3)_3C^\bullet$ and $CH_3C^\bullet O$ is $\approx$ 0.00015 or 2.5$\mu$T, whilst the proton coupling in the $(CH_3)_3C^\bullet$ radical is greater than 2.2mT.

Fig.(4.3.5)

A Demonstration Of Limiting And Intermediate Examples Of RPM.

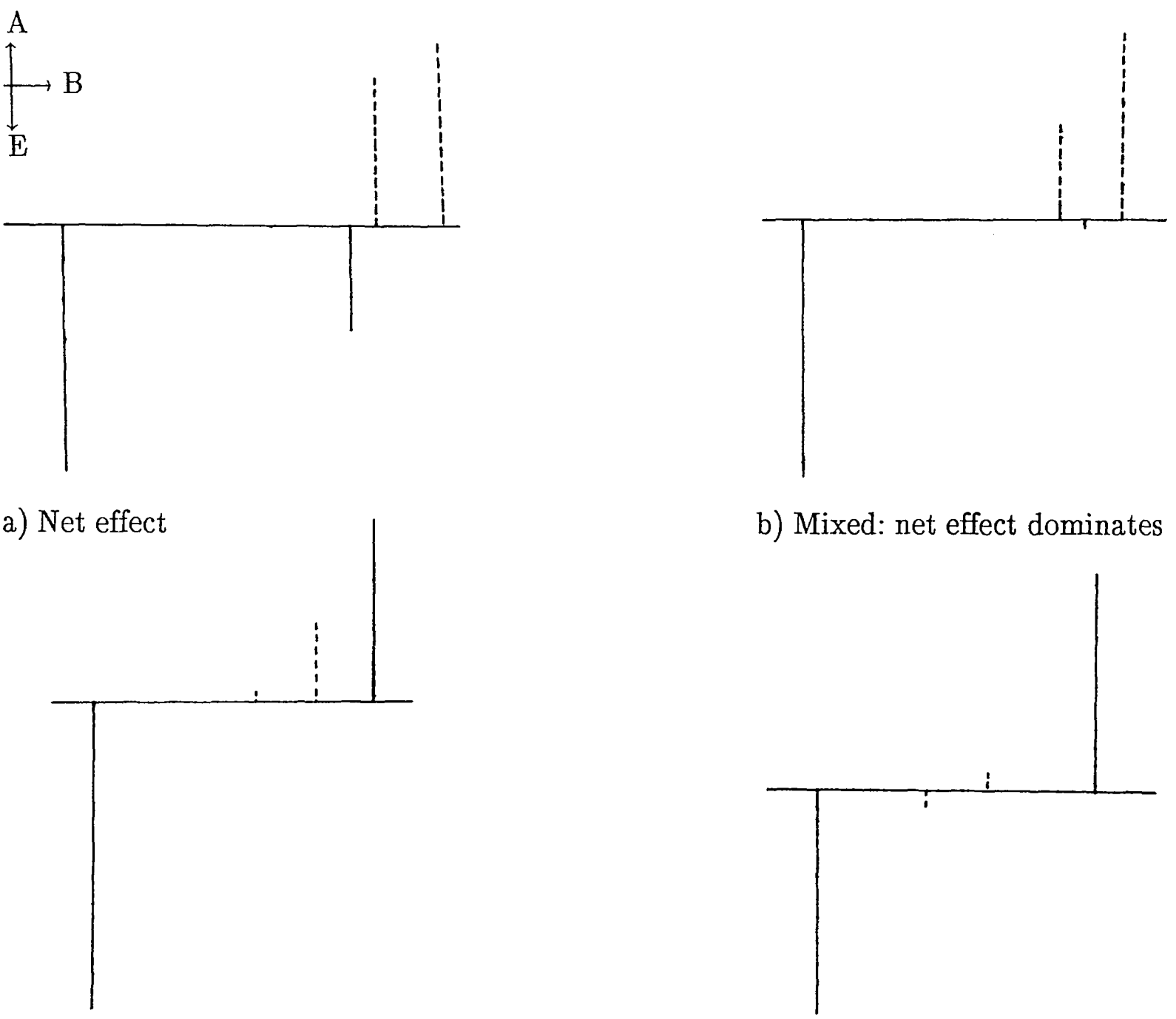


a) Net effect

b) Mixed: net effect dominates

c) Mixed: multiplet effect dominates

d) Pure multiplet effect

Couplings are ≈ 0.4mT and ≈ 1.9mT.

the centre field of the counter radical spectrum [45]. To either side of this point the ensemble average will either be positive or negative, and this will result in an appropriate phase of polarization. This last point is illustrated nicely by Fig.(4.3.5b) in which the phase of lines is E/A/E/A from low to high field. No example of this kind of net effect has been demonstrated, though similar mixed–phase behaviour can arise from other sources – see Chapter 5. The effects of isotropic hyperfine (multiplet) and isotropic g–factor (net) polarization have, in other respects, been thoroughly examined since this semi–quantitative theory was developed [46,47].

(4.3.4) Making The Theory Fully Quantitative

We begin by assuming that all re–encounters involve a radical pair that experiences an average exchange interaction $2J_r$ over a time $t_j$, and that, at the point of the first separation the only component of $\underline{\Pi}(r,t)$ that is non–zero is $\Pi(0)$. The probability of re–encounter after a time $t_q$ is $\mathcal{F}(t_q)$, which is also the time for which S–$T_0$ mixing occurs. Thus the polarization generated on radical 1 upon re–encounter, and for all possible re–encounter times is

$$Pol_{1,ab} = \Pi_z(0)\sin(2J_r t_j).\int_0^\infty \mathcal{F}(t_q).\sin(2Q_{ab}t_q)dt_q \qquad (4.3.9)$$

Replacing a re–encounter probability with time by one that varies with number of diffusive steps taken, N, and time per diffusive step $\tau_d$ ($t_q = N\tau_d$) gives a re–encounter probability distribution of [48]

$$Pr(N) = \frac{0.24}{\sqrt{(N + 0.44)^3}} \qquad (4.3.10)$$

Polarization is given, then, by [37]

$$Pol_{1,ab} = 0.24\Pi_z(0).\sin(2J_r t_j).\int_2^{\infty}\left\{\frac{\sin(2Q_{ab}\tau_d N)}{\sqrt{(N+0.44)^3}}\right\}dN \qquad (4.3.11)$$

where the integration limit of two follows from the need for radicals to separate and then re–encounter. For a small degree of mixing this approximates to

$$Pol_{1,ab} \approx 0.85\Pi_z(0).\sin(2J_r t_j).[Q_{ab}\tau_d]^{\frac{1}{2}} \qquad (4.3.12)$$

Using realistic approximations of $Q_{ab} \approx 10^8 rads^{-1}$, $\tau_d \approx 10^{-11}s$, $\sin(2J_r t_j) \approx 0.1$ [40], gives a value of $Pol_{1,ab}$ of about $10P_{eq}$. This is for one singly degenerate line ,a, on radical 1, with one counter–radical line b: the ensemble average polarization is then

$$Pol_{1,a} = (1/x_2).\sum_n Pol_{1,ab_n} \qquad (4.3.13)$$

where $x_2$ is the total number of states, $b_n$ on radical 2. The reduced form of the polarization expression (4.3.12) predicts that we should see a dependence of $\sqrt{|Q_{ab}|}$ on the contribution to a line on radical 1 from each line in radical 2, and this is found to hold for nearly all experimental systems under conditions of normal viscosity. We could regard the oscillation between S and $T_0$ states that $Q_{ab}$ tries to establish as being weakly damped by $T_1$ and $T_2$ and severely damped by the fall–off in re–encounter probability. As the viscosity of solution increases then this condition of small S–$T_0$ mixing is violated and a more complex dependence is found [43]. For moderate

Fig.(4.3.6)

The Oscillatory Nature Of RPM Polarization Generation

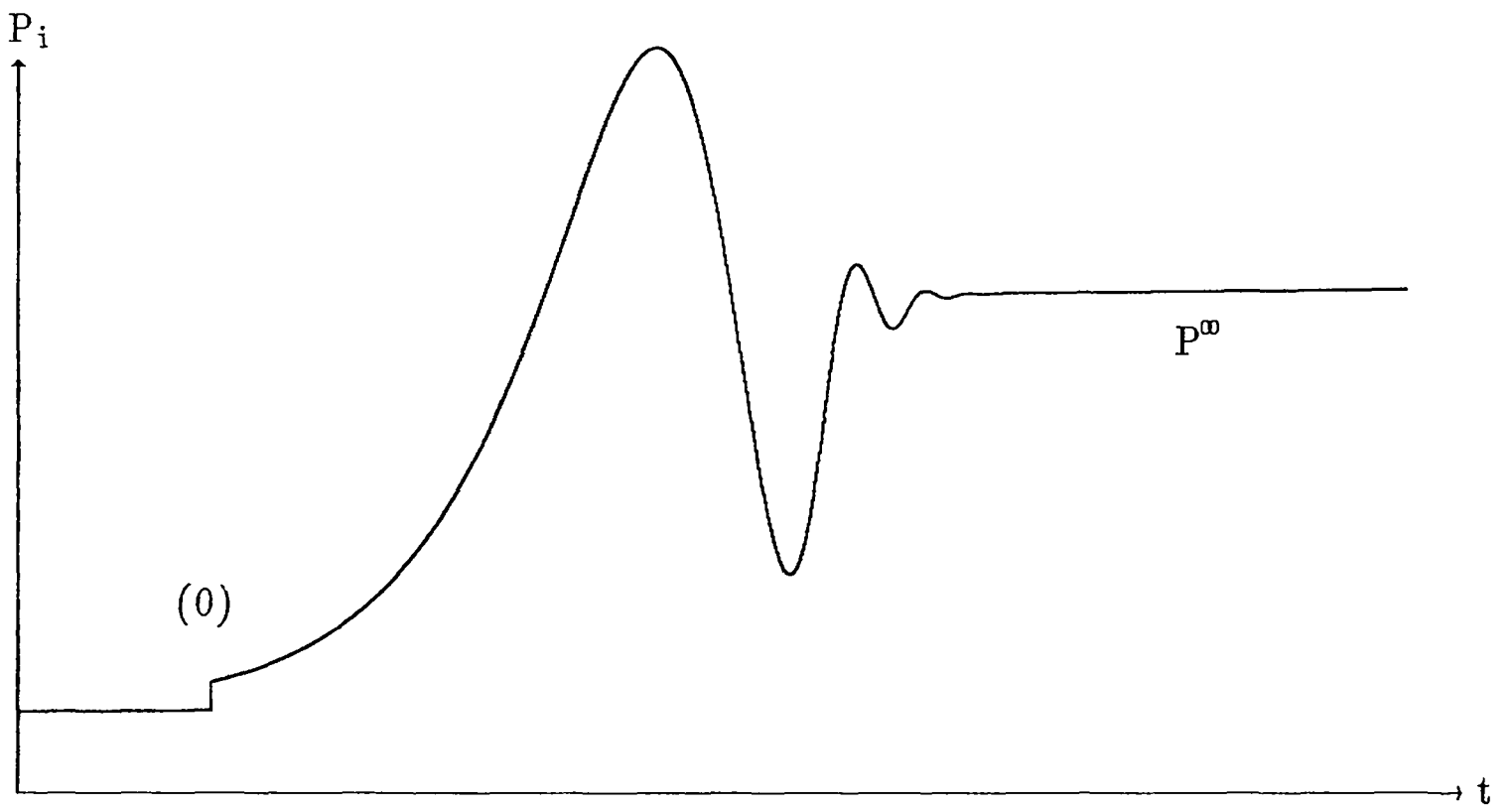


Modelled for an exponential exchange. (log.scale).

viscosities, however, the polarization should vary with $\sqrt{\tau_d}$, which may be substituted by $(\eta/T)^{\frac{1}{2}}$. The resulting variation of polarization with viscosity $\eta$ has been confirmed [49].

(4.3.5) A Rigorous Mathematical Model Of The Radical Pair

To treat the behaviour of an ensemble of spins that diffuse and evolve where the two processes are interlinked involves a higher level of sophistication than that of the vector model. Two components that influence this evolution may be identified. These are a spin Hamiltonian that is spin– and distance–sensitive, $\mathscr{H}_{rp}(\underline{r},\underline{S}_1,\underline{S}_2)$ and a diffusion operator that is just sensitive to separation, $D\Gamma_r$. A complete equation for the motion of the density matrix is [50]

$$\frac{\partial \Pi(\underline{r},t)}{\partial t} = -i[\mathscr{H}_{rp}(\underline{r},\underline{S}_1,\underline{S}_2), \Pi(\underline{r},t)] + D\Gamma_r.\Pi(\underline{r},t) \qquad (4.3.14)$$

D is the diffusion coefficient for the pair of radicals, and in isotropic solution $\underline{r}$ may be replaced by r. This is an analytically insoluble equation but, by allowing the radical pair to diffuse in a stepwise manner through discrete but closely separated values of r, a matrix is built up that contains spin and separation terms. This is a stochastic solution and the whole expression is termed the Stochastic Liouville equation [50]. Its construction is treated at more length in appendix C. For each set of D, $J_r$ and $Q_{ab}$ a different matrix of solutions is generated. There is, of course, a full numerical solution available to us [51] employing the finite differences between values of r, modelling exchange and diffusion as simple analytical functions and considering the separation at which radicals react as a reflective boundary and that separation from which they are unlikely to re–encounter as an absorptive outer boundary. Further refinements [52] have concentrated upon the anisotropy of $J_r$ and $Q_{ab}$, and the effect of spin upon

diffusional trajectories, but the net effect in all these models is found to be small.

Exchange is most conveniently written as

$$J_r = J_0.e^{-\lambda r} \qquad (4.3.15)$$

where $\lambda$ is an *ad hoc* parameter that may be varied to investigate the influence of long or short range exchange interactions upon polarization. Diffusion is also conveniently reduced to

$$D \approx d^2/3\tau_d \qquad (4.3.16)$$

where d is the distance of closest approach of the radical pair (the inner reflecting boundary). Using these expressions and assuming that mixing is small ($|Q_{ab}.\tau_d| \ll 1$), an asymptotic solution may be forced [53],

$$Pol^{\infty}_{1,ab} = (\pi/2).\frac{|Q_{ab}J_0|}{Q_{ab}J_0}.\frac{\sqrt{3}\Pi_z(0)}{\lambda d}.[|Q_{ab}|\tau_d]^{\frac{1}{2}} \qquad (4.3.17)$$

which agrees well with the full treatment [51]. For very fast diffusion (not found in practice), then $P_{1,ab} \alpha Q$, and when diffusion is slow $P_{1,ab} \alpha Q_{ab}{}^{\epsilon}$ where $\epsilon$ lies between 0 and $\frac{1}{2}$. A more thorough treatment still gives

$$Pol^{\infty}_{1,ab} = (Q_{ab}d^2/D)^{\epsilon}.\left[\frac{2|J_0|\tau_1(\lambda) + (\lambda d)^{\epsilon'}.(2J_0\tau_1(\lambda))^2}{1 + (2J_0\tau_1(\lambda))^2}\right] \qquad (4.3.18)$$

for an initial triplet state in the absence of reaction, and for which $(Q_{ab}d^2/D) \leq 0.016$.

$\tau_1(\lambda) \approx (d/D\lambda)[1 + (\lambda d)^{-1}]$ ; $J_r = J_0 e^{-\lambda(r-d)}$ ; $\epsilon = \frac{1}{2}$ ; $\epsilon' = 1$. $\epsilon$ and $\epsilon'$ are reduced as the small mixing condition is violated. This $Q^{\frac{1}{2}} - aQ$ polarization dependence has been demonstrated for alkyl radicals in high–viscosity paraffins [43]. As was the case for the TM the absolute enhancements of lines is difficult to determine, but unlike the TM the relative intensities of lines provide a very sensitive test of polarization theory. One point about the last observation of a dependence on $Q_{ab}$ in high viscosity solutions is that this linear term will be exaggerated as it arises from the separation of radicalsalone; all radical pairs we observe will have separated but only about one third will return to re–encounter their partner. Furthermore, the oscillatory generation of polarization has been derived theoretically [55] and tested experimentally [56,57]. With this weight of evidence behind the RPM it can be justifiably used to probe the exchange interaction between radical pairs in highly viscous media [58] and in bi–radical chains of varying lengths [59]. A final point ought to be made: G– and F–pair polarizations are mono– and bi–molecular respectively and will therefore have different time and concentration dependences. This has been demonstrated in Fig.(2.3.3) for a suitable range of conditions.

(4.4.1) The Mixing Of S and T$_-$ States

Whilst it was pointed out in Fig.(4.3.2) that S and T$_-$ states became degenerate over a small range of r, the possibility of their mixing was dismissed. It is found that this holds good for carbon–centred radicals in solutions of normal viscosity. We shall encounter non–carbon–centred species and high viscosity media in later chapters so a short discussion of ST$_-$ mixing is necessary.

The magnetic Hamiltonian is written as

$$\mathscr{H}_s = g\mu_B S_z.B_0 + \sum_n a_n \underline{S}.\underline{I}_n \qquad (4.4.1)$$

If we consider degenerate nuclei as being coupled together so that $I = \sum_n I_{equiv}$ for n equivalent nuclei, then I can take the values of k, k − 1, . . . 0, and $I_z$ can take values between k and − k, where k = n/2. For a first–order *e.s.r.* spectrum $\mathscr{H}_s = S_z.I_z$ so that all combinations of spins that give a total momentum of k are degenerate. To *second order*, however, the non–secular terms $S_xI_x$ and $S_yI_y$ contribute effectively to split hyperfine lines up (this is clearly resolved in the spectra of radicals such as $(CH_3)_3C^\bullet$). For a change from $\beta$ to $\alpha$ spin in an electron a simultaneous flip from a nuclear $\alpha$ to $\beta$ state must take place. These spin–flips are generated by the $S_+$ and $S_-$ operators and since these terms will vary across the second order components of a line it is possible to distinguish the effects of $ST_-$ polarization from $ST_0$ or TM polarizations (strictly speaking this ought to read $T_-S$ as it will usually be observed as a transition from a separating triplet pair to a singlet one).

(4.4.2) The Second Order Effect

Taking the electron/nuclear interaction

$$a\underline{S}.\underline{I} = a(S_zI_z + S_yI_y + S_xI_x) = a[S_zI_z + \tfrac{1}{2}(S_+I_- + S_-I_+)] \qquad (4.4.2)$$

where $S_\pm = S_x \pm iS_y$ and $I_\pm = I_x \pm iI_y$. $S_zI_z$ cannot mix $T_-$ and S states and $S_-I_+$ cannot occur for a pure $T_-$ state. However, the term $S_+I_-$ does have a non–zero matrix element connecting $T_-$ and S, if $I_z \neq -I$, since

$$\langle T_-,I,I_z-1|\, S_+I_-|\, S,I,I_z\rangle = [I(I+1)-I_z(I_z-1)]^{\frac{1}{2}} \qquad (4.4.3)$$

The strength of this mixing is proportional to the square of the matrix element, $a^2[I(I+1)-I_z(I_z-1)]$. Clearly the extent to which ST$_-$ mixing occurs will be a sensitive measure of the coupling constants (a nice illustration of this is given by the $^{27}$Si–centred radical from reaction of tri–ethyl silane with $^t$butoxyl radical, which shows a weak net emission from ST$_-$ mixing ($a(^{27}Si) > 20mT$)[3], though the non–magnetic isotope, which by contrast has a small spectral spread, is observable in net absorption.

This gives a hyperfine–dependent polarization to the radical observed but since this is developed in a region for which $J_r \neq 0$ we must also consider all possible ST$_-$ contributions that the second radical could produce on the first: simply, it is an average of all the ST$_-$ polarizations that the second radical can produce, distributed evenly over each hyperfine state of the first radical. If the coupling constant on radical 1 is large then its spectrum will be dominated by the hyperfine–dependent part of the ST$_-$ mixing; if radical 2 possesses an unusually large coupling then the spectrum of radical 1 will be dominated by the hyperfine–independent part. This is demonstrated by the spectra of di–ethoxy phosphonyl and propan–2–olyl radicals [60]. Another feature of the ST$_-$ mechanism is that it is dependent both on the sign of the coupling constant and on whether the radical pair separates as a triplet or a singlet. Neither prediction has been rigorously tested. The phenomenon has been treated to a full stochastic Liouville analysis, in which a series of models for the exchange interaction have been employed

---

[3] This radical has been examined by myself and J. G. Buglass but the spectra are unfortunately not of a high enough quality to be analysed for more than their apparent content.

[61] and numerical solutions have been derived. This full theory agrees with the simplest experiments, performed on identical pairs of radicals which possess just one large hyperfine coupling constant [62] and the $ST_-$ polarization may thus be incorporated into the polarization expressions for $ST_0$ mixing where necessary. A simulated $ST_-$ spectrum is displayed in Fig.(4.4.1).

Fig.(4.4.1)

The ST$_-$ Effect – Origins And Appearance

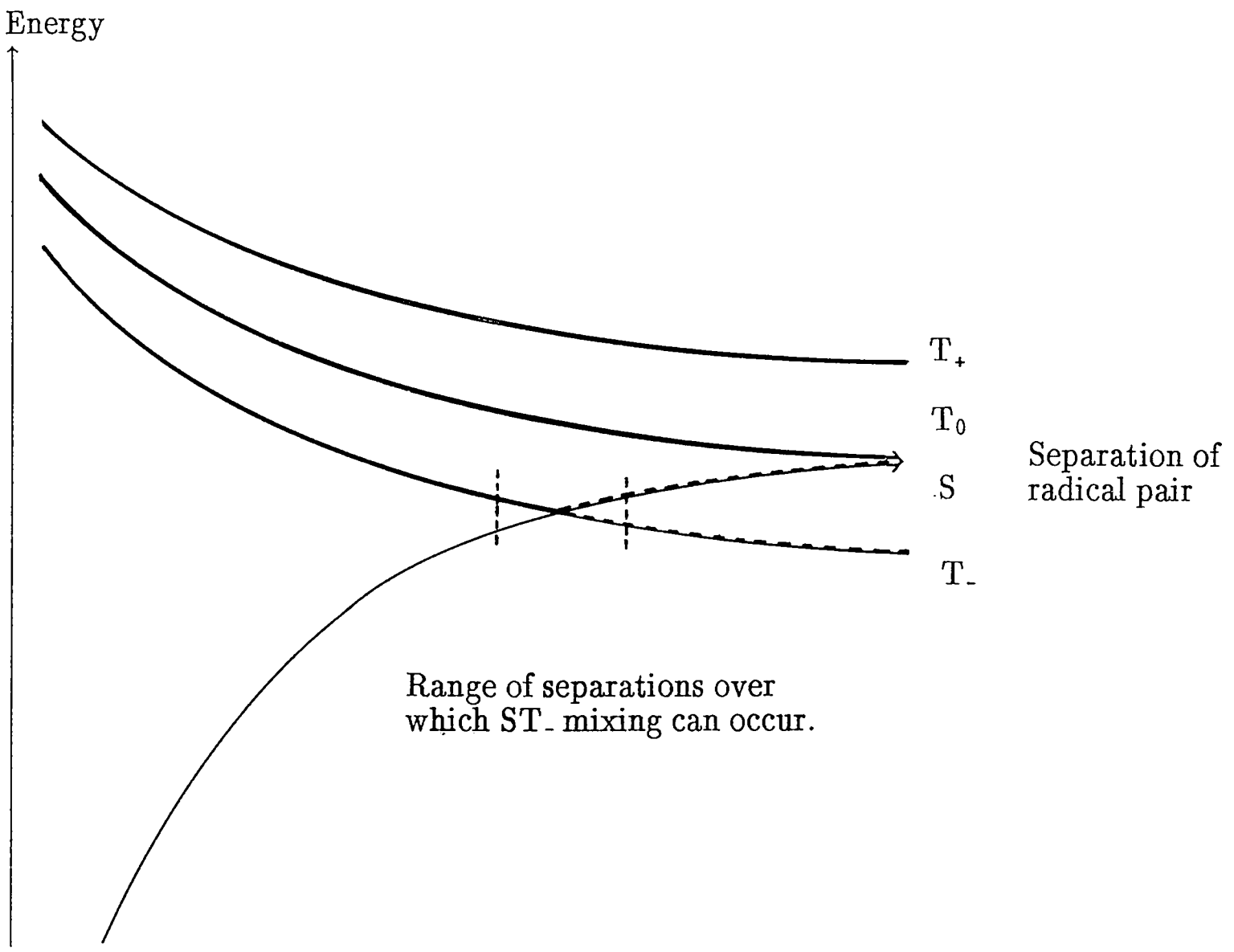


A Simulated ST$_-$ Spectrum

| | $K_i$ | 1 | 2 | 2 | 1 |
|---|---|---|---|---|---|
| 2I | | | | | |
| 2 | | 1 | 1 | 1 | 1† |
| 1 | | | 2 | 2† | |

Those states marked by † are already in the highest possible coupled nuclear states and cannot therefore contribute to the spectrum.

This produces a hyperfine–independent part,

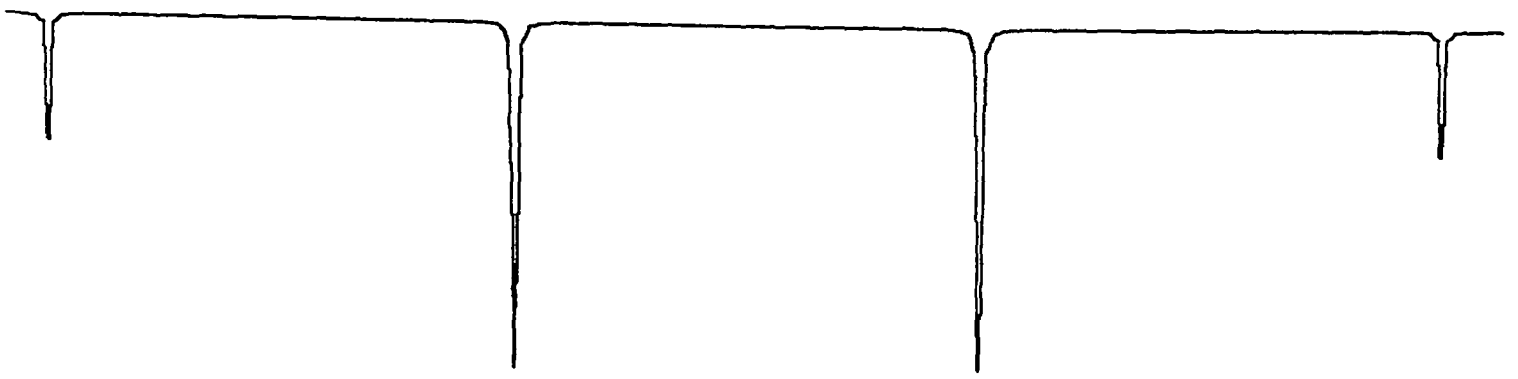

and a hyperfine dependent part

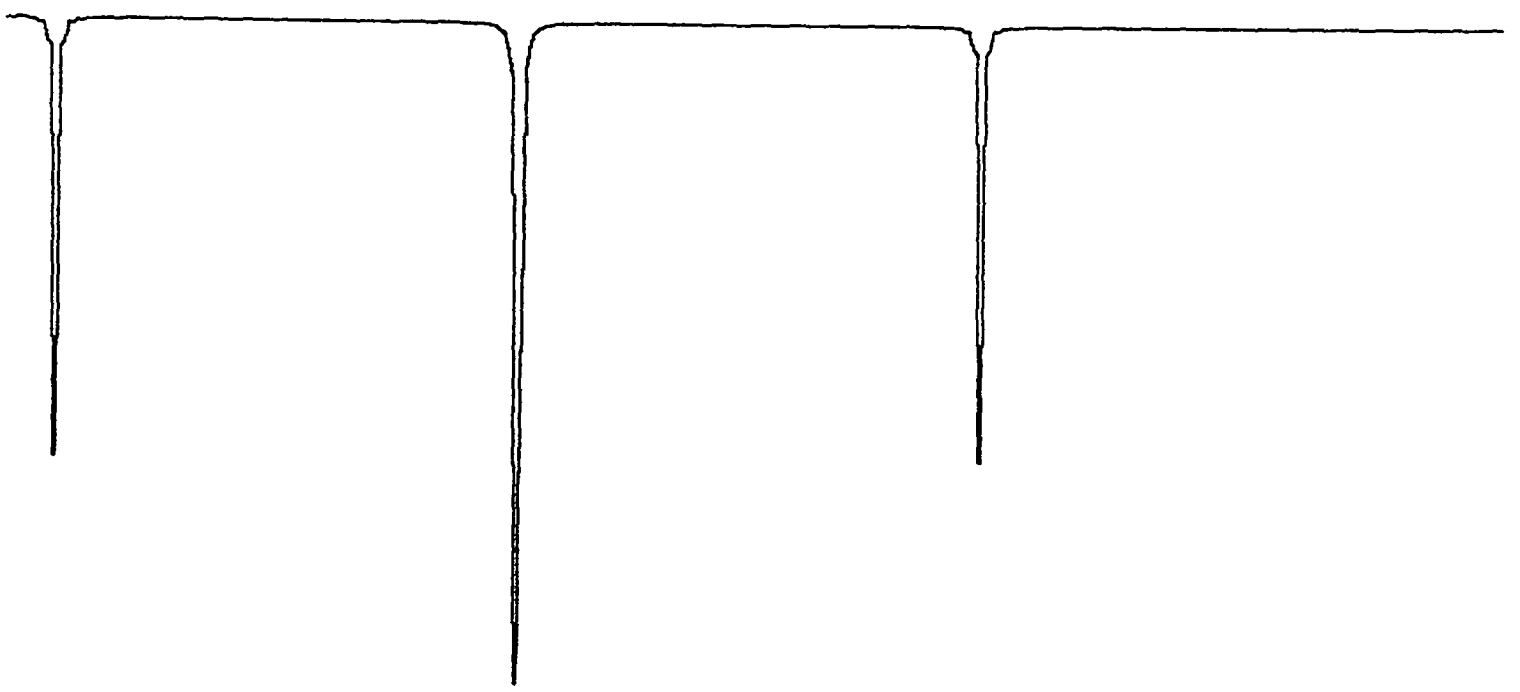

combining to give the complete spectrum.

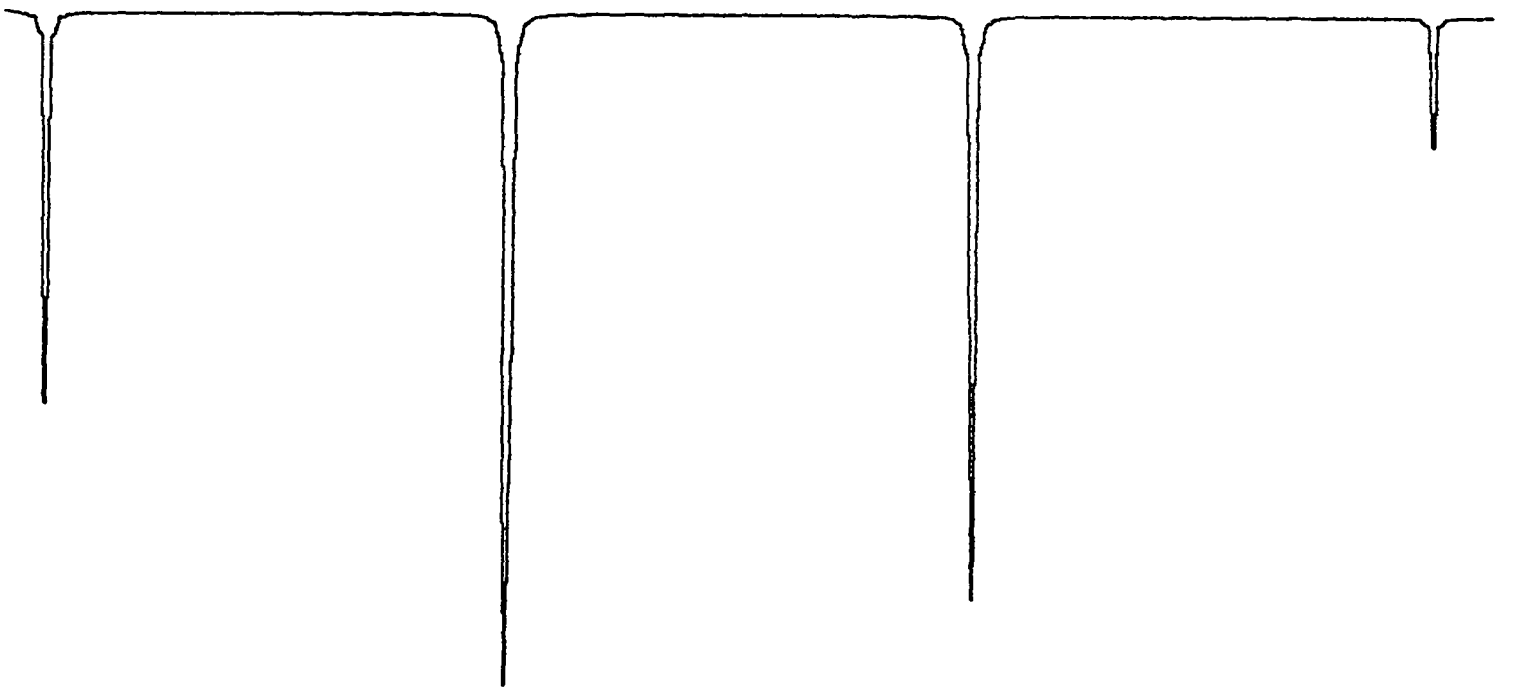

## REFERENCES – CHAPTER 4


1 Fessenden R.W., Schuler R.H. *J.Chem.Phys.* (1963) 39, 2147.

2 Ward H.R., Lawler R.G. *J.Am.Chem.Soc.* (1967) 89, 5518.

3 Fischer H., Bargon J. *Acc.Chem.Research* (1969) 2, 110.

4 Basu S., McLauchlan K.A., Sealy G.R. *Chem.Phys.Lett.* (1982) 88, 84.

5 Buckley C.D., McLauchlan K.A. *Mol.Phys.* (1985) 54, 1.

6 Buckley C.D., McLauchlan K.A. *Chem.Phys.Lett.* (1989) 164, 517.

7 Basu S., Grant A.I., McLauchlan K.A. *Chem.Phys.Lett.* (1983) 94, 517.

8 Carmichael I., Paul H. *Chem.Phys.Lett.* (1979) 67, 519.

9 McLauchlan K.A., Simpson N.J.K.
*J.Chem.Soc. Perkin Trans.II* (1990) – in the press.

10 Atkins P.W., Dobbs A.J., McLauchlan K.A. *Chem.Phys.Lett.* (1973) 22, 209.

11 Atkins P.W., Buchanan I.C., Gurd R.C., McLauchlan K.A., Simpson A.F.
*Chem.Commun.* (1970) 513.

12 Takagi Y. *Chem.Phys.Lett.* (1985) 119, 5.

13 Van Vleck A. *Rev.Mod.Phys.* (1951) 23, 213.

14 Atherton N.M. "*Electron Spin Resonance*" (Pub. Ellis Horwood, 1973).

15 McGlynn S.P., Azumi T., Kinoshita M.
"*Molecular Spectroscopy Of The Triplet State*" (Pub. Prentice Hall, 1969).

16 Gehrtz M., Bräuchle C., Voitländer J. *Chem.Phys.Lett.* (1982) 91, 217.

17 Buckley C.D., McLauchlan K.A. *Chem.Phys.* (1984) 86, 323.

18 Buckley C.D., McLauchlan K.A. *J.Photochem.* (1984) 27, 311.

19 Buckley C.D., Grant A.I., McLauchlan K.A., Ritchie A.J.D.
*J.Chem.Soc.Farad.Disc.* (1984) 78, 257.

20 Wong S.K., Hutchinson D.A., Wan J.K.S. *J.Chem.Phys.* (1973) 58, 985.

21 Atkins P.W., Evans G.T. *Mol.Phys.* (1974) 27, 1633.

22 "*Electron Spin Relaxation In Liquids*" (Ed. Muus L.T., Atkins P.W.)
(Pub. Plenum N.Y., 1972).

23 Pedersen J.B., Freed J.H. *J.Chem.Phys.* (1975) 62, 1706.

24 Adrian F.J. *J.Chem.Phys.* (1974) 61, 4875.

25 Dobbs A.J., McLauchlan K.A. *Chem.Phys.Lett.* (1975) 30, 257.

26 Yamauchi S., Tominaga K., Hirota N. *J.Phys.Chem.* (1986) 90, 2367.

27 McLauchlan K.A., Stevens D.G. *Mol.Phys.* (1987) 60, 1159.

28 McLauchlan K.A., Sealy R.C., Wittmann J.M.
*J.Chem.Soc.Farad.Trans.II* (1977) 73, 926.

29 Adeleke B.B., Choo K.Y., Wan J.K.S. *J.Chem.Phys.* (1975) 62, 3822.

30 Atkins P.W., Dobbs A.J., Evans G.T., McLauchlan K.A., Percival P.W.
*Mol.Phys.* (1974) 27, 769.

31 Atkins P.W., Dobbs A.J., McLauchlan K.A. *Chem.Phys.Lett.* (1974) 29, 616.

32 Grant A.I., McLauchlan K.A. *Chem.Phys.Lett.* (1983) 101, 120.

33 Schulten K., Steark H., Weller A., Werner H.J., Nickel B.
*Z.Phys.Chem.Natur.* (1976) 101, 371.

34 Closs G.L. *J.Am.Chem.Soc.* (1969) 91, 4552.

35 Kaptein R., Oosterhoff L.J. *Chem.Phys.Lett.* (1969) 4, 195, ibid 214.

36 Adrian F.J. *J.Chem.Phys.* (1971) 54, 3912.

37 Adrian F.J. *J.Chem.Phys.* (1971) 54, 3918.

38 Freed J.H., Pedersen J.B. *Adv.Magn.Reson.* (1976) 8, 1.

39 Trifunac A.D., Thurnauer M.C. "*Time Domain e.s.r.*" (Eds. Kevan K., Schwartz R.N.) Chapter 6. (Pub. J.Wiley N.Y., 1979).

40 Adrian F.J. *Rev.Chem.Int.* (1979) 3, 1.

41 Feynmann R.P., Vernon F.L., Hellworth R.W. *J.Appl.Phys.* (1957) 28, 49.

42 Atkins P.W. *Chem.Phys.Lett.* (1973) 18, 290.

43 McLauchlan K.A., Stevens D.G. *J.Magn.Reson.* (1985) 63, 473.

44 Kaptein R. *Chem.Commun.* (1971) 732.

45 Buckley C.D., McLauchlan K.A. *J.Magn.Reson.* (1984) 58, 334.

46 Trifunac A.D., Avery E.C. *Chem.Phys.Lett.* (1974) 27, 141.

47 Trifunac A.D., Avery E.C. *Chem.Phys.Lett.* (1974) 28, 294.

48 Noyes R.M. *Progr.React.Kinet.* (1961) 1, 129.

49 Atkins P.W., Duggan J.K., McLauchlan K.A., Percival P.W. *Chem.Phys.Lett.* (1974) 24, 565.

50 Kubo R. *Adv.Chem.Phys.* (1969) 15, 101.

51 Pedersen J.B., Freed J.H. *J.Chem.Phys.* (1973) 58, 2746.

52 Pedersen J.B., Freed J.H. *J.Chem.Phys.* (1973) 59, 2869.

53 Monchick L., Adrian F.J. *J.Chem.Phys.* (1978) 68, 4376.

54 Zientara G.P., Freed J.H. *J.Chem.Phys.* (1979) 70, 1359.

55 Freed J.H. *Ann.Rev.Phys.Chem.* (1972) 23, 265.

56 Eliav U., Freed J.H. *J.Chem.Phys.* (1984) 88, 1277.

57 Veselov A.V., Melekhov V.I., Anisimov O.A., Molin Y.N. *Chem.Phys.Lett.* (1987) 136, 263.

58 Buckley C.D., Hunter D.A., Hore P.J., McLauchlan K.A. *Chem.Phys.Lett.* (1987) 135, 307.

59 Closs G.L., Forbes M.D.E. *J.Am.Chem.Soc.* (1987) 109, 6185.

60 Buckley C.D., McLauchlan K.A. *Chem.Phys.Lett.* (1987) 137, 86.

61 Monchick L., Adrian F.J. *J.Chem.Phys.* (1979) 71, 2600.

62 Burkey T.J., Luztyk J., Ingold K.U., Wan J.K.S., Adrian F.J. *J.Chem.Phys.* (1985) 89, 4286.

# CHAPTER V : AN INVESTIGATION INTO TRANSFER POLARIZATION

# AN INVESTIGATION INTO POLARIZATION TRANSFER

## (5.1.1) Introduction

The work presented in this chapter has two main thrusts, one of them qualitative, the other analytical. This follows the chronology of the experimental results, for the initial effort was directed towards demonstrating a phenomenon but in the course of this investigation a series of chemical systems were experimented upon that, once their complex chemistry had been straightened out, were found to be near–ideal subjects for quantitative analysis. This has permitted the first application of a relatively ancient piece of theoretical work on the transfer of CIDEP polarization from one radical to another, chemically distinct one [1,2].

CIDEP has been employed previously for kinetic purposes [3–5] where no knowledge of the polarization mechanism had been pre–supposed (though the subtlety of CIDEP may well prove such a cavalier approach to be foolhardy). It has been used more exactly and accurately to separate and measure first order and second order effects and then to extract kinetic data from these values [6]. There has been, to date, only one case of hyperfine–dependent polarization transfer which has been analysed [7], in that case to assess the rate of exchange between two conformers of the cyclohexanolyl radical. However, whilst radical populations may only be measured with great difficulty, the polarization present in a radical ensemble at any time is an intrinsic quantity, observable in an *e.s.r.* experiment. Clearly, the amount then imparted to a secondary species will be a function of the rate of decay of that polarization and rate of formation of the secondary from the primary species.

(5.2.1) A Non–quantitative Appraisal

The stimulus for this work arose from attempts to explain an observation reported in the spectra of polarized radicals in micelles [8]. While the true reason for the remarkable appearance of these spectra has since been shown to come from the action of a small splitting caused by the exchange interaction in the radical pair [9] the arguments put forward are still perfectly valid [10]; it was argued that, provided the primary radical possessed hyperfine–dependent polarization and that at least one nucleus remained coupled to the electron throughout the reaction, then that hyperfine dependence would be reflected in the appearance of the secondary radical – a point that had been recognised previously but not followed through [11]. The essence of this effect is displayed in Fig.(5.2.1).

When no correlation exists between nuclei in initial and final radicals then only a hyperfine–independent or "net" polarization ( equivalent to the consequences of electron transfer in radical anions) is carried over [12]. The difficulty with this kind of study is that absolute signal intensities and enhancements are harder to determine than relative hyperfine intensities. When, however, coupling to the same magnetic nucleus exists in two generations of radicals then the resulting hyperfine–dependent RPM, clearly distinguishable from the TM or equilibrium effects, may be borne over into specific hyperfine states of the daughter radical. Before subsequent relaxation and polarization can destroy this "fingerprint" of the original species we might expect to observe patterns similar to those displayed in (5.2.1b) and (5.2.1c); the latter corresponds to a case in which the sum of the couplings generated in the new species exceeds that of the coupling to the nucleus that remains correlated through the reaction. It is conceivable that, by a combination of RPM effects, a spectrum could be produced that has a Q–dependence such that it appears similar to (5.2.1b), given that the normal secondary radical RPM

Fig.(5.2.1) Level Ordering And Populations Induced By RPM On A Primary Radical

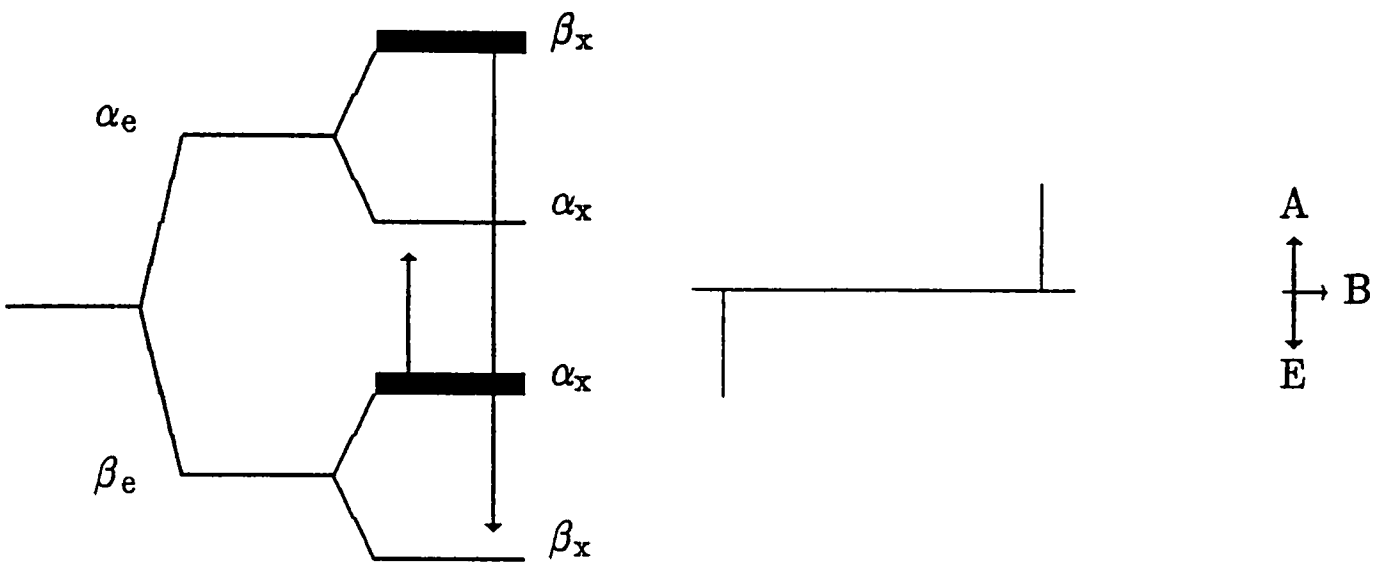


These populations, when transferred to a secondary species, with one spin–½ nucleus and positive coupling, as for the primary, gives

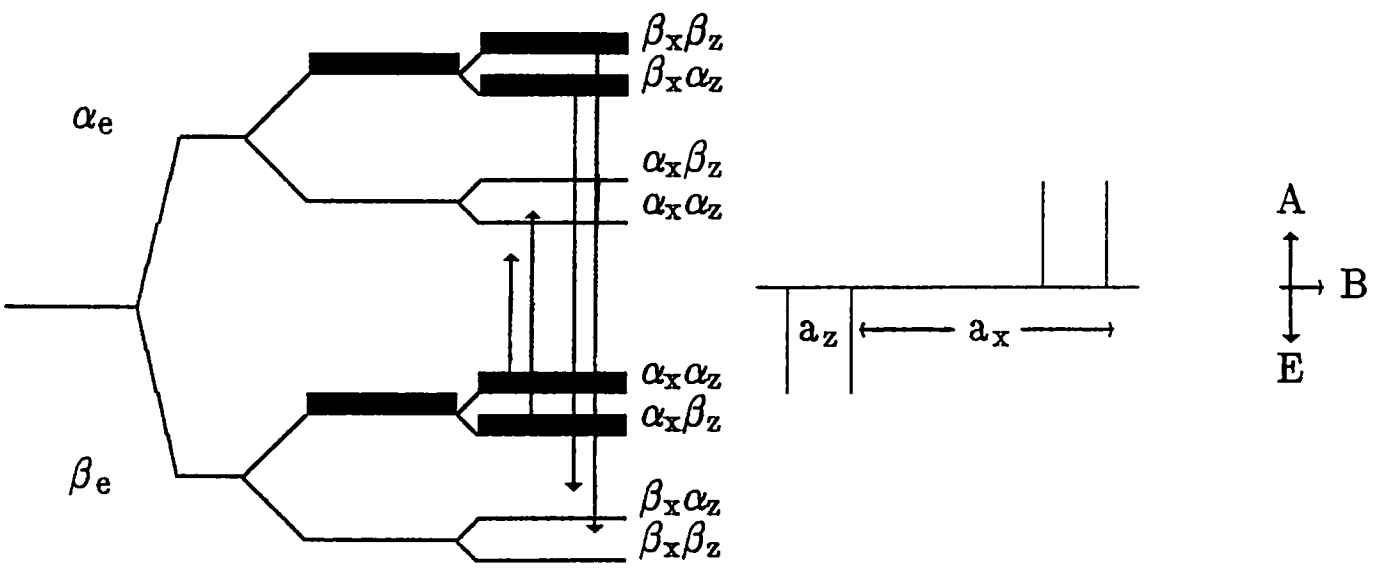


where $a_x > a_z$ and both are positive. This contrasts with normal RPM: each hyperfine line would have a different polarization.

When the new couplings in the secondary species exceed that to the coupling of the correlated nucleus, then a different pattern arises –

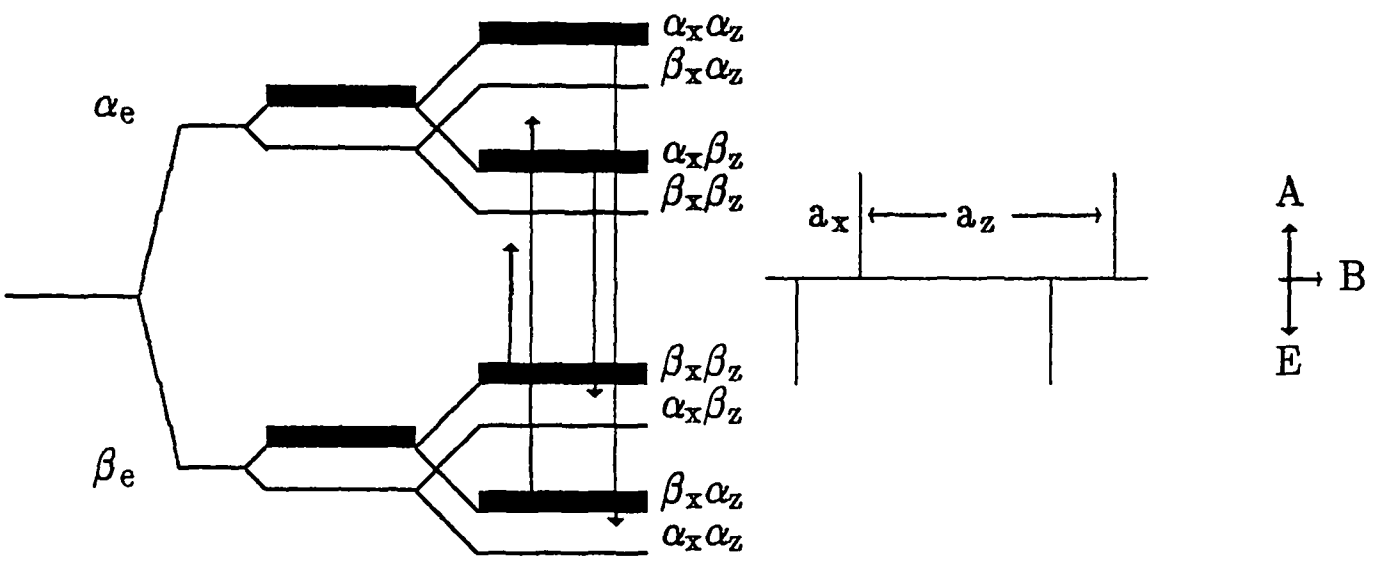

polarization will certainly modify the observed transfer–polarized hyperfine intensities; the mixed–phase spectrum portrayed in the last diagram would require an inconceivable combination of $\Delta g$ and hyperfine parameters. Examples of both kinds of transfer extremes will be presented, and we may note that the requirement for the observation of general transfer of an excess of one spin state over another is not stringent: free radical reactions mostly take place at rates well above that of a typical reciprocal spin–lattice relaxation time.

The effect was first unequivocably demonstrated for the addition of a phosphonyl radical onto an alkene [13]. Correspondence of the adduct spectrum with (5.2.1c) is unmistakable.

It is evident that, should a radical coupling change sign upon reaction, then the low–to–high field hyperfine dependence of each doublet in the primary will be reversed in the secondary, as intimated when first considered [10]. Further, systems in which a series of competitive or chain reactions are taking place will contain a wealth of kinetic data. The effect of transfer polarization on TIS spectra has been dealt with elsewhere [14] but the very nature of TIS means that time–information is lost. Such systems would readily lend themselves to the surface–mode of spectrometer operation, since the spectral components arising from each radical will have been produced under identical operating conditions. Their relative growth or decay may then be directly compared.

### (5.2.2) A First Illustration

In this, as in all following work in this chapter, the "primary radical" is, in fact, a secondary one. To explain, a convenient photo–initiator (found to be both efficient and clean) is di–tertbutyl peroxide, commercially available in high purity. Its absorption maxima lie well away from 308nm but sufficient photolysis occurs to yield a maximum

concentration ($\approx 10^{-3}$M ) of $^t$butoxyl radicals. It is unclear through what state the peroxide dissociates in solution, or even in the gaseous state [15,16], though it is likely that it is singlet–dissociative in these experiments[1]. Whatever the pathway, the very rapid relaxation of the $^t$butoxyl radical ($T_1 \simeq 10^{-9}$s) means that for the sake of these investigations, not only do we see no sign of it because of relaxation–broadening, but nor will it have an effect on the polarization of the radicals it generates. Instead, the radical we shall consider as our primary is the di–alkoxyphosphonyl, generated by H–abstraction from the phosphite present, thus –

$$(CH_3)_3C\text{–}O\text{–}O\text{–}C(CH_3)_3 \xrightarrow{h\nu(308nm)} 2(CH_3)_3C\text{–}O^{\bullet} \qquad (A)$$

$$(CH_3)_3C\text{–}O^{\bullet} + O{=}P(H)(OR)_2 \xrightarrow{k} (CH_3)_3COH + O{=}\dot{P}(OR)_2 \qquad (B)$$

$k \approx 10^7$ $dm^3mol^{-1}s^{-1}$. from comparison with rate constants of similar reactions. The recombination rate for the phosphonyl radical is $3.3 \times 10^9$ $dm^3mol^{-1}s^{-1}$ (R = Et or Me)[2]. It is this di–alkoxy radical which will be referred to hereinafter as the primary species. Unless stated otherwise, the stock solutions employed were a 50:50 v/v mix of di–tertbutyl peroxide and di–ethyl phosphite, or a 10:10:3 v/v/v mix of di–tertbutyl

---

[1] A CIDEP study of di–tertbutyl peroxide, photolysed in a high concentration of di–tertbutyl phenol yielded emissive spectra with a weak A/E RPM pattern superimposed on this. Photolysis of the phenol alone in an inert solvent yielded a net emission overlaid by an E/A component. Fig (5.2.2) indicates that peroxide is dissociating primarily through a singlet state.

[2] Values come from Landolt – Börnstein Neue Serie II (Pub. Springer Verlag Berlin 1983). Reaction rates were taken from sub–vols. 13c and 13d; comparative coupling constants were taken from 17b and 17c.

Fig.(5.2.2) The Spectrum Of 2,6 Di–tertbutyl Phenol.

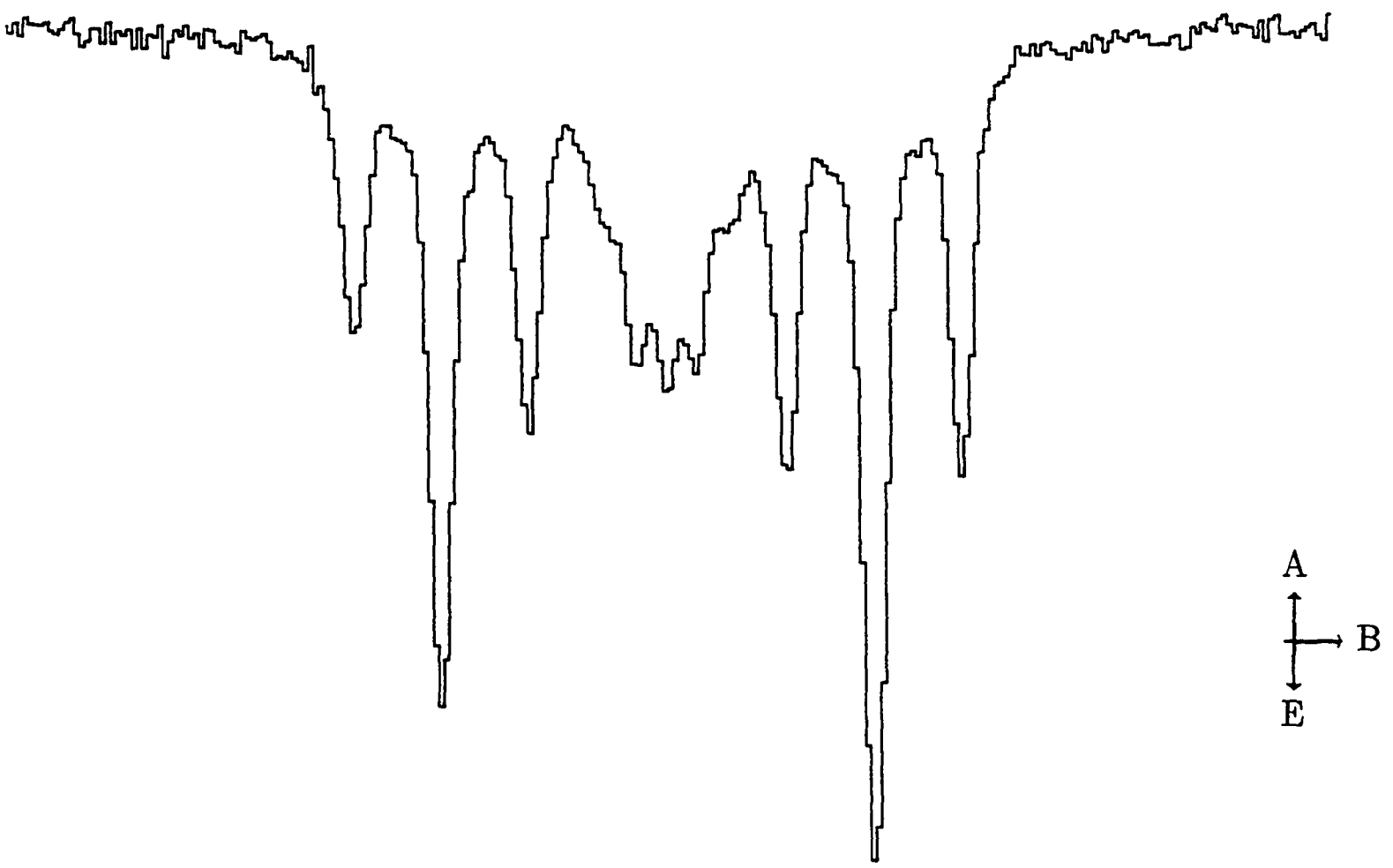


Formed by H–abstraction in a 50:50 vol/vol. solution of di–tertbutyl peroxide and propan–2–ol.

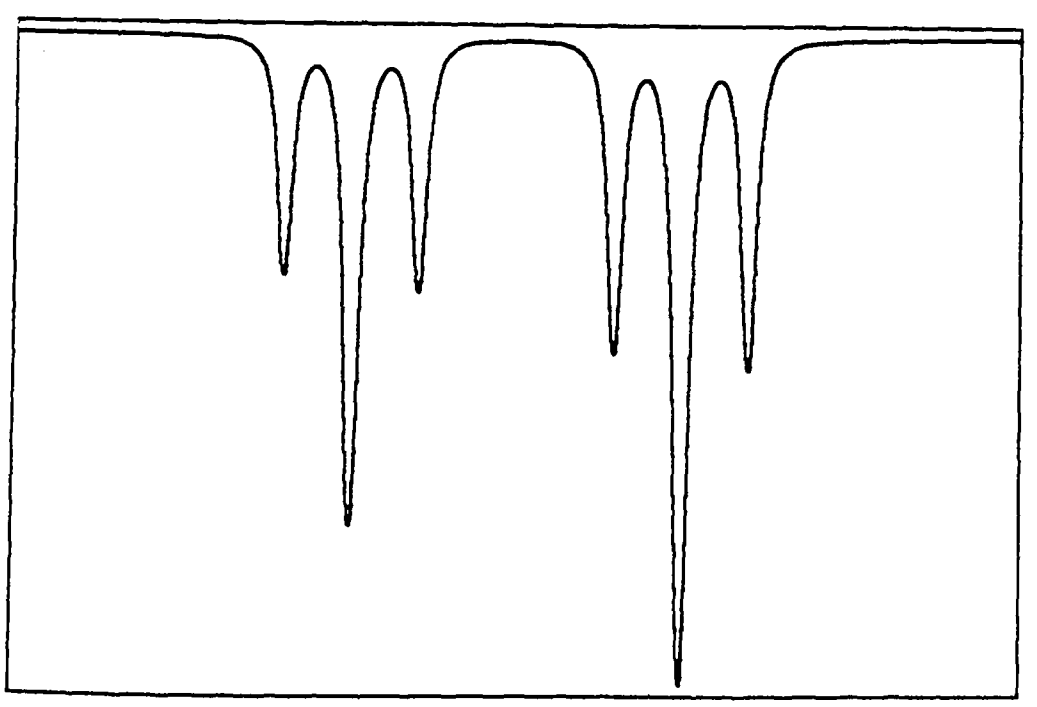

peroxide, di–methyl phosphite and di–chloro methane[3], so the phosphonyl radicals and their polarization are created instantaneously with respect to the spectrometer response. The phosphonyl spectrum exhibits a simple two–line E*/A pattern, $T_- \rightarrow S$ mixing arising from the large coupling constants ($a_p$(R=Me) = 70.8mT; $a_p$(R=Et) = 69.8mT). This spectrum has been well characterised elsewhere [17], where reference is made to contamination by abstraction of ethyl hydrogens. None such is apparent in Fig.(5.2.3). We are concerned with how this initial polarization will manifest itself in the radical adducts of these phosphonyl radicals with unsaturated compounds. The mechanism of addition and the products therefrom have been thoroughly investigated [18,19] but we need consider only three major findings: i) a high alkene concentration will inhibit the phosphonyl addition reaction by scavenging the $^t$butoxyl radical before it encounters a phosphite molecule – a situation that is carefully avoided in all these experiments; ii) a moderate alkene concentration will favour the formation of oligomers and telomers [20] ; iii) a low concentration of alkene will favour mono–adducts. In practice, our spectra correspond to an intermediate state between case ii) and iii). When an appropriate scavenger is added the phosphonyl radical will add to it to yield what shall be termed a secondary radical, in which the phosphorus retains electron spin density throughout the course of the reaction, but with a much reduced coupling in the product, typically of 6 to 10mT. For example,

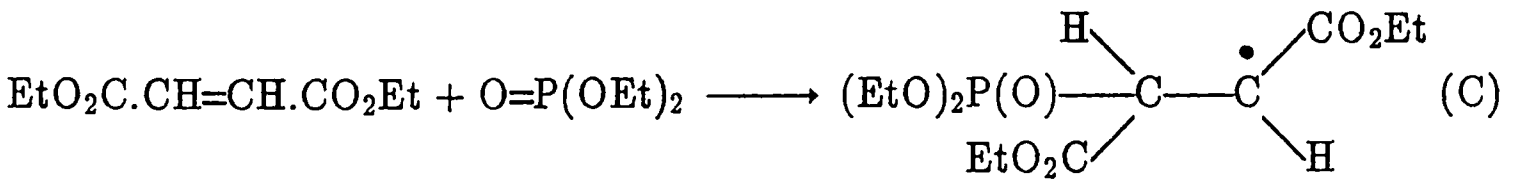


(C)

---

[3] All solvents and solutes were used in their purest commercially available form and, where necessary, they were dried over anhydrous sodium sulphite and de–oxygenated by passage of $O_2$–free nitrogen prior to, and during the experiment.

Fig.(5.2.3) The Spectrum Of The Di–ethoxy Phosphonyl Radical

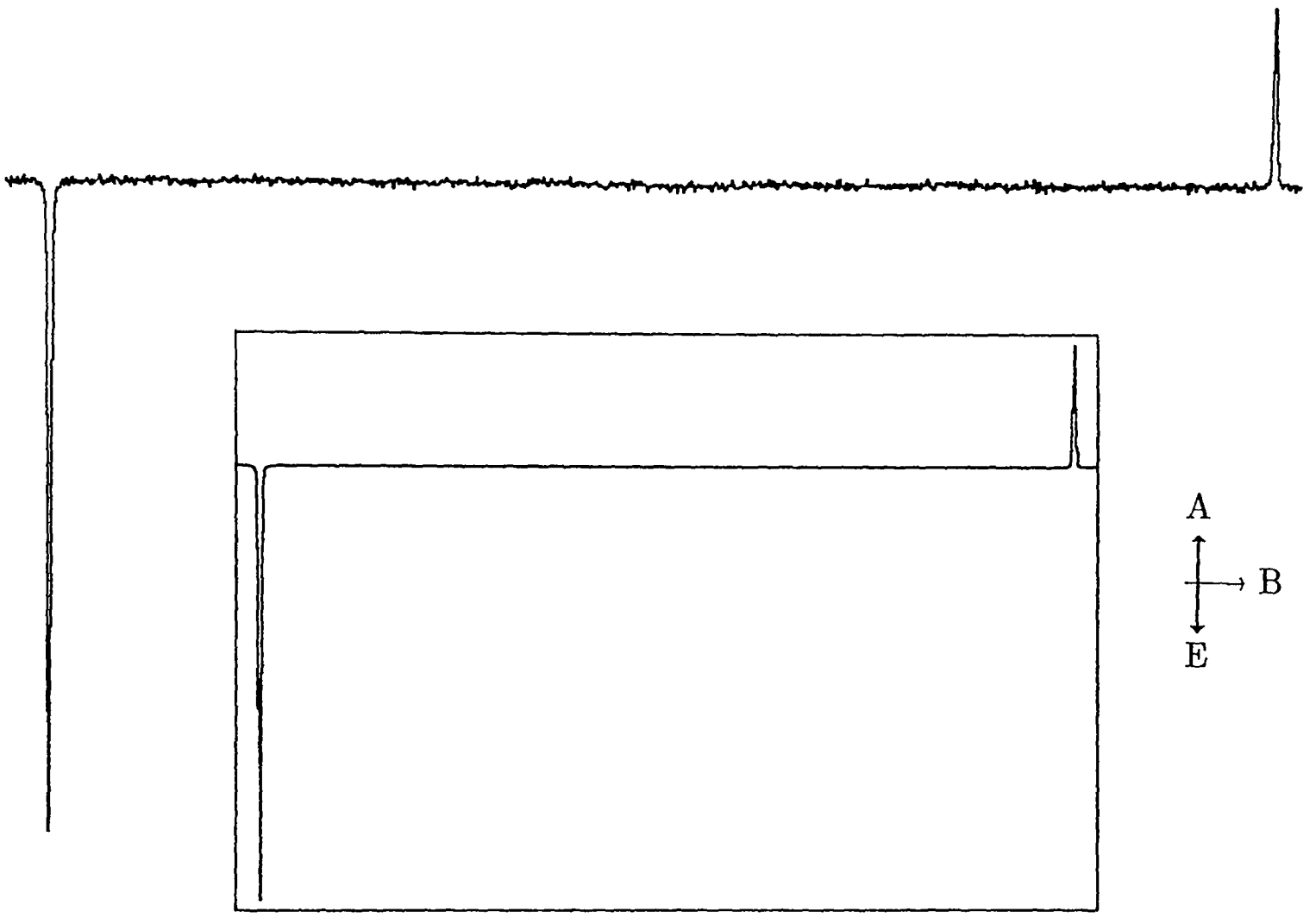


Produced on photolysis of a 50:50 vol/vol. solution of di–ethyl phosphite and di–$^{t}$butyl peroxide. A short $T_1$ and $T_2$ were used in the theoretical calculation, in keeping with a highly anisotropic electron–nuclear dipolar interaction[1]. $a_P = 69.8mT$, $a_{\gamma H} = 0.1mT$. Ratio of $ST_-:ST_0$ RPM is 0.57.

---

[1] Measured as $B_{parallel} = 11.3mT$ by Kerr C.M.L., Webster K., Williams F. *J.Phys.Chem.* (1975) 79, 2650.

The spectrum is shown in Fig.(5.2.4), in which both primary and secondary radicals can be simultaneously observed. Both di–ethyl fumarate and di–ethyl maleate were used in this study, and to all intents and purposes the adduct spectra were identical, indicating free rotation about the central C–C$^{\bullet}$ bond in the adduct radical.

Provided that polarization is allowed to build up fully between pairs of phosphonyl radicals before they are scavenged the adduct spectrum, recorded before relaxation destroys the signal and subsequent RPM comes to dominate it, should reflect the phosphonyl spectrum, with relative intensities of high and low field lines between the two spectra being equivalent. These conditions are met rather easily in this case. The simplest system to model is found to be that in which formation of adduct is sufficiently fast to ensure that the primary radical is entirely consumed within the first couple of microseconds, so that any polarization generated thereafter can only originate from pairs of identical radicals and, moreover, radicals in which the complications of ST-polarization are largely absent[4]. This is achieved by monitoring the time–decay of the phosphonyl doublets as quencher concentration is increased. A sequence of adduct spectra are displayed in Fig.(5.2.5), which indicate the gradations of behaviour with increase in time and scavenger concentration, from pure transfer polarization to almost pure RPM. Simulation of this effect is straightforward; analysis is not and the most one may infer from these field–swept spectra is that a polarization mechanism consistent

---

[4] Simulation of transfer–polarized spectra involves the calculation of hyperfine–dependent sub–spectra corresponding to each spin state of the nucleus that retains its coupling to the electron after addition. The sub–spectra are added together with a separation between their centres equal to that coupling in the product radical, and to this framework one may add, as appropriate, all other polarization effects. See appendix A.

Fig.(5.2.4) Spectrum Of Di–ethoxy Phosphonyl And Adduct With Di–ethyl Maleate


$0.5 - 1.5\mu$s post–flash. The apparent heights of adduct peaks are misleading, as the field resolution is not great enough, over this field sweep, to include the actual maxima of all lines.

Fig.(5.2.5) The Adduct Spectrum Of Di–ethoxy Phosphonyl With Di–ethyl Maleate.

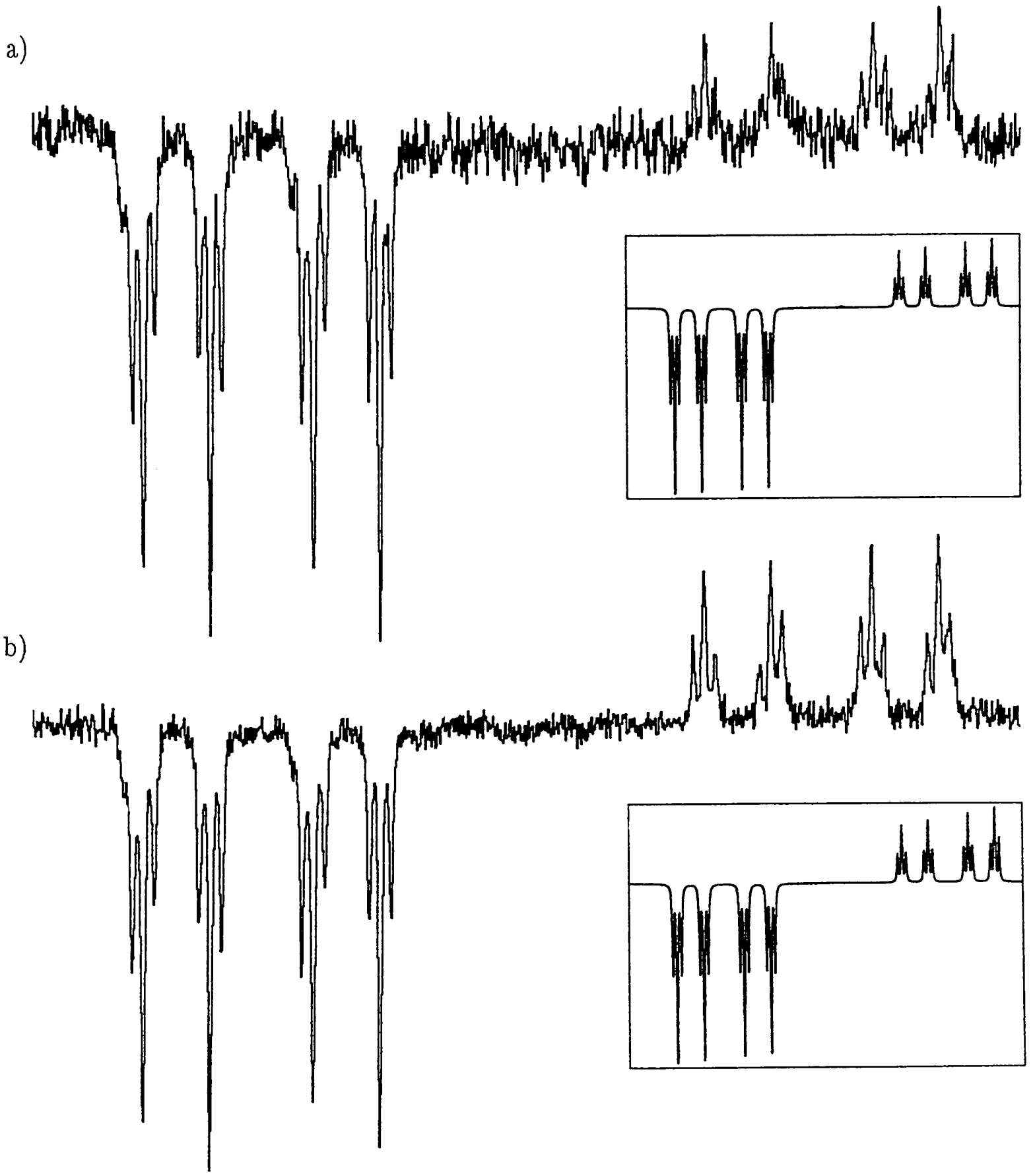

c)

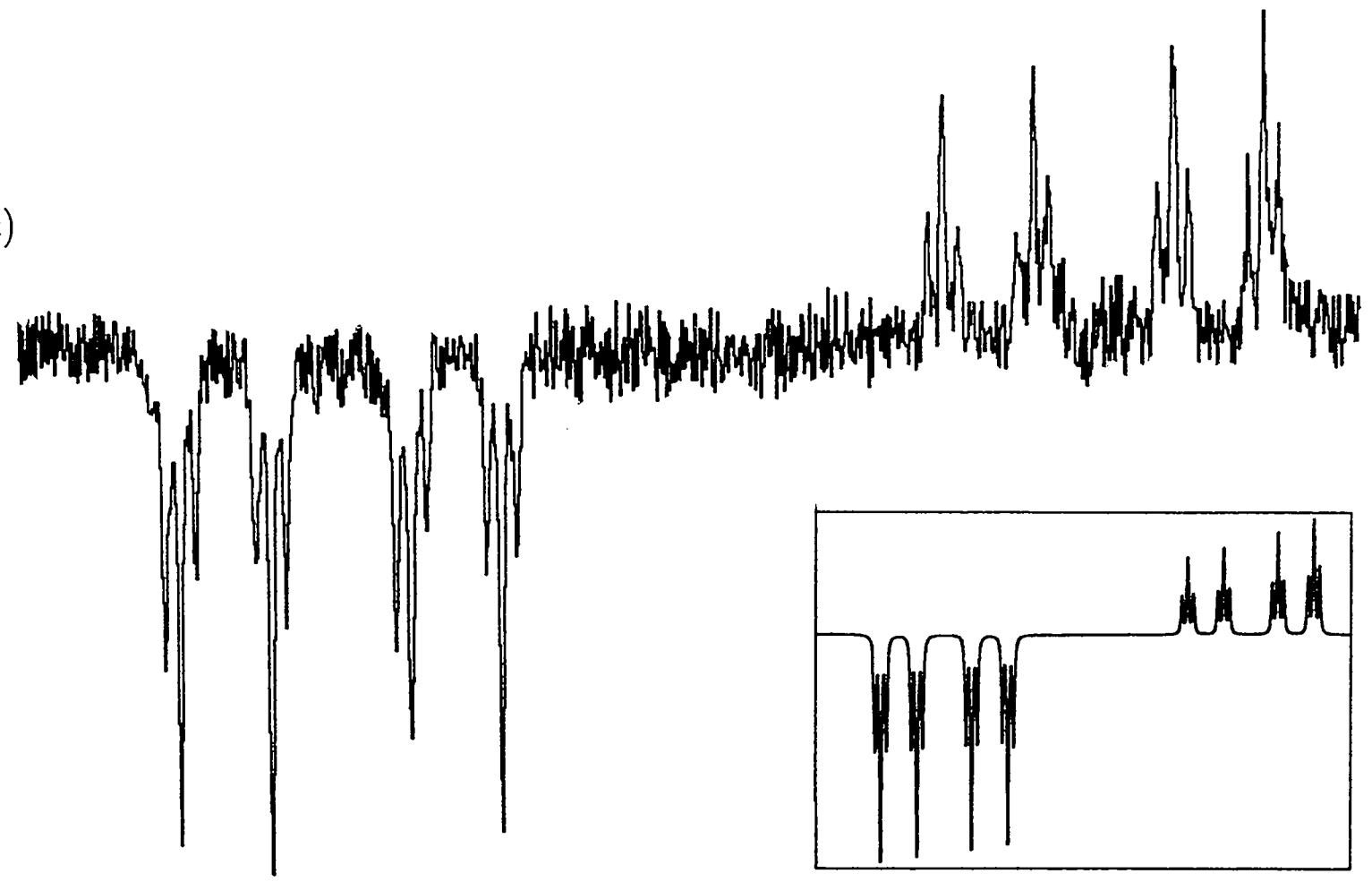

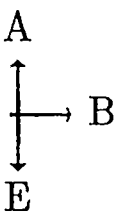


These are all recorded at 1.0 – 2.0$\mu$s after the laser flash. Concentrations of di–ethyl maleate radical scavenger are 0.13 Molar, 0.56 Molar and 1.03 Molar respectively, in the 50:50 vol/vol. stock solution of phosphite and peroxide.

These simulations use the following couplings: $a_P = 6.84$mT; $a_{\beta H} = 0.81$mT; $a_{\alpha H} = 2.03$mT; $a_{\delta H} = 0.13$mT. No simple relationship seems to hold between scavenger concentration and transfer:RPM polarization ratios.

Fig.(5.2.5) Spectra from the same solutions recorded at later times.

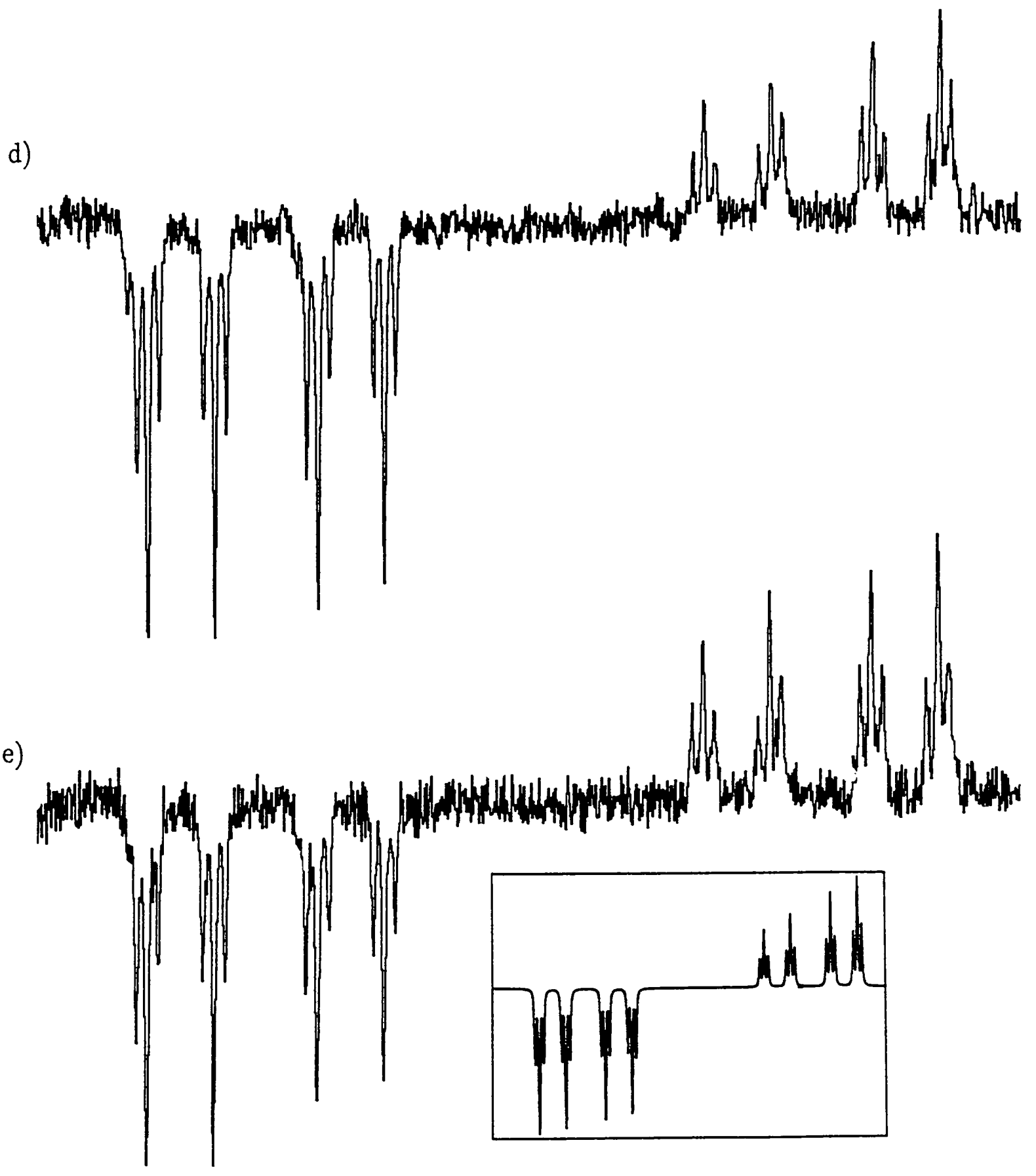

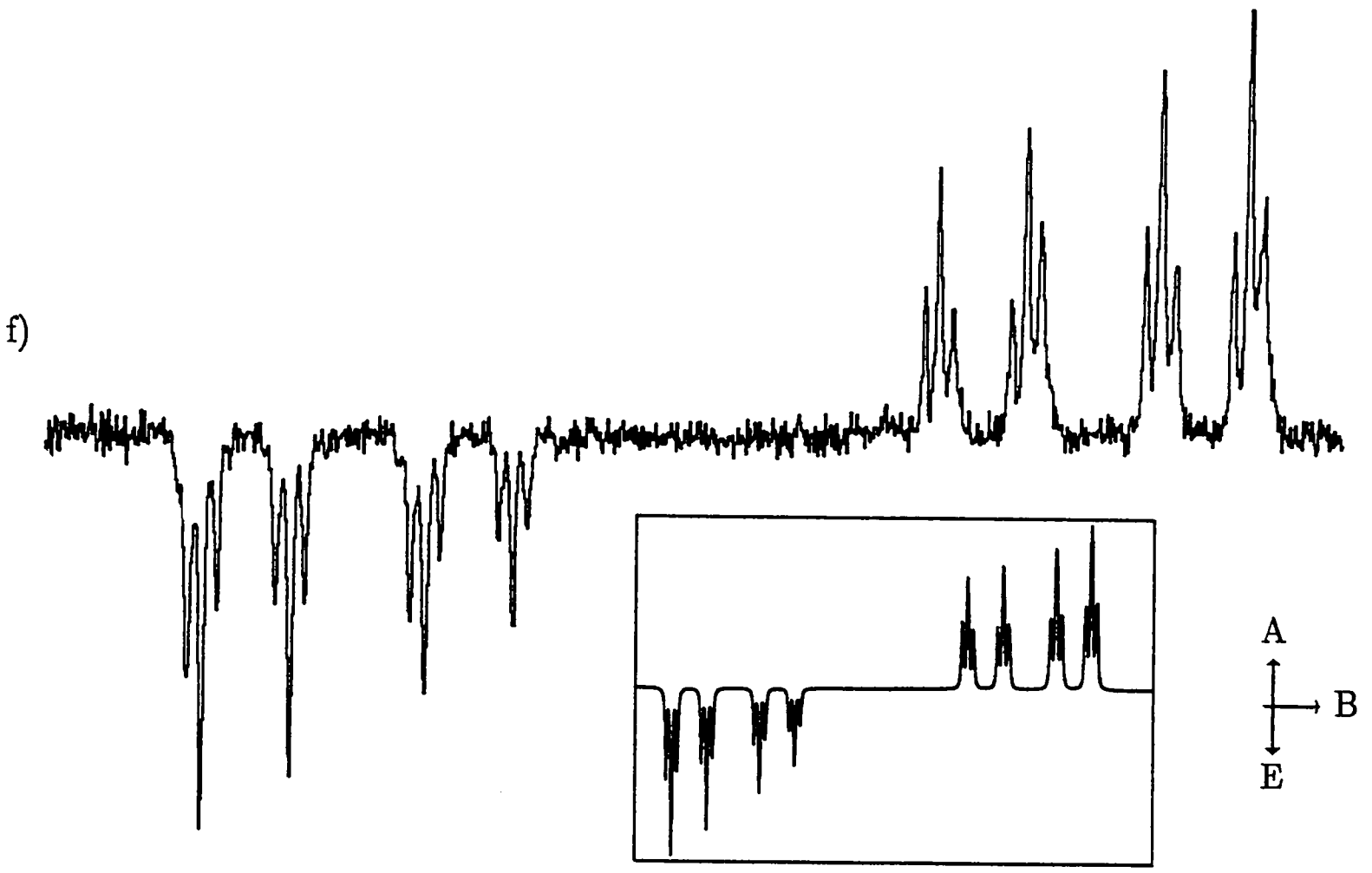


All spectra recorded over 2.0 – 7.0$\mu$s after the laser flash. By this time transfer polarization has relaxed considerably, and been largely replaced by normal F–pair RPM.

with transfer from a phosphonyl species seems to be occurring with a correlation of coupling constant between primary and secondary radicals. This kinetic problem will be returned to.

Turning aside from the polarization aspects momentarily, we may note that the relative intensities within each hyperfine sub–spectrum show inequalities from which a clear pattern of hyperfine–dependent relaxation emerges, the lines that relax the fastest appearing less intense than those that relax more slowly. Whenever RPM polarization or exchange can operate, the continual re–population of hyperfine states will tend to obscure any such effect so it is hardly surprising that it has rarely been reported by researchers in the field of CIDEP [21]. The advantages that transfer polarization confer in this respect are that degenerate exchange with ground state molecular precursors of the free radicals is eliminated, and the complicating effect of RPM hyperfine dependence is reduced: an initially polarized signal will be more sensitive to differential relaxation rates between hyperfine lines than a non–polarized one.

Drawing on the material of chapter 2, for a single *e.s.r.* transition [22,23],

$$1/T_1 = A + BM_i + CM_i^2 \qquad (5.2.1)$$

for which $M_i$ is the total magnetic quantum number for that line and B and C are constants resulting from the inner products of the $\underline{\underline{g}}'$ tensor with the hyperfine coupling tensor, $\underline{\underline{a}}'$, and of the $\underline{\underline{a}}'$ tensor with itself. The prime signifies that only the traceless part of the full tensor is considered. For $\varrho$ such coupled nuclei (5.2.1) must be extended to [24]

$$1/T_1 = A + \sum_{\varrho} B_{\varrho} M_i(\varrho) + \sum_{\varrho} C_{\varrho} M_i(\varrho)^2 + \sum_{\varrho \neq \xi} D_{\varrho\xi} M_i(\varrho).M_i(\xi) \qquad (5.2.2)$$

Thus, for a nucleus with a negative coupling constant the high–field line in the *e.s.r* spectrum corresponds to a nuclear spin of $+\frac{1}{2}$: if the $BM_i$ term dominates the relaxation then the high field line, for which the $BM_i$ term will augment the relaxation rate, will be relaxed fastest; the relative intensity of this line to the other will be reduced. Provided that the two important contributions to relaxation come from the B and C terms in (5.2.2) it should be possible to determine the sign of the coupling constant for each nucleus [25]. Unfortunately, no combination of signs of coupling constants involving just these parameters is sufficient to account for the observed spectrum. In our case it is possible to find a combination that includes the D term, which arises from the modulation of the coupling between two dissimilar nuclear spins, that reproduces the observed spectrum perfectly well. However, it will be seen to make it impossible to predict signs of coupling constants with complete confidence. For instance, with the cross–product between the couplings of $a_{\delta H}$ and $a_{\beta H}$, $D_{\beta\delta}$ the relaxation equation (5.2.2) may be condensed down to the form

$$1/T_1 = A^* + D_{\beta\delta}(M_i(\beta).M_i(\delta)) \qquad (5.2.3)$$

in which $A^*$ contains all other terms except for this one inner product. We do not know for certain what the sign of $D_{\beta\delta}$ is unless we know the precise form of $g'$ and $a_\delta{}'$ for this radical, and without this knowledge we can select either positive or negative couplings for $\beta$ and $\delta$ protons and produce a hyperfine–dependent relaxation scheme that is consistent with the observed spectrum. A tentative conclusion may be drawn, however, since $a_\beta$ is, according to theoretical calculation [26], positive. Assuming that

$|a_\alpha| > |a_\beta|$ [5] our relaxation expression for each triplet, from low to high field, is then

$$A^* + D_{\beta\delta}(+\tfrac{1}{2})(\pm 1) \text{ if } a_{\delta_H} \text{ is positive} \qquad (5.2.4)$$
$$A^* + D_{\beta\delta}(+\tfrac{1}{2})(\mp 1) \text{ if } a_{\delta_H} \text{ is negative}$$

which is compatible with the observed spectrum only if $D_{\beta\delta}$ and $a_\delta$ have the opposite sign. Ascribing appropriate spin states to each line in accordance with this gives a level–ordering diagram of

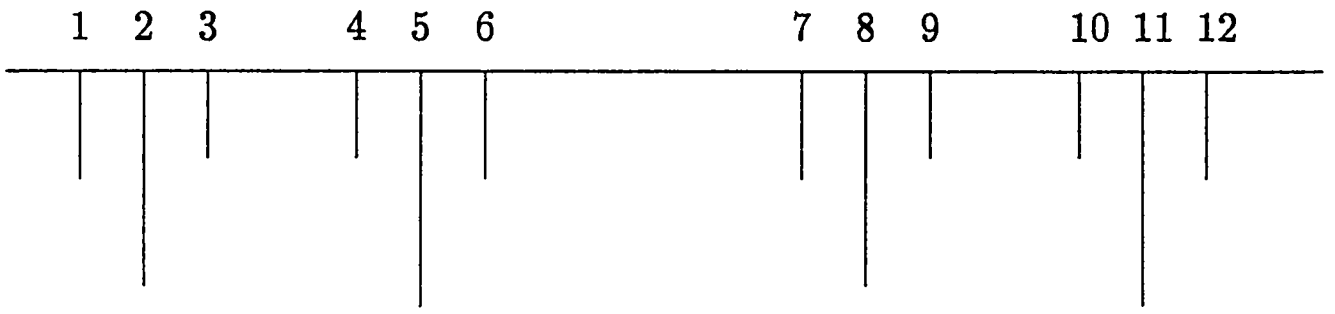


for the low–field half of the spectrum, for which the lines have the following nuclear assignments:

| | | | | | |
|---|---|---|---|---|---|
| $M_{\alpha_H}$ | $-\frac{1}{2}$ | $-\frac{1}{2}$ | $+\frac{1}{2}$ | $+\frac{1}{2}$ | |
| $M_{\beta_H}$ | $+\frac{1}{2}$ | $-\frac{1}{2}$ | $+\frac{1}{2}$ | $-\frac{1}{2}$ | |
| $\Sigma\ M_{\delta_H}$ | 1 0 –1 | 1 0 –1 | 1 0 –1 | 1 0 –1 | $a_{\delta_H}$ is positive |
| $\Sigma\ M_{\delta_H}$ | –1 0 1 | –1 0 1 | –1 0 1 | –1 0 1 | $a_{\delta_H}$ is negative |

---

[5] The size of $\alpha$–couplings in such species are consistently found to lie around 2mT whereas those for protons attached to carbons that are bonded to phosphorus are smaller than the equivalent phosphorus–free radicals. Landolt – Börnstein Neue Serie again provide the data.

The major finding of this study is that the coupling of phosphorus to electron in the first radical (primarily a contact interaction of electron with nucleus upon which it resides) is of the same sign as that in the adduct radical, in which the phosphorus is attached to a carbon atom $\beta$ to the radical centre. This result applies to all the spectra reported here and, indeed, for all phosphonyl addition reactions studied ,alkenes and alkynes alike.

(5.2.3) Adducts With Maleic Anhydride And Maleic Anhydride Derivatives

A considerable body of work has been published on maleic anhydride, primarily because of its importance in polymerization [28,29] and in the Wittig reaction [30,31]. It has also received a study purely for the CIDEP content of its photochemistry [32]; being weakly photo–active at 308nm, a small proportion of direct photolysis product is observable in some of the spectra which follow.

As found for the addition of phosphonyl radical to the di–esters of maleic and fumaric acid, the phase of the transfer–polarized spectrum mimics that of the initial phosphonyl, for both maleic and methyl maleic anhydrides, shown in Figs.(5.2.6) and (5.2.7) respectively. This latter case is particularly interesting for it illustrates two salient points: firstly, the two phosphorus sub–spectra in the adduct spectrum overlap in the central region, giving the second example of mixed–phase behaviour, this having been observed originally from the adduct of di–ethoxy phosphonyl radical with 2–methyl propene [13]; the second is that the two sub–spectra, corresponding to each phosphorus nuclear state, have a set of relative hyperfine intensities that are almost equivalent to those in the equilibrium spectrum (in other words, RPM and other hyperfine–dependent polarizations are overwhelmed by the transfer effect). Assuming that relaxation and reaction rates for the two possible radicals, namely –

Fig.(5.2.6) The Adduct Of Di–ethyl Phosphonyl With Maleic Anhydride.

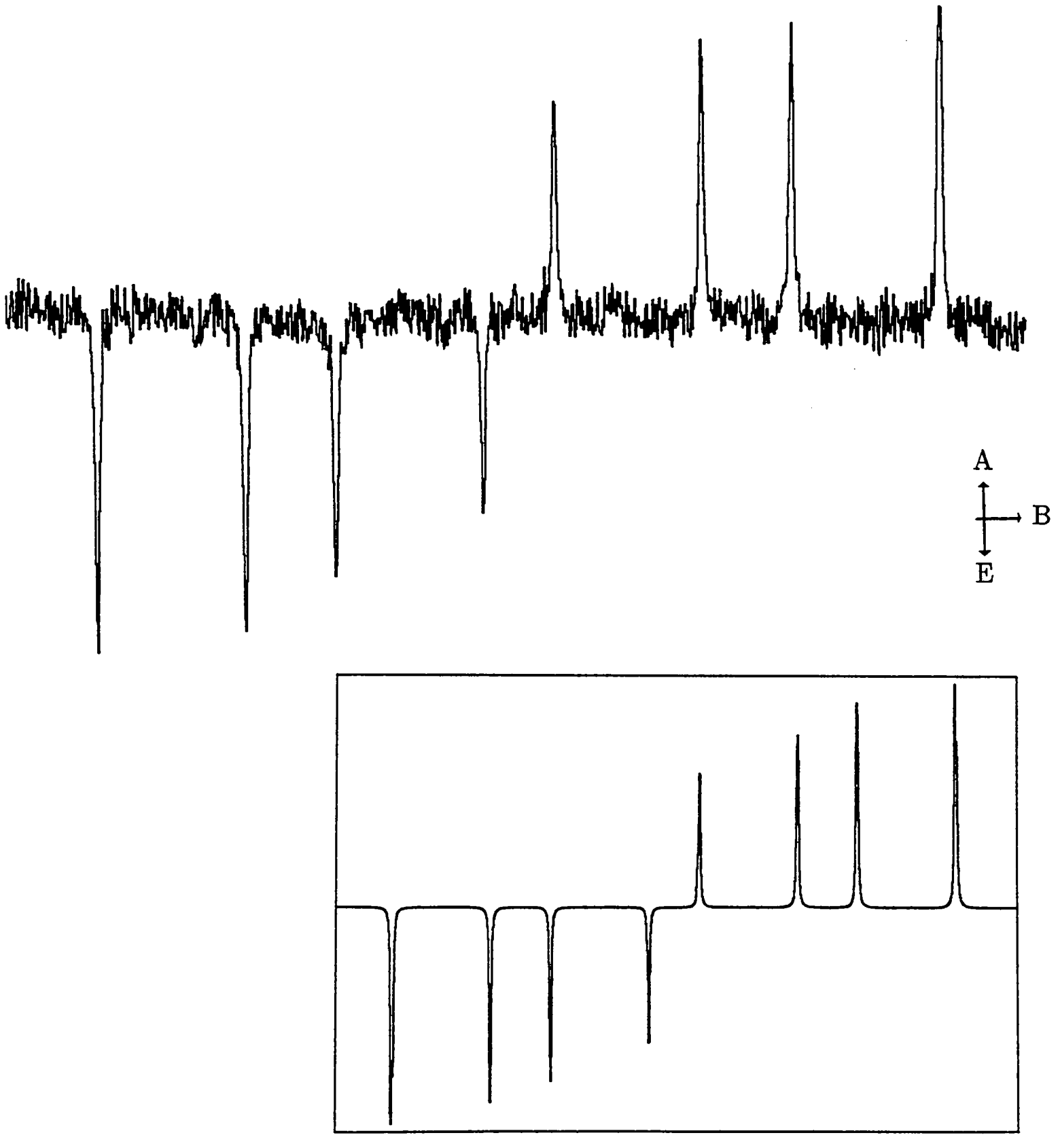


Spectrum recorded 0.5 to 1.5$\mu$s after the laser flash, over 14mT. The coupling constants used are $a_P = 6.31$mT; $a_{\alpha H} = 2.02$mT; $a_{\beta H} = 3.25$mT.

Fig.(5.2.7) Adduct Spectrum Of Di–ethyl Phosphonyl With Methyl Maleic Anhydride.

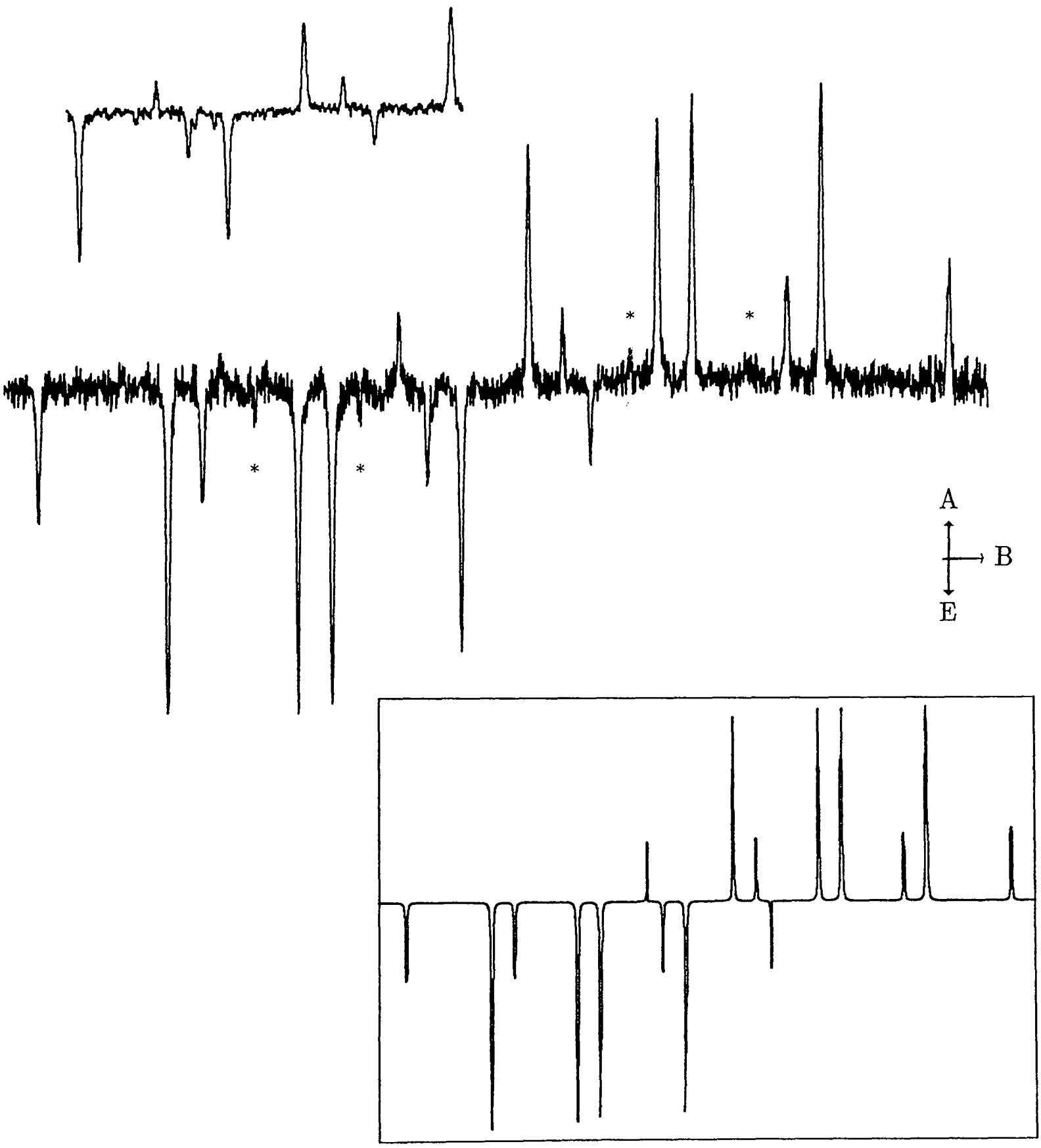


The complete scan is over 17mT, the central section of which has been examined separately to allow more efficient signal–averaging (Inset is over 6mT) The peaks of the minor product are asterisked. Coupling constants used in the simulations are $a_P = 6.23\text{mT}$; $a_H = 2.80\text{mT}$; $a_{Me} = 2.21\text{mT}$.

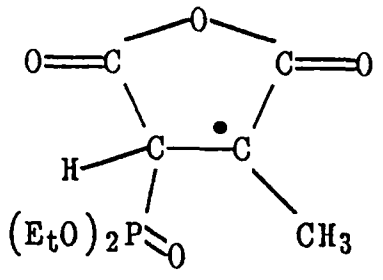

D

$a_P = 6.23mT$

$a_{\beta H} = 2.80mT$

$a_{Me} = 2.21mT$

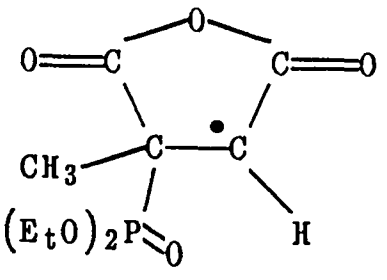

E

$a_P = 6.48mT$

$a_{\alpha H} = 1.84mT$

are equal, then their relative product yields may be assessed by "integrating" the spectrum (the digital nature of the field–swept spectrum allows this to be done simply by summing the values of all field points). This yields a ratio of D to E in the product radicals of 98% to 2% – a result in good agreement with other product analysis studies [33]: steric hindrance virtually precludes attack at the carbon atom attached to the methyl group.

In both cases, while transfer polarization is evidently present, the strong net emission observed between phosphonyl radical pairs is not seen in the adducts. Maleic anhydride is about 150 times, and methyl maleic anhydride about 30 times as susceptible to attack by phosphonyl as di–ethyl maleate [33] so that, even at the low concentrations of anhydride used in these experiments the likelihood of a pair of phosphonyl radicals encountering each other is vastly reduced. The net emission developed by $ST_-$ mixing is therefore minimised compared to the hyperfine–dependent $ST_-$ and RPM processes (a lower proportion of phosphonyls are adding on to the double bond after undergoing polarization by encounter with a second phosphonyl).

The higher the scavenger concentration the more it will disrupt the evolution of $ST_0$ and ST- polarization. At very high anhydride concentration the spectrum is dominated by an absorptive component that far outweighs the E/A RPM effect, even in systems where the only photo–active component is the peroxide[6], and in the above system an emissive TM, if any, would be predicted [32]. This implies that the absorptive phase arises upon radical–radical encounter, as a consequence of a hitherto unrecognised aspect of RPM since it cannot be accounted for simply by removing any possible ST- emissive elements of the spectrum. It is tempting to speculate that it is related to the unexplained absorptive component of the polarized propan–2–olyl radical spectrum. This matter will be returned to in chapter seven. At any rate, this observation does imply that direct photolysis of the anydride is insignificant at the lower concentrations used for these spectra, when compared to the efficiency of photolysis of peroxide and ensuing radical reactions. Were it to be an important photochemical pathway then we should begin to see the emissive TM coming through as concentrations were increased.

The interest in maleic anhydride as a reagent in the Horner–Emmons modification of the Wittig reaction [30,31] has led to a study of the electron affinities of maleic anhydride and its derivatives [35]. The free–radical analogue of a common Wittig

---

6 See, for example, the spectra recorded at high alkene concentration by C.T.Holder (Chemistry Part II Thesis, Oxford (1987)). The system used was a phosphite/peroxide stock solution similar to those employed here, addition taking place to 2,3–dimethyl but–2–ene. It is clear from these studies that the transfer of emissive polarization from the phosphonyl radical has been annulled by an absorptive polarization.

reagent, F, may be conveniently generated if a suitable base is present, since the H atom attached to the C–P carbon is the only labile one in the molecule.

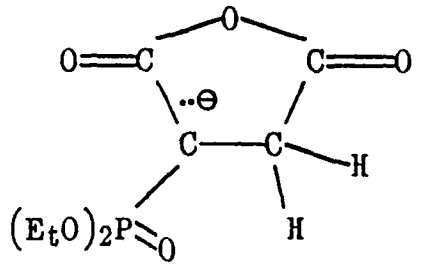

F

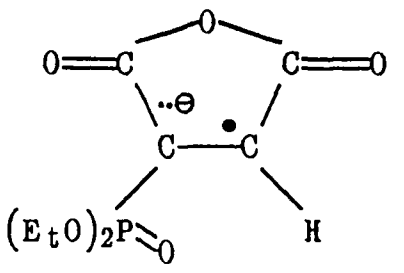

G

A suitable non–photoactive base was found to be sodium methoxide which, when present in low concentrations did not cause a severe disruption of the chemical system (whilst it would be impossible to prevent base–catalysed reactions such as the Michael addition from taking place they do not interfere with our observed photolytic reactions).

A four line spectrum should result, its growth coinciding with the disappearance of the initial adduct spectrum. This sequence of events is shown in Fig.(5.2.8). Since the overall signal intensity from the secondary radicals we are interested in has been reduced by their reaction, those unwanted signals from the direct photolysis of the scavenger are observed more clearly. There will be lines visible from the radicals shown below, all of which have been identified elsewhere [36]. Those of the carboxylate radical signal, in particular, will be enhanced.

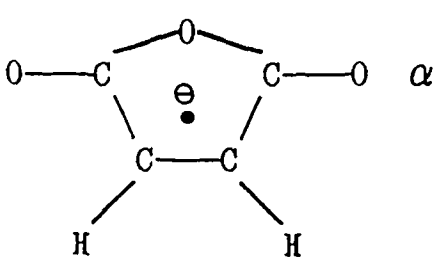

$\alpha$

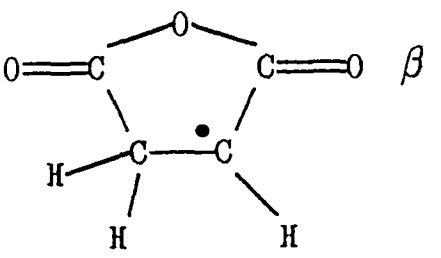

$\beta$

Fig.(5.2.8) Spectra Of The Maleic Anhydride / Di–ethyl Phosphite / Peroxide System.

Upon The Addition Of Base.

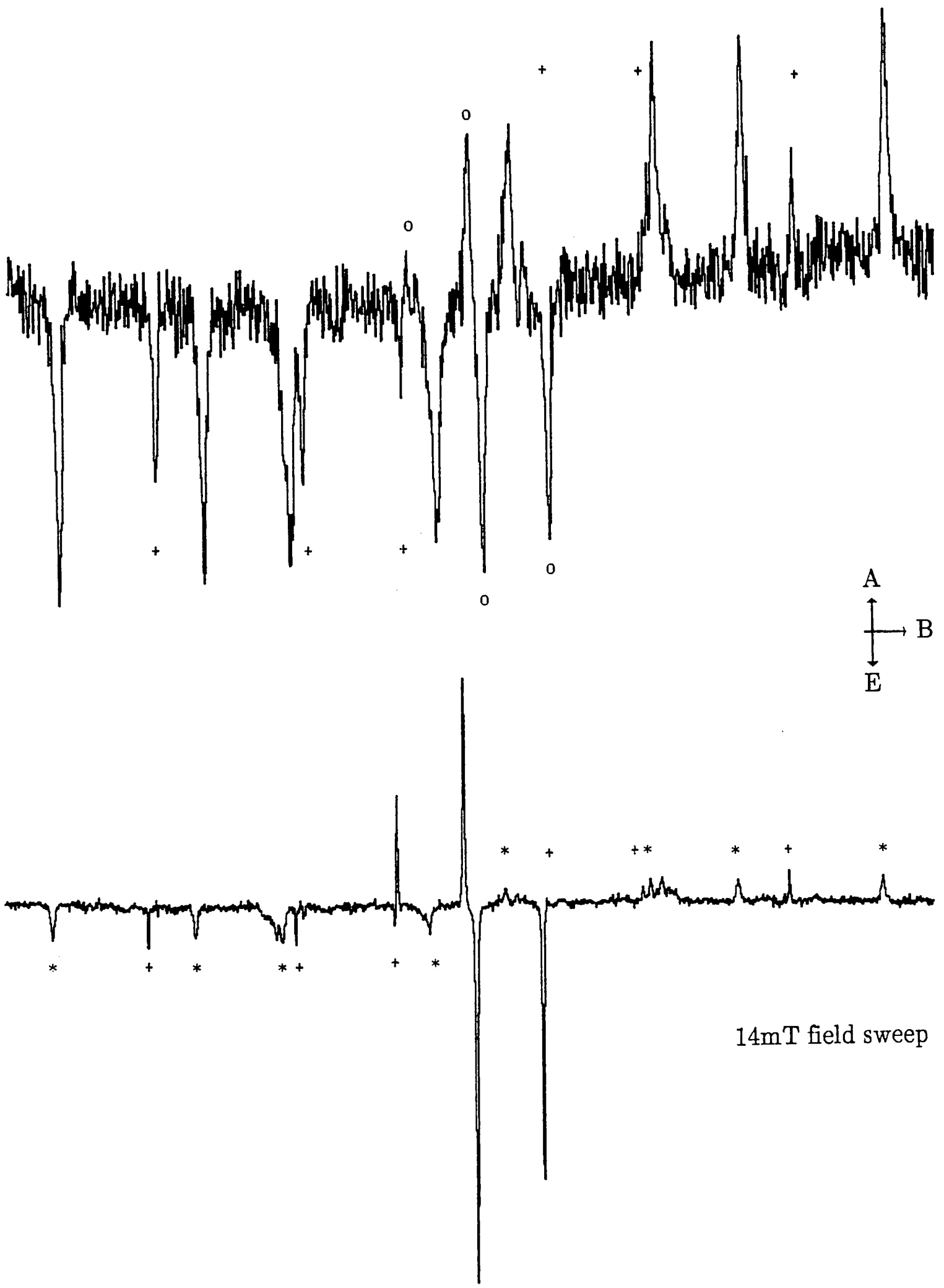

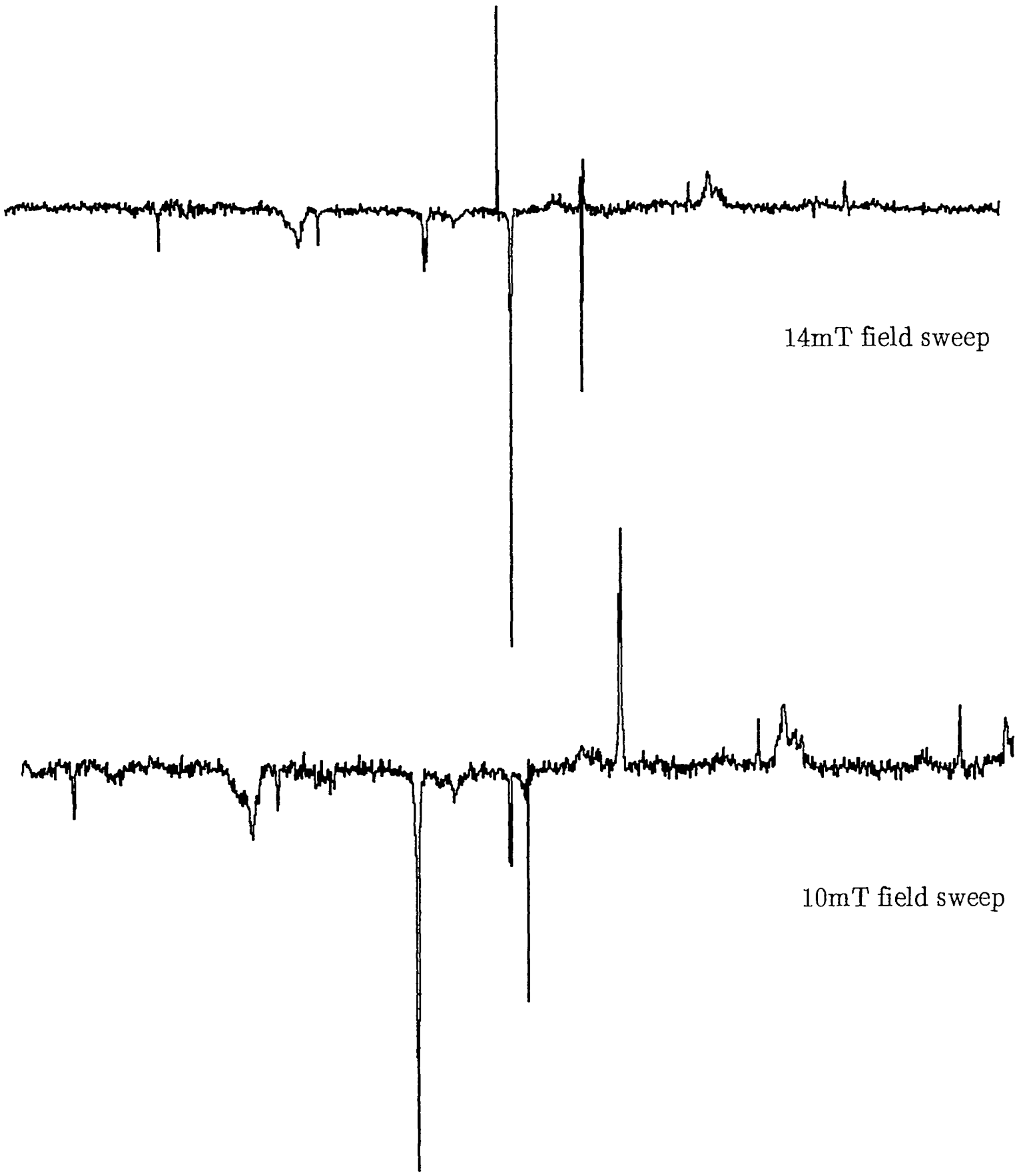


Spectra recorded at $0.1 - 1.0\mu s$, $1.0 - 2.0\mu s$, $2.0 - 3.0\mu s$ and $3.0 - 4.0\mu s$ post flash. Those species $\alpha$ through to $\delta$ are marked by crosses to differentiate them from the initial adduct lines (Fig.(5.2.6)) which are asterisked. Those lines resulting from species G are indicated by circles. The growth of these lines, at the expense of the initial adduct lines, is clearly shown.

Simulations of each known component to the spectrum are shown, using values from references [29] and [32] and the following, calculated from the spectrum, for the tertiary radical: $a_P = 1.13$mT; $a_H = 0.96$mT. This does not reproduce the spectrum exactly; the creation of a range of short–chain polymeric species, each with slightly different couplings would be expected to give the broader peaks, and these have not been modelled.

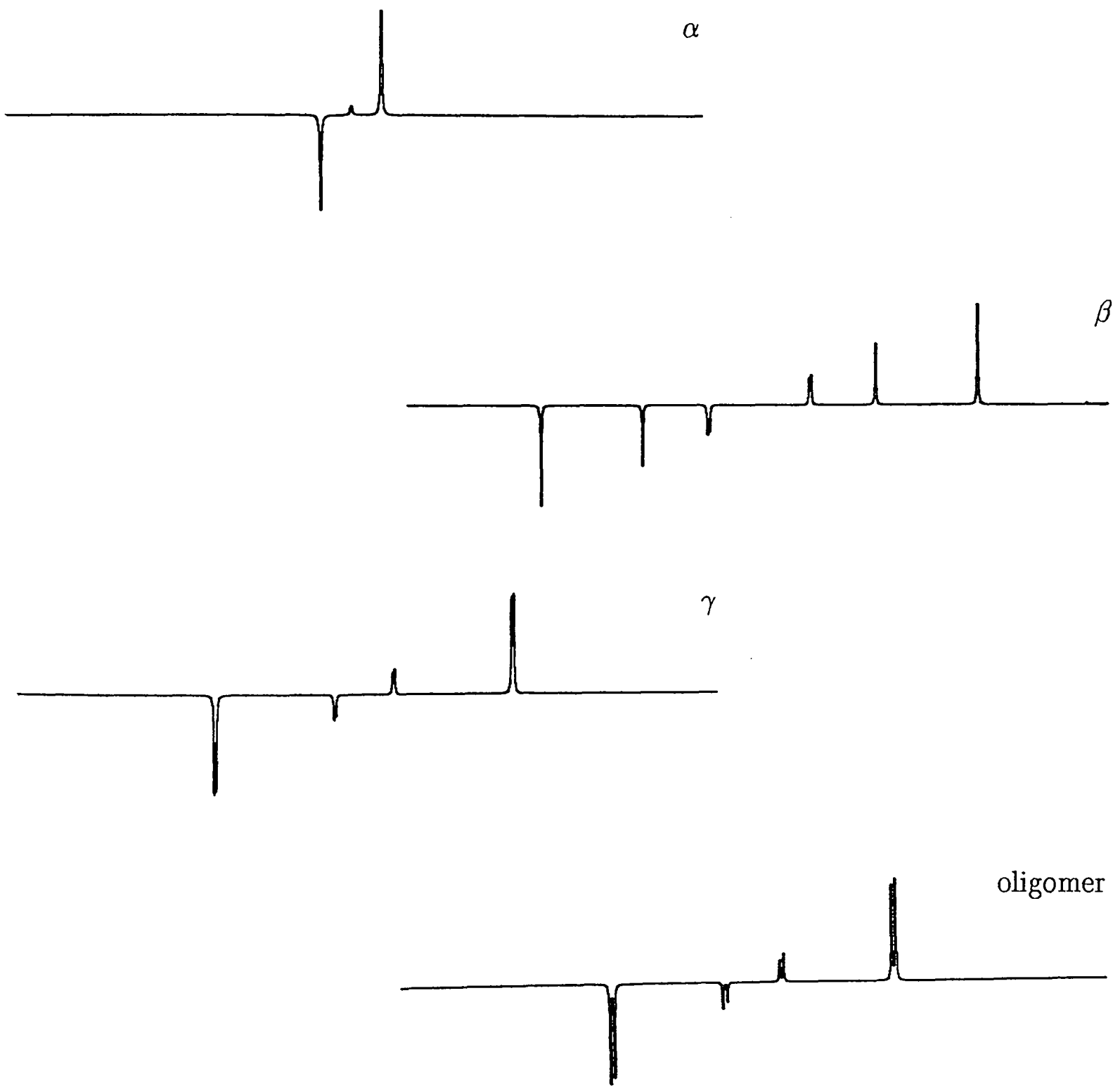


Pure RPM $ST_0$–polarized spectra.

Pure transfer–polarized spectra –

see appendix A for method of simulation.

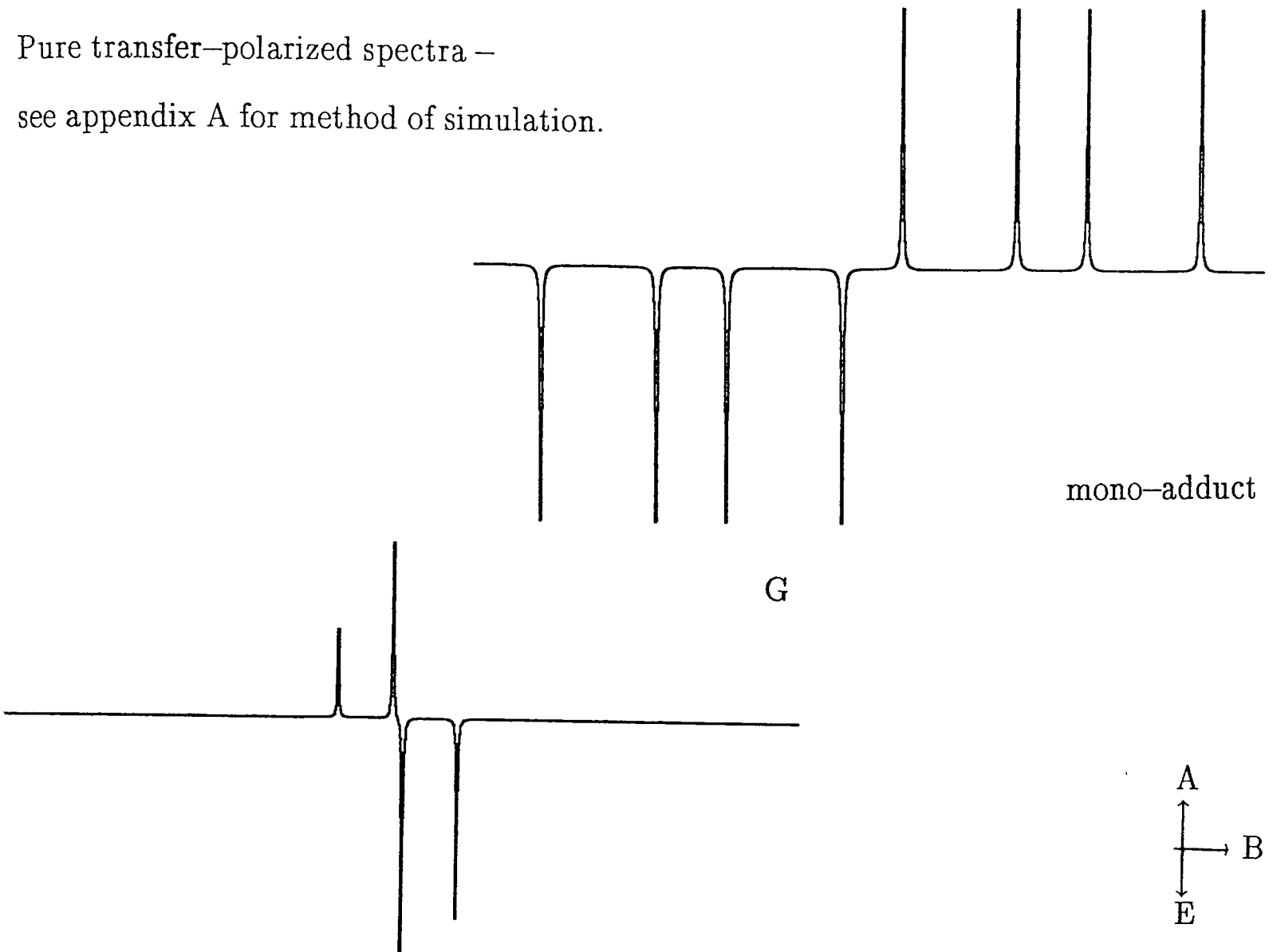

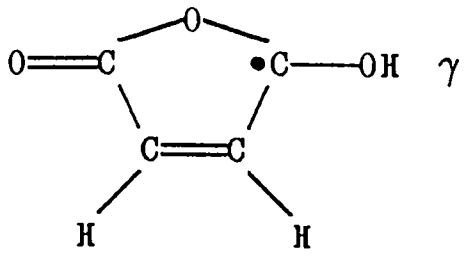

γ

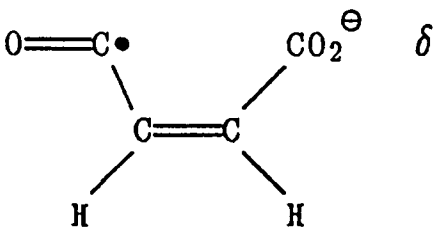

δ

These lines are marked with crosses; those from the initial adduct are indicated by asterisks. However, the phase of the central four lines is A/E at early times, reverting only slowly to E/A, as shown in Fig.(5.2.9). Clearly the rate of generation of these lines is too slow for the radical to have arisen from an excited singlet state reaction, and we must therefore conclude that the remarkable phase results from a reversal in sign of one of the coupling constants between the inital adduct and species G. Another surprising observation is the size of the couplings (0.96mT and 1.13mT). They are consistent with those calculated [37] and observed – Fig.(5.2.10) – for a closely related radical anion, H.

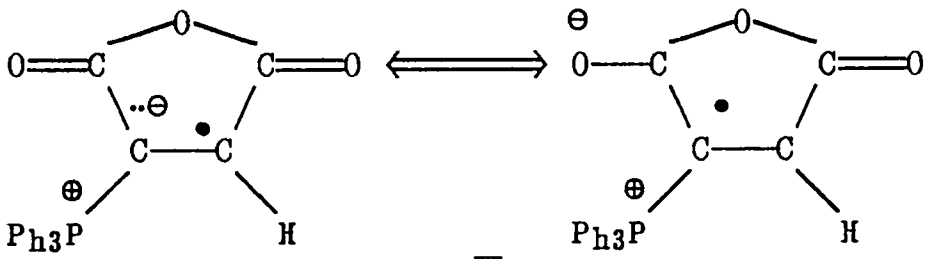

H

This radical was created by photolysis of the parent ylid in a di–tertbutyl peroxide/di–ethyl phosphite stock solution (Observation of this radical at low concentration was greatly facilitated by the strong ST$_-$ polarization conferred upon it by the much more numerous phosphonyl radicals).

We are unable to tell from this spectrum which coupling constant – P or $\alpha$H – has changed sign. Inspection of the equivalent methyl–maleic anhydride radical spectrum under basic conditions, Fig.(5.2.11), shows conclusively that it is the phosphorus

Fig.(5.2.9) The Central Four Lines Of The Maleic Anhydride System.


Spectra were recorded over $0.8 - 1.8\mu$s and $6.0 - 13.0\mu$s. In the latter the normal (weak) RPM has re–asserted itself, and is visible with an equilibrium component. Both spectra cover 3mT

Fig.(5.2.10) The Tri–phenyl Phosphoranylidene Radical

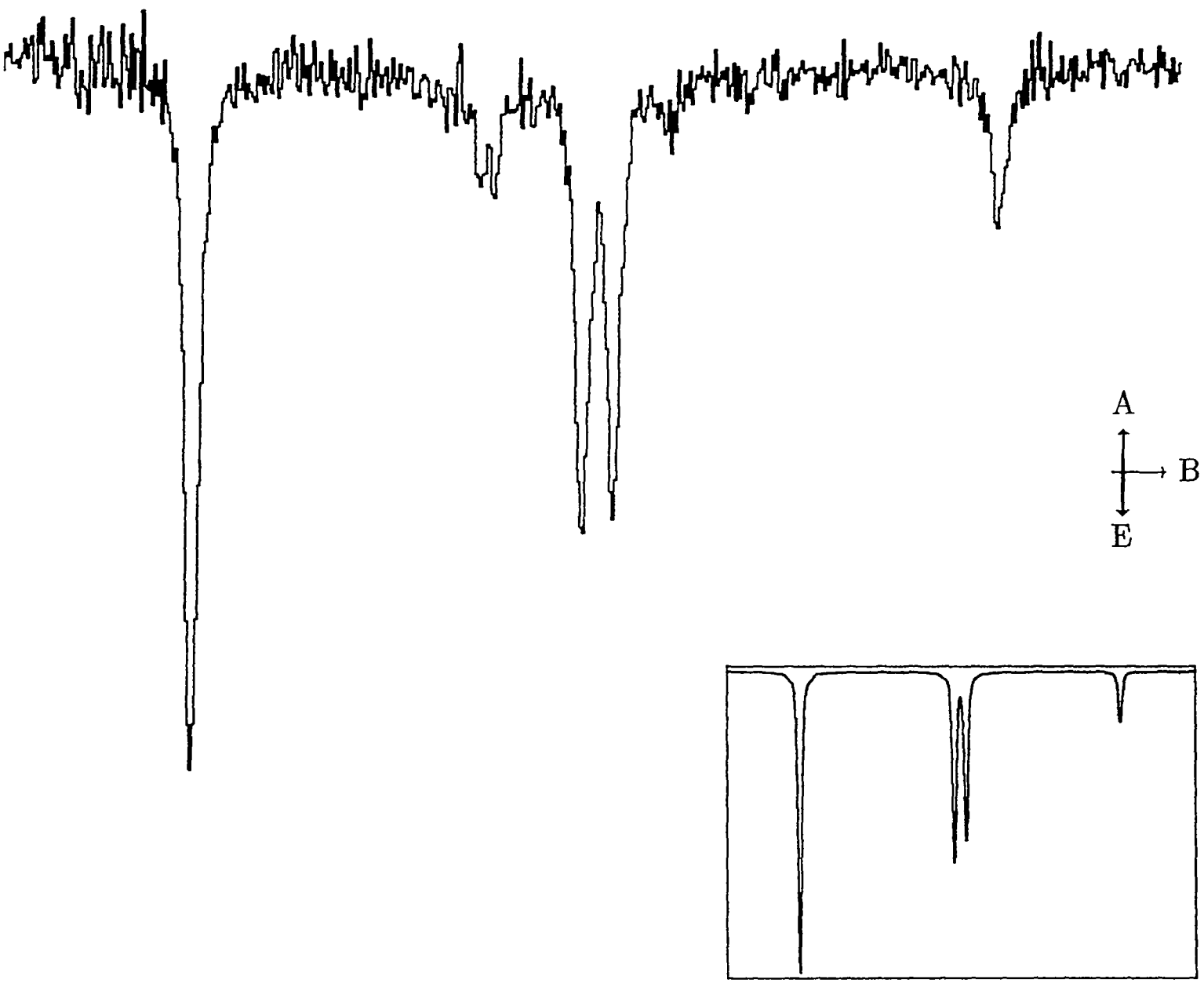


Recorded over $0.5 - 2.0\mu s$. Couplings are $a_P = 1.063$mT; $a_H = 0.987$mT. A 3mT field sweep is used.

Fig.(5.2.11) The Central Section Of The Methyl Maleic Anhydride Spectrum In The Presence Of Base.

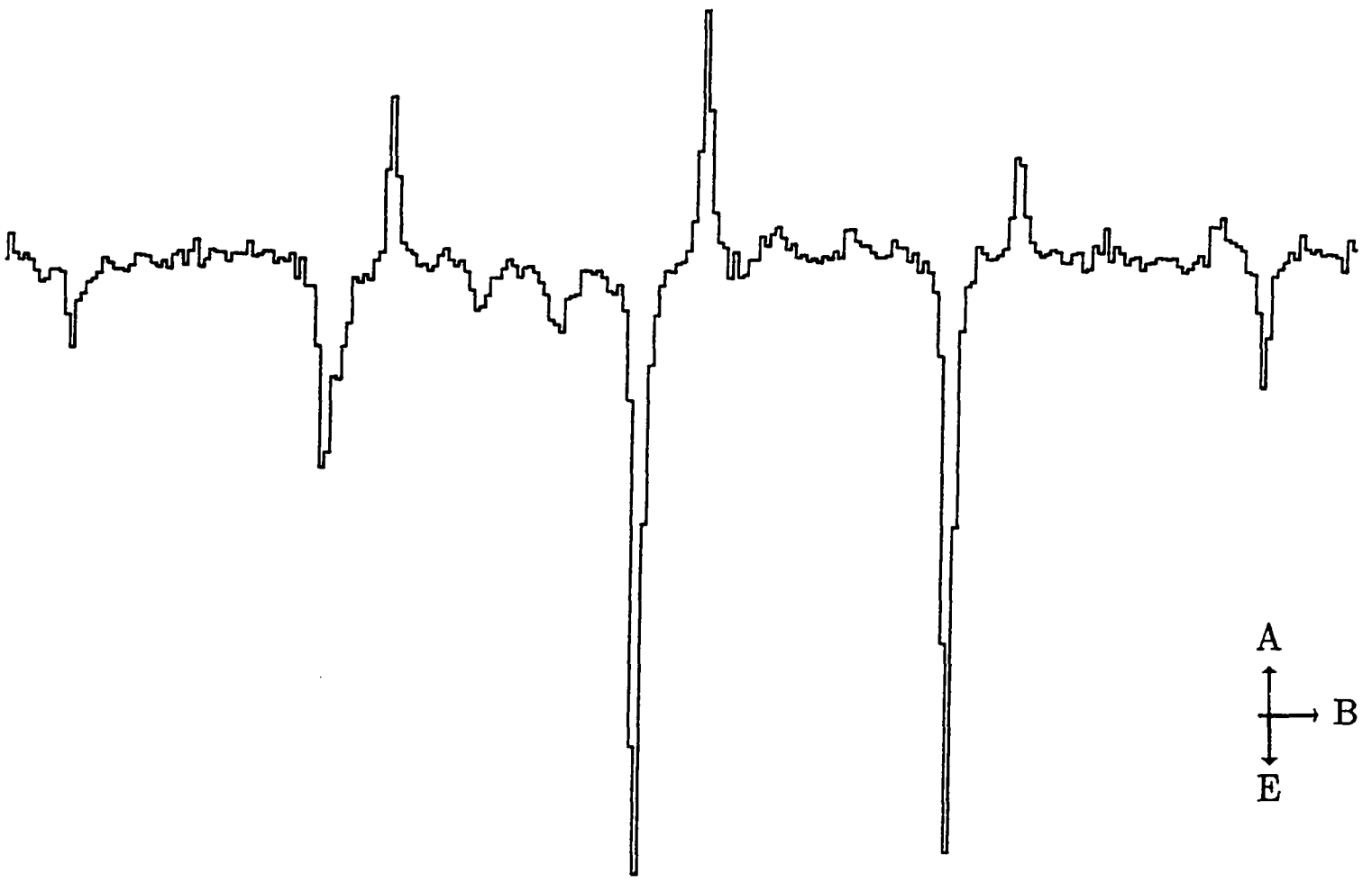


Recorded 1.0 – 2.0$\mu$s post–flash. The simulation uses the couplings $a_P$ = 1.64mT; $a_{Me}$ = 2.06mT. The lowest field line is already in emission: the greater spectral spread of this radical compared to that of species G means that transfer:RPM ratios will be lower, and it was not therefore possible to observe that line in absorption at any time after the flash, as a consequence.

coupling, with each phosphorus doublet being A/E in phase[7] (though the line to lowest field does not show in absorption as the normal RPM for this line is of the same magnitude but opposite sign to the imparted transfer polarization: the high–field lines have a much stronger transfer component). This is as we might expect, for the geometry of the intervening carbon atom will have been affected by the transition from tetra– to tri–valent bonding upon proton abstraction. According to the McConnell–Heller equation [38], the coupling for a proton can be described by

$$a_{\beta H} = (\lambda_0 + \lambda \cos^2\theta).\varrho_{2p_\pi} \qquad (5.2.5)$$

where $\varrho_{2p_\pi}$ denotes the spin density in the $2p\pi$ radical orbital, which in a cyclic five–membered radical with no $\pi$–conjugation is likely to be unity, and the other parameters are usually found to lie in the range (this applies to protons only) $0.3\text{mT} \leq \lambda_0 \leq 0.5\text{mT}$ and $4\text{mT} \leq \lambda \leq 5\text{mT}$. $\theta$ is the dihedral angle between the axis of the unpaired electron orbital and the bond to the nucleus under investigation. For a phosphorus nucleus attached to a five–membered ring the initial angle is estimated to be $60^\circ$ but an estimate of spin density in the $2p\pi$ orbital is difficult in this case, since it will certainly be reduced by interaction with the adjacent carbonyl function. Upon formation of the carbanion this would go to $90^\circ$, in which case the $\lambda_0$ term would dominate the coupling interaction; at a dihedral angle of $60^\circ$ the $\lambda$ term is most important. What is interesting is that according to this interpretation the $\lambda$ and $\lambda_0$ terms are, for this species, of opposite sign.

---

[7] Under no conditions could the di–methyl maleic anhydride adduct radical be induced to form any such tertiary radical.

An account of the chemical implications of this work has been published [39], together with the relaxation analysis and comments on the nature of the CIDEP observed.

(5.3.1) The Kinetic Problem

There are two methods of analysis of the kinetics of such sequential reactions; simply, we may monitor either the decaying signal of the parent radical or the signal of the daughter species as it grows in with time. Inherent in both is the assumption that there exists a relationship between the size of an *e.s.r.* signal and concentration of that radical giving rise to the signal. The complexity of the kinetic expressions that will be used lies only in this relationship and will reflect the way that polarization will change with concentration, in the first approach taken, and with the way that a transfer polarization signal will be "damped" by rate of formation of the associated radical in the second approach.

The first method will be seen to be flawed but, for the di–ethoxy phosphonyl radical that it is employed upon, this failing is minimised. It will also be seen to be the most generally applicable, since the crucial period of analysis lies well away from the first microsecond of radical existence, during which the spectrometer response will be critical. The central two lines in the spectrum of the tertiary radical will allow us to use the second method but, as indicated by the fact that this is the first time it has been demonstrated, this method will only rarely be able to be employed.

(5.3.2) Decay Of A Parent Radical Population

The adduct of di–ethoxy phosphonyl radical with di–ethyl maleate gives an adduct in which each of the hyperfine lines will develop RPM polarization over time, through

encounters with phosphonyl or other adduct radicals. Likewise, each di–ethoxy phosphonyl radical and its encounter partner are polarized but substantially more so than for the adduct encounters, as a result of the large $Q_{ab}$ term and the ST$_-$ effect. It is a reasonable assumption, therefore, to say that the polarization of each phosphonyl line may be taken as arising exclusively from phosphonyl/phosphonyl encounters. The reaction of phosphonyl with radical scavenger is simply a pseudo–first order reaction at the scavenger concentrations used. Spectral parameters and second order kinetics are extracted by fitting values to the field–swept spectrum and the decay lineshape, employing expression (2.3.25), which includes all kinetic and polarization–creating terms,

$$\dot{\underline{M}}(t) = \underline{\underline{L}}\underline{M}(t) + T_1^{-1}n(t)P_{eq}.\begin{pmatrix}0\\0\\1\end{pmatrix} + k_2n(t)^2P_f.\begin{pmatrix}0\\0\\1\end{pmatrix} + \frac{\dot{n}(t)}{n(t)}.\underline{M}(t)$$

The second term is included in the simulations though it may well be omitted as being insignificant when compared to the third and fourth terms (hardly surprising, considering the polarization expected from such a large $Q_{ab}$ term) at concentrations pertaining in these experiments. Comparison of rates of H–abstraction from similar species suggests a rate constant of around $10^7 dm^3mol^{-1}s^{-1}$ for the reaction with phosphite. We may expect, therefore, that geminate polarization would be negligible, the oxyl radicals having separated to several molecular diameters before reacting to give a phosphonyl pair. Interestingly, it was found necessary to include a geminate

---

[8] For instance, that of the reaction $(CH_3)CO^{\bullet}$ with $(EtO)_3SiH$ is $2 \times 10^6 dm^3mol^{-1}s^{-1}$. and competitive reaction rates for di–ethyl phosphite and silyl H–abstraction suggest that the former are about five times as fast.

polarization term, of the same magnitude as the F–pair term. This has been noticed before and remarked upon [17]. It may result from the non–uniform distribution of radicals (that is, that they are still grouped as pairs even after a few nanoseconds) though the spatial distribution of radicals, taken as pairs, is uniform. This is illustrated in Fig.(5.3.1), along with the "best fit" values.

Time–decays relating to two different scavenger concentrations are shown in Fig.(5.3.2) and simulations are shown alongside which use the scavenging pseudo–first order rate constants shown. This yields a value for the scavenging reaction rate constant for (C) of $1.6 \times 10^6 dm^3 mol^{-1} s^{-1}$. An error estimation on this figure is hard to gauge, as the assumption about the strength of polarization produced by adduct/phosphonyl pairs is not a reliable one; if these encounters do contribute substantially to the size of the phosphonyl signal then the rate constant we have derived would be too small; this experiment does, at least, set an upper bound upon it and one that compares well with chemically similar reactions. Further, the sensitivity of the decay curve to small changes in first order reaction rate is marked, and a variation of $\pm 0.3 \times 10^6$ is clearly detectable, the two calculated reaction rates being within this band. Since this reaction appears not to be diffusion controlled a temperature study was considered. Unfortunately, however, the complication arises at higher temperatures of a competing thermodynamically controlled attack on the carbonyl oxygen group, as demonstrated for the addition of Group IV radicals to maleic anhydride [40].

(5.3.3) A Kinetic Treatment Of Radical Formation

A more satisfactory method of analysis is to find a system in which the time dependence of a resonance transition is effectively a function only of the current polarization of the parent radical and its rate of formation. If the parent radical has

Fig.(5.3.1.) The Low–field Line Of The Phosphonyl Doublet Spectrum.

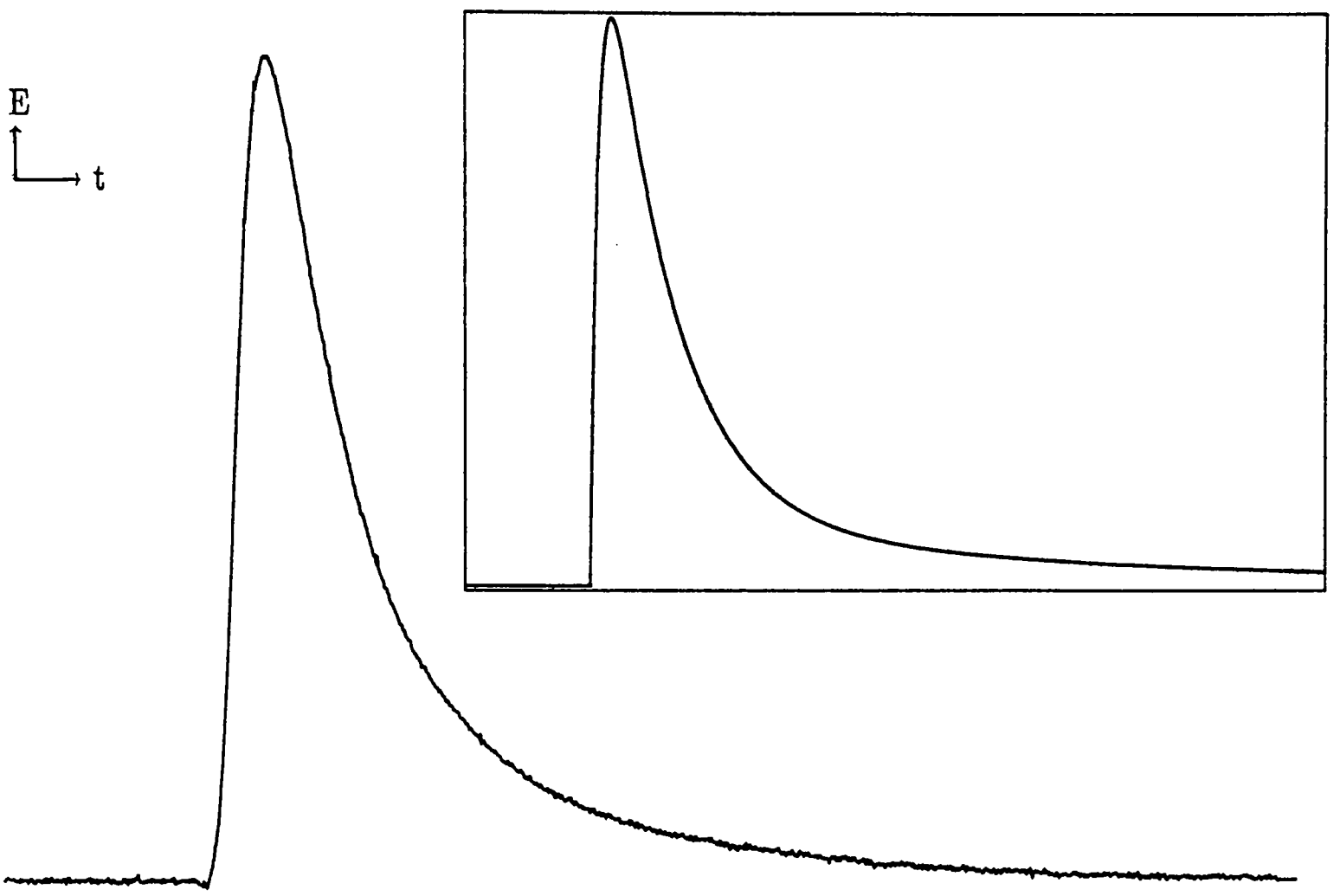


Trace covers 20.5$\mu$s. It was found necessary to include an initial polarization that was half the size of F–pair encounter polarization in order to model this curve accurately. Under these conditions the initial concentration of radical is not very important to the shape of the curve, as the initial polarization dominates.

Bimolecular recombination was taken as $3.3 \times 10^{9}$ $dm^3mol^{-1}s^{-1}$. Initial radical concentration was modelled as $5 \times 10^{-6}$ $mol.dm^{-3}$. $T_1 = 1.5\mu s$.

Fig.(5.3.2) On–resonance Decays For The Low–field Line Of The Phosphonyl Radical Under Two Scavenger Concentrations.

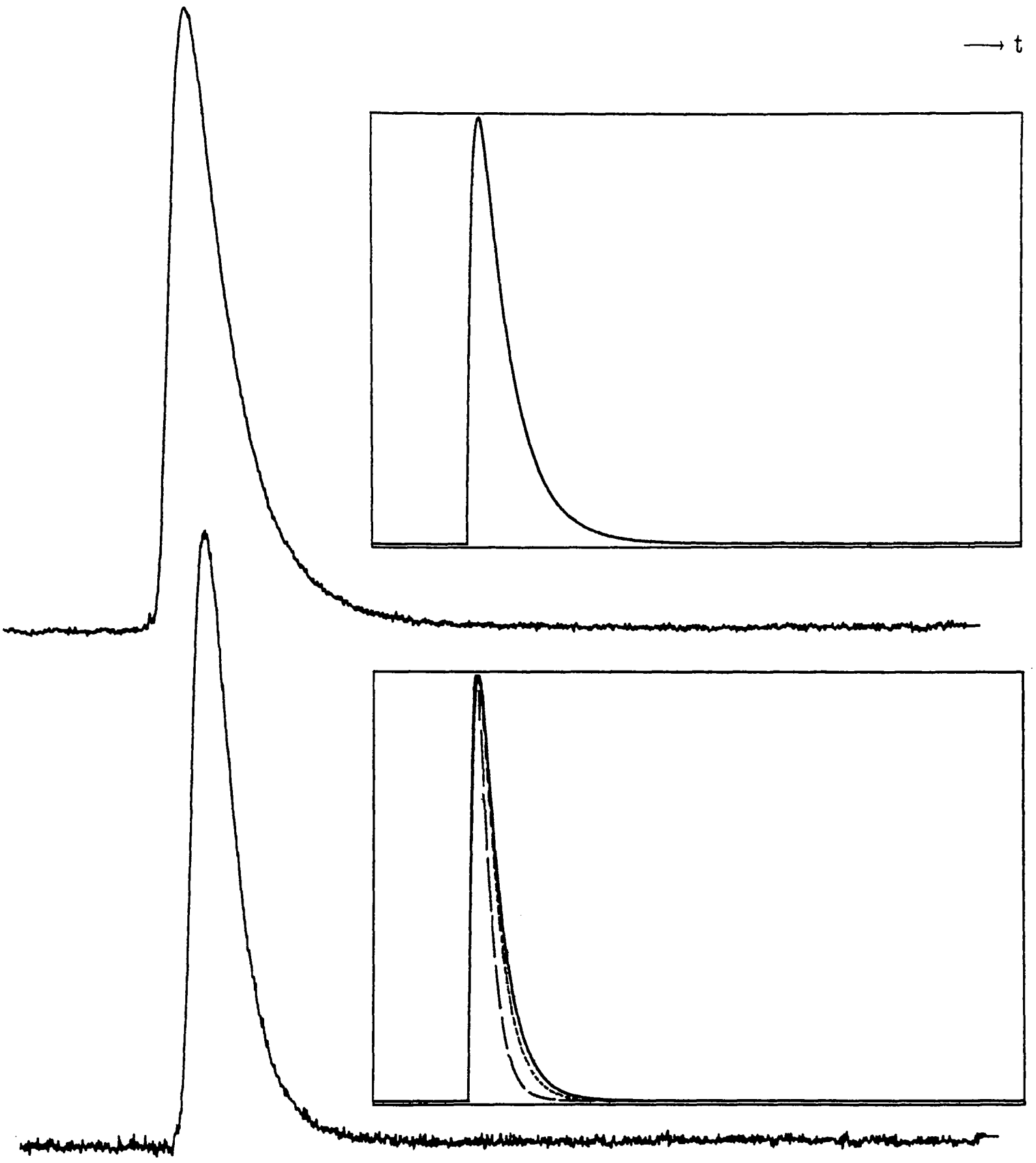


Each trace covers a 20.5$\mu$s time window. Scavenger concentrations were 0.30 Molar and 0.56 Molar di–ethyl maleate. Insets show the kinetic simulation of these curves together with, in the last case, two dashed lines, to give an idea of the sensitivity this method offers. Pseudo–first order rate constants of $5 \times 10^5$ $s^{-1}$ and $1.0 \times 10^6$ $s^{-1}$ are best fit values. The two sample curves use the values $2.0 \times 10^6$ $s^{-1}$ – – – –

and $1.2 \times 10^6$ $s^{-1}$ · · · · ·.

developed a steady state polarization by, say, F–pair RPM, and is likely to produce a daughter radical over a timescale for which this polarization remains essentially constant, then we may view the polarization of the secondary species as a convolution of the decay lineshape for that radical with its formation function. These are very restrictive criteria since the radicals invariably develop RPM polarization after creation, or undergo exchange–like processes that confuse the kinetics and cause rapid reaction. If we examine the tertiary radical created in the maleic anhydride system, however, we see that they are virtually all met: the central two lines are so close to the centre of the spectra of all radicals present in the system at the time they appear, so as to allow any contribution from the RPM to be satisfactorily ignored; the anionic nature of this radical means that kinetic decay by radical–radical reaction is impeded (and it is a relatively stable de–localised species anyway); since no ground–state ions of this species are present, and because it will be in low concentration, having been formed from three selective reaction steps, degenerate electron exchange will not be effective. Two further advantages are that the reaction rate is slow enough to ensure that no phosphonyl/anion encounters occur and that spectrometer response does not mask the signal growth. Reaction rate is fast enough, however, such that the relaxation behaviour and change in polarization magnitude of the parent species over the period of tertiary formation are not critical. A final point is that though these two lines are close together they do not overlap, either with each other or with any line of their precursor radical, so only z–components of magnetization can be transferred in the formation step.

As with the analysis in the previous section various spectral parameters must be extracted; an example is shown in Figs.(5.3.3) for the daughter radical ${}^{s}T_2^{-1}$. Fig.(5.3.4) shows the time dependence of both central lines over a 20$\mu s$ time span. It is revealing in that it not only demonstrates how slow the termination reaction for the radical anion is,

Fig.(5.3.3) A Fit Of $T_2$ To The Low–field Central Line

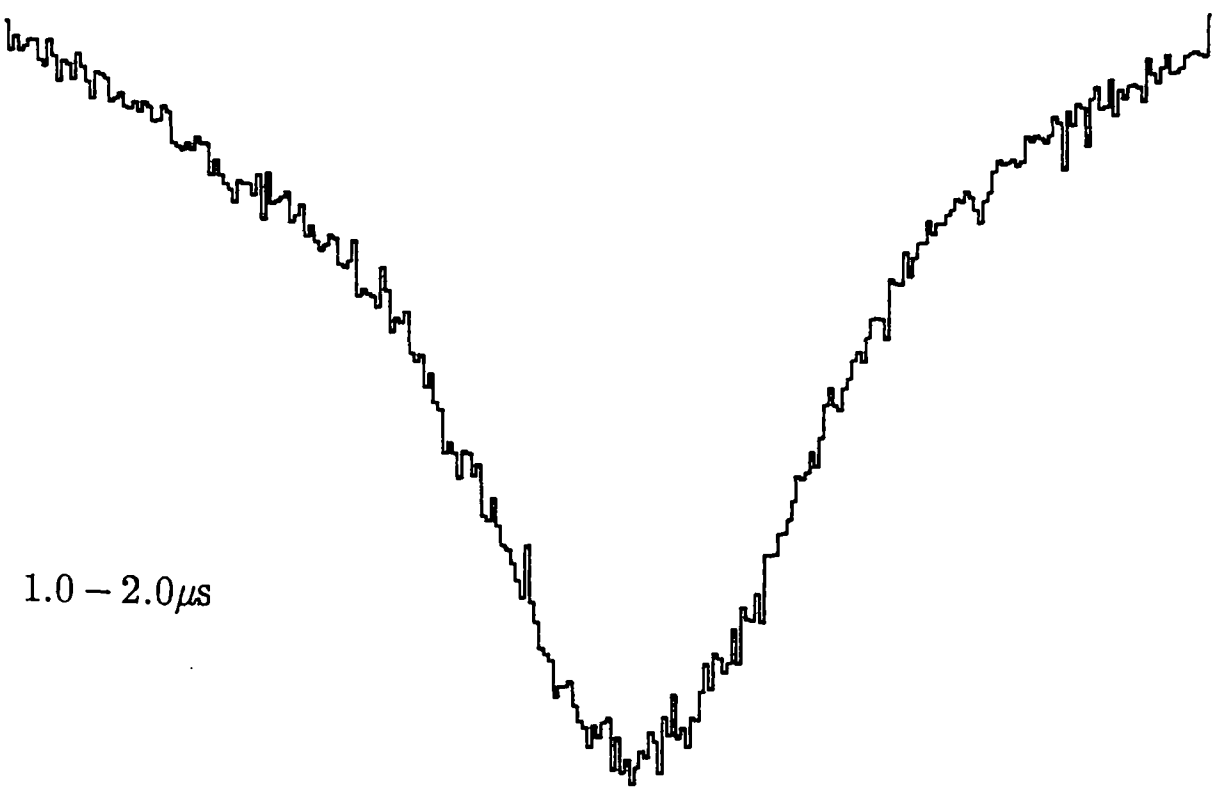


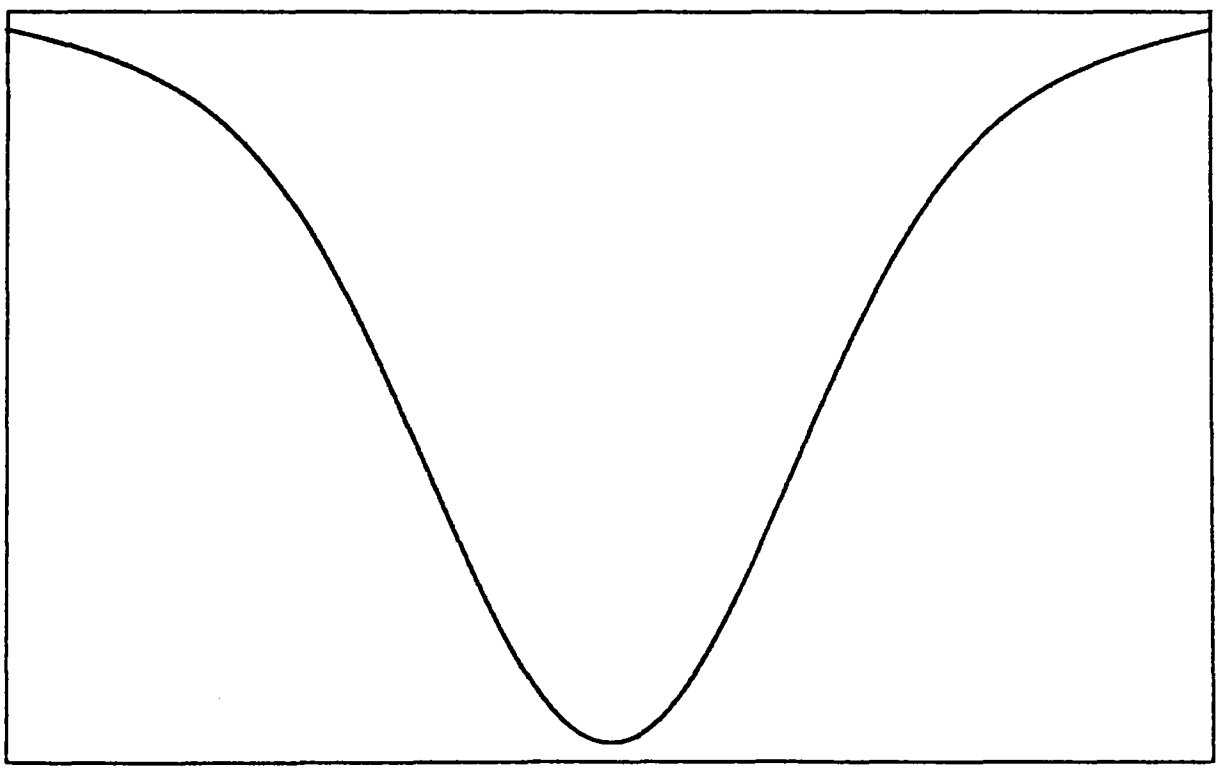

Sweep width is 0.05mT. A value of $T_2$ appropriate to this is 1.20$\mu$s. This is an approximate value, as the method of modelling relies upon the instantaneous creation of radicals, rather than their slow formation.

Fig.(5.3.4) The Two Central Lines In The Tertiary Radical Spectrum.

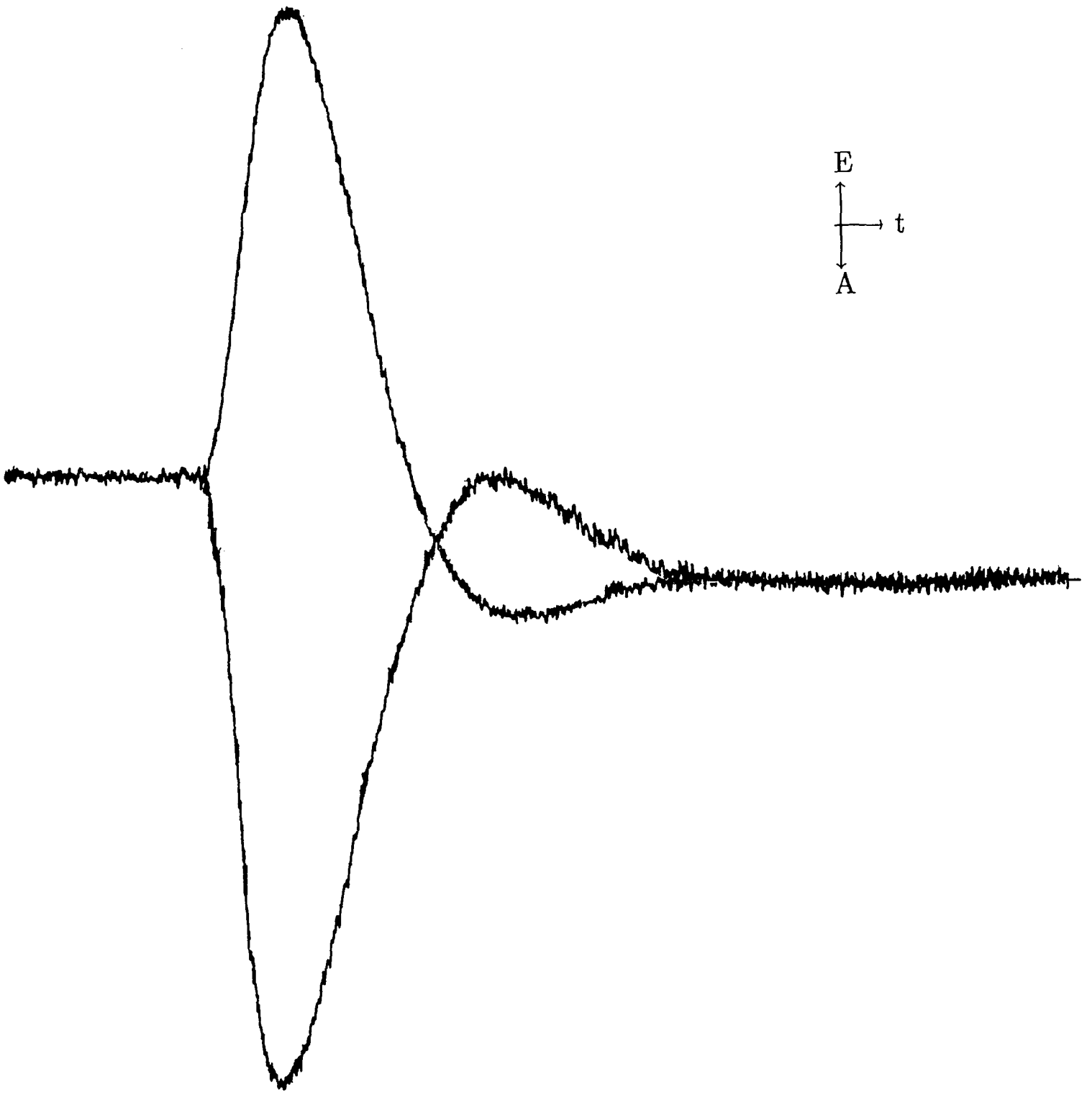


Taken over a 20.5$\mu$s window. The initial polarization can be seen to relax to an equilibrium level in about 12$\mu$s,

but it also shows that we are right to neglect RPM polarization, which should be equal and opposite between the two lines, and distinguishable when the transfer polarization has relaxed away. What follows is a heuristic approach to arrive at the equation for transfer of polarization from one radical to another. A fuller and rigorous mathematical description is given in Appendix D.

Let us first define some terms: the superscripts $^{p}$ and $^{s}$ will refer to the primary and secondary species; $k_1$ is the pseudo–first order rate constant for the formation of secondary radicals; $P_i$ is the initial polarization of the primary radical. If we look at the $_{r}$th component of the $_{k}$th hyperfine line of the secondary radical then the quantity we must evaluate is $^{s}M_{y,kr}$. However, if we assume that the time dependence of all lines in primary and secondary radicals are identical then the $_{k}$ and $_{r}$ subscripts may be replaced by a simple weighting factor, c, that relates the number of lines in the primary radical that are correlated with the line under observation in the secondary. For instance, in the species we are analysing, a proton coupling has been lost on producing the radical anion, so each line in the product species correl ates with two lines in the parent radical spectrum. Further, we assume that all lines of the secondary radical are well separated from all those in the primary one. This reduces the problem greatly for we only need to consider the z–component of primary radical polarization, as mentioned above.

At a time t the magnetization of the primary is given by

$$^{p}\dot{M}_z(t) = \{[P_i - P_{eq}].e^{-t/^{p}T_1} + P_{eq}\}.^{p}n(0).e^{-k_1 t} \qquad (5.3.1)$$

At the same time, the magnetization instantaneously inherited by the secondary must then be

$$\dot{{}^{s}M}_z(t) = ck_1{}^{p}M_z(t)$$

$$= ck_1{}^{p}n(o)\{[P_i - P_{eq}].e^{-t/{}^{p}T_1} + P_{eq}\}.e^{-k_1 t} \qquad (5.3.2)$$

This equation has two distinct parts: the terms including $e^{-t/{}^{p}T_1}$ contain the non–equilibrium polarization being transferred; the last term holds the equilibrium polarization of the primary radical and that, too, is introduced into the secondary magnetization.

As the system evolves to a time t′ this instantaneously transferred polarization will be transported into the y–axis according to a lineshape function $\Lambda_{yz}(t)$ where $\Lambda_{yz}(t)$ is just the solution of equation (2.3.3). Thus, if ${}^{s}\Delta\omega = 0$,

$${}^{s}\Lambda_{yz}(t) = (\omega_1/b)e^{at}.\sin(bt) \qquad (5.3.3)$$

where $a = -\frac{1}{2}\,({}^{s}T_1{}^{-1} + {}^{s}T_2{}^{-1})$; $b = [\omega_1{}^2 - \frac{1}{4}({}^{s}T_2{}^{-1} - {}^{s}T_1{}^{-1})^2]^{\frac{1}{2}}$

The magnetization inherited at time t has then evolved, by time t′ into[9]

$${}^{s}M^{*}_{y}(t')_{pol} = ck_1{}^{p}n(0)\left\{[P_i - P_{eq}].e^{-t/{}^{p}T_1} + P_{eq}\right\}e^{-k_1 t} \times {}^{s}\Lambda_{yz}(t' - t) \qquad (5.3.4)$$

where the star signifies that we are only considering that polarization transferred at time t. At the same time, the secondary radical will accrue its own equilibrium polarization

---

[9] This assumes that no secondary radical termination reactions occur over this time.

$$ {}^{s}M_{y}^{*}(t')_{eq} = cP_{eq}{}^{s}n(t').{}^{s}\Lambda_{yz}(t'-t)/{}^{s}T_{1} $$

or

$$ {}^{s}M_{y}^{*}(t')_{eq} = cP_{eq}{}^{s}T_{1}{}^{-1}.{}^{p}n(0)[1-e^{-k_{1}t}].{}^{s}\Lambda_{yz}(t'-t) \qquad (5.3.5) $$

The total magnetization in the y–direction at time $t'$ is the sum of equations (5.3.4) and (5.3.5) over all possible formation times.

$$ {}^{s}M_{y}(t') = ck_{1}{}^{p}n(0)P_{i}.\int_{0}^{t'} e^{-(k_{1}+{}^{p}T_{1}{}^{-1})t}.{}^{s}\Lambda_{yz}(t'-t)dt + $$

$$ ck_{1}{}^{p}n(0)P_{eq}.\int_{0}^{t'}\left[e^{-k_{1}t}-e^{-(k_{1}+{}^{p}T_{1}{}^{-1})t}\right].{}^{s}\Lambda_{yz}(t'-t)dt + $$

$$ c^{p}n(0)P_{eq}{}^{s}T_{1}{}^{-1}.\int_{0}^{t'}\left[1-e^{-k_{1}{}^{1}t}\right].{}^{s}\Lambda_{yz}(t'-t)dt \qquad (5.3.6) $$

or, more neatly

$$ {}^{s}M_{y}(t') = ck_{1}{}^{p}n(0)P_{i}.{}^{s}\Lambda_{yz}(t') \oplus e^{-(k_{1}+{}^{p}T_{1}{}^{-1})t'} + $$

$$ ck_{1}{}^{p}n(0)P_{eq}.{}^{s}\Lambda_{yz}(t') \oplus \left[e^{-k_{1}t'}-e^{-(k_{1}+{}^{p}T_{1}{}^{-1})t'}\right] + $$

$$ c^{p}n(0)P_{eq}{}^{s}T_{1}{}^{-1}.{}^{s}\Lambda_{yz}(t') \oplus \left[1-e^{-k_{1}{}^{1}t'}\right] \qquad (5.3.7) $$

where $a(t') \oplus b(t')$ signifies the convolution $\int_{0}^{t'} a(t'-t).b(t')dt$.

By this route we arrive at the same expression as that derived from a non–phenomenological approach. An illuminating substitution into (5.3.7) is to set $k_f$

equal to $(k_1 + {}^{p}T_1^{-1})$ and assume that $P_i \gg P_{eq}$. Under these conditions the form of (5.3.7) is

$$ {}^{s}M_y(t') = P_i {}^{p}n(0).{}^{s}\Lambda_{yz}(t') \oplus k_1 e^{-k_f t'} \qquad (5.3.8) $$

In other words, it is the result of a primary radical decay convoluted with the function $k_1 e^{-k_f t'}$, an effective formation function for polarized radicals.

(5.3.4) Application Of The Kinetic Expression

We shall apply equation (5.3.7) in its entirety to the signals derived from the central two lines of the maleic anhydride–derived tertiary radical, over a range of microwave powers and base concentrations (unfortunately the range of basic strengths is limited by the complications caused by base–catalysed reaction of the anhydride). Computation of this expression is straightforward but time–consuming, so it helps to have an idea of which parameters have the greatest influence on the time–decay. It is also worth pointing out that we may juggle the effective first order reaction rate by varying base strength, so that it lies in a region where the signal is most sensitive to changes in kinetics ( if the rate is too fast kinetic information will be masked by the spectrometer response).

As observation will centre upon the time–dependence of one line, exactly on resonance, the expression given for ${}^{s}\Lambda_{yz}(t)$ given above may be used (the field–frequency lock was employed to maintain precise resonance). The constant terms $c^{p}n(0)$ can be omitted as they will only affect the overall signal magnitude, so the actual expression used for all simulations was

$$
\begin{aligned}
{}^{s}M_y(t') \;\alpha\; k_1 P_i/P_{eq}.{}^{s}\Lambda_{yz}(t') \circledast e^{-(k_1 + {}^{p}T_1^{-1})t'} \;+ \\
k_1.{}^{s}\Lambda_{yz}(t') \circledast \left[ e^{-k_1 t'} - e^{-(k_1 + {}^{p}T_1^{-1})t'} \right] + \\
{}^{s}T_1^{-1}.{}^{s}\Lambda_{yz}(t') \circledast \left[ 1 - e^{-k_1 {}^{1} t'} \right] \qquad (5.3.9)
\end{aligned}
$$

This leaves the variables $k_1$, $P_i/P_{eq}$, ${}^{p}T_1$, ${}^{s}T_1$, ${}^{s}T_2$ and $\omega_1$ – still too long a list to allow worthwhile fit with experimental results. However, the latter three may be separated from the former at higher reaction rates (such that $k_1 \gg {}^{p}T_1^{-1}$, ${}^{s}T_1^{-1}$, ${}^{s}T_2^{-1}$ and $\omega_1$ , which is easily achieved in our system). ${}^{s}T_2^{-1}$ can be extracted from the field–domain lineshape, and $\omega_1$ and ${}^{s}T_1^{-1}$ can then be fitted to the signal decay, noting that $P_i/P_{eq}$ will not influence the period of oscillations. In order to maximise the kinetic effect a comparison of signal with varying $\mu$–wave field strength was made. The results, shown in Fig.(5.3.5) indicate the 10 to 15 dB range to be the most suitable.

Returning these values to (5.3.9) allows us to adjust just three parameters. Indeed it is found that for rates of reaction apparent in the examined system, variation of simulated signal with ${}^{p}T_1$ is barely detectable. A value of $k_1$ and $P_i/P_{eq}$ then fall out of the analysis fairly easily, since their respective effects upon the lineshape are very different. These lineshapes and their simulations are shown in Fig.(5.3.6), along with extremes of fast and slow radical formation and high and low $P_i/P_{eq}$ terms. In these experiments the base concentration was varied linearly, and an effective first order rate constant has been measured as $2 \times 10^{8} dm^{3} mol^{-1} s^{-1}$. Again, the error is difficult to assess but an appreciable difference in appearance of simulated lines can be seen if the formation rate is adjusted by $\pm\ 5 \times 10^{7} dm^{3} mol^{-1} s^{-1}$. It must be stressed that this error is estimated from the effect of varying the pseudo–first order rate constant in the simulations: these use values for $\omega_1$, ${}^{s}T_2$ and ${}^{s}T_1$ that are unlikely to be very accurate,

Fig.(5.3.5) The Variation Of Signal With Microwave Field Strength.

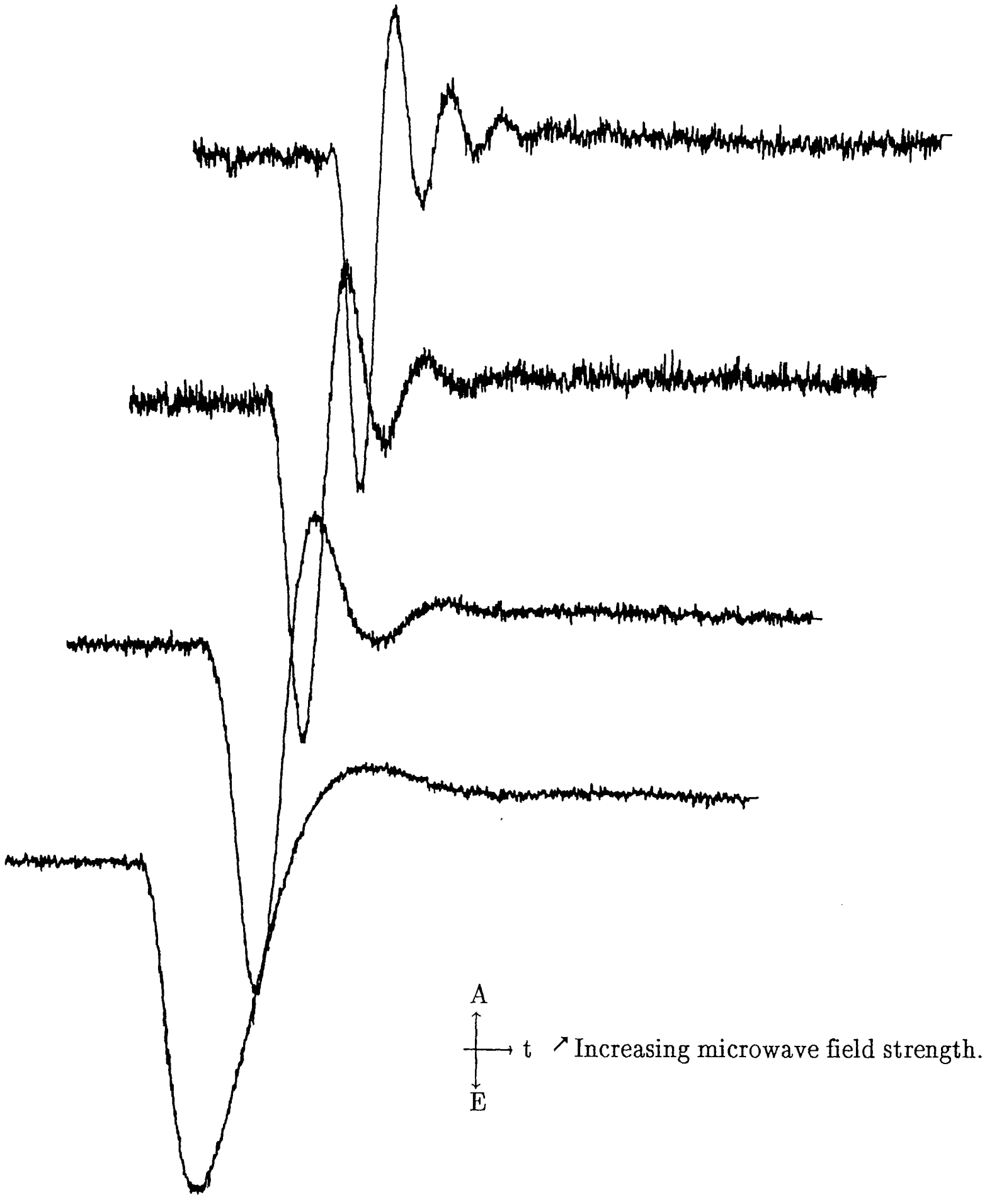


Attenuations of 20, 15, 10 and 5 dB were used: the appearance of the signal is most informative at 15 and 10 dB, below which response is too slow, and above which tuning and noise problems arise.

Fig.(5.3.6) Decay Curves For Various Base Concentrations And Two Microwave Field Strengths.

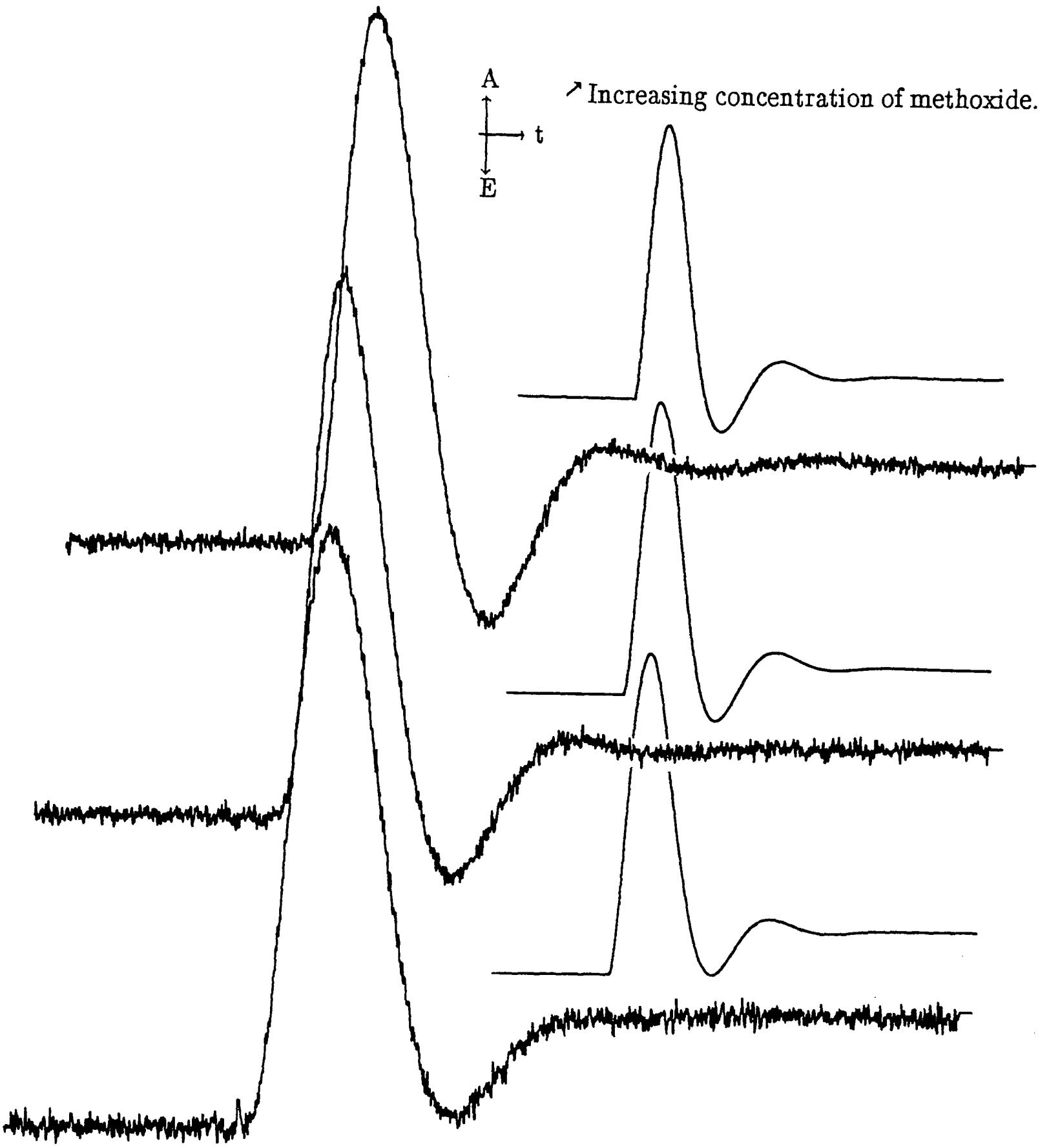


Attenuation = 15 dB. Base concentration are 0.005, 0.01 and 0.04 Molar.

Simulations use pseudo–first order rate constants of $1.1 \times 10^6$, $2.2 \times 10^6$ and $4.4 \times 10^6$ $s^{-1}$, in ascending order of base concentrations.

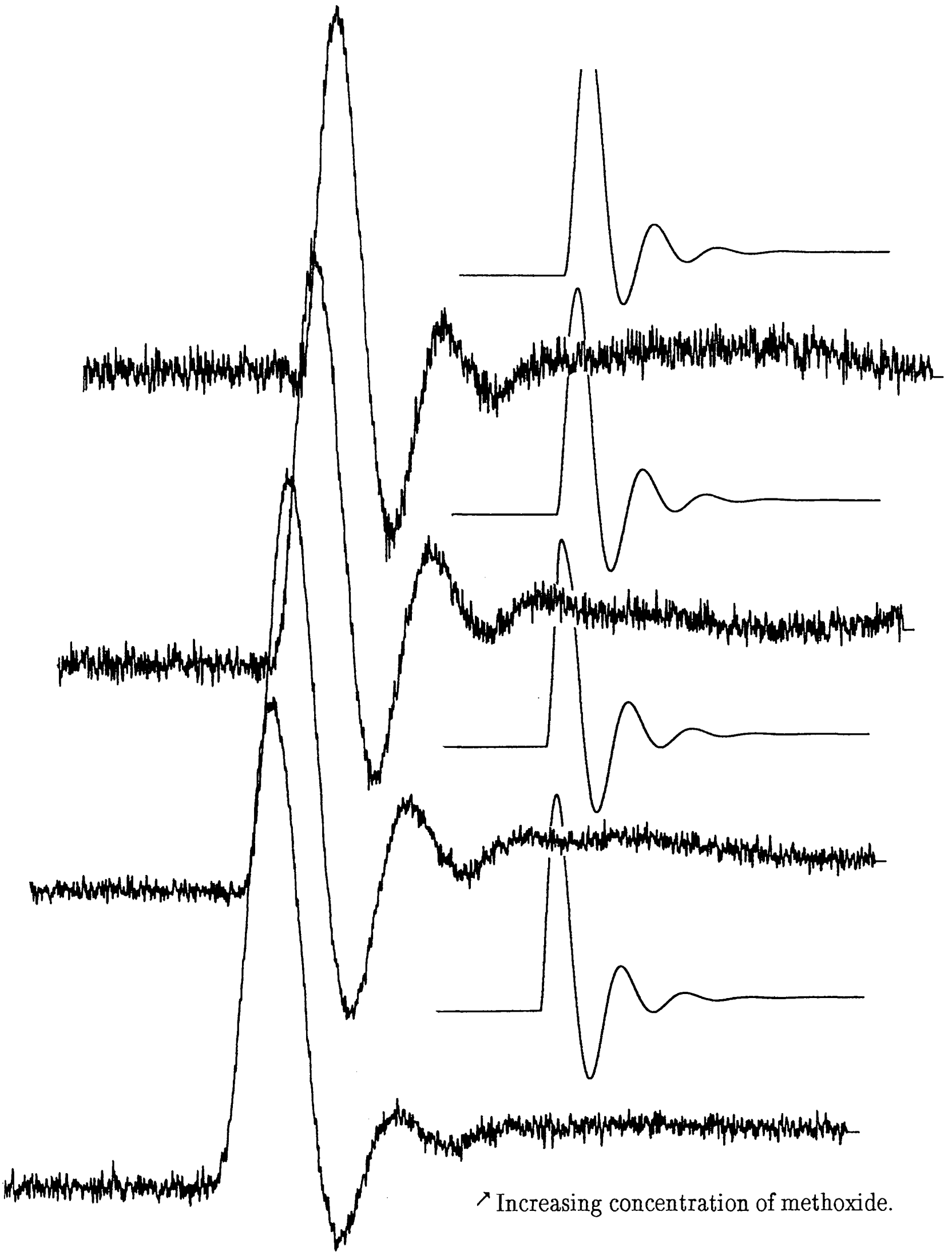


Attenuation = 10 dB. Base concentrations are 0.005, 0.01, 0.02 and 0.03 Molar.

Simulations use pseudo–first order rate constants of $1.1 \times 10^6$, $2.2 \times 10^6$, $4.4 \times 10^6$ and $6.6 \times 10^6$ $s^{-1}$. Above base concentration of 0.02 M $dm^{-3}$ no detectable difference in signal with concentration is observed.

and while the effect of ${}^{s}T_1$ is small, that of ${}^{s}T_2$ and $\omega_1$ are considerable. Consequently, this error band ought to be regarded as an error minimum, rather than a maximum. The order of magnitude for this reaction does, however, seem plausible, and it would be hard for a combination of the above parameters to cause a deviation in apparent rate of as much as $5 \times 10^8$. More importantly, with a chemical system as complex as this, we are probably not justified in assuming that the base put in will equal the active base in the reaction. This does, as did the other method, allow us to put a band on the minimum rate of reaction since we obviously cannot observe a higher effective base concentration than was in the original solution. This work has been submitted as the first practical demonstration of this form of kinetic spectroscopy [41].

(5.4.1) Conclusions

The series of experiments described here demonstrates many aspects of polarization, kinetics and free–radical chemistry. Identification of free–radical intermediates, free–radical kinetics and hyperfine–dependent relaxation are all assisted by the enhancement of signal strength by transfer of spin populations from and to specific hyperfine states in the course of a chemical reaction.

A prediction has been borne out by the observation of A/E polarization in a tertiary species, and it should stand as a reminder that the rate of formation of radical species must be considered if we are to avoid mis–assigning or drawing erroneous conclusions from polarized spectra. In the course of these investigations the relative signs of coupling constants in a large number of species have been inferred by a simple qualitative test.

Two methods of kinetic analysis have been expounded, both of which have their draw–backs but do permit otherwise difficult measurements to be made. I envisage

neither as having wide–scale potential as analytical tools, but they do furnish us with alternative ways of probing radical chain reaction rates.

As a final thought, the carbanionic radical is, as mentioned before, very closely related to a carbanion widely used in a modification of the Wittig reaction [30]. The presence of a radical centre adjacent to the nucleophilic carbon atom may well open a non–intrusive window through which the mechanism of the Wittig reaction could be viewed. The photo–activity of ketone groups at 308nm make it an inappropriate reaction to be studied under our experimental conditions. However, a set–up that would allow formation of this radical outside a microwave cavity, followed by a period of rapid mixing within it (assisted by the apparent long lifetime of the carbanionic radical) may well make it possible to investigate the attack and breakdown stages of the reaction.

## REFERENCES – CHAPTER 5


1 McLauchlan K.A., Sealy R.C., Wittmann J.M. *Mol.Phys.* (1978) 35, 51.

2 Hore P.J., McLauchlan K.A. *Mol.Phys.* (1981) 42, 533.

3 Ayscough P.B., Lambert G. *J.Chem.Soc. Faraday Trans.I* (1978) 74, 2481.

4 Ayscough P.B., Lambert G., Elliot A.J.
*J.Chem.Soc. Faraday Trans.I* (1976) 72, 1770.

5 Fessenden R.W. *J.Chem.Phys.* (1973) 58, 2489.

6 Paul H. *Chem.Phys.* (1979) 40, 265.

7 McLauchlan K.A., Stevens D.G. *J.Chem.Phys.* (1987) 87, 4399.

8 Sakaguchi Y., Hayashi H., Murai H., I'Haya Y.J.
*Chem.Phys.Lett.* (1984) 110, 275.

9 Buckley C.D., Hunter D.A., Hore P.J., McLauchlan K.A.
*Chem.Phys.Lett.* (1987) 135, 307.

10 McLauchlan K.A., Stevens D.G. *Chem.Phys.Lett.* (1985) 115, 108.

11 Wong S.K., Hutchinson D.A., Wan J.K.S. *J.Chem.Phys.* (1974) 60, 2987.

12 Pedersen J.B. *F.E.B.S.Lett.* (1979) 97, 305.

13 McLauchlan K.A., Simpson N.J.K. *Chem.Phys.Lett.* (1989) 154, 550.

14 Basu S., McLauchlan K.A., Sealy G.R. *Mol.Phys.* (1984) 52, 431.

15 Evleth R.M. *J.Am.Chem.Soc.* (1976) 98, 1637.

16 Dorer F.H., Johnson S.N. *J.Chem.Phys.* (1971) 75, 3651.

17 Burkey T.J., Lusztyk J., Ingold K.U., Wan J.K.S., Adrian F.J. *J.Phys.Chem.* (1985) 89, 4286.

18 Stacey F.W., Harris J.F. *Org.React.* (1963) 13, 218.

19 Barnes G.W., David M.P. *J.Org.Chem.* (1960) 25, 1191.

20 Parshall G.W., England D.C., Lindsay R.V. *J.Am.Chem.Soc.* (1959) 81, 4801.

21 McLauchlan K.A., Stevens D.G. *Mol.Phys.* (1987) 60, 1159.

22 Kivelson D. *J.Chem.Phys.* (1960) 33, 1094.

23 Atkins P.W., Kivelson D. *J.Chem.Phys.* (1966) 44, 169.

24 Carrington A., Hudson A., Luckhurst G.R. *Proc.Roy.Soc.* (1965) A284, 582.

25 DeBoer E., Mackor E.L. *J.Chem.Phys.* (1963) 38, 1450.

26 Wilson R., Kivelson D. *J.Chem.Phys.* (1966) 44, 154.

27 Akiyama K., Wan J.K.S. *Abstracts Am.Chem.Soc.* (1988) 195, 116.

28 Ricca G., Severini F. *Polymer* (1988) 29, 880.

29 Roth H.K., Wünsche P. *Acta.Polymerica* (1981) 32, 491.

30 Bautagy J., Thomas R. *Chem.Rev.* (1974) 74, 87.

31 Kayser M.M., Breau L. *Tet.Lett.* (1988) 29, 6203.

32 Chen K.S., Foster T., Wan J.K.S. *J.Phys.Chem.* (1980) 84, 2473.

33 Giese B., Gretzschmar G. *Chem.Berischte* (1984) 117, 3175.

34 Basu S., Grant A.I., McLauchlan K.A. *Chem.Phys.Lett.* (1983) 94, 517.

35 Paul G., Kebarle P. *J.Am.Chem.Soc.* (1989) 111, 464.

36 Kasperski H., Linke J., Wünsche P., Roth H.K.
*Polymer Photochem.* (1982) 2, 151.

37 Geoffroy M., Rao G., Tancic Z. *private communication/"Abstracts, 31st Rocky Mountain Conference On Analytical Chemistry"*, Denver CO, USA (1989).

38 Heller H.C., McConnell H.M. *J.Chem.Phys.* (1960) 32, 1535.

39 McLauchlan K.A., Simpson N.J.K.
*J.Chem.Soc.Perkin Trans.II* (1990) in the press.

40 Alberti A., Hudson A., Pedulli G.F. *Tetrahedron* (1982) 38, 3749.

41 McLauchlan K.A., Simpson N.J.K. Submitted for publication.

# CHAPTER VI : A STUDY OF HYPERFINE–DEPENDENT POLARIZATION

# A STUDY OF HYPERFINE–DEPENDENT POLARIZATION

## (6.1.1) Introduction

This is a short chapter, included since it provides a useful reference point for chapter 7, and because, in its unfolding, several novel features of CIDEP will be encountered. The subject chosen for study is the photolysis of di–tertbutyl ketone and di–isopropyl ketone in high viscosity paraffins, and it was chosen because under such conditions an uniquely strong RPM signal is obtained. This fact, combined with the ten and fourteen line spectra resulting from the tertbutyl and isopropyl radicals (each line with associated second order components) suggested that it would be an ideal study for evidence of $ST_-$ mixing, unusual $ST_0$ Q–dependences and possible separation of F– and G–pair effects. These expectations have been fully realised and, in the course of the study it has been shown that hitherto unexplained hyperfine intensities in micellar media and high viscosity solutions appear to have a related and simple explanation.

## (6.1.2) A Brief Review Of Di–alkyl Ketone Photochemistry

The photolysis pathway for a di–$^t$butyl ketone is well characterised. Thus [1,2]

$$(CH_3)_3C.\overset{O}{\overset{\|}{C}}.C(CH_3)_3 \xrightarrow{UV} \text{singlet/triplet} \longrightarrow (CH_3)_3C^{\bullet} + {}^{\bullet}\overset{O}{\overset{\|}{C}}.C(CH_3)_3 \qquad (A)^1$$

---

[1] The initial bond scission has been measured as $9 \times 10^9$ $s^{-1}$ by Yang N.C., Feit E.D., Hui M.H., Turro N.J., Dalton J.C. in *J.Am.Chem.Soc.* (1970) 92, 6974. $k_d = 3.5 \times 10^5$ $s^{-1}$.

$$\bullet\overset{\overset{O}{\|}}{C}.C(CH_3)_3 \xrightarrow{k_d} CO + (CH_3)_3C^{\bullet} \qquad (B)$$

$g\{(CH_3)_3C^{\bullet}\} = 2.0026$ ; $g\{(CH_3)_3C.C^{\bullet}O\} = 2.0008$. This reaction, a Norrish type I process, takes place within a few nanoseconds.

Di–$^{i}$propyl ketone can undergo a "type III" reaction,

$$(CH_3)_2CH.\overset{\overset{O}{\|}}{C}.CH(CH_3)_2 \longrightarrow CH_3.CH{=}CH_2 + CH_3.\overset{\overset{O}{\|}}{C}H \qquad (C)$$

but this does not appear to be taking place at the wavelength of excitation used here.

Recombination rate constants for $^{t}$butyl, $^{i}$propyl and ethyl radicals in the gas phase lie in the range $5 \times 10^{8}$ to $5 \times 10^{11}$ $dm^3mol^{-1}s^{-1}$ (i.e. $\approx \frac{1}{4}$ of the collision frequency, as expected from spin statistics for pure singlet reactivity), and the activation barrier for the ethyl/ethyl reaction is estimated as 3.5 $kJmol^{-1}$, being too small to be measured by light modulation techniques[2]. The $^{t}$butyl radical bimolecular termination rate constant in cyclohexane has been measured as $1.1 \times 10^{9} dm^3mol^{-1}s^{-1}$ [3] and it decreases with $\eta^{-0.8}$, as predicted by diffusion theory. An independent measurement in benzene [4] gives a rate constant of $9.6 \times 10^{9}$ $dm^3mol^{-1}s^{-1}$. Further work has confirmed this trend towards lower recombination rates at higher viscosities [5], indicating specifically that the percentage of cage–recombinant to free–encountering products varied from 80% in very

---

[2] Only one in four gas phase collisions can give rise to reaction, and this may still be true in highly mobile solutions, though any kind of restriction upon radical mobility will make this prediction very unlikely. Rates of reaction may be impeded in solution if $J_r$ shows marked anisotropy and the solvent molecules hinder radical/radical re–orientation.

viscous (decalin) solvents, to 15% in pentane [6]. Two re–encounter reaction routes exist for either radical pair indicated in (A) and (B): illustrating this for a pair of $^{t}$butyl radicals, these are the simple recombination

$$2\,(CH_3)_3C^{\bullet} \longrightarrow (CH_3)_3C{-}C(CH_3)_3 \qquad (D)$$

which could, in solution, be an activated process, and the "disproportionation",

$$(CH_3)_3C^{\bullet} + H{-}CH_2.C^{\bullet}(CH_3)_2 \longrightarrow (CH_3)_3C{-}H + CH_2{=}C(CH_3)_2 \qquad (E)$$

which is able to take place via a singlet or triplet biradical and may have a lower activation energy for hindered tertiary or secondary radicals than the singlet route [7].

(6.2.1) Experimental Conditions

All spectra were recorded from the photolysis of 0.1 Molar di–$^{t}$butyl ketone or 1.0 Molar di–$^{i}$propyl ketone (of > 99% purity) in heavy paraffin that had been rigorously de–gassed under vacuum and then saturated with $O_2$–free nitrogen. The formation of bubbles of carbon monoxide upon photolysis and the changes in viscosity caused by the change in temperature at which spectra were recorded meant that the normal method of capillary flow to regulate flow rate had to be exchanged for a pump, buffered by an air chamber to smooth the passage of the sample. Solutions were thus drawn upward through the cavity region, carrying these bubbles with the flow, thereby avoiding cavity de–tuning. A range of temperatures were studied to try to assess the magnitude of the ST$_-$ effect upon the second order components of each hyperfine line, and to attempt, for the $^{i}$propyl radical, to compare signs of $\alpha$– and $\beta$– coupling constants. Separation and

re–encounter/free–encounter should also be retarded in higher viscosity solvents, so the geminate polarization would be expected to persist, undistorted by F–pair effects for longer. This, for our purposes, is an ideal situation, only very rarely achieved; radicals are always created in pairs in photolytic experiments but their precise nature is not always defined, and where they appear to be so in CIDEP experiments, the results are often at variance with product analysis or kinetic studies[3].

(6.2.2) A Coarse Analysis Of The Spectra

This section allows us to dismiss various aspects of the spectra before we concentrate on the quantitative side. Fig.(6.2.1) shows a signal–to–noise ratio for the strongest lines well in excess of a hundred. One unfortunate aspect of digital field sweeps is that the combination of a large spectrum width and narrow lines makes it possible to step over the true line maxima, upon advancing from one field point to the next, giving apparent intensities that differ markedly from the true ones. Under these conditions a coupling for the $\beta$H is measured as 2.287mT. Natural abundance of $^{13}C$ is 1.11% so the radical $H_3{}^{13}C—C^{\bullet}(CH_3)_2$ should be observable at a 3% abundance: these are the weak peaks to either side of each $^{12}C$ peak, with a coupling to the carbon nucleus measured from the spectrum of 1.25mT, which is in excellent agreement with that measured at a lower temperature on a steady–state photolysis rig [9], and indicates substantial non–planarity at the radical centre. This is the first record of lines observed for $^{13}C$ at its natural abundance on a time–resolved experiment; they are too weak to be

---

[3] As an example, the photolysis of propanone in propan–2–ol yields both oxygen– and carbon–centred species [8], but the transient *e.s.r.* spectrum reveals just what would be expected from the RPM of two identical ketyl radicals, and with a net absorption on top of this.

Fig.(6.2.1)

The $^{t}$Butyl Radical Spectrum

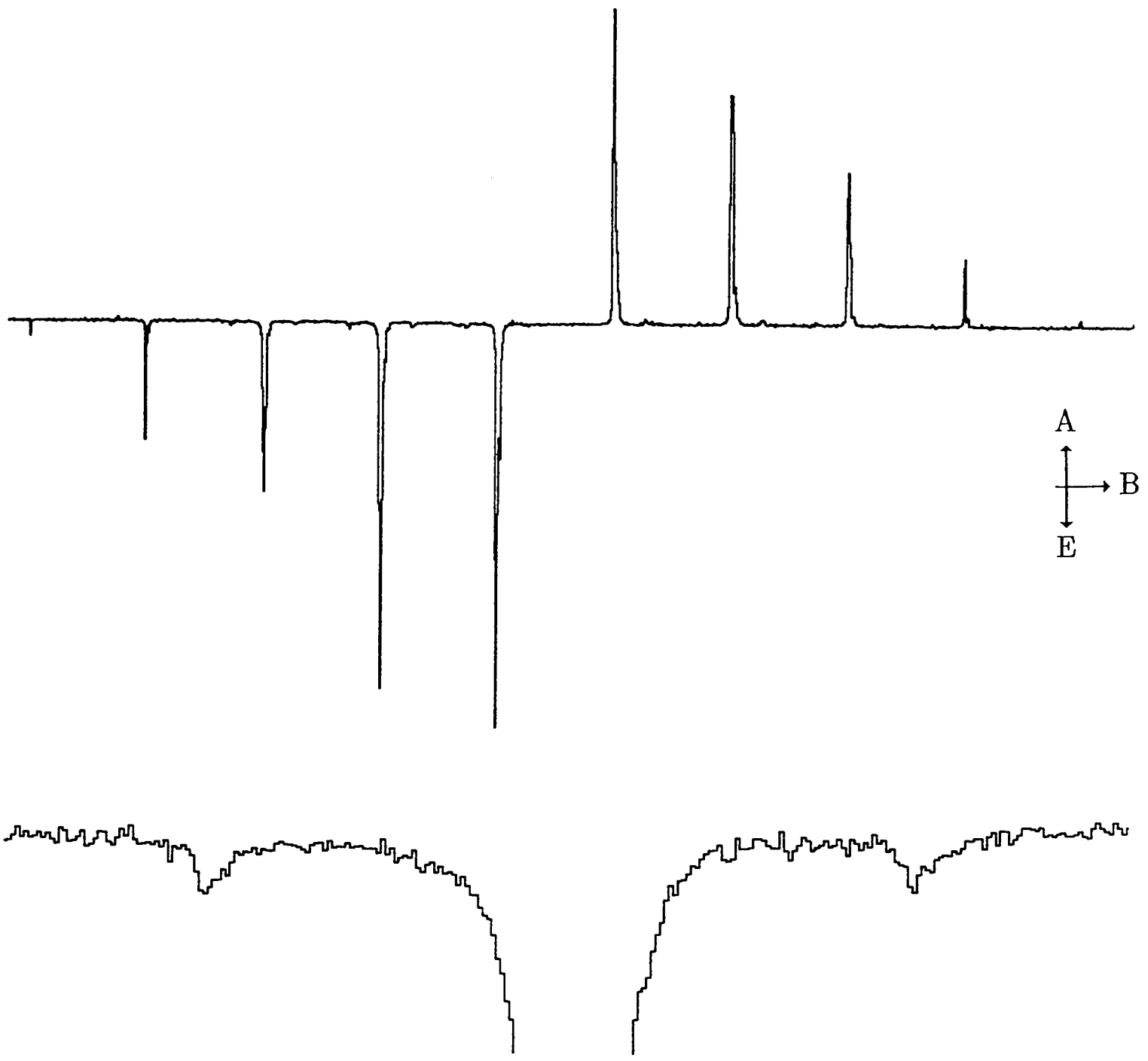


An indication of the strength of signal from a carefully prepared sample is given by the 3% (1.5% per peak) of signal that arises from the $^{13}$C on the $\alpha$–Carbon, appearing as weak satellites to either side of each line. This is shown below the main spectrum, in expanded scale, over 2mT.

This spectrum was recorded from 0.2 to 6.2 $\mu$s, over 22mT (apparent heights of major lines are not reliable indications of true intensities on this scan, as explained in the text).

used for quantitative work, but anyway, those of real interest would be of the $^{13}C(CH_3)_3$ radical, for the size of its coupling, and its relaxation properties would be more helpful in determining the extent of non–planarity: these peaks are not observed at all.

A second feature is that the lines broaden and lose the second order structure as the viscosity increases, while the centre lines gain intensity with respect to the outer lines. This sequence of events is shown in Fig.(6.2.2). The first of these observations is a consequence of a shorter $T_2$, as the rotational correlation time increases.

The second warrants more explanation, since a hyperfine–dependent relaxation dominated by the $CM_i$ term is not consistent with the observed linewidths (a single $T_2$ is appropriate for all the lines across each spectrum). Polarization may be generated by one of two possible radical pairs: taking the di–$^t$butyl ketone system, these are either a pivaloyl/$^t$butyl or a $^t$butyl/$^t$butyl couple, which, in the absence of any effect such as differential relaxation between one of the species that comprise the pair, would be expected to polarize equally if the small RPM net effect is ignored. However, acyl radicals are known to have a short $T_1$ (though clearly not so short as to disrupt $ST_0$ mixing: i.e. $T_1$, $T_2 > 10^{-8}$s), and with no $\alpha$ or $\beta$ protons to couple to, will have a small spectral spread[4]. The g–factor difference between the pivaloyl and $^t$butyl radicals is fairly insignificant when compared to the $\beta$H couplings, so the pivaloyl radical would develop only a weak RPM. Therefore, even if it were to have a long lifetime, on the scale of the spectrometer response, it would still not be seen. It has been the absence of any acyl signal in both $^i$propyl and $^t$butyl photolyses that has led experimenters to conclude that somehow the kinetic measurements are wrong, and that the CIDEP spectrum could be simulated by the effect of identical radical encounters. A comparison

---

[4] They have been observed in temperatures below – 70°C, under steady–state photolysis [10].

Fig.(6.2.2)

The Effect Of Viscosity Upon The $^{t}$Butyl Spectrum.

Two spectra, recorded at 32°C and 2°C, and covering 20 and 22mT respectively – the longer $T_2$ in the former made it necessary to reduce sweep width to ensure that true line intensities were recorded. The net absorption is reduced with a reduction in temperature.

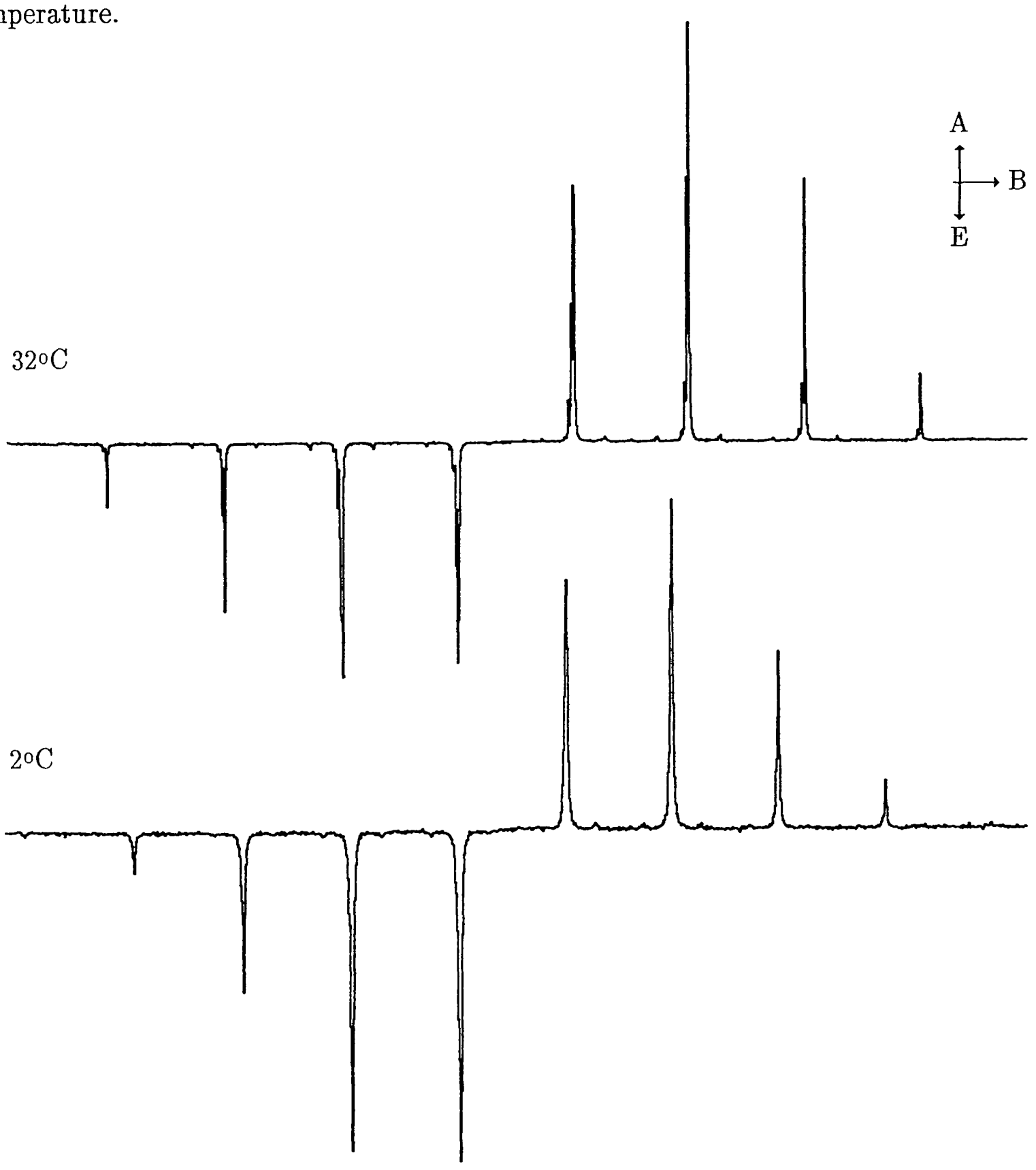

of the differences between the two models is shown in Fig.(6.2.3). The important point is that this dissimilar radical pair enhances the centre field lines at the expense of the outermost ones, as is to be expected from the ensemble–averaging effect of the RPM process, over all lines of the counter–radical. The result is similar, but not equivalent to that of violation of the "small mixing" condition, which gives rise to a $Q^{\frac{1}{2}} - aQ$ hyperfine dependence[5] [11]. What this means in practice is that the radical pair's relative diffusion is slowed to such an extent that appreciable $ST_0$ mixing occurs as the radicals separate, so a re–encounter is not necessary to generate RPM polarization. The only published example of this effect [12] was carried out in heavy paraffin upon the photo–products of di–$^{i}$propyl ketone: a study to separate and quantify these two effects is given in § (6.2.3).

What we are witnessing can be directly related to what is happening on a microscopic scale as, by changing the viscosity we are trapping more radicals into the region around the solvent cage in which they were formed, so that until the slow de–carbonylation step has occurred, encounter between identical alkyl radicals is almost precluded. Whilst the lifetime of the pivaloyl radical is short compared to the observation time, it is long when compared to the time taken for geminate RPM to develop and so, provided little F–pair polarization is present, it will leave an unmistakeable fingerprint upon the spectrum of the observed radical.

A similar set of hyperfine intensities has been noted in the polarized spectra of benzyl radicals formed in high viscosity solutions [13], and in micelles [14], in which diffusion is known to be hindered, and there is evidence that radicals are actually

---

[5] The units of **a** in this equation are conveniently expressed in $\text{Gauss}^{\frac{1}{2}}$.

Fig.(6.2.3)

The Effect Of An Acyl Counter–radical Upon RPM Polarization

Simulations are shown of the spectrum of the $^{t}$butyl radical polarized by encounter with another $^{t}$butyl radical and with an acyl one. These are shown for stick spectra with second order corrections to line positions, and for spectra with appropriate lineshapes convoluted upon them. The effect upon the relative heights of third and fifth lines from either end is striking.

$^{t}$butyl/$^{t}$butyl pair

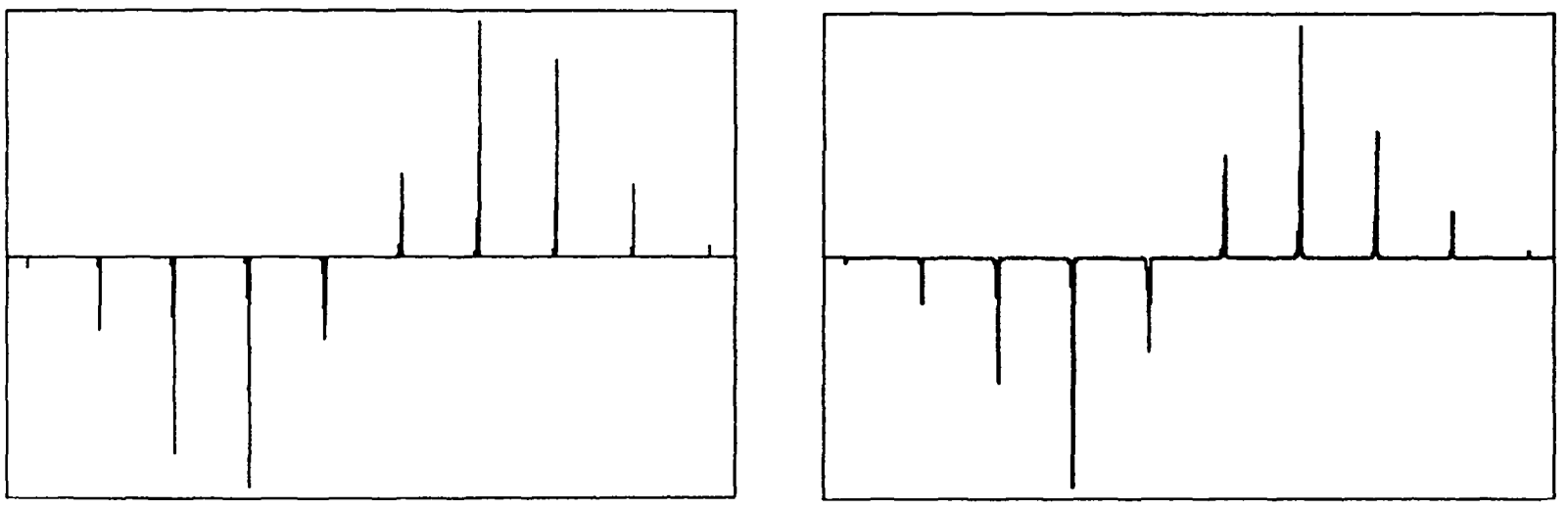

pivaloyl/$^{t}$butyl pair

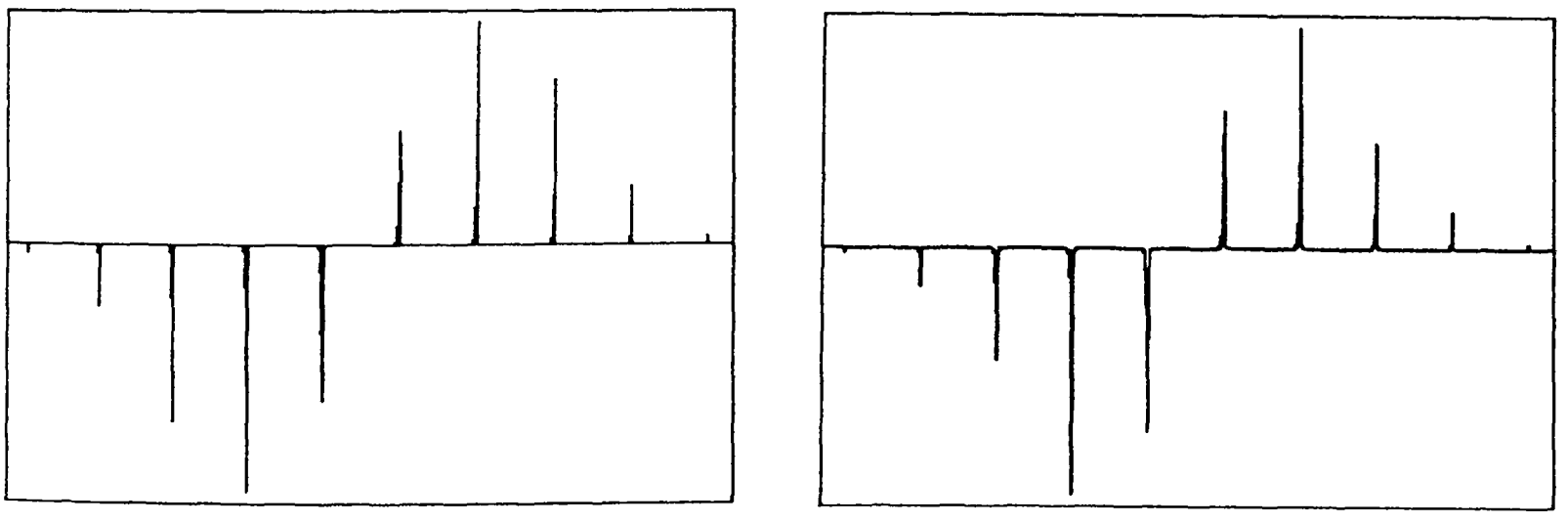

When the effect is allied with a small correction term, linear in $Q_{ab}$ then correspondence with spectra in Figs.(6.2.1) and (6.2.2) can be attained. This term has deliberately been over–compensated for in these simulations: a = 0.09.

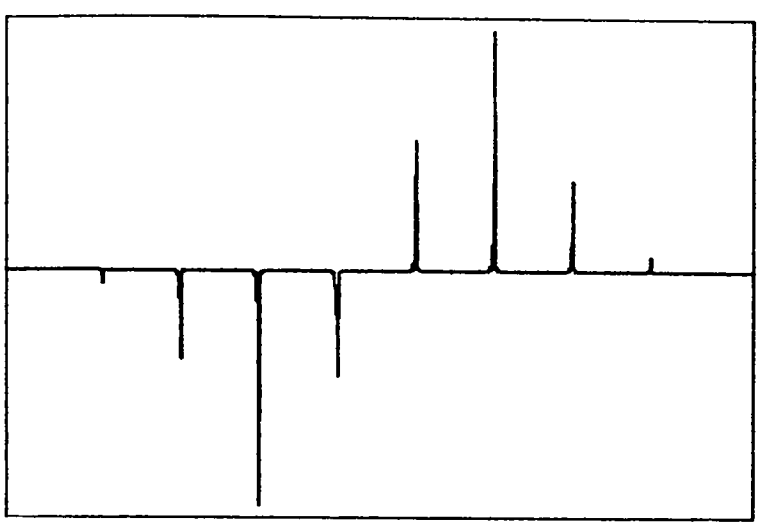

$(CH_3)_3C^{\bullet} + (CH_3)_3C^{\bullet}$

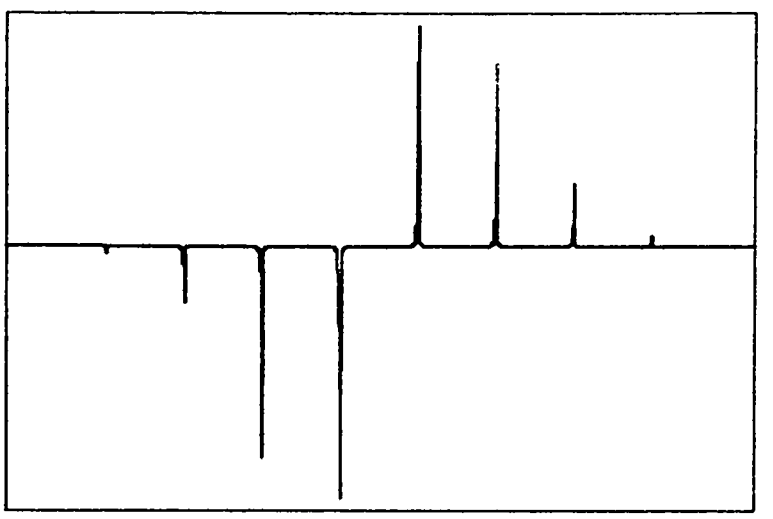

$(CH_3)_3C^{\bullet} + {}^{\bullet}\overset{\overset{O}{\|}}{C}.C(CH_3)_3$

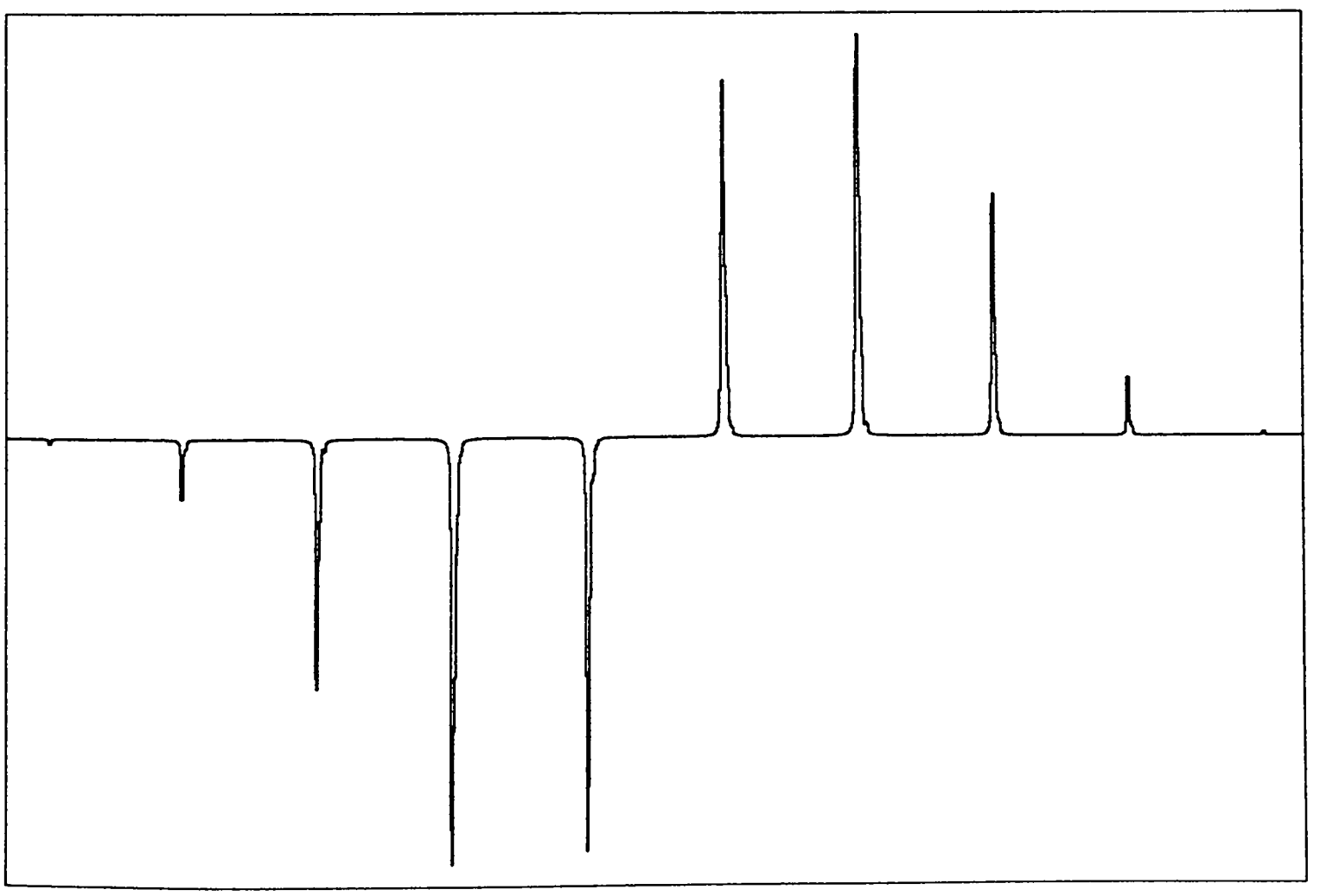

Simulation of (6.2.2b) incorporating A:B in the ratio 3:10. a = 0.06.

prevented from re–encountering one another because of attraction to to micellar walls [15] and because of the dynamic destruction and reformation of micelles on a microsecond timescale [16]. Both effects will damp out non–geminate polarization, so that geminate polarization, even if very weak, will be observed.

Perhaps this simple explanation may have been overlooked until now because of the inability of most workers to convolute a lineshape upon the RPM stick spectrum. This tends further to enhance the central field lines because of overlap of their many second order components. Without this one must resort to modifying the Q–dependence of the RPM to bring apparent signal intensities into line with the observed ones. This is shown in Fig.(6.2.3). The conclusion is satisfying because it invokes no new polarization process and is consistent with the known kinetics of the ketone photolysis.

A last observation concerns the net absorptive component to the spectrum, noted before and ascribed then to the TM [17]. Certainly it is of the expected phase, for aliphatic ketones are predicted in general to show absorptive TM [13]. The initial bond–breaking process is fast enough to generate TM before relaxation of the triplet, and an increase in viscosity would be expected to increase $ST_-$ and decrease $T_1$. This assumes that our system is in that region for which $T_1$ and $T_2$ are approximately equal – Fig.(2.2.2). Both act to reduce the observed net absorption. In addition, photolysis of phenyl–$^t$butyl ketone (0.05 Molar in heavy paraffin) shows a weak net emission, the parent chromophore being expected to behave as an aromatic ketone and give an emissive TM. A comparison of these two types of behaviour is made in Fig.(6.2.4). However, a detailed discussion of this matter is reserved for Chapter 7.

Fig.(6.2.4)

The Central Six Lines Of The $^{t}$Butyl Spectrum

Photolysis of 0.1 Molar di–$^{t}$butyl ketone in heavy paraffin.

Note the very weak net absorption.

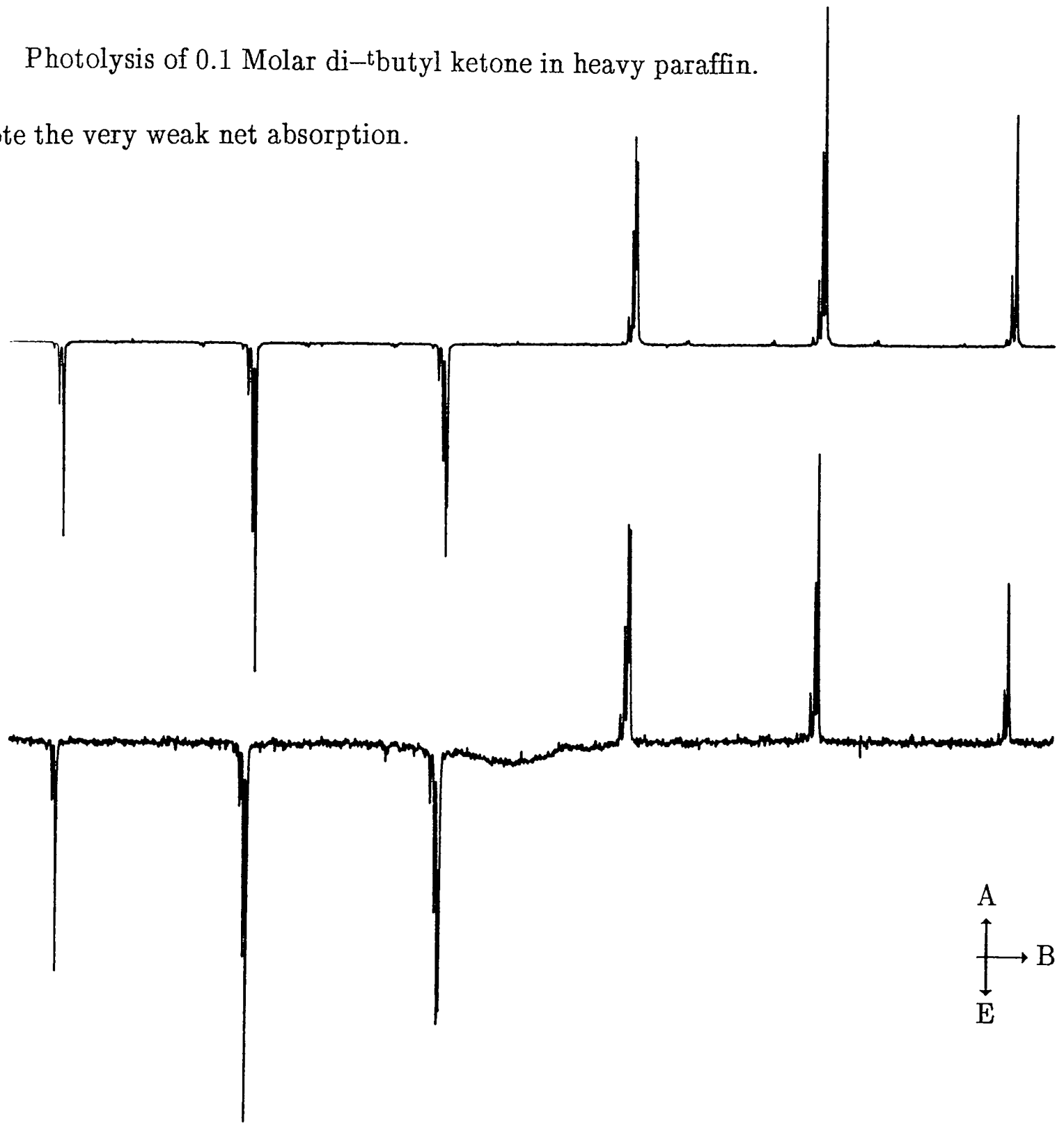


Photolysis of 0.05 Molar phenyl $^{t}$butyl ketone in heavy paraffin. The $^{t}$butyl radical appears in net emission and a weak, broad central feature – the acyl radical – is visible, entirely in emission. Both spectra were recorded over 1 to 4$\mu$s and 11mT.

(6.2.3) A Perfect Fit

The foregoing discussion has paved the way for a full analysis of the high quality spectra obtained from both the $^{i}$propyl and $^{t}$butyl systems. This section will be correspondingly brutal.

A single hyperfine line is focused upon so that the best field resolution can be obtained. We shall examine the oscillations to either side of the peaks of the second order spectrum of the second line to low field of centre. These second order components are discussed in §(4.4.1) and the oscillations in field domain are shown in Fig.(2.2.4). The interference between these second order components are shown by simulation to be extremely sensitive to microwave power, $T_1$ and $T_2$. However, in order to observe these nutations we require an observation period that is much smaller than the period of nutations. This condition represents a delicate balance – a high microwave power generates a strong signal but very short nutation period, whereas a lower power will generate more easily observed nutations but at a far lower intensity. The strength of the signal obtained from the $^{t}$butyl radical allows a new approach, for rather than play with incident microwave power we can choose a single point in the digitised time decay curve at each field position.

Fig.(6.2.5) shows just how effective the experimental set–up is at achieving high quality time–resolved signals. Both were recorded from just one time point on the decay of a resonance transition, clearly showing the transient nutations as a consequence of $\omega_1$ field and interference amongst the second order components. Comparison with simulations for just one time sample show in each case that the oscillations in observed spectra can be seen to be damped with respect to these simulations. That they are damped is a consequence of the small but continuous generation of F–pair RPM, which will prevent the application of a simulation based upon the initial generation of

Fig.(6.2.5)

Spectra And Simulations Made Over A Very Narrow Time Band

Three spectra are displayed, recorded at 1.1$\mu$s and 0.75radMHz and 1.18radMHz microwave field strengths and at 1.2$\mu$s and 0.75radMHz. Experimental spectra of the second low–field line of the $^{t}$butyl radical were taken from a single address in the transient recorder. For the reasons explained it was necessary to use a small range of sample points (20 samples) to reproduce the results exactly.

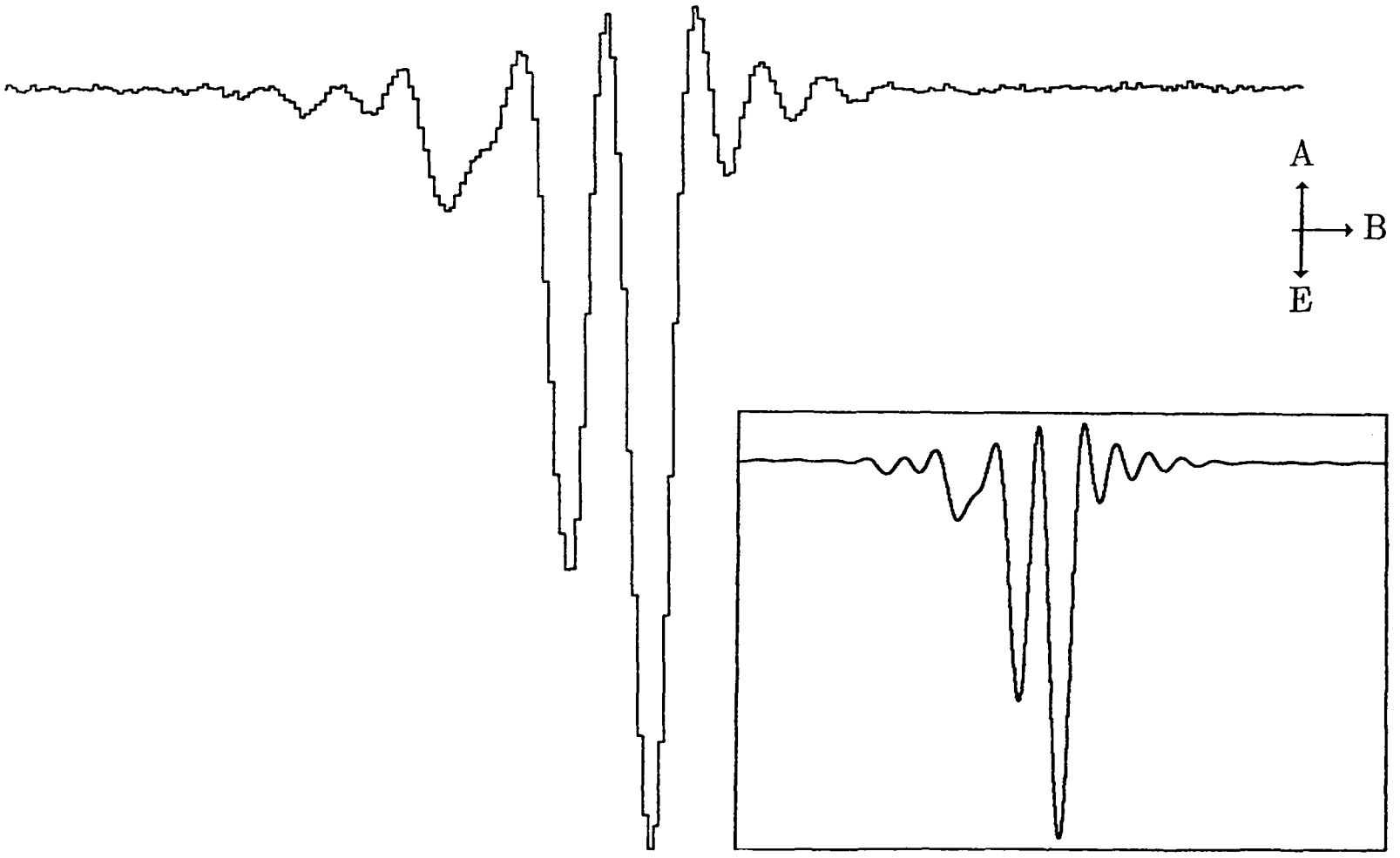

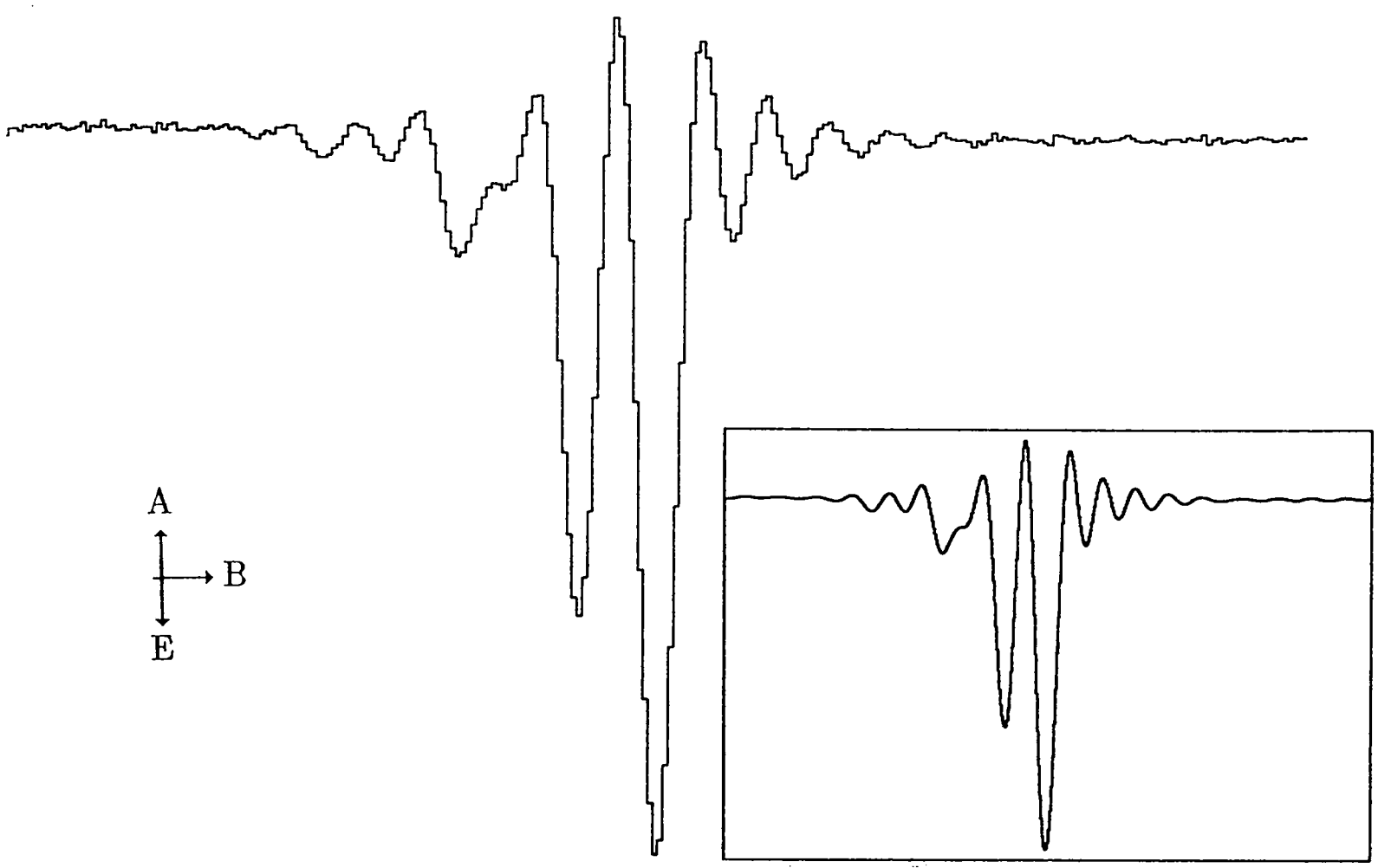


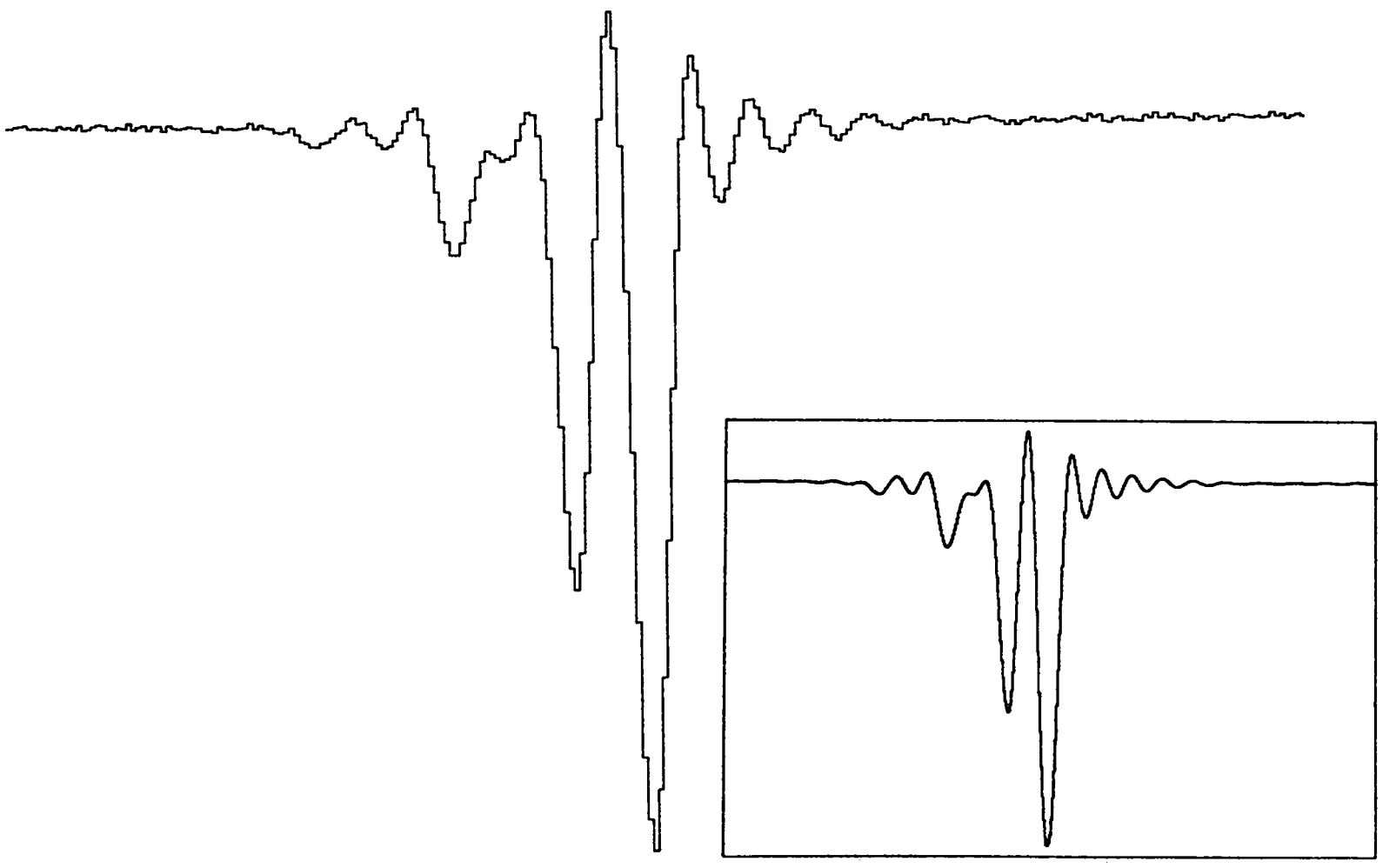

Perfect fits were found for a $T_1$ of 2.5$\mu$s and $T_2$ of 1.0$\mu$s. It was impossible to measure a polarization ratio from this analysis since the polarization was too strong. Ideally one would require a ratio of unity to make accurate analyses.

polarization alone, and by the "jitter" on the laser (that time between the laser being triggered and actually firing). The latter is estimated as being within ± 50 ns of the trigger with, presumably, a statistical distribution of firing times after that trigger is received. The trigger circuitry itself has been found to be subject to uncertainties of ± 50ns. This can be modelled by synthesising a spectrum not for a single time point, but for a small range, consistent with the uncertainty in formation point of radicals. A second simulation, taking this range from the above estimates as 20 time points (200ns) gives a spectrum that reproduces the experimental one excellently. In all other respects this is a true 10 ns time–resolved *e.s.r.* spectrum. Values of $T_1$ and $T_2$ calculated from these plots are given with the figures. They prove remarkably sensitive to variations in any of the parameters, though a reduction in $T_1$ and a lengthening of time of observation are hard to distinguish. These values are used in the simulations, wherever $T_2$ can be seen not to have been shortened by an increase in viscosity.

Fig.(6.2.6) displays two simulations : each of these represents a pure form of RPM, in the absence of any other polarization source, for the encounter of an $^{i}$propyl/$^{i}$propyl pair and for an acyl/$^{i}$propyl pair; it has not been found necessary to include any equilibrium term in synthesising Figs.(6.2.5), so that if a discrepancy in the net signal from a spectrum appears in the simulation, it can be corrected by a TM adjustment.

Fig.(6.2.7) is recorded at a lower temperature than the first spectrum, and the effect of encounters between dissimilar radicals is therefore enhanced. A higher temperature, and hence a lower viscosity will have the reverse effect, tending to accelerate the evolution of F–pair polarization for otherwise identical conditions. This is shown in Fig.(6.2.8). A similar effect is found for radicals obtained at later times, when encounters, if they occur at all, are between similar pairs of radicals. In all these simulations a lower multiplying factor than that published for this system [12], for the

Fig.(6.2.6)

The Effect Of An Acyl Counter–radical Upon The $^{i}$Propyl Spectrum.

Two simulations are shown, as for the $^{t}$butyl radical, of the effect of identical and dissimilar radical encounters upon the RPM. The $(CH_3)_2C^{\bullet}H$ radical pair is shown above that of the $(CH_3)_2CH.C^{\bullet}O$ / $(CH_3)_2C^{\bullet}H$ pair. In particular, emission from net RPM effect is conferred upon the observed radical, that is quite distinct from an emissive TM or ST$_-$ effect.

a)

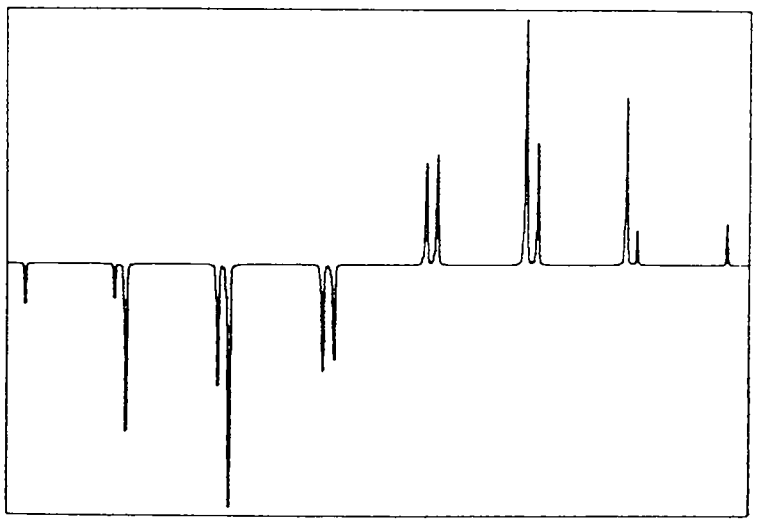

b)

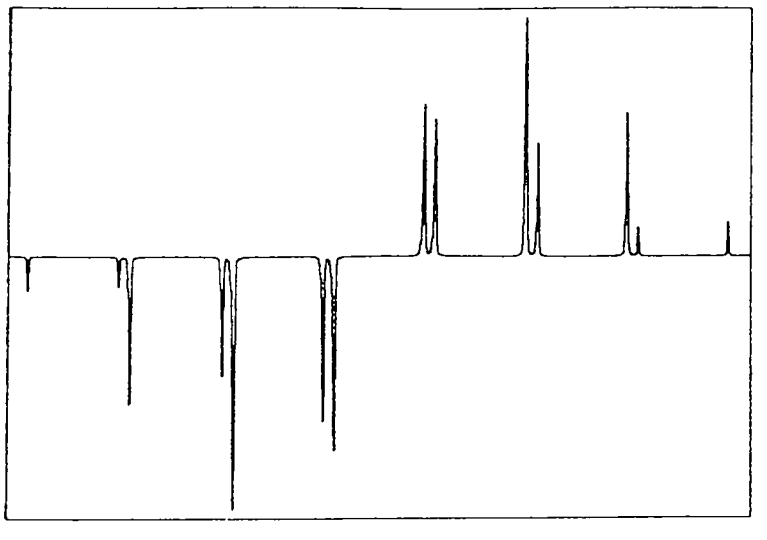

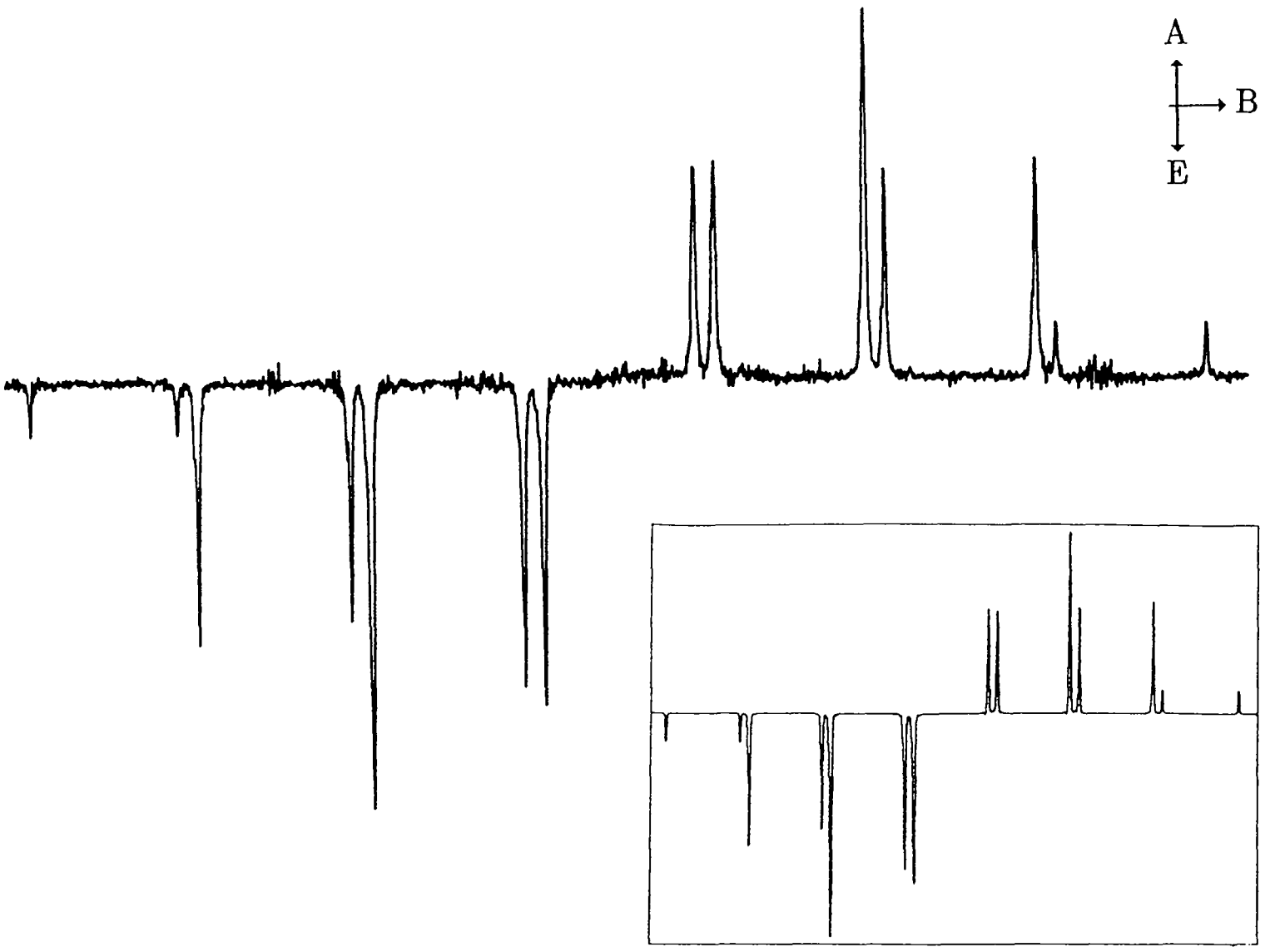


A sweep over 18mT at 26°C and from 0.25 to 1.25$\mu$s gives a spectrum that may be modelled by a 1:2 ratio of (a) to (b), with a linear correction to $Q_{ab}$ of 0.06.

Fig.(6.2.7)

A Higher Temperarature Study

All spectral conditions are as for Fig.(6.2.6), except for the temperature: 46°C. $T_2$ appears to be slightly longer at this temperature. A simulation incorporating alkyl/alkyl and acyl/alkyl pairs in a 1:1 ratio is given; interestingly it was still necessary to include a linear correction factor of 0.06 to reproduce the outer peaks accurately.

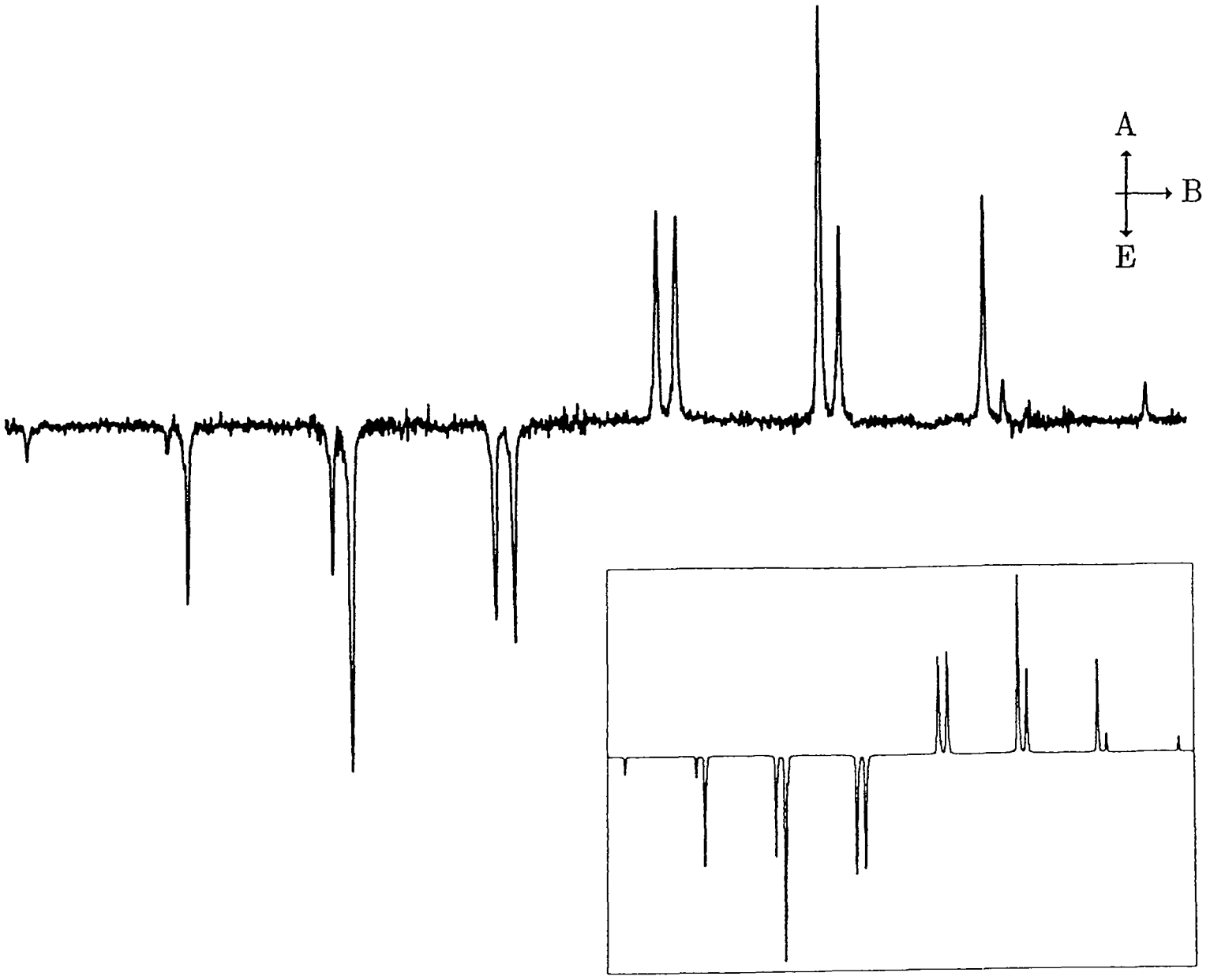

Fig.(6.2.8)

The Effect Of Lowering Temperature.

All parameters as for Fig.(6.2.6) except for temperature : 0°C. The simulation uses a ratio of alkyl/alkyl to acyl/alkyl encounters of 1:10, though this is only an estimate as the spectrum again becomes insensitive beyond this point. The linear term is once more modelled as 0.06. The simulation also shows the effect of a 5% ST- contribution. The low–field half of the spectrum is exaggerated even at this low level of mixing.

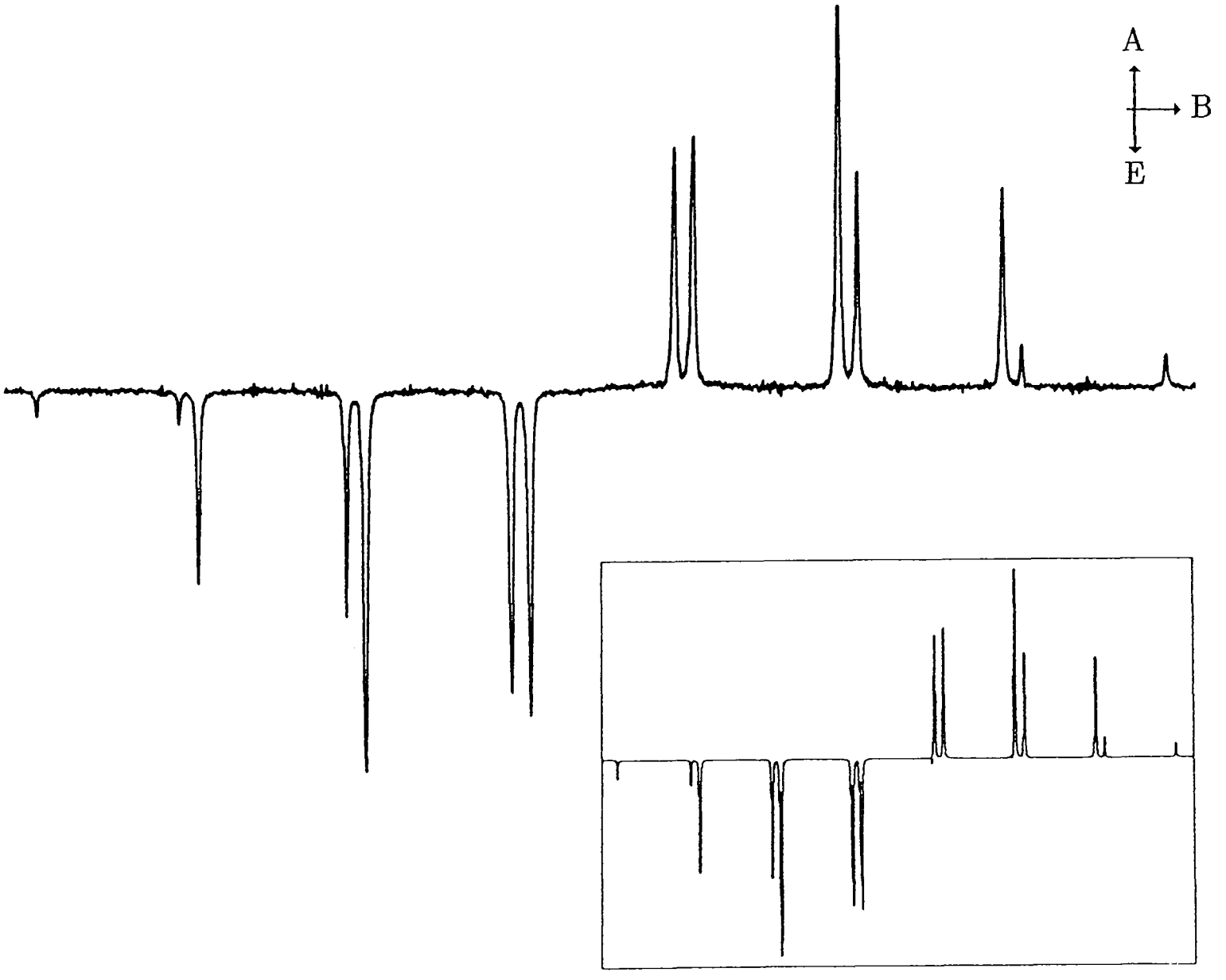

linear term in $Q_{ab}$ was used: as predicted, the effect was exaggerated by not considering the true nature of the radical pair.

To quantify any ST$_-$ effect we focus in on two hyperfine lines and model their second order components. The reasons for looking at second order components are discussed in §(4.4.1). This contribution increases with viscosity, but a look at the equations relating residence time in the region for which $J_r \approx g\mu_B B_0$ with temperature reveal that the relationship, even without approximations, would be complex (From the Einstein–Schmoluchowski equation, the residence time in the region where S and T$_-$ levels are degenerate, at a distance $r_{st-}$, is $d^2/2D_{ab}$ where d is the size of diffusive jump and $D_{ab}$ is the diffusion coefficient for radical $_a$ in solvent $_b$; we may equate d with $r_{st-}$ and see that ST$_-$ mixing is incomplete if $D_{ab} \leq r_{st-}{}^2$ and $D_{ab}$ is proportional to $1/\eta$, $\eta$ being the solvent viscosity[6]). The real viscosity around the radical pair would, anyhow, be less than that for the bulk solution, as a result of dissipation of excess energy absorbed by the ketone upon photolysis. Fortunately these problems do not concern us, for in no spectrum could significant (i.e. > 5%) ST$_-$ mixing be detected. This finding contrasts sharply with that for ketyl radicals in alcoholic solvents, for which strong ST$_-$ polarization, and even a splitting caused by the $J_r$ interaction, become dominant well above solidification of the solvent [14]. The $^t$butyl radical would be expected to possess a larger molecular radius than the propan–2–olyl radical, suggesting that it is the strength of the hydrogen bonds present in the latter in alcoholic solvents, that prevent pairwise separation. In other words the Van der Waals radius of $^t$butyl in paraffin is smaller than that of $^i$propolyl in alcohols. An estimation of the viscosity dependence of

---

[6] This uses the Stokes–Einstein relationship evaluated in Appendix C. Estimations of $D_{ab}$ for the $^t$butyl and $^i$propyl radicals in heavy paraffin over a range of $-10^oC$ to $+30^oC$ lie between $10^{-10}$ and $10^{-7}$ $cm^2s^{-1}$.

$ST_-$ mixing is demonstrated in Fig.(6.2.9) for two low field lines, over a small sweep to allow us to examine the second order components. An important point with the $^i$propyl radical is that the $\alpha$– and $\beta$– couplings are of opposite sign, and the relative dependence upon $ST_-$ mixing of each hyperfine level should reflect this. A simulation of the effect of equal and opposite signs of couplings upon $ST_-$ is shown in Fig.(6.2.10).

Returning to the relative proportions of acyl/alkyl and alkyl/alkyl encounter polarization we may conclude that, provided each encounter produces an equal polarization, then the relative ratios of cage–recombinant to escape–product–forming radicals can be estimated. Taking the ratios used in these spectra give values of between 50% and 91% of cage products, depending on temperature of the paraffin solvent. The lower bound is as expected from the values quoted at the beginning of this chapter, but the upper limit is surprising, suggesting that at 0°C the heavy paraffin solvent is more viscous than decalin at room temperature.

Clearly there are further factors to consider. For a start, the absorptive component, as mentioned above, is awkward to separate from an equilibrium term, yet we may compare how the theories of RPM:equilibrium and TM:equilibrium polarizations should vary with viscosity [18,19]. TM increases linearly with $\eta$ in the "slow motion" limit, for which an increase in viscosity – and hence of rotational correlation time – results in $T_1$ increasing. The RPM, on the other hand, varies with $\eta^{\frac{1}{2}}$ whether the small mixing limit applies or not. The conclusion drawn is that it *is* consistent with a weak equilibrium term, for the reasons specified above, which decreases with increasing $\eta^{\frac{1}{2}}$ relative to the RPM effect.

Fig.(6.2.9)

Estimation Of ST- Mixing.

The two central low–field lines are displayed, with simulations, at 48°C and 2°C. The second order structure is very sensitive to ST- polarization, the sub–line to lowest field being strongly enhanced and that to highest field developing no polarization if the coupling is positive. Relative alkyl/alkyl and acyl/alkyl proportions are derived from the spectra in Figs.(6.2.7) and (6.2.8) respectively, and simulations use a 3% ST- addition to these bases. Even this is apparently too large, though there is evidence for a weak effect. (The two second order components to highest field in the high–field line are not resolvable into separate lines).

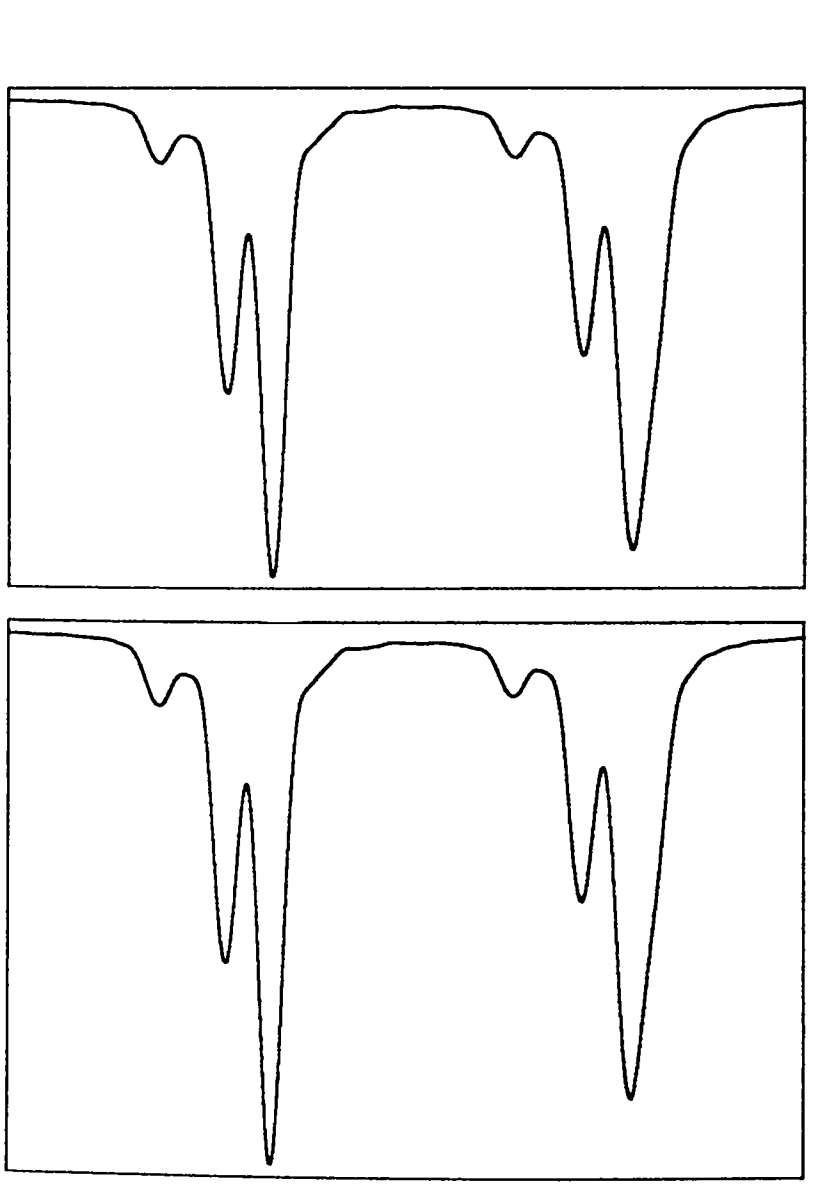

Fig.(6.2.10)

An Illustration Of ST$_-$ Mixing Upon The $^{i}$Propyl Radical.

This simulation models a pure ST$_-$ effect for a radical that has one negative and six positive (and identical) couplings. The net trend from low to high field is for emission to decrease, but for each doublet the higher–field line is more strongly enhanced.

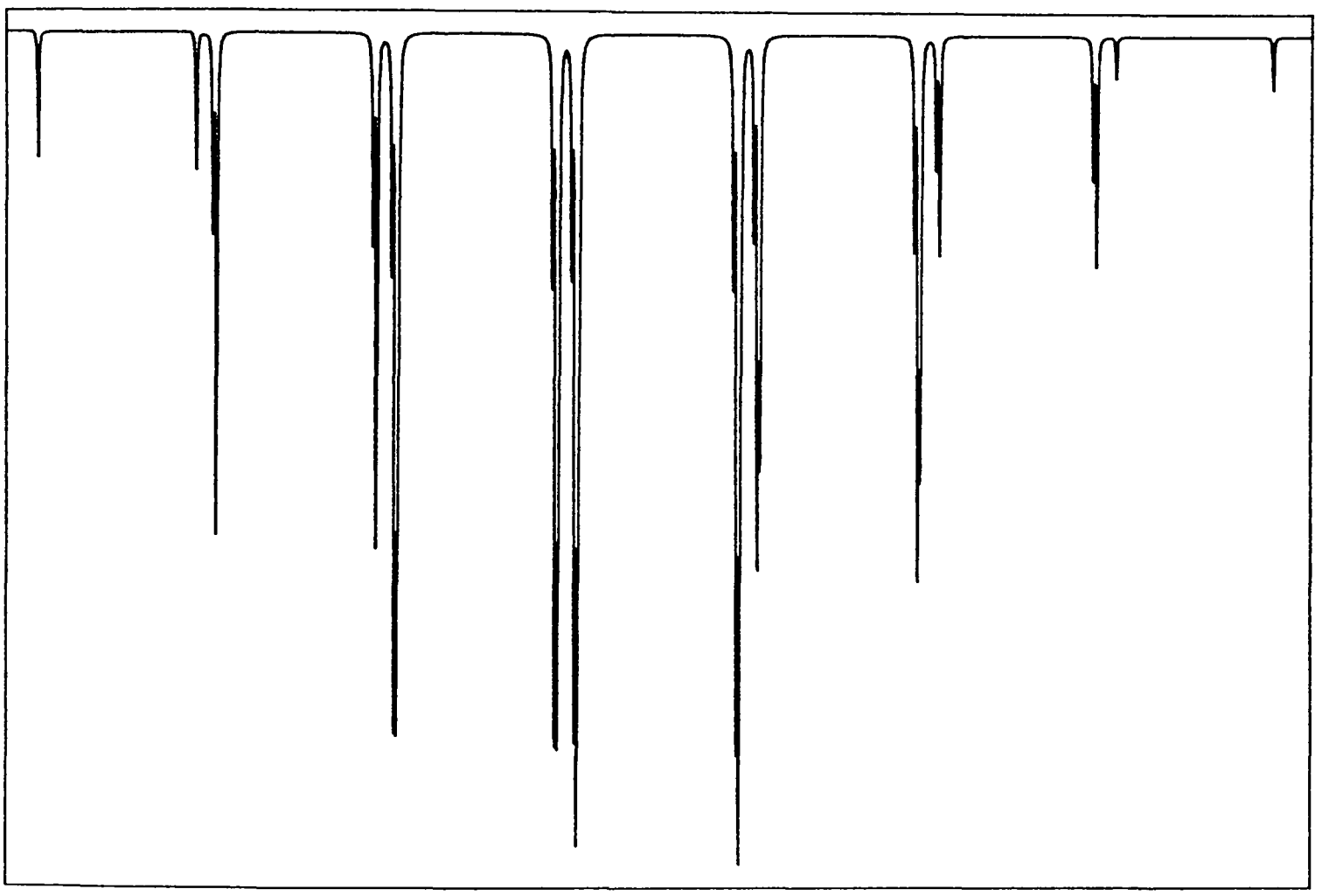

(6.3.1) Conclusions

What has been presented in this chapter is a review of the various known polarization mechanisms, and their illustration by a series of spectra of exceptional quality. At short times after the laser flash these spectra can be analysed completely in terms of these mechanisms. It is also shown that the contributions to the total spectrum from all possible sources vary as one would expect with time and viscosity. It is unfortunate that no accurate method of determining polarization ratios is currently available, for otherwise those generated between acyl and $^{t}$butyl, and between a pair of $^{t}$butyl radicals, for instance, could be used to provide cage–to–escape ratios of free radicals, which would be useful for kinetic and CIDNP studies.

Along the way the first transient spectrum of a $^{13}C$ radical at its natural abundance was revealed, and a resolution of the problem of "unusual" hyperfine intensities in highly viscous solutions and micelles has been given. The reasons for this explanation having not been advanced before are discussed in the light of retrospective wisdom. In addition, previous work purporting to show a violation of the small–mixing condition in RPM polarization development has been re–considered, and that violation was found to have been exaggerated, even in the very viscous paraffin solutions. Material from this chapter will be drawn upon freely in the next.

## REFERENCES – CHAPTER 6


1 Norrish R.G.W., Bamford C.H. *Nature* (1937) 140, 195.

2 Vollenweider J.K., Paul H. *Intern.J.Chem.Kinet.* (1986) 18, 791.

3 Carlsson D.J., Ingold K.U. *J.Am.Chem.Soc.* (1968) 90, 7047.

4 Weiner S., Hammond G.S. *J.Am.Chem.Soc.* (1968) 90, 1659.

5 North A.M. *Quarterly Rev.* (1966) 20, 421.

6 Sheldon R.A., Kochi J.K. *J.Am.Chem.Soc.* (1970) 92, 4395 & 5175 (ibid).

7 de Kanter F.J.J., Kaptein R. *J.Am.Chem.Soc.* (1982) 104, 4759.

8 Ledger M.B., Porter G. *J.Chem.Soc. Faraday Trans.I* (1972) 539.

9 Krusic H.K., Meakin P. *J.Am.Chem.Soc.* (1976) 98, 228.

10 Paul H., Fischer H. *Helv.Chim.Acta.* (1973) 56, 1575.

11 Freed J.H., Pedersen J.B. *Adv.Magn.Reson.* (1976) 8, 1.

12 McLauchlan K.A., Stevens D.G. *J.Magn.Reson.* (1985) 63, 4735.

13 Grant A.I., McLauchlan K.A. *Chem.Phys.Lett.* (1983) 101, 120.

14 Buckley C.D. *D.Phil.Thesis, Oxford* (1988) Chapter 6.

15 Steiner.U.E. (Universität Konstanz) *personal communication* (1988).

16 Aniansson A.G., Wall S.N., Almgren M., Hoffmann H., Kielmana I., Ulbricht W., Zana R., Lang J., Tondre C. *J.Chem.Phys.* (1976) 80, 905.

17 Carmichael I., Paul H. *Chem.Phys.Lett.* (1979) 67, 519.

18 Freed J.H. "*Chemically Induced Magnetic Polarization*" (Ed. Muus L.T. *et al.*) Chapter 19 (Pub. D.Reidel, 1977).

19 Atkins P.W., Evans G.T. *Mol.Phys.* (1974) 27, 1633.

# CHAPTER VII : THE TROUBLE WITH KETONES

# THE TROUBLE WITH KETONES

## (7.1.1) Introduction

This chapter will fall into two distinct sections: one concerns the puzzling early–time absorptive component observed upon photolysis of all aliphatic ketones and dealt with exhaustively elsewhere [1–5]; the other focuses on the equally perplexing long–time behaviour of RPM signals that appear to invert from an E/A multiplet to an A/E phase many microseconds after radical creation [2,6–8] – a quite different effect from the A/E signals observed for secondary radicals in Chapter 5.

Following on from the well–behaved system in the previous chapter, the scope of the chemistry will be expanded considerably to include two indirect radical–generating reactions. That these phenomena do not have an interpretation that can be easily tested will become apparent, though it will prove possible to reject some models and explanations. In a sense, then, this chapter provides a summary of the work carried out to date on both problems, and attempts a review of the only two CIDEP anomalies that appear to have a general physical significance.

## (7.2.1) Propanone Photochemistry

Propanone, and most other aliphatic ketones, are strongly excited at 308nm to yield an excited singlet that intersystem–crosses to the $n\pi^*$ triplet state. Measurements of fluorescence times and Stern–Volmer plots with amine quenchers suggest that the triplet is less than, or as reactive as the singlet state (the quenching rate is very sensitive to steric effects) [9], and insensitive to the nature of the amine, suggesting a charge transfer initially into the $n\pi^*$ state from the lone pair on the amine Nitrogen atom;

reduction potentials for ketones govern the quenching rate, being far greater than the oxidation potentials for amines [10]. These results are confirmed by independent kinetic and CIDEP studies, specifically upon propanone photoreduction by amines over a range of temperatures [11]. In passing, an attempt was made to measure the triplet lifetime and quantum yield for propanone photolysis by a thermal lens method, as described elsewhere [12]. On the equipment available to us we were unable to reproduce any kind of effect, though several approaches were tried both on the apparatus described in Chapter 3 and on a dedicated Optically Detected Magnetic Resonance rig. This is very unfortunate since both quantities are vital to a proper consideration of TM and RPM processes.

Intersystem–crossing to the triplet state is rapid and would, if kinetic conditions are favourable, give rise to a TM polarization but whether in absorption or emission is unclear: the zero field splitting of propanone has been taken as positive from comparison with other aliphatic carbonyls [13] and from this an absorptive TM was predicted, yet a more recent study [14] has demonstrated that D is negative in the triplet molecule isolated in an inert matrix at low temperature. We have noted no such effect on the CIDEP spectrum, even down to the solidification point of alcohols in which the photo–reduction is proceeding, but ST$_-$ effects and those from the spectrum of the radical pair itself ($J_r \neq 0$) are found to dominate, anyhow [15]. Excited singlet propanone shows a distortion from the ground state with the C=O bond lying between 30 and 40$^o$ out of the plane [16]. If such a distortion also applies to the excited singlet molecule then the selection rules for symmetry–driven ISC cannot be justifiably applied ($C_{2v} \rightarrow C_s$).

It is known that certain strained ketones show differing triplet sub–level reactivity [17] and also that, just as spin–orbit coupling can populate triplet sub–levels anisotropically, so it can de–populate them by conferring greater singlet character upon those same states [18], leading either to deactivation or to chemical quenching. It has

been demonstrated for some molecules [19] but experiments on propanone show no measurable difference in triplet sub–level reactivity [20] and, to my knowledge, no work on deactivation rates has been attempted. Biphotonic processes in aliphatic ketones can encourage $\alpha$–scission products [21] by Norrish Type I mechanisms, and a CIDEP study on the complex reaction of biphotonic propanone excitation has been undertaken [22], confirming that even if a high proportion of reaction is via such mechanisms no untoward CIDEP behaviour is observed (Indeed a pure E/A spectrum with no complicating A component results).

(7.2.2) Propanone Free Radical Chemistry

The major photo–product of propanone in alcohols or amines is the propan–2–olyl radical, $(CH_3)_2C^{\bullet}$—OH and this is the only radical that we observe under our experimental conditions in propan–2–ol. The spectrum that results is shown in Fig.(7.2.1). Coupling constants of $a_{\beta H} = 1.950$mT and $a_{OH} = 0.075$mT are found to fit the observed spectrum ideally [23]. A $T_2$ of 0.67$\mu$s reproduces the linewidth and a $T_1$ of 3.5 has been determined under similar conditions [24] by a spin–echo technique. This could not be confirmed by a microwave–swiched experiment on our equipment since this requires that the polarization is formed in the geminate pair alone, but this can only be applied accurately to more slowly decaying signals, anyhow.

The photolytic scheme of interest is[1]

---

[1] Singlet reactivity, though high, cannot compete with ISC so that, for propanone in 1.3 Molar propan–2–ol it contributes only 0.6% of the total reaction [25].

Fig.(7.2.1)

The spectrum of propan–2–olyl radical produced by photolysis of propanone in propan–2–ol. Field sweep is 1.25mT and the simulation uses coupling constants to the $\beta$–protons of 1.95mT and to the hydroxylic proton of .075mT.

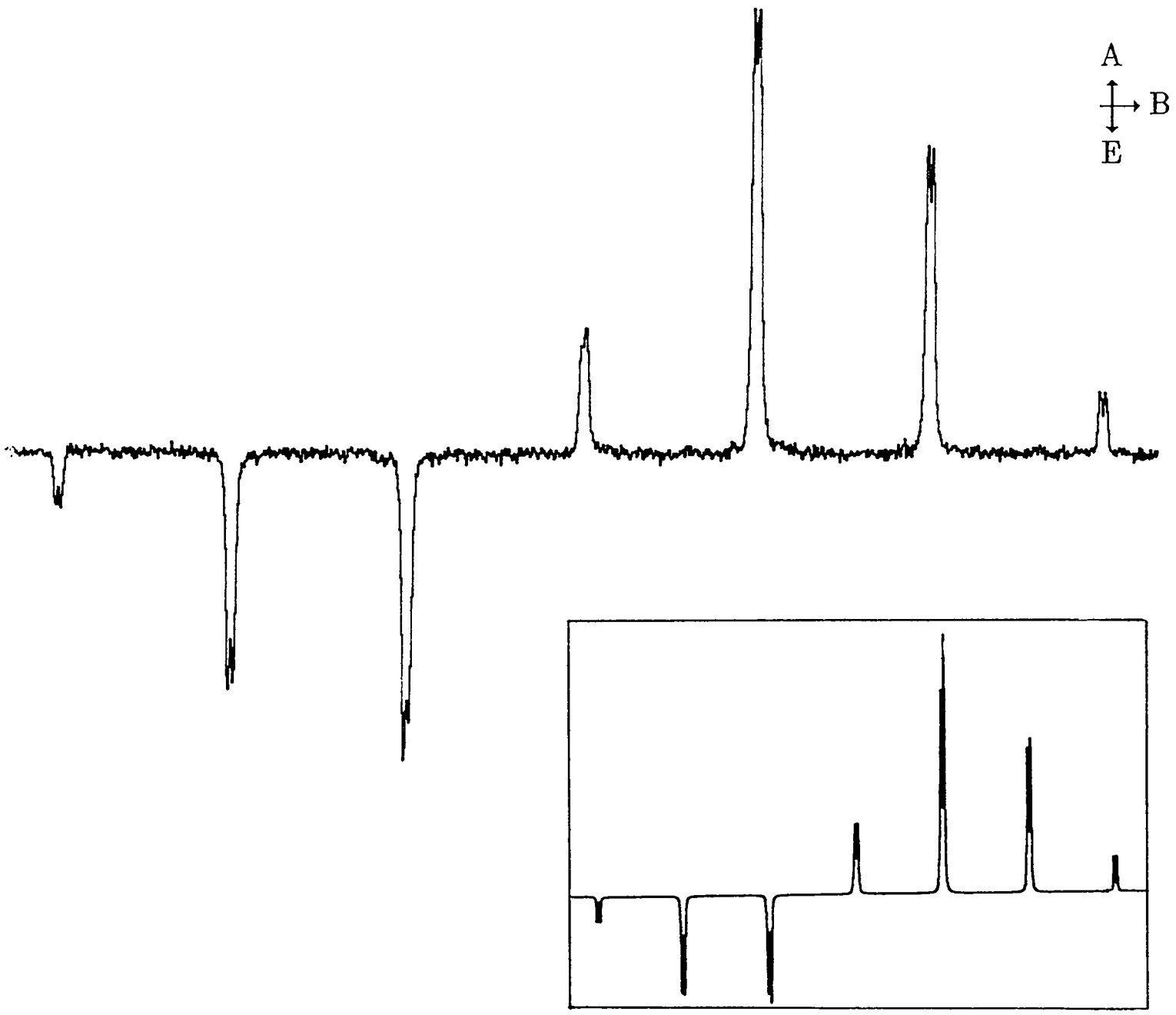

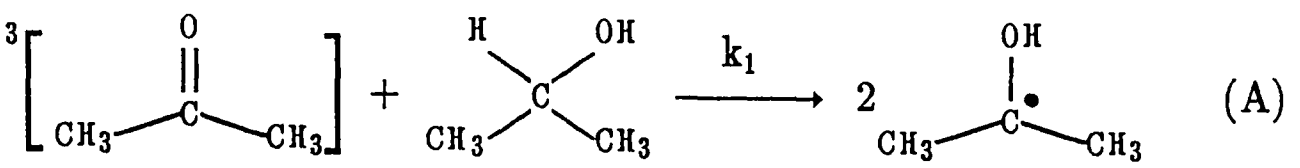

(A)

$k_1 = 9.7 \times 10^5\ M^{-1}s^{-1}$ [25]. Two other reactions,

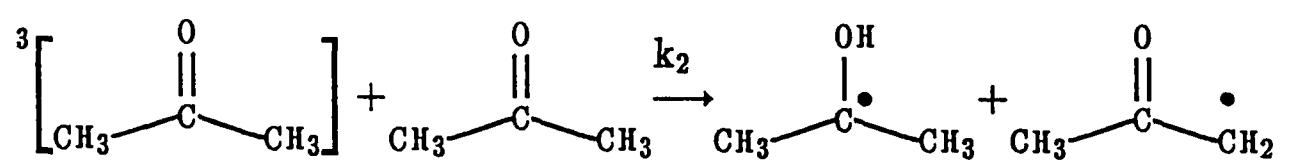

(B)

$k_2 = 5 \times 10^4\ M^{-1}s^{-1}$ [26], and

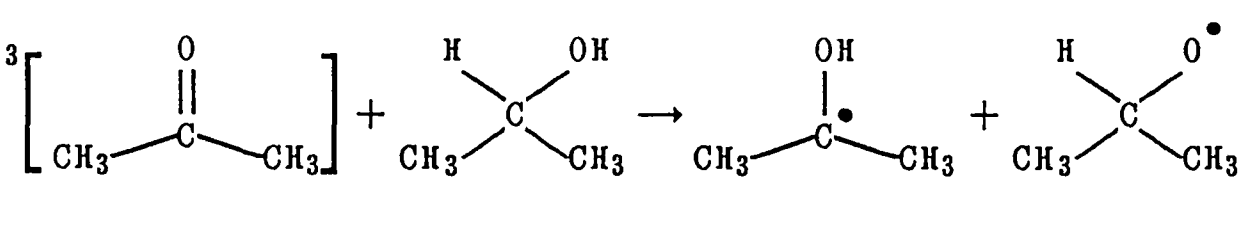

(C)

are known to take place [27 – 29], aside from the $\alpha$–scission. Since in all experiments carried out and reported in this chapter the concentration of propanone was lower than that of the quencher, reaction (B) is an insignificant pathway. Reaction (C) deserves more consideration; there is evidence, both theoretical and experimental, that this mechanism is important for small non–cyclic ketones suffering photo–reduction in their related alcohols. However, the oxygen centered species has a degenerate ground state and is therefore relaxed very efficiently by the spin–orbit contribution to $T_1$ and $T_2$ as it tumbles in solution. This would serve to destroy any polarization and, in keeping with this, no net hyperfine–dependent effect consistent with a high (or even a low) g–value counter–radical is observed. In addition to this the reaction

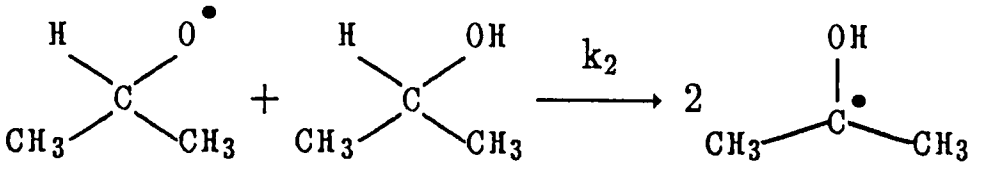

(D)

($k_2 = 2 \times 10^6$ $dm^6M^{-1}s^{-1}$ [30]) is important at high concentrations of propan–2–ol, so that only the geminate radical pair would be affected in any case. Equation (A) is therefore the reaction that prevails, and whilst the photochemistry of the system is potentially complex, under all conditions which pertain in the following experiments it may be treated very simply.

A temperature–dependent transient *e.s.r.* study of propanone in propan–2–ol [31] reveals a full range of $ST_0$ and ST- polarizations, along with, at very low temperatures, the spectrum of the radical pair [15]. An estimate of TM:RPM:Equilibrium polarizations of 8:40:1 is in accordance with the few cases where $\gamma$ for TM [32] and RPM [33] have been measured.

A second study, using a light–modulated technique separates out hyperfine line enhancements for first and second order processes [34], and extracts a rate constant for bimolecular termination (which gives rise to RPM) of $1.4 \pm 0.7 \times 10^9$ $dm^3mol^{-1}s^{-1}$. This implies that the reaction is governed by diffusion rates for the propan–2–olyl radical (in agreement with a series of rates determined at various temperatures [35]). The second order component was found to be a pure E/A multiplet with the expected relative RPM polarizations between hyperfine lines: taking an oversight of the polarization theory into account the ratio of $P_f$:$P_g$ is approximately unity. In keeping with the slow formation rate of radicals ($\tau_T \approx 0.8\mu s$) only a weak net absorption ($1.5 \pm 0.5$ $P_{eq}$) is reported, as would be expected from equilibrated triplet reaction ($1.5$ $P_{eq}$).

Only two products have been identified [36].

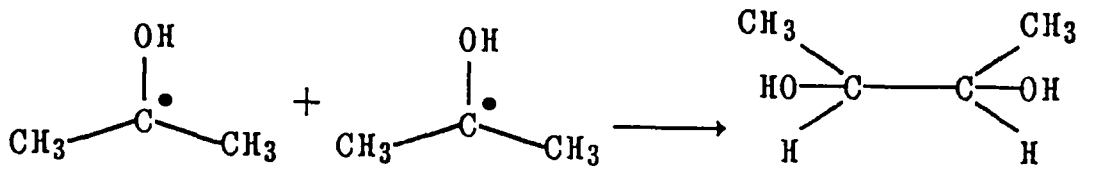

(E)

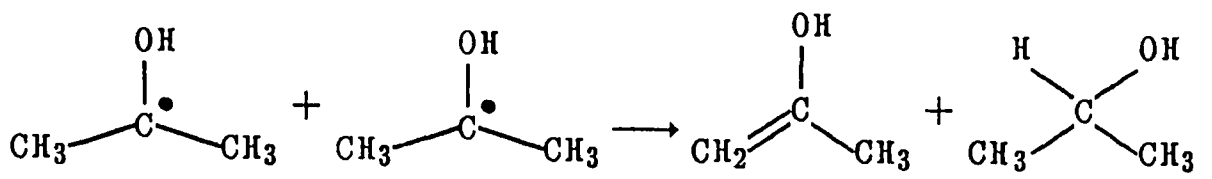

(F)

It would appear that the dominant route at room temperature has a very low activation barrier.

(7.2.3) A Collection Of Experimental Results

The problem, then, is that whilst early–time RPM behaviour is predictable and quantifiable, there is no agreement on either the size or, consequently, the origin of the net absorption. In this section a range of experiments have been carried out, some duplicating previous work to confirm that the earlier experiments were not affected by freak conditions. A recent proposal and demonstration of a radical pair mechanism that can give rise to net, hyperfine–dependent polarization is also examined.

It is a simple process to demonstrate that not only is the absorptive component polarized, but that it is polarized to the same extent as the hyperfine–dependent part. Referring back to equation (2.3.8) it is apparent that a variation in $\omega_1$ will affect polarized and equilibrium terms differently. This is shown in simulations, against which easy comparisons with observed spectra can be made. No correspondence is observed in Figs.(7.2.2) and (7.2.3) for a spectrum consisting of just RPM and equilibrium terms.

Let us consider, now, that by some fluke of rate constants, a small number of excited triplets react with the alcohol within the first few nanoseconds (the rate constant does not permit the bulk of triplets to react within typical $^3T_1$ times), leading to

Fig.(7.2.2)

The effect of a low $\omega_1$ power upon the absorptive component of the propan–2–olyl spectrum, with a simulation using a calculated value of $\omega_1$ of 0.4radMHz. Field sweep is over 8.5mT and the spectrum was sampled from 0.6 to 1.6$\mu$s.

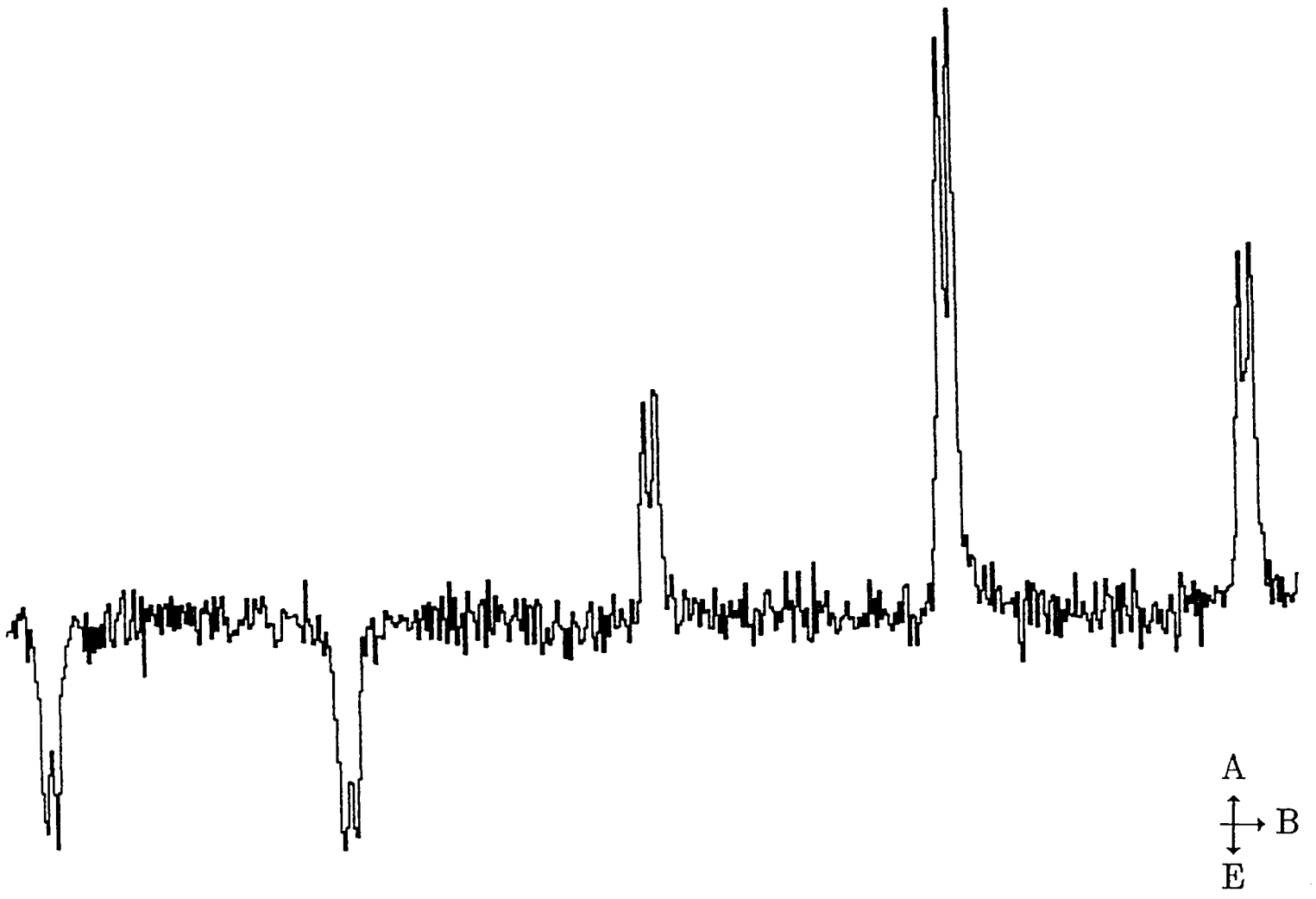


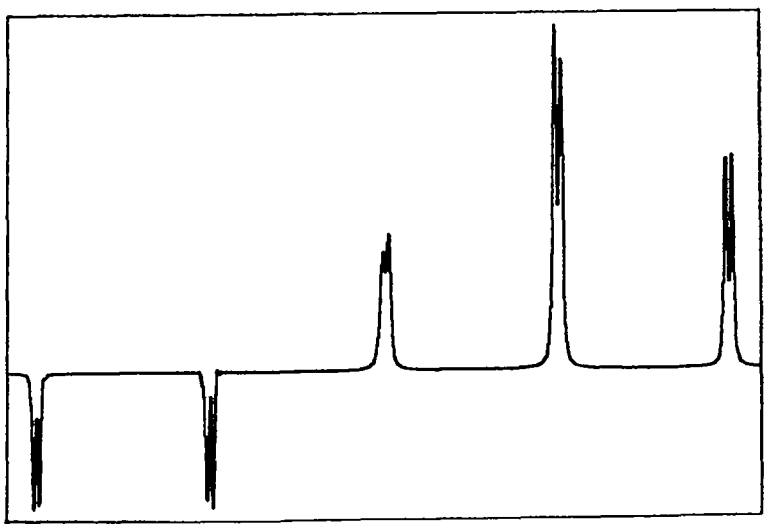

Fig.(7.2.3)

The same spectrum but recorded under very much higher microwave power: $\omega_1 = 1.9 \text{radMHz}$. The simulation, which takes the value of $\gamma$ for the absorptive envelope used in Fig.(7.2.2), bears little relation to the observed spectrum.

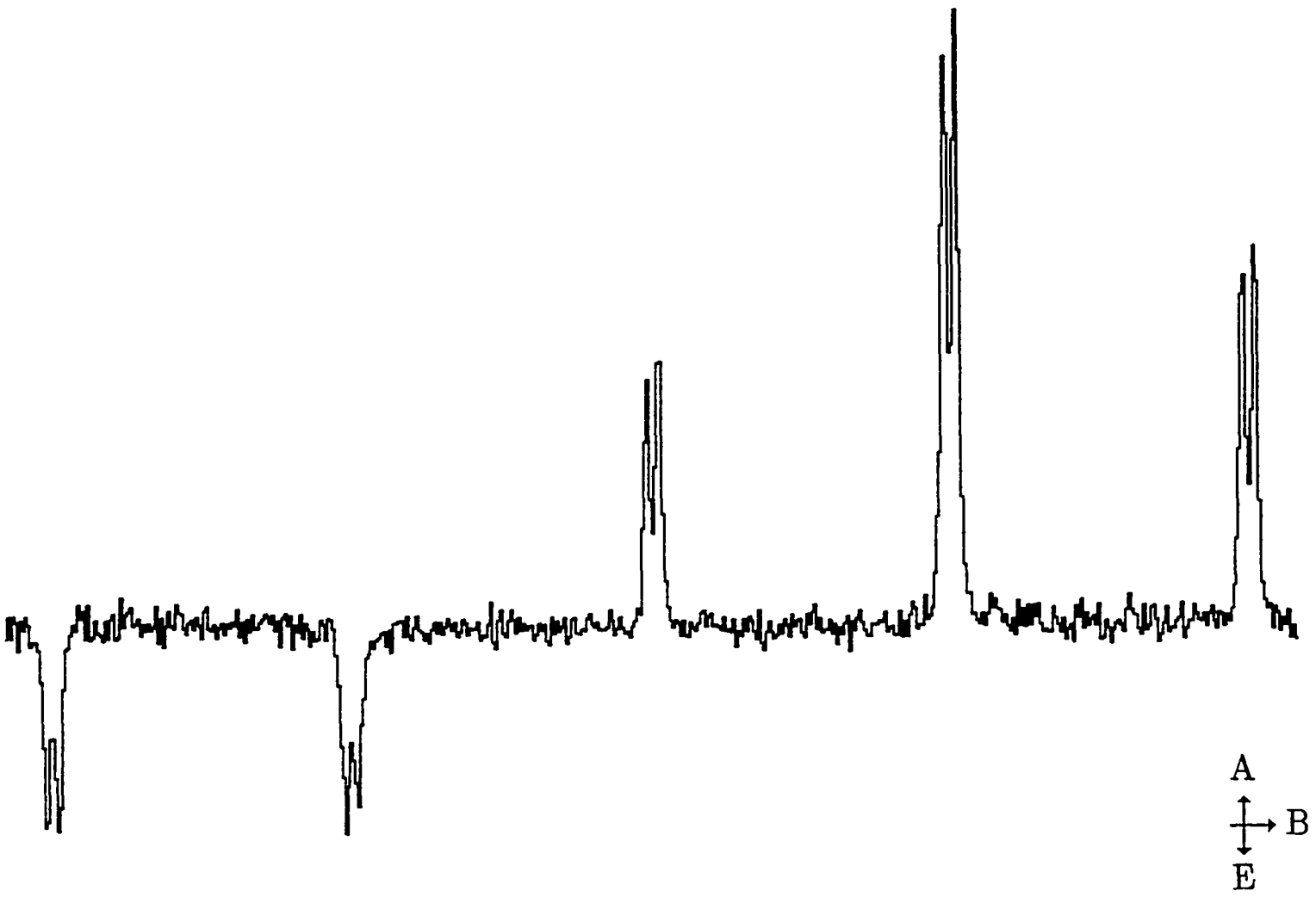


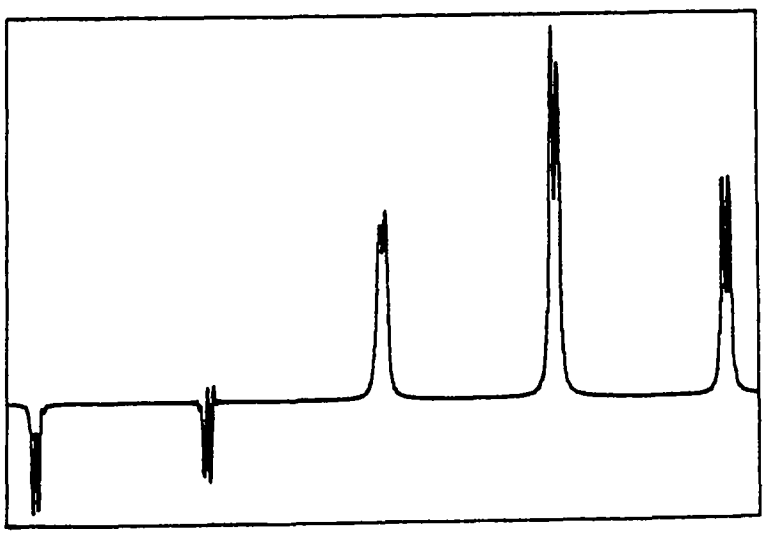

TM–polarized radicals, thereby dragging up $\gamma$ for the ensemble of radicals. For such a scenario the observed TM would be highly sensitive to quenching rate. Reduction of TM would occur upon dilution of the alcohol to one half of its original concentration by a far less reactive co–solvent, 1,4–dioxan. Spectra recorded 1.0 to 2.0$\mu$s after the flash are shown in Fig.(7.2.4), in which the sum of third and fifth peaks are the same within experimental error, though by reference to equation (4.2.18) we should expect to see a near–linear decline in the TM polarization. The second direction we can take is to increase quenching rate by substituting alcohols by amines [11], the relative rate for the amine being three orders of magnitude higher than for the alcohol [9]. Thus, as amine concentration is increased we should expect to see first an increase in TM, followed by a decrease as triplet scavenging becomes too fast to allow development of polarization in the laboratory frame. This pre–emptive quenching of TM would occur at a lower reaction rate than we would observe the scavenging of excited singlets, but at even higher levels singlet reactivity becomes evident by the A/E phase of multiplet RPM. The results are displayed in Fig.(7.2.5), and clearly demonstrate the increase in singlet reactivity: if one assumes $P_{s_{RPM}}$ is approximately the same as $P_{t_{RPM}}$ then the singlet/triplet quenching achieves parity at a concentration of 3.0 Molar tri–ethyl amine, giving an ISC rate of $10^{10}s^{-1}$. The remarkable feature of all these spectra is that the relative magnitude of the central line, and its absolute size compared to the background noise, is constant – sufficient evidence to exempt the TM from further consideration[2].

---

[2] It should be mentioned that an apparent variation of this absorptive phase with orientation of plane of plane–polarized exciting light [4] has been shown to have been mis–interpreted [5]. The effect observed was almost certainly a consequence of non–isotropic transmission of the exciting radiation by the sample cell.

Fig.(7.2.4)

The effect of adding inert co–solvent to a reaction mixture. The two spectra below, recorded over 8.5mT show no apparent variation in relative size of R.P.M. and absorptive components, though reduction in quenching rate from that observed in pure propan–2–ol would reduce TM polarization linearly.

Photolysis of propanone in a 50:50 vol/vol mix of propan–2–ol and dodecane.

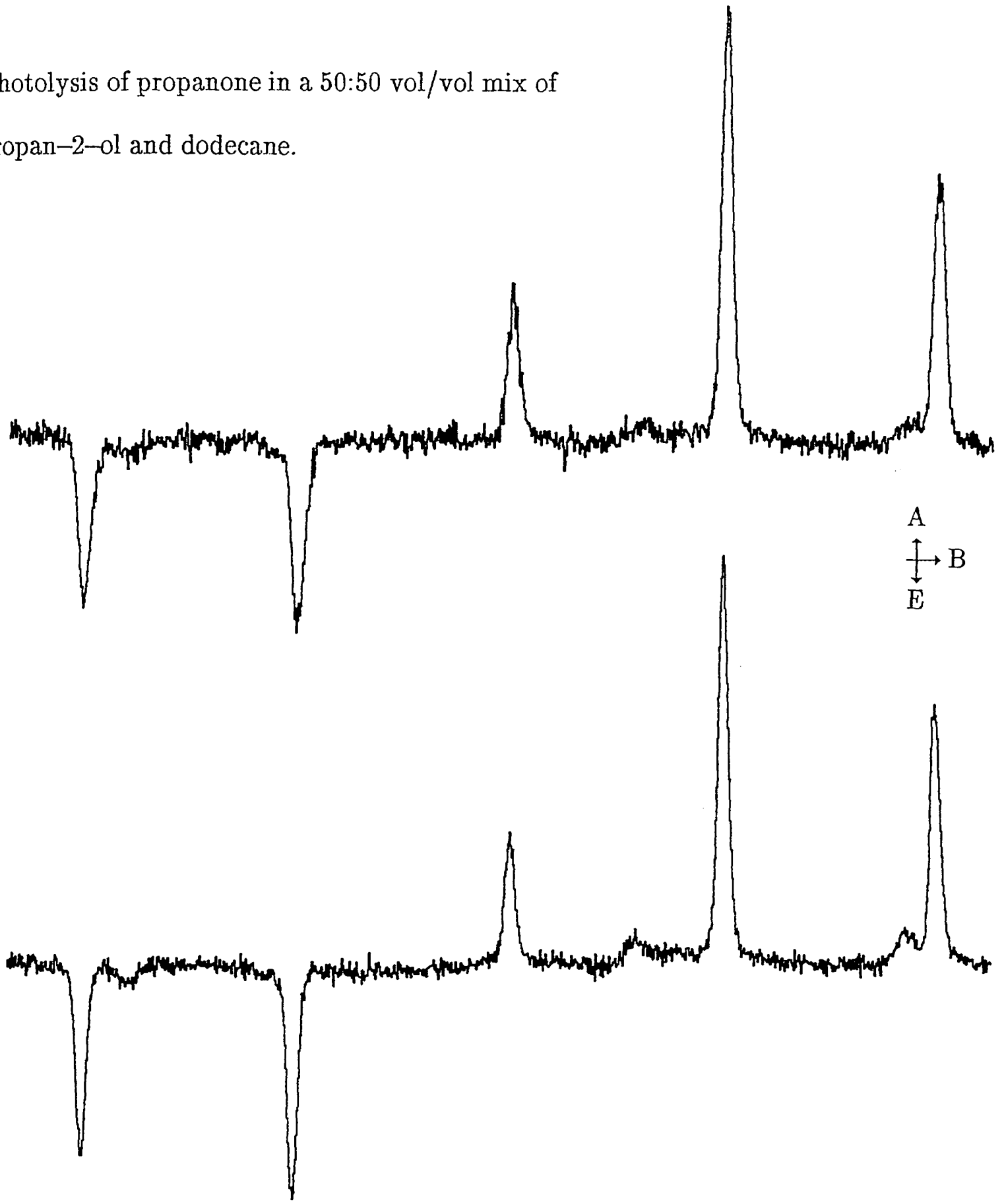


Photolysis of propanone in a 25:75 vol/vol mix of propan–2–ol and dodecane.

Fig.(7.2.5)

The effect of amine quenchers upon triplet propanone reaction.

As concentration of tri–ethyl amine is increased the E/A multiplet, indicating triplet reactivity, gives way to an A/E multiplet, indicative of overriding singlet reaction. All spectra are recorded over 9mT and from 0.4 to 1.6$\mu$s.

1 Molar $Et_3N$ / 1.4M propanone in benzene.

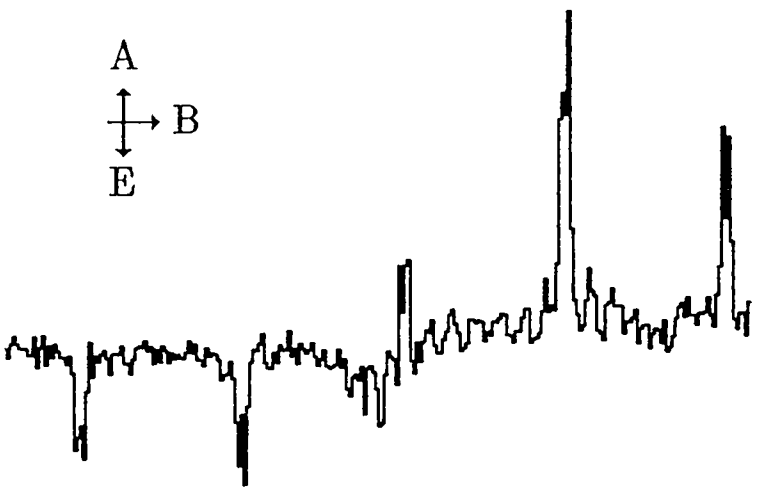


3 Molar $Et_3N$ / 1.4M propanone in benzene.

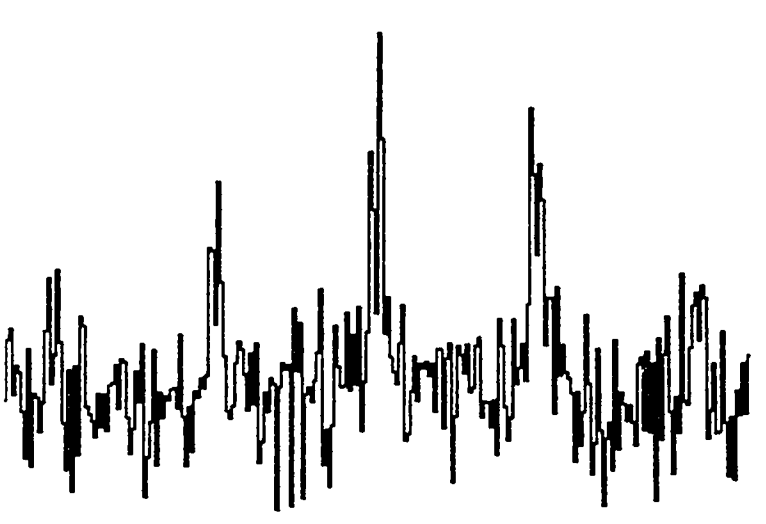

Neat $Et_3N$ / 1.4M propanone.

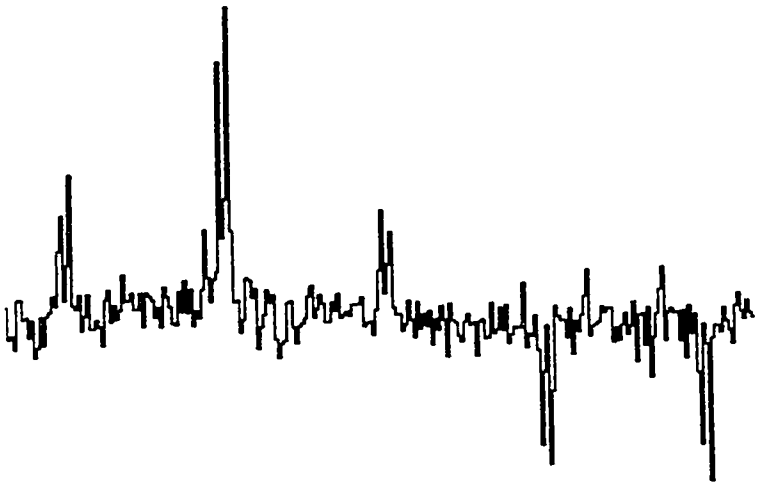

(7.2.4) Spin–Rotation – A Scalar Interaction.

The coupling between the electron spin and molecular rotational motion was shown to give rise to relaxation in §(2.2.2). It may be a very efficient relaxation process and is known to be the major source of relaxation in $CH_2^{\bullet}OH$ ($T_1 = T_2$) [37]. The interaction is of the same form as the hyperfine coupling between a nucleus and an electron, and it is thus capable of generating polarization. It will differ from the RPM in that the polarization so produced will be hyperfine–independent, as the rotational state and the nuclear spin state of a radical are independent (their operators, $\underline{I}$ and $\underline{J}$, commute). A criterion that

$$\Delta\omega.\Delta\tau \geq 1 \qquad (7.2.1)$$

must be met for a significant polarization to be built up ($\Delta\omega$ is the level separation in frequency units, $\Delta\tau$ is the time for which the radical is resident in that level). Under our conditions $\Delta\omega \approx 5 \times 10^{10}$rad.s$^{-1}$ and $\tau_c$ is less than $10^{-12}$s [38]. the product of $\Delta\omega.\Delta\tau$ is thus far too small to discriminate between levels.

If we consider a radical pair, however, for which $J \gg g\mu_B B_0$ then, provided that the spin rotation interaction is large enough to couple S and $T_1$ states, by virtue of the far larger size of $\Delta\omega$, the product may be close to, or even exceed unity. In addition the above value for $\tau_c$ was calculated from studies on transition–metal complex ions, whereas we are dealing specifically with an alcohol–related radical which is fairly planar and capable of hydrogen bonding. Both effects may allow $\tau_c$ along one axis, at least, to be substantially larger[3].

---

[3] There is a precedent here: Schuh H.H. and Fischer H. noted a limited singlet reactivity between pairs of encountering alkyl radicals and ascribed it to steric

Another matter to consider is that, unlike nuclear perturbations on electronic energies, which for the timescale of RPM generation are static, the imbalance in rotational energy levels necessary to cause this effect is transient, and will subside at a rate that is equivalent to $\tau_c$, the rotational correlation time. Where might such an imbalance arise? On creation of a radical pair the chromophore and its surroundings will be very hot, a high degree of electrical energy having been dissipated, so that, to achieve rotational thermal equilibrium with its surroundings, the radical pair will acquire higher rotational energy at the expense of the spins. As an example,

$$|\langle T_{+1}^{+}|\ \mathscr{H}_{sr}|\ S^{-}\rangle|^2 = c^2/8 \qquad (7.2.2)$$

where c is the spin–rotation coupling constant and $T_{+1}^{+}$ represents a higher rotational state, $S^{-}$ a lower one. Such a simple picture could be extended to cover long–time re–encounters for which high relative rotations of the two radicals would act as an instantaneous activation barrier, favouring the separation of those radicals in higher rotational states. The resulting net polarization on the spins would therefore be opposite to that observed for geminate separation.

The foregoing speculation can be simply tested, for the relative contributions of spin–rotation to relaxation decrease between $CH_2^{\bullet}OH$ and $CH_3C^{\bullet}(OH).CH_3$ whilst the RPM increases. If spin–rotation is responsible then the net absorption should dominate the spectrum of the former, and should be less important in the latter. Fig.(7.2.6) shows spectra and simulations of these two radicals produced under identical conditions: it is immediately apparent that a slightly larger effect is present in the spectrum of the

---

constraints and a slower rotational diffusion of "radical/solvent aggregates" in *Helv. Chim. Acta* (1978) 61, 2130.

Fig.(7.2.6)

Comparison of two radicals: the radical derived from methanol by H–abstraction is expected to have a higher spin–rotation term than that for propan–2–olyl radical; a simulation of the spectrum for the methanolyl radical required a TM–like absorptive phase of magnitude 3 times the RPM polarization. Inclusion of an identical size contribution to the spectrum of the propan–2–olyl radical gives the simulation shown.

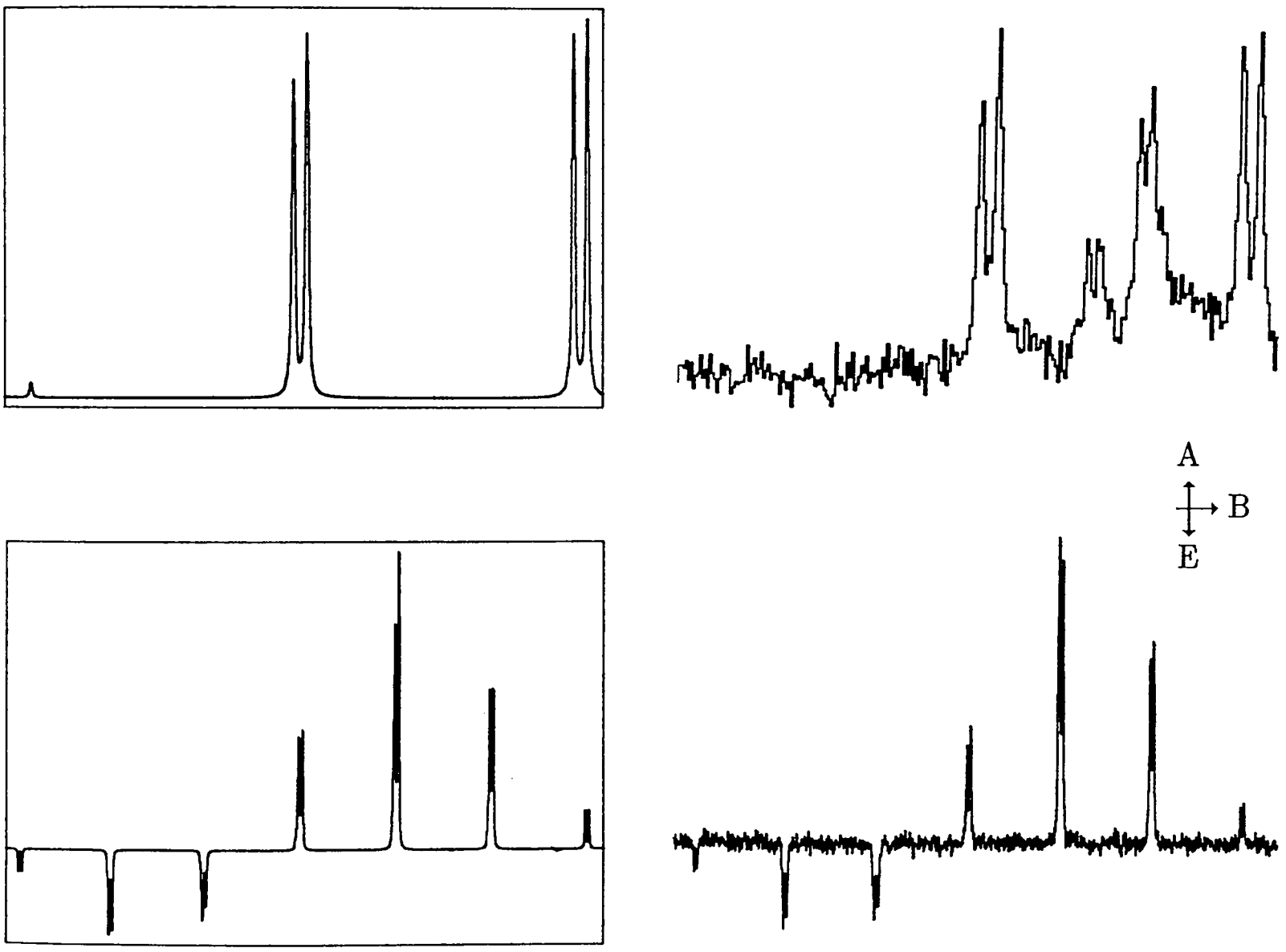


Counter radical peaks from octan–2–ol are visible in the upper spectrum. The inclusion of an identical magnitude component in the spectrum of the acetolyl simulation only marginally over–emphasises the observed absorption.

$CH_2^{\bullet}OH$ radical (the viscosity of the methanol/peroxide solution was adjusted by addition of octan–2–ol to match that of the propan–2–ol solution). The effect is not large but it is interesting to note that it lies at the top end of the range for aliphatic ketones that have been experimented upon, whilst those of larger parent molecules, such as the cyclohexanolyl radical show a very small net effect. As pointed out in the previous chapter absorption is reduced as viscosity is increased, yet that apparent reduction cannot be modelled in terms of a stronger ST_ polarization.

(7.2.5) The Radical/Triplet Encounter Pair.

A recently proposed theory [39] which has been satisfactorily tested involves the encounter and separation of a radical and a long–lived triplet. The systems chosen were the relatively unreactive benzil and naphthalene triplets, encountering alkyl radicals. The results showed that net hyperfine–independent emission could be created in the spectrum of the observed radical. This was analysed in terms of ISC and energy–transfer quenching [40]

Two major inconsistencies between theory and experiment lead us to reject this idea for our systems: firstly the polarization is expected to increase with $\eta$, the viscosity, whereas in fact the reverse is observed, relative to the normal radical/radical RPM [14,15]; secondly the theory implies that net polarization will always be emissive[4], irrespective of the sign of the zero–field splitting, D.

Since the acetone triplet and possible un–purged oxygen are the only species capable of causing such an effect in this system, two simple tests are demonstrated.

---

[4] Clearly this is out of keeping with our findings, though it may well be that the bulk of reportings of "emissive TM" in the photolysis of a lot of aromatic molecules may have been mis–ascribed.

Fig.(7.2.7a) shows an identical A + E/A spectrum to that recorded for acetone, though here the photoinitiator is di–$^t$butyl peroxide. As mentioned in §(5.2.2) its dissociation state is not known for certain but we can be sure that the excited state does not hang around as a triplet for a microsecond or more! The second test employs varying oxygen concentrations, from the completely de–oxygenated to an $O_2$–saturated solution. No variation was reported save an increasing disruption of polarization with oxygen concentration – no signal was observable in the $O_2$–saturated sample. A nearly saturated sample gives the spectrum shown in Fig.(7.2.7b)

(7.2.6) Assorted Experiments.

Variation of pH betwen 5 and 8 in aqueous propan–2–ol and selective deuteration of the OH postion revealed no detectable change in the relative heights of hyperfine lines – Fig.(7.2.8) and Fig.(7.2.9). In addition, photolysis of propanone ($d_8$) in propan–2–ol ($d_9$) has been carried out [41]. Once again it is apparent that RPM:net polarizations are the same.

The absorption in propan–2–olyl radicals is observable from the earliest times and its growth seems to be limited by the response time of the equipment. This is not the case for the closely related cyclohexanol/cyclohexanone system (exchange between conformers interchanges line positions at an intermediate rate at room temperature [42] which serves to broaden six of the nine potential lines). Of interest to us is the slower growth of the absorptive phase compared to that for the propan–2–olyl spectrum. Such an observation is consistent with the slower exchange of electron spin level populations by internal motion: exchange between conformers is slow compared to the rotation of methyl groups in the propan–2–olyl radical. In other words we might look for an explanation in terms of some internal spin–rotational cross–relaxation, but this

Fig.(7.2.7)

Comparison of two spectra of the propan–2–olyl radical, recorded under identical conditions apart from the degree of de–oxygenation carried out on the sample before photolysis: the lower trace was recorded for a solution near–saturated with $O_2$. Both were recorded over 13.0 and 12.5mT.

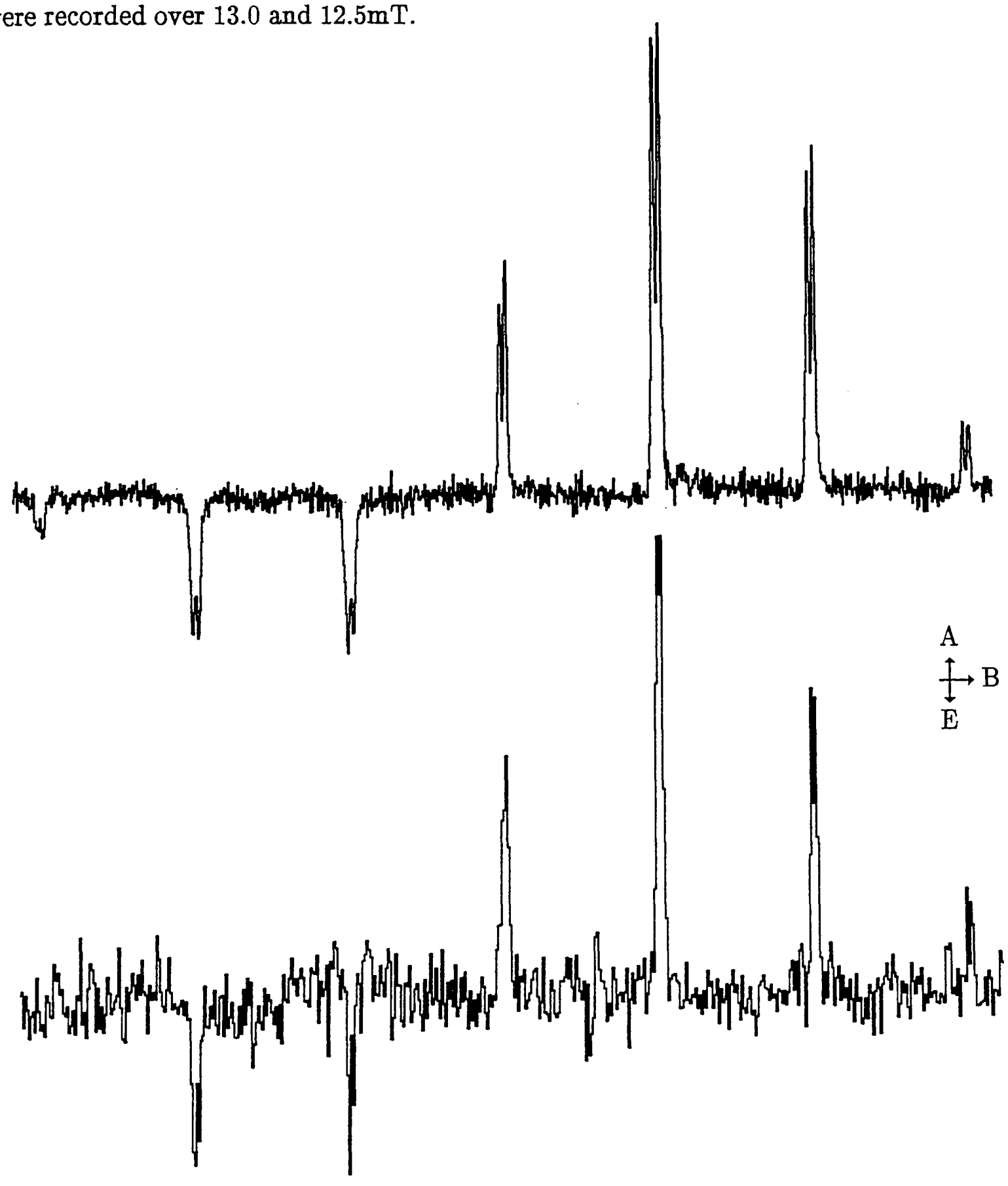

Fig.(7.2.8)

The effect of increasing acidity upon the absorptive component of the propan–2–olyl radical. Both spectra were recorded over 13.0mT and from 0.5 to 1.5$\mu$s.

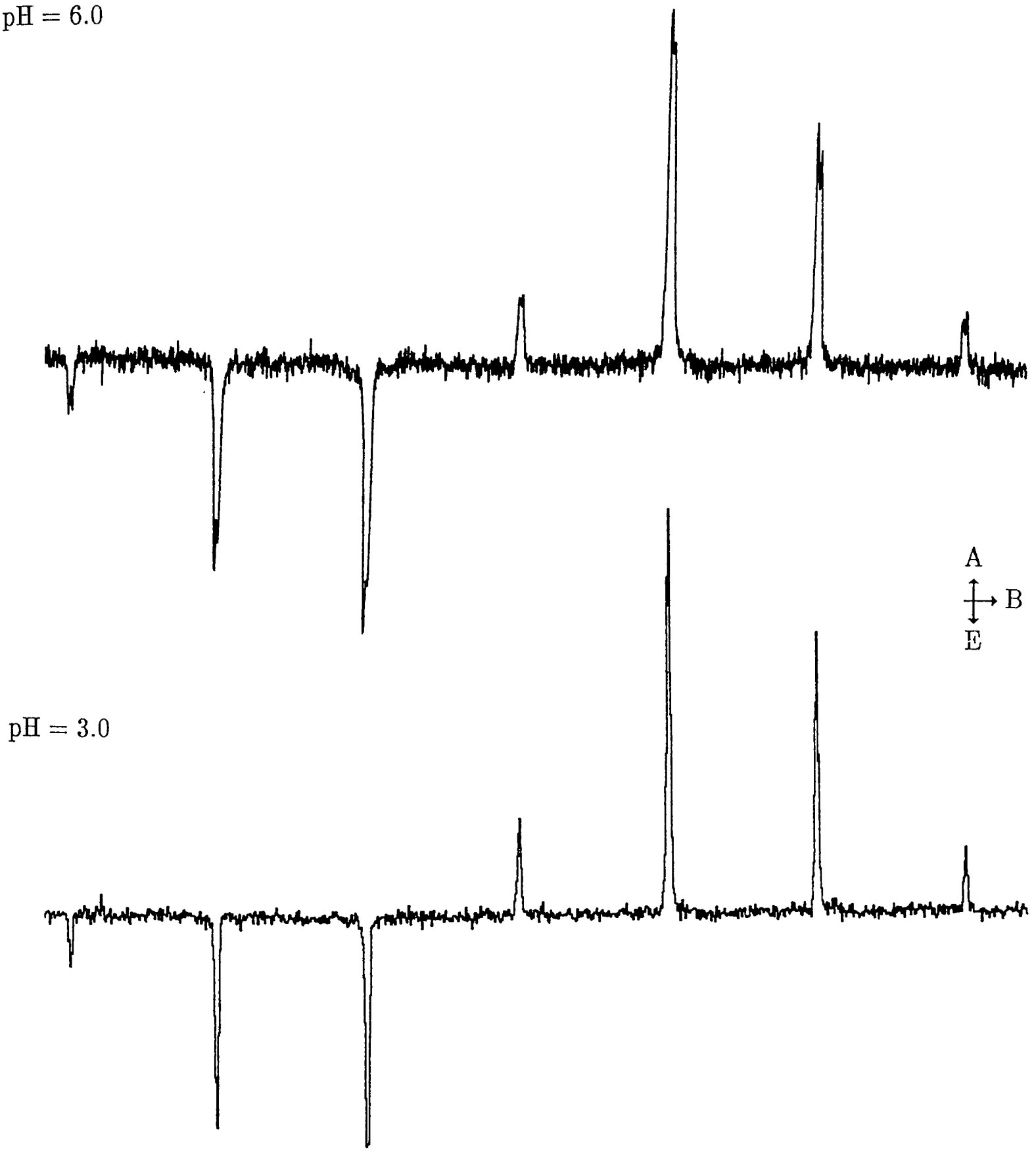

Fig.(7.2.9)

The effects of deuteration upon a spectrum of the propan–2–olyl radical derived from photolysis of propanone in propan–2–ol/water mixture (B.pt = 91°C) at pH 6. All spectra are recorded over 13.0mT and from 0.1 to 1.5$\mu$s.

Solvent is $(CH_3)_2C(H)OH$

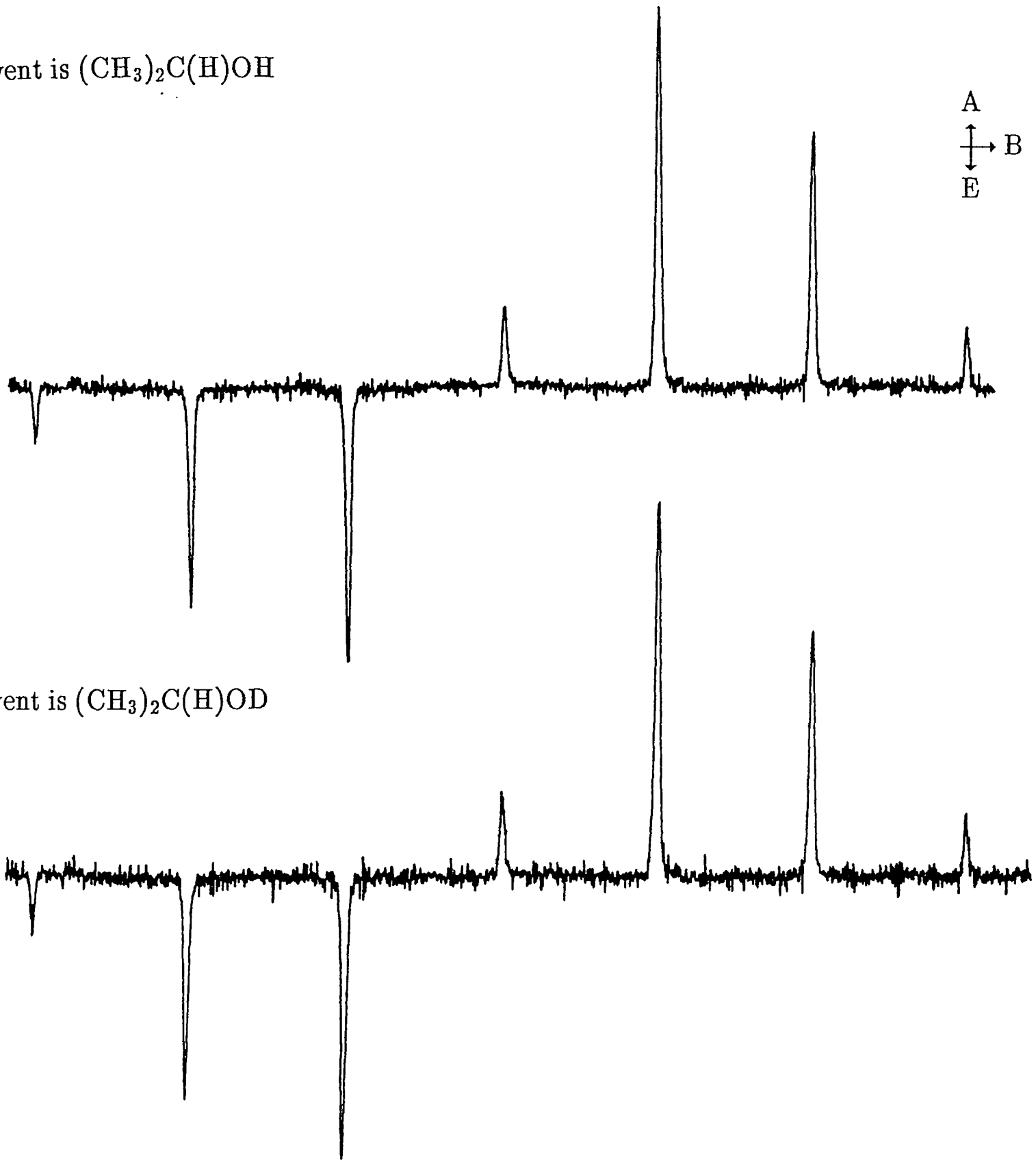


Solvent is $(CH_3)_2C(H)OD$

explanation would have to exclude the $CH_2^{\bullet}OH$ radical for which none is possible. And once more the viscosity plays a part, for cyclohexanol is very much more viscous than propan–2–ol.

(7.2.7) A Summary

Such conclusions as can be drawn from all this are largely negative. Thus we know that TM and equilibrium polarization, triplet/radical and internal motion are incapable of providing unique and general solutions to this problem. Sadly, no quantitative and reliable method of measuring polarization ratios exists as yet, and until one is developed it seems that the problem will remain. It has encouraged a re–think of the CIDEP phenomenon, however, and perhaps most importantly, the absorptive envelope has proven to be well behaved – that is, it has not swung wildly in magnitude or reversed its phase with a change in experimental conditions. Nor has it apparently affected the development of other forms of polarization. We may continue, then, to treat it as a predictable anomaly, incorporating it as an *ad hoc* parameter in the simulations of polarized spectra.

(7.3.1) Long Time Inversions Of Phase.

The history of this problem is even longer than that of the previous section. The matter to be addressed is why an early–time E/A signal, which is in all other respects well–behaved, should invert to become A/E at longer times as though radicals were reacting through the singlet state. An example is given in Fig.(7.3.1).

The earliest observation of unusual behaviour was made on the photolysis of $^t$butyl phenyl ketone [43] which was being investigated in order to separate TM and RPM processes, since both fragments of the photolysis could be identified. At long times after

Fig.(7.3.1)

Two genuine examples of phase changes in the multiplet spectra of free radicals:

a) Photolysis of 0.5M 3,3 di–methyl butan–2–one in heavy paraffin. Spectra are recorded over 1.0 to 2.0$\mu$s and 21.0mT and 50 to 70$\mu$s and 12.0mT respectively.

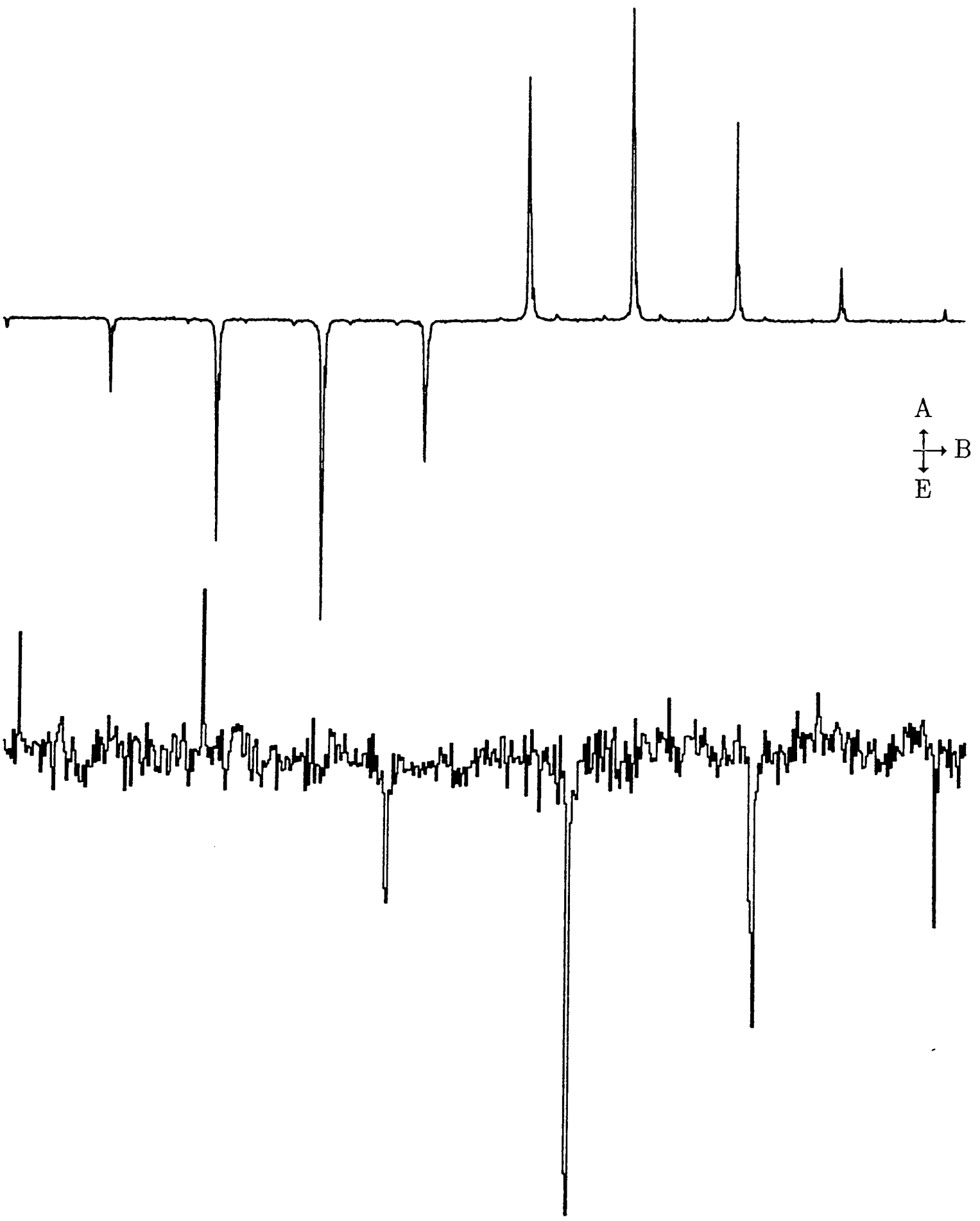

b) Photolysis of 0.1M $^{t}$butyl phenyl ketone in heavy paraffin. Spectra are recorded over 1 to 3$\mu$s and 12.5mT and 20 to 85$\mu$s and 7.5mT respectively. The central feature is the benzoyl radical, and interestingly, it remains in emission throughout the period of observation.

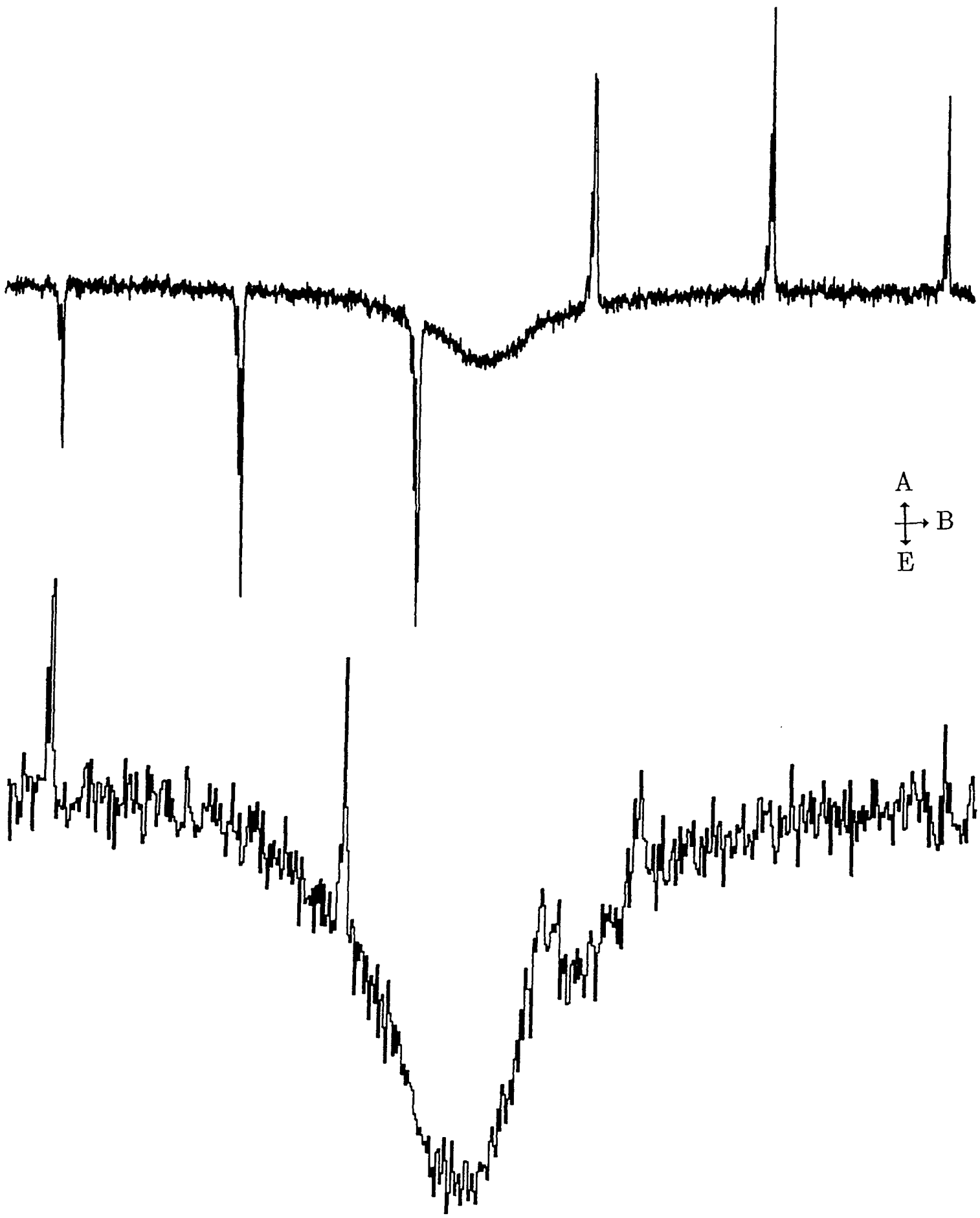

the flash the $^{t}$butyl lines appeared to develop a slowly rising polarization of the opposite phase to the earlier one. The possibility was advanced that singlet encounter pairs could be polarized more strongly than triplet ones, and this idea has been treated thoroughly since [44]. A triplet exciplex mechanism (postulating a positive $J_r$ for a small range of encounter distances), and an activated singlet reaction pathway have also been proposed, the latter arising from observations of CIDNP which indicated that the simple coupling recombination product, given in reaction (7.2.5) was only favoured at higher temperatures.

Clear E/A to A/E behaviour has since been published for pairs of $^{t}$butyl radicals [6], $^{i}$propyl radicals [7], propan–2–olyl radicals [2] and several related ketyl species, recorded on the apparatus described in Chapter 3, similar flash–photolysis *e.s.r.* rigs, and on a completely different detection device, employing sinusoidally modulated exciting radiation, which functions by picking up signal that varies with the frequency of the exciting light (mono–molecular reaction such as geminate re–combination) and the frequency squared (bi–molecular reaction such as F–pair reaction) [6]. This latter is an important point for it is a simple matter to generate spurious phase inversions of signals by pulsed *e.s.r.* experiments that employ a continuous, sampling microwave field – I have eliminated a consistent artifact in spectra recorded upon our apparatus before 1989, which arises from the presence of coupling capacitors in both transient recorder and amplification devices. The reason for experimenters' failure to recognise this artifact is that the end result upon each spectrum and for each set of experimental conditions, including temperature and solvent, is different. A subtle interplay of effects can give rise to spectra recorded at long times that are anything but mirror–images of those at shorter times, so a simple reflection of the strong early signals, caused by the discharge of potential stored in these capacitors, is seldom observed. One case where it is is presented

in Fig.(7.3.2) but even here the behaviour of signal with time is superficially plausible, with an intermediate stage in which pure absorption is visible, at which point it was argued the early and late time "polarization processes" cancelled each other out. Since recognising this fault and removing it I have been unable to reproduce the inversion of the di–ethoxy phosphonyl doublet (E*/A to A*/E) or the penta–fluoro benzene sulphonyl spectrum (A*/E to E/A) reported in reference [8], and various unpublished results of oscillating or inverting RPM signals have also been shown to arise form the same source. *a.f.c.* circuitry has also been considered as a possible source of phase inversions, so a re–examination of the *a.f.c.* sample–and–hold circuitry has been carried out by us and other workers [46], and a final check was made by gating the microwaves off for the first 10$\mu$s of radical spin evolution after the flash before being re–applied. All these results attest to the genuineness of the observations for the ketyl radicals to be described, and for the $^{i}$propyl and $^{t}$butyl radicals.

Attempts at explaining this phenomenon may be neatly divided into those that separate F– and G–pair behaviour and those that do not. The former class will be examined first.

(7.3.2) Qualitative Differences Between F– and G–Pairs

We have at our disposal several possible methods of generating A/E style polarizations if we make this distinction between behaviour of radical pairs, and further, it is not an arbitrary distinction for we should expect markedly different behaviour from the two examples. We may reject singlet–geminate reaction as a source of the A/E multiplet, however, for a combination of relaxation times, polarization evolution rates and microwave powers ensures that this geminate signal dies away usually within a couple of microseconds, to be replaced by the more common E/A RPM pattern (an

Fig.(7.3.2)

The appearance of a spurious phase inversion from E/A to A/E, caused by a coupling capacitor in the transient recorder. This effect gives a long time signal that is a mirror image of that at early times, provided that no substantial genuine signal is present by that time. Sweep width is 13.0mT and sampling times are 1 to 2$\mu$s and 50 to 75$\mu$s.

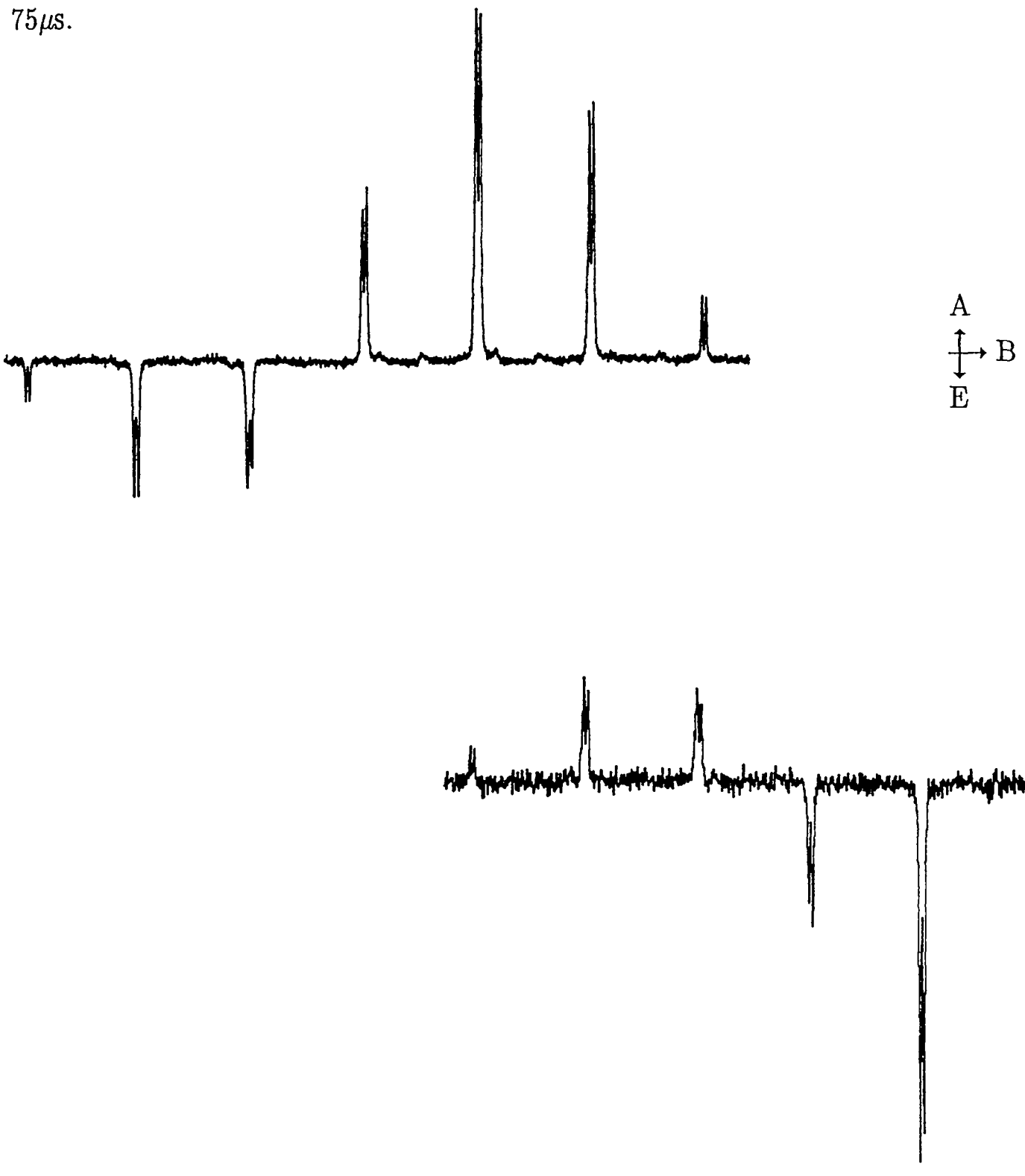

example will be shown later on). In other words an early–time A/E multiplet can transmute into a longer–time E/A, but the reverse cannot happen. A simulation of the decay curve for singlet–geminate reactive radicals that react upon free encounter in solution predominantly via the singlet state is shown in Fig.(7.3.3).

Two models merit consideration, both relying upon the different relative diffusional trajectories of G– and F– encounter pairs.

Firstly, it is clear that the geminate pair will be created at a separation that is smaller than that at which radicals encountering each other in solution will become spin–correlated (and hence either reacting or diffusing apart as an initially correlated S or $T_0$ pair). Over the entire cycle of separation and re–encounter for an F–pair, then, a different total exchange will be experienced than for a G–pair. Let us propose a bi–phasic exchange interaction, $J_r$, such that it is positive over a small range of r. This is not without precedent for a positive exchange has been invoked to account for the magnetic behaviour of some near–rigid electron transfer agents in biochemical systems [47]. Using such an exchange interaction it has been shown that G– and F–pairs can produce opposite polarizations for the same hyperfine line [48]. In terms of Adrian's vector model for RPM this is equivalent to a clockwise rotation about the z–axis for G–pairs and an anti–clockwise one for F–pairs.

A second explanation, recognised as a possibility long before any experimental evidence had been garnered [49], and given a thorough treatment elsewhere [44] is that as singlet encounter pairs may have different diffusional trajectories from triplet pairs – explicitly, that they will be held together for longer than their triplet counterparts by virtue of the attractive exchange potential – they may be more strongly polarized than triplet pairs. All that is then required is that a large enough number of singlet pairs do not react, so that the free radicals remaining evolve with a net singlet polarization across

Fig.(7.3.3)

A simulation of the effect of singlet reactivity upon a radical that was born in a singlet radical pair state, and that reacts predominantly through the singlet state upon encounter with another radical. This simulation employs the following values: $T_1 = 2.5\mu s$; $T_2 = 0.8\mu s$; $\omega_1 = 0.5$radMHz; $P_i = P_f = 20\ P_{eq}$; $n(0) = 1 \times 10^{-4}M$; bi–molecular recombination rate $= 1 \times 10^{9}dm^{3}M^{-1}s^{-1}$. The whole trace represents a $100\mu s$ time window, and inversion of the simulated transient from E to A occurs after $3.5\mu s$

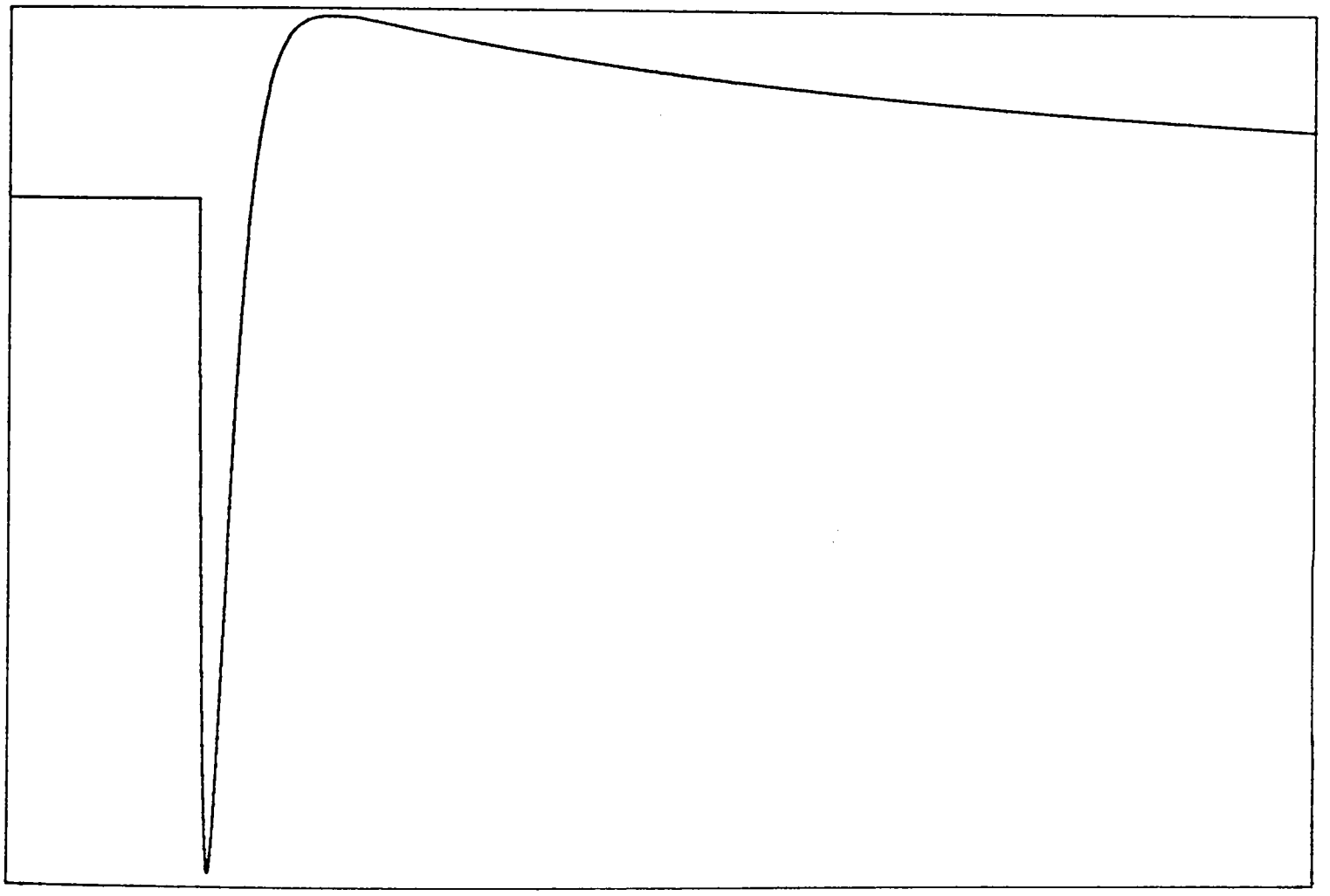

the ensemble. Why should G–pairs differ from F–pairs? At the point of radical creation a high enough proportion of pairs are created in triplet states for $n(T_0).P(T_0)$ to exceed n(S).P(S). Credible decay curves may be obtained by simulating this in terms of fractional reaction probability of singlet pairs and singlet/triplet RPM polarization ratios, as shown in Fig.(7.3.4)

(7.3.3) Experimental Separation Of G– And F–Pairs

The consequences of first and second order kinetics can be separated by effect–modulated experiments and it was this that first provided unequivocal evidence for A/E phases in $^t$butyl F–pairs and E/A for the preceeding G–pairs [6]. However, a similar study for the propan–2–olyl radical revealed that both contributions to polarization were of identical phase and nearly equal magnitude. I have dwelled very briefly upon these models since, whilst we cannot separate F– and G–pair effects so simply in a pulse–correlated experiment, it is possible to study limiting cases in which only F–pair or only G–pair polarization could possibly be observed. Firstly we can take advantage of the singlet reactivity of ketones towards amine quenchers, to generate singlet–geminate pairs of ketyl radicals and observe how the polarization varies thereafter: initial RPM is singlet geminate and according to either model the subsequent evolution of polarization should also *appear* to be singlet–geminate.

Following the conditions described in §(7.2.3) and Fig.(7.2.5) a time decay of lines in the propan–2–olyl radical spectrum were recorded: within a couple of microseconds the A/E signal from this inital singlet reaction has subsided into an E/A pattern, indicative of "normal" RPM evolution (shown in Fig.(7.3.5)); that is, that it is consistent with either a monotonic exchange interaction or that the singlet encounter pairs that separate again are not significantly more polarized than the re–combinant triplet pairs. Viscosity

Fig.(7.3.4)

A demonstration of the effect of limited singlet reactivity of radical pairs upon encounter. Three lines are modelled, using initial polarizations of –20, 0 and +20 $P_{eq}$, with 20% of singlet free–encounter pairs reacting upon encounter and with $P_{f,singlet}$:$P_{f,triplet} = 40 : -20$ ($\times P_{eq}$).

Inversion of the high–field line (A → E) occurs at 12.6$\mu$s and that of the low–field line (E → A) occurs at 9.6$\mu$s.

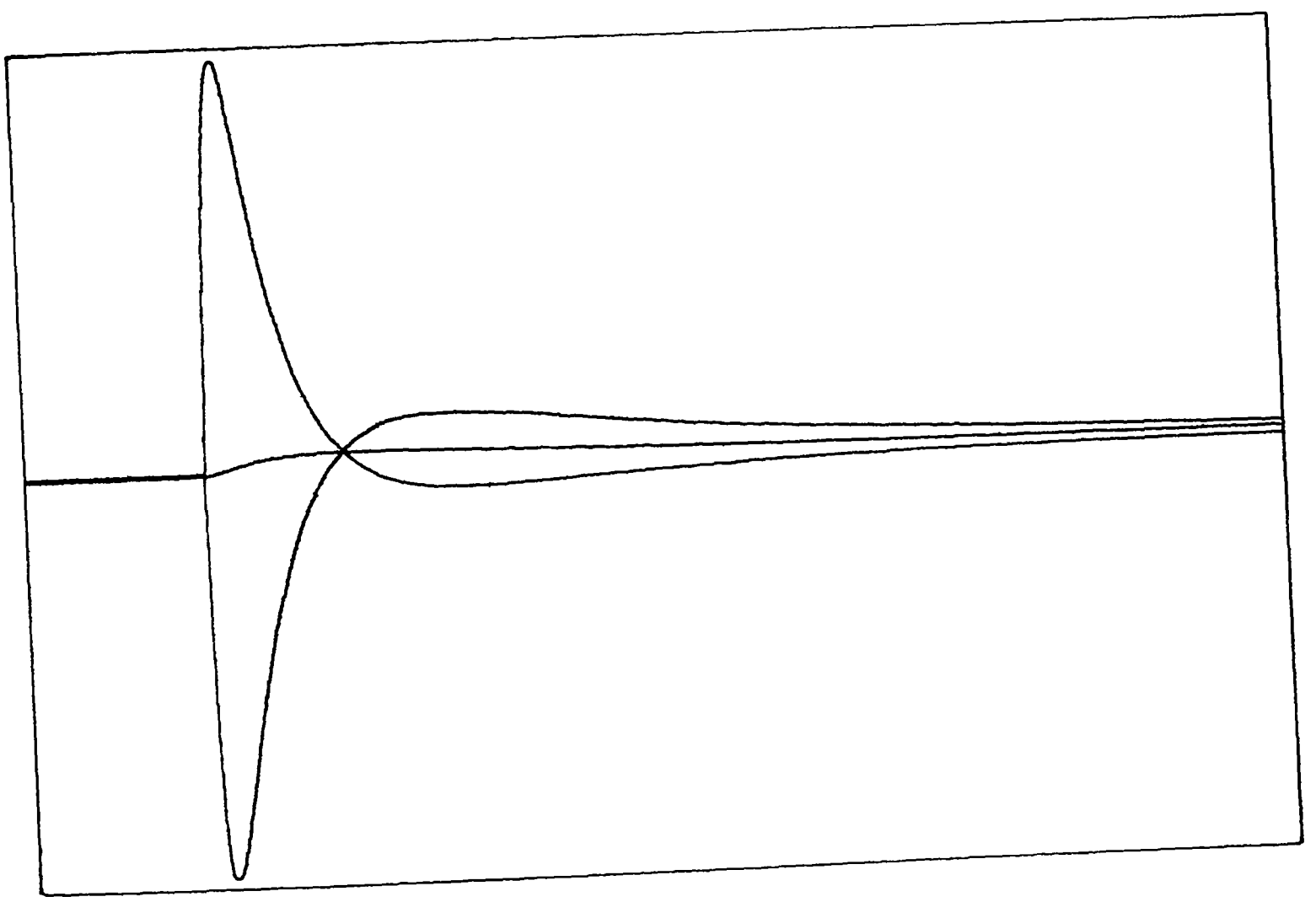

$T_1 = 2.5\mu s$; $T_2 = 0.8\mu s$; $\omega_1 = 0.5$radMHz.

Entire transient simulation is over 102.4$\mu$s.

Fig.(7.3.5)

The first low and high field lines from the centre of the spectrum of the propan–2–olyl radical derived from the excited singlet state of propanone in neat tri–ethyl amine. Rapid relaxation of initial A/E polarization and replacement by E/A phase RPM within a couple of microseconds gives the time decays shown. This demonstrates the speed with which initial polarization is replaced by F–pair RPM polarization.

Both traces are recorded over 40$\mu$s.

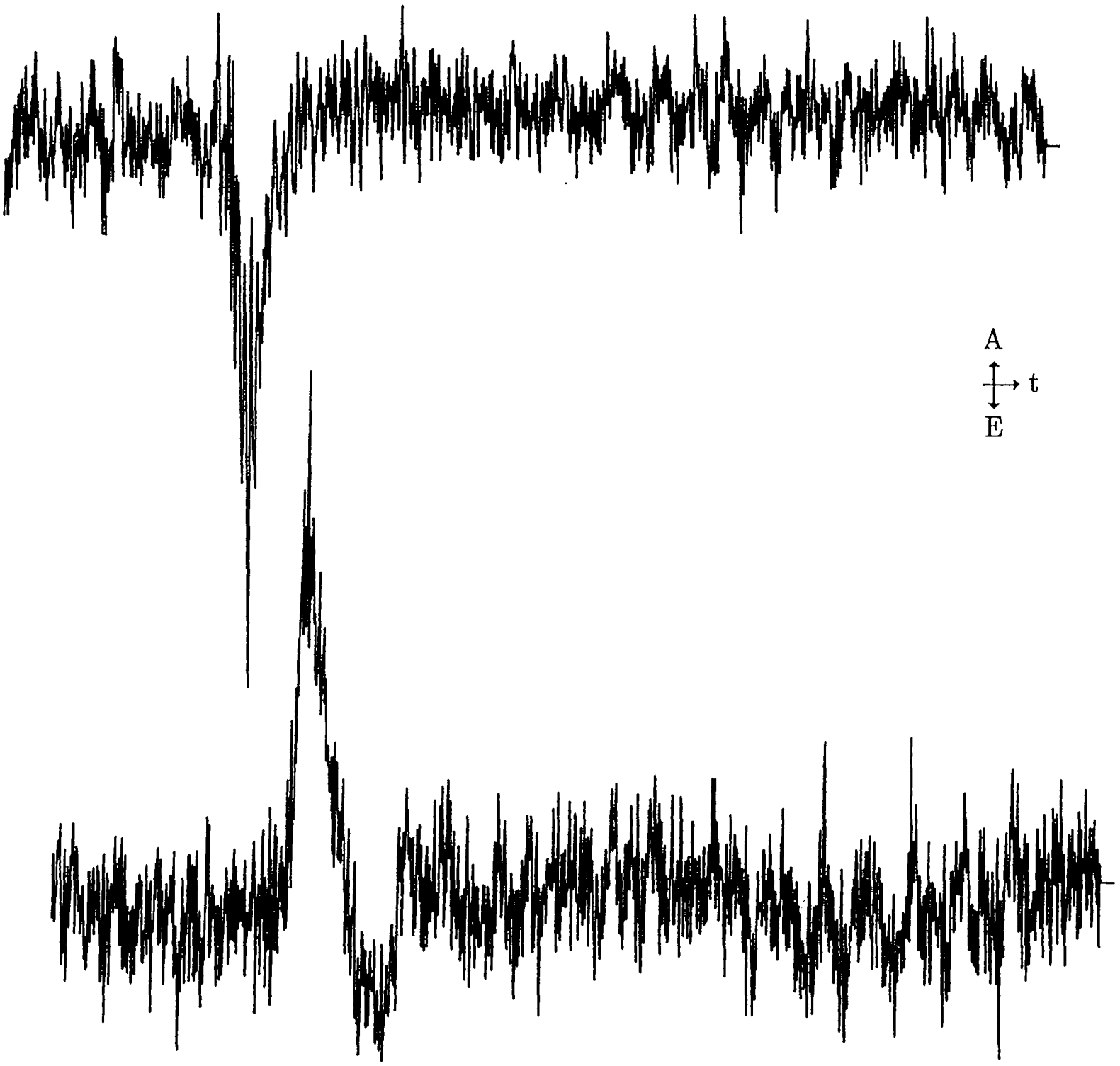

and dielectric constants of tri–ethyl amine and propan–2–ol are not so very different that one should upset the polarization development that is taking place in the other (unlike the heavy paraffin solvent employed in the previous chapter, which restricted diffusion to such an extent that in some cases RPM was only observed between the photo–fragments in the geminate cage).

This seems a good place to make an observation: it is argued that $J_r$ is going to affect both the relative diffusional motion of the radical pair and its polarization, yet the two processes operate at very different exchange strengths; polarization is most efficient when $\tau_e J_r \ll 1$ so a value of $J_r \approx 10^{-11}$s is often employed [50], whereas the polarization is destroyed before $J_r$ becomes large enough to disrupt diffusion *by itself* (kT is four orders of magnitude larger).

The second test makes use of a chemical method to prevent the observation of geminate polarization. We employ the following two reaction schemes:

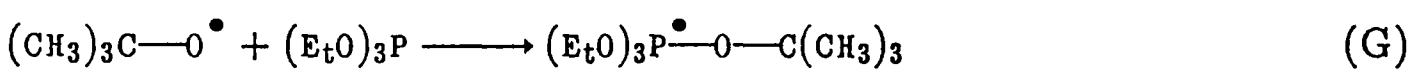

(G)

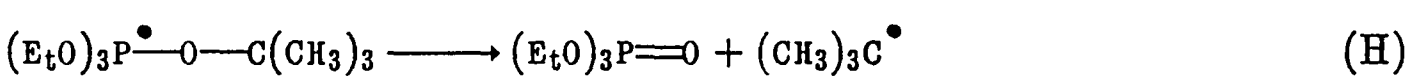

(H)

the bimolecular rate constant is $1.7 \times 10^9$ $dm^3mol^{-1}s^{-1}$; the unimolecular one is $3.5 \times 10^5 s^{-1}$

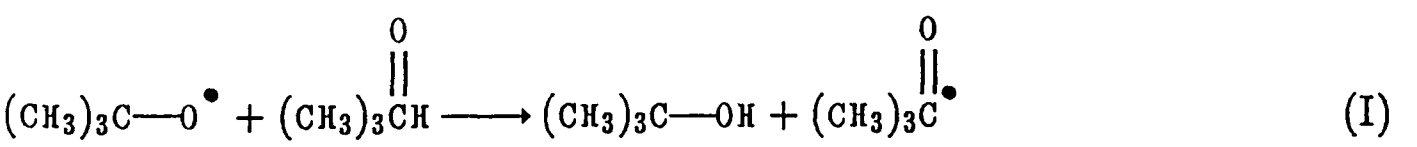

(I)

(J)

H–abstraction[5] rate is between $10^5$ and $10^6$ $dm^3mol^{-1}s^{-1}$; decarbonylation rate is $3.5 \times 10^5 s^{-1}$.

These reactions were carried out in a 40:10:50 v/v/v peroxide/$^t$butanol/phosphite mixture and a 0.1M 2,2–dimethyl propanal in 40:60 v/v solvent of peroxide and $^t$butanol. Both phosphorus– and carbon–centred radicals are observable – Fig.(7.3.6). At all times of observation shortly after the flash the $^t$butyl species is visible as an E/A multiplet, though the weak signal made it hard to follow through to longer times. That of the $^t$butyl radical created in reactions (I) and (J) is also visible as an E/A multiplet, which seems at long times to invert, too, though the signal is so deeply buried in the noise that this could not be confirmed even after repeated averaging. Again it could be argued that viscosity or solvent polarity effects prevent the A/E polarization from being observed but in this case both lie between those of paraffin and propan–2–ol solutions, and the A/E multiplet has been observed in both cases.

Further contradictory evidence comes from independent radiolysis work [51] in which the spectra of alkyl and ketyl radicals are found to be entirely consistent with those from photolysis studies. It is not known for certain how the excited species in radiation spurs interact but it is clear that no initial correlation exists, so that, even if polarization is generated largely within a spur, the net behaviour will be as though from F–pairs. In all reported spectra, both directly after and several microseconds after radiolysis the E/A RPM pattern dominates.

---

[5] Values for the rate constants quoted are taken from Vollenweider J–K., Fischer H., Hennig J., Leuschner R. in *Chem.Phys.* (1985) 97, 217, Roberts B.P., Scaiano J.C. *J.Chem.Soc.Perkin Trans. II* (1981) 6, 905 and from comparisons of similar H–abstraction rates in Landolt – Börnstein Neue Serie II (Pub. Springer–Verlag, Berlin, 1983) sub–vol. 13c.

Fig.(7.3.6)

Two line spectrum of the intermediate (G) in the production of $^{t}$butyl radicals. These two lines, separated by 91.1mT are shown in close–up, with the stretch of featureless, interlying baseline removed. Both lines are visible in absorption, despite the possibility of a strong ST$_-$ effect. The ensuing $^{t}$butyl radical takes on a weak absorption but develops its own strong E/A re–combinant polarization. This was taken over 2 to 4$\mu$s and 12.0mT.

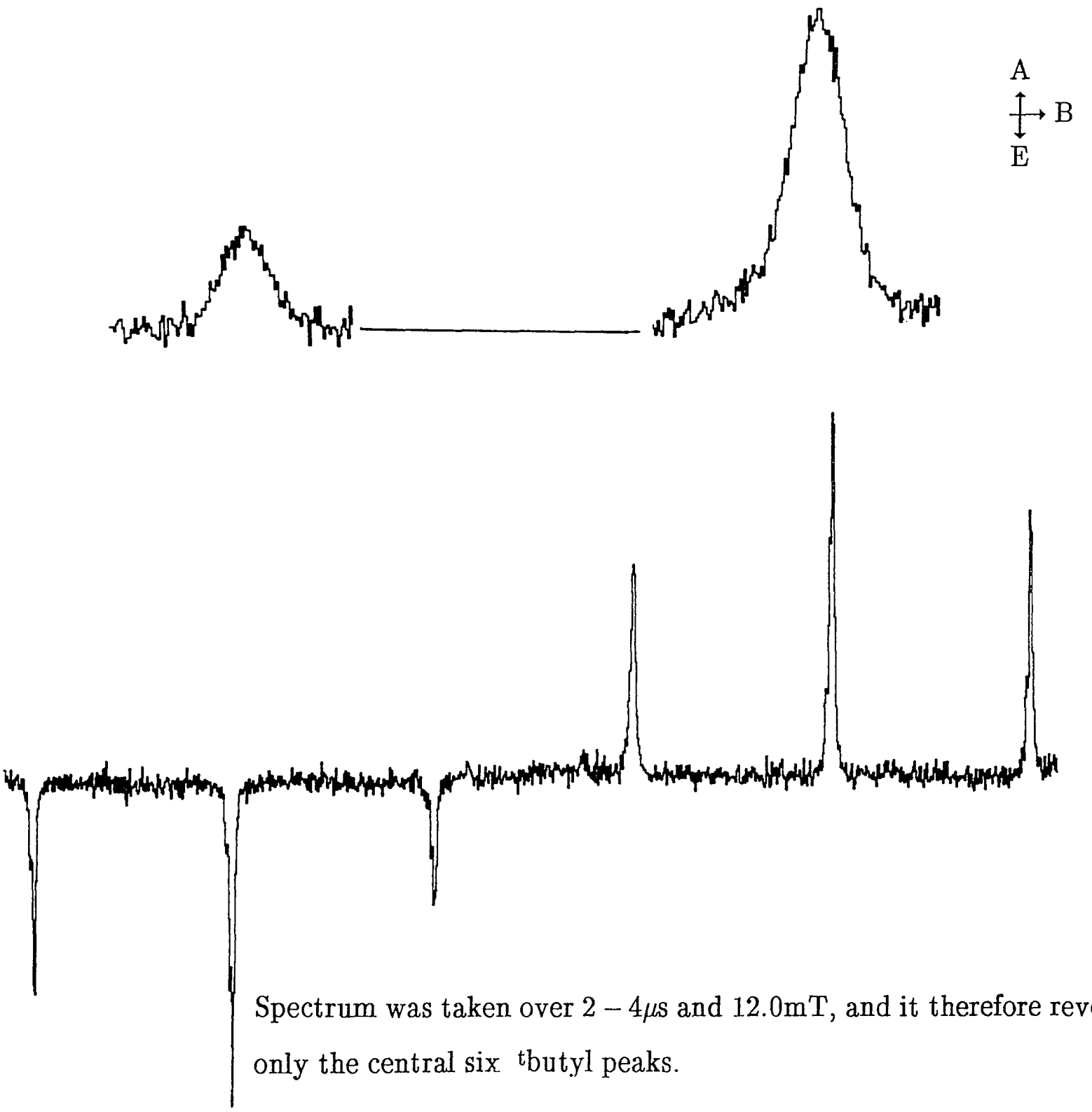


Spectrum was taken over $2-4\mu$s and 12.0mT, and it therefore reveals only the central six $^{t}$butyl peaks.

A final nail in the coffin comes from an experiment in which a microwave field is boosted to a saturating level at radical creation, and then stepped down a few microseconds later: polarization still evolves as the E/A pattern [52] before developing slowly into an A/E multiplet.

(7.4.1) Cross Relaxation – A Real "Dynamic" Polarization?

The problem as it stands, then, is that a real difference exists between early and later time polarizations, that cannot be resolved in terms of distinctions between geminate and re–combinant radical pairs. The time at which inversion takes place is shown to vary with radical concentration [53], and this will be further illustrated later on. These studies throw up contradictory results for it is shown that the cyclohexanolyl and propan–2–olyl spectra invert only at higher radical concentrations whereas, working with very low laser powers (and hence radical concentrations) the $^{i}$propyl spectrum inverts faster than at higher concentrations. This first anomaly will be returned to. Here we consider that, since bimolecular and unimolecular reactions do not give opposite polarizations at times close to the initiating laser flash, the origin of the A/E multiplet may lie in physical effects.

The timescale of inversion is consistent with nuclear spin relaxation rates in radicals [54]. Concurrent with CIDEP is the nuclear analogue, CIDNP, and because of the differing gyro–magnetic ratios of electron and nucleus ($\gamma_e/\gamma_n \approx 10^3$), the Overhauser effect – the simultaneous flipping of electron and nuclear spins – is often observed [55] and has been implicated in the creation of CIDNP from CIDEP [56,57]. The inverse Overhauser effect is a rarity, by contrast, since that same ratio that facilitates the Overhauser effect makes its converse unlikely – rather like the tail wagging the dog! A schematic of the CIDNP polarization mechanism is to be found in Fig.(7.4.1).

Fig.(7.4.1)

A Schematic Of The CIDNP Mechanism

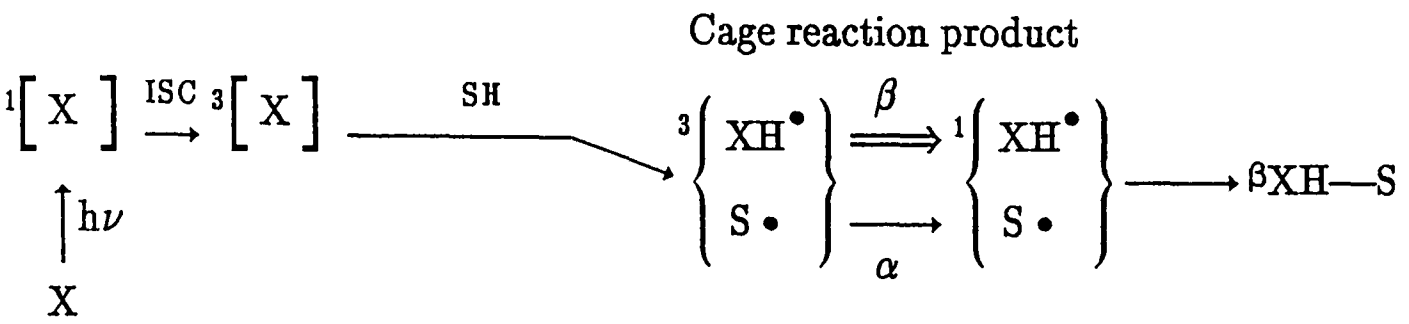


The escape product for XH will therefore have an excess of $\alpha$–nuclear spins. This scheme gives rise to the following *n.m.r.* spectra for the stable products of cage and escape reactions:


The spectra resulting from such a scheme would, if reaction took place from the excited singlet state, be reversed. The double arrow between the two $XH^{\bullet}$ species within the spin–correlated radical pair indicates a faster development of singlet character for those pairs in which $XH^{\bullet}$ is in the $\beta$ state (effected by g–value and hyperfine interactions, as for RPM CIDEP). *e.s.r.* only allows us to detect the escape radicals, and even then we cannot observe the stable products arising from them. It should be remembered that while CIDNP polarizations of only a hundred $P_{eq}$ have been measured in the escaped radical products, the polarization prior to reaction and cross–relaxation may be much higher.

Provided that CIDNP is very large (${}^{n}P_{cidnp} > {}^{n}1000P_{eq}$) it could be possible for a reverse process to occur and give the electron a polarization greater then ${}^{e}P_{eq}$. This would be a true "dynamic" or cross–relaxational polarization mechanism. To see how CIDNP could be transferred to electron spins we use two simple case of a pair of radicals with one nuclear coupling and a pair with two dissimilar couplings. Two cross–relaxations are identified: the dipolar (or "flip–flip") mechanism operates according to the selection rule $\Delta m = \pm 2$, and would be expected to dominate in those species for which a large END term in the relaxation expression is found; the scalar (or "flip–flop") process, arising from scalar modulation of an electron–nuclear coupling by internal motion such as the rotation of methyl groups, and the buffeting by solvent molecules, operates according to the selection rule $\Delta m = 0$. These two cross–relaxations provide a means of shuffling spin polarizations between electrons and nuclei and the effect upon the spin of the electron will be manifest in the spin populations of the radical's nuclei.

Let us first examine the effect of a net CIDNP polarization transfer [58] in Fig.(7.4.2a). We define four radical eigenstates for a positive hyperfine coupling: $|1\rangle = \alpha_s\alpha_i$ ; $|2\rangle = \alpha_s\beta_i$ ; $|3\rangle = \beta_s\beta_i$ ; $|4\rangle = \beta_s\alpha_i$. The effect of cross–relaxation upon this system is shown in a hypothetical *e.s.r.* spectrum beneath each final eigenstate population diagram, after the relaxation process has occurred. A simple sign rule may be extracted from (7.4.2a) for the polarization conferred upon the electron, along the lines of the Kaptein sign rules for CIDEP and CIDNP.

$$\Delta\Gamma^{S}_{net} = R^{SI}.\Gamma^{I}_{net} \qquad (7.3.1)$$

in which the phase of the CIDNP effect is defined as positive for enhanced absorption and negative for enhanced emission. $R^{SI}$ is positive if the dipolar relaxation rate $R_2$

Fig.(7.4.2)

a) Net CIDNP Polarization Transfer For A Radical With One Nucleus.

Scalar relaxation, $R_0$ , $\Delta m = 0$; dipolar relaxation $R_2$ , $\Delta m = \pm 2$; coupling constant, $a_H$, is positive. The energy levels connected by each process are indicated by diagonal arrows.

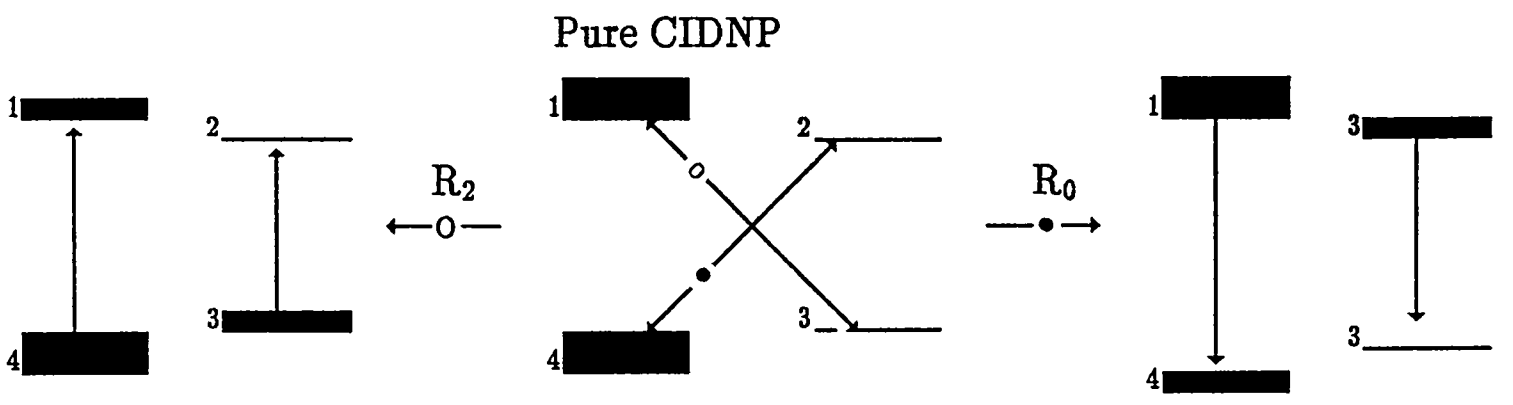


Effect upon the *e.s.r.* signal is

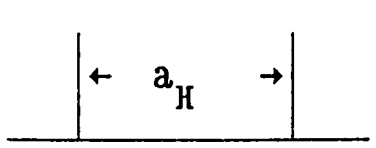


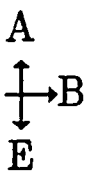


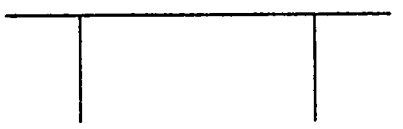

$|1\rangle = \alpha_s\alpha_i$; $|2\rangle = \alpha_s\beta_i$; $|3\rangle = \beta_s\beta_i$; $|4\rangle = \beta_s\alpha_i$.

b) Transfer Of Multiplet CIDNP Polarization From A Radical With Two Identical Nuclei.

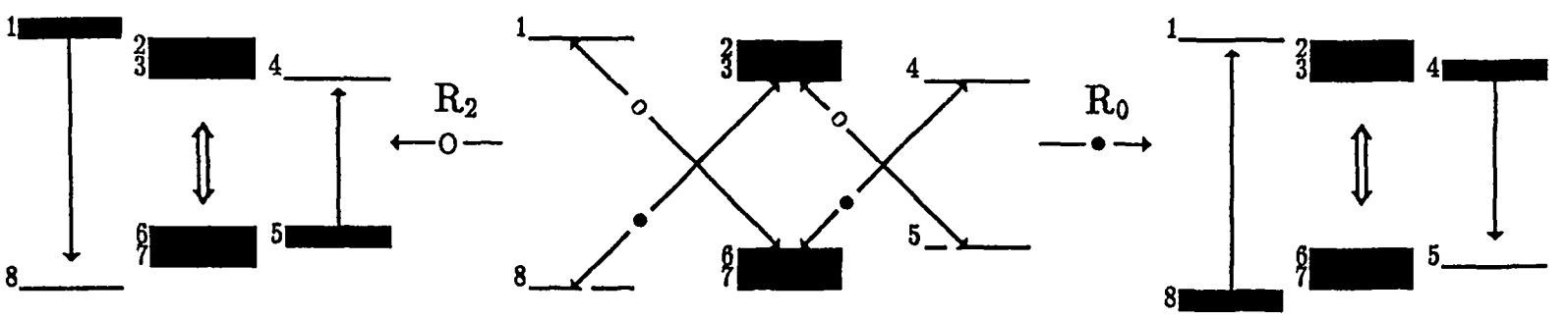


Effect upon the *e.s.r.* signal is

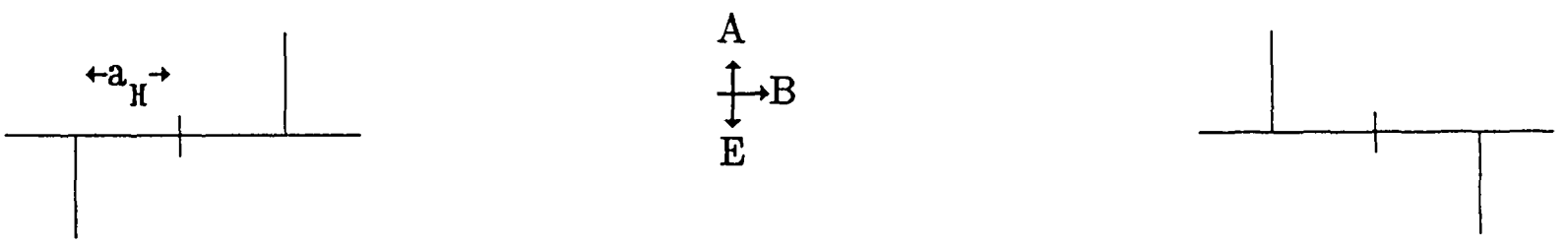


The corresponding eigenstates are

$|1\rangle = \alpha_s\alpha_i\alpha_j$; $|2\rangle = \alpha_s\alpha_i\beta_j$; $|3\rangle = \alpha_s\beta_i\alpha_j$; $|4\rangle = \alpha_s\beta_i\beta_j$

$|5\rangle = \beta_s\alpha_i\alpha_j$; $|6\rangle = \beta_s\alpha_i\beta_j$; $|7\rangle = \beta_s\beta_i\alpha_j$; $|8\rangle = \beta_s\beta_i\beta_j$.

dominates ($R_2 > R_0$), and is negative otherwise. If $\Delta\Gamma^{S}_{net}$ is positive then the contribution to the *e.s.r.* signal is absorptive, and if negative then the contribution is emissive.

The effect of a multiplet CIDNP enhancement is more complex, since we must have two or more magnetic nuclei on each radical in order to produce a nuclear multiplet effect. Fig.(7.4.2b) depicts a radical with two identical couplings[6]. Again $a_H$ is positive and the corresponding eigenstates are given alongside the diagram. If, as shown, CIDNP confers an excess of anti–parallel nuclear spins then the dipolar route will generate an E/A multiplet and the scalar route will generate an A/E one. These deductions can also be cast into a sign rule equation:

$$\Delta\Gamma^{SJ}_{multiplet} = A^{SJ}.R^{SI}.\Pi^{IJ} \qquad (7.3.2)$$

in which $A^{SJ}$ is the sign of the hyperfine coupling to nucleus J and $\Pi^{IJ}$ is positive for an excess of anti–parallel spins and negative otherwise. We shall state that $A^{SJ}$ is positive since we are considering radicals in which the hyperfine structure is dominated by alkyl $\beta$ protons. The Kaptein rules [58] predict that the radical should have an A/E phase CIDNP multiplet if the internuclear couplings are positive, and an E/A phase if they are negative. Either way round, the result is an excess of antiparallel spins in the radical. Under such strictures we require that $R^{SI}$ be negative for $\Delta\Gamma^{SJ}_{multiplet}$ to be negative (i.e. A/E). In other words a cross–relaxation must be driven by a scalar interaction (and a

---

[6] This choice requires an explanation, for the multiplet CIDNP would not be observed in an *n.m.r.* experiment – the emission on one spin would be cancelled by the enhanced absorption on the other. For dissimilar spins an *n.m.r.* spectrum with an IJ CIDNP multiplet would be converted into an SJ CIDEP multiplet, where I and J are labels of the two nuclei and S is that for the electron spin [8].

very efficient one, too; the rate of transfer of nuclear polarization must exceed the electron spin–lattice relaxation rate) for this reservoir of nuclear spin polarization to be tapped and converted into electron spin polarization. Unfortunately, the equivalence of protons in every radical bar the $^{i}$propyl means that the size of the multiplet CIDNP effect is hard to assess, let alone quantify. However, a calculation for a radical with two equivalent spins [46] sets a figure of $P_n = 3 \times 10^{-2}$ in order to observe high and low field *e.s.r.* lines crossing over from E/A to A/E, when realistic values of $T_1$, F–pair CIDEP and exchange have been compensated for. Even then, the equilibrium electron polarization dominates the decay profile and the assumption is made that no dipolar relaxation can take place.

Setting aside these reservations we may identify two major mechanisms of scalar relaxation in the radicals studied: internal rotation of methyl groups or conformational exchange in cyclic systems cause hyperfine coupling constants to be modulated; inversion at the radical centre, known to be non–planar, as mentioned in the previous chapter [59], and modulation of the double well potential at the radical centre by the buffeting of local solvent molecules (at $\approx$ 10GHz) will also modulate the couplings.

The former may be tested by the behaviour of the 4–$^{t}$butyl cyclohexanolyl radical, in which internal motion is prevented by the $^{t}$butyl group, which effectively locks the ring in one conformation, as evinced by the well–resolved $\gamma$–proton couplings. Clearly there can be no rapid or even slow interchange – optical isomers of the stable alcohol may be resolved – between conformers, so any internal motion in the radical can be dismissed. Observing this radical over time reveals that it does invert from a symmetric E/A to an A/E* pattern after a hundred microseconds or so – Fig.(7.4.3). This was used as a piece of evidence for rejecting the cross–relaxational theory in the original paper [8] because the possibility of the radical centre inversion giving rise to cross–relaxation was overlooked.

Fig.(7.4.3)

The spectrum of 4–$^{t}$butyl cyclohexanolyl radical in 4–$^{t}$butyl cyclohexanol. A symmetric E/A multiplet at 1.0 to 2.5$\mu$s has developed into an A/E multiplet with a weak absorptive envelope by 100$\mu$s. $\gamma$–couplings of 0.04 and 0.08mT are resolvable.

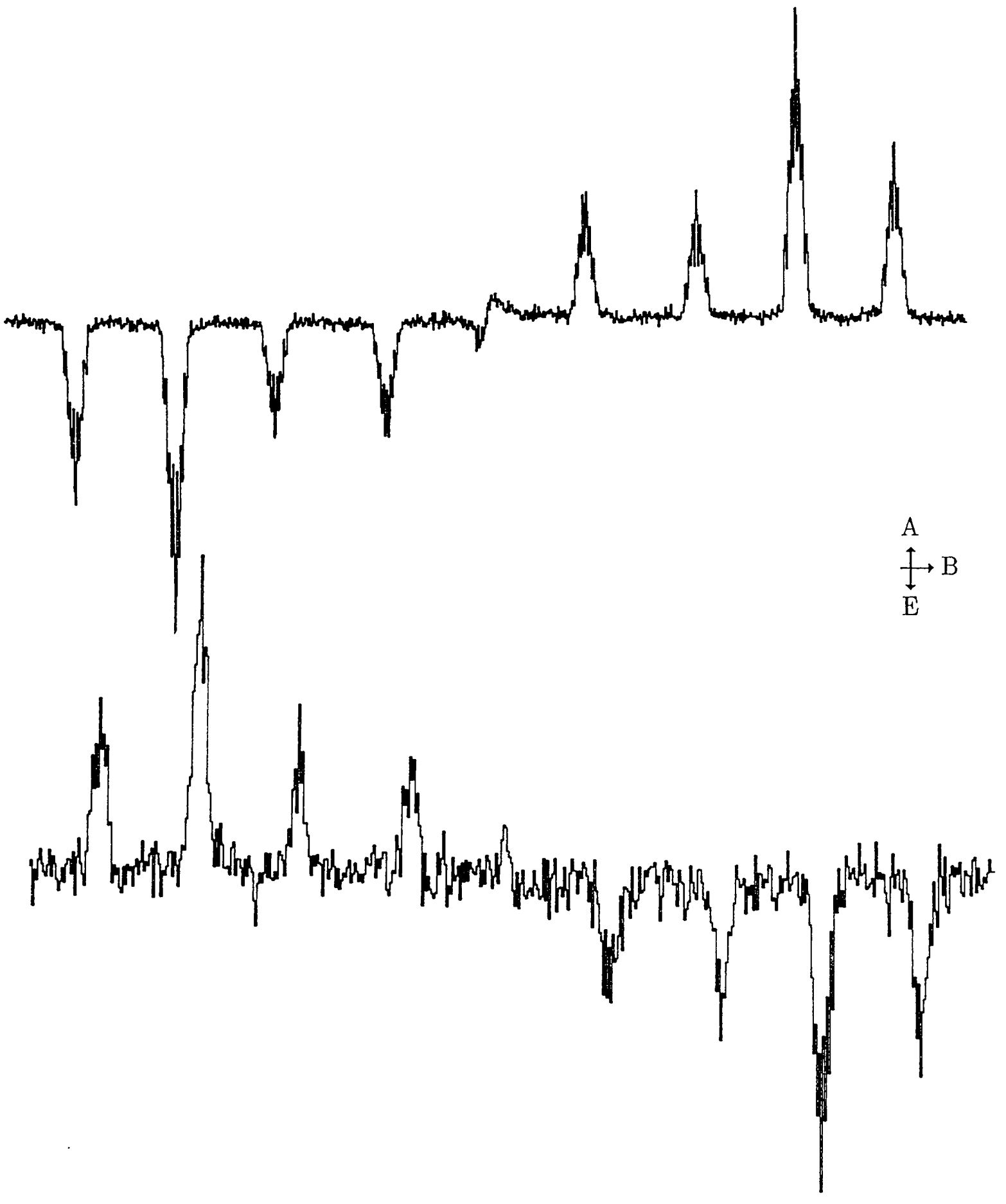

The other two spectra published in that communication I have since shown to have been largely influenced by the spurious experimental signal discussed earlier. If this radical–centre inversion or modulation is responsible for setting up very efficient cross–relaxation then radicals in which planarity is induced by $\pi$–conjugation of the lone electron to aromatic or carbonyl groups would not be expected to show such inversions, and experiments have been conducted on systems in which the radicals are believed to be planar: the results demonstrate that no phase inversion is observed [46], but since the phenomenon will, according to this model be concentration (residual F–pair polarization will frustrate the evolution of the unimolecular cross–relaxational effect) and temperature dependent these experiments are only useful pieces of evidence rather that confirmatory tests.

A simulation that introduces cross relaxation into the *e.s.r.* decay transient is given in Fig.(7.4.4). A description of the method of simulation is reserved for appendix E but certain details require explanation here. What is presented is the $M_y$ component of a 1:2:1 triplet of *e.s.r.* lines, which possess an initial multiplet polarization of $P_i$, 0 and $-P_i$, expressed as ratios of the equilibrium polarization for the electron. Similarly F–pair effects are treated as $P_f$, 0 and $-P_f$. Both are variable parameters but they have been entered as $P_i = P_f$ in all simulations given here. The time dependence of each component, initial and F–pair, varies as has been demonstrated in chapter 2. All necessary parameters are entered before each simulation. Those values that were derived or quoted in the previous chapter for the $^t$butyl radical have been used in what is a complete model of the cross–relaxation process. Nuclear polarization is introduced as an initial condition (present from the moment the radical pair escapes from the geminate cage) which decays over time with a characteristic relaxation rate. This feeds

Fig.(7.4.4a)

An illustration of the effect of transfer of CIDNP, via a scalar relaxation mechanism, to an electron spin system consisting of an electron coupled to two degenerate nuclei of spin $\frac{1}{2}$. The z–component of magnetization, in the absence of a microwave field, has the following behaviour:

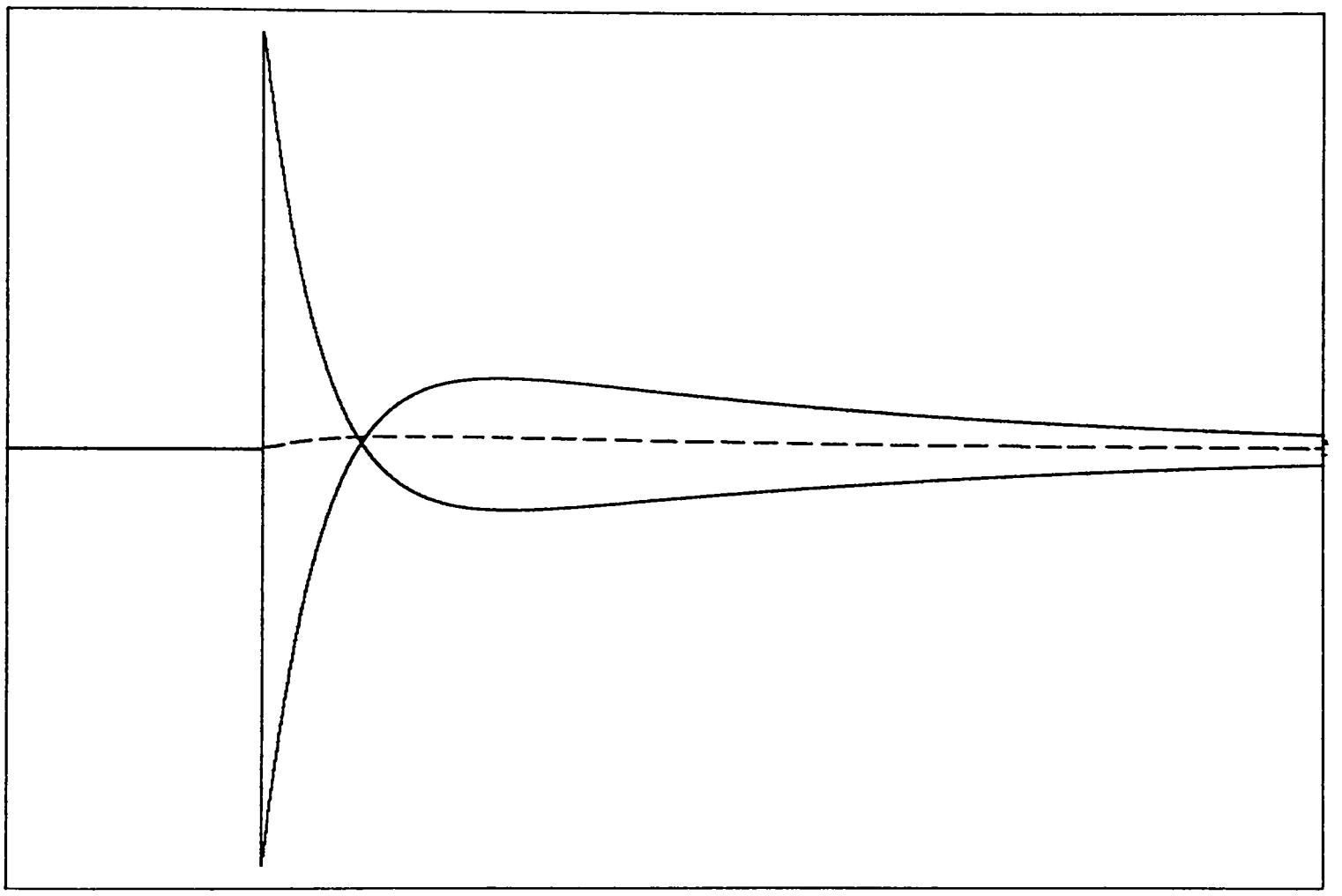

Total time window is $50\mu s$: bimolecular rate constant, $k_2 = 1 \times 10^9 dm^3 M^{-1} s^{-1}$; scalar cross–relaxation rate, $k_x = 5 \times 10^4 s^{-1}$; ${}^eT_1 = 2.5\mu s$; ${}^eT_2 = 0.8\mu s$; ${}^nT_1 = 25\mu s$; $\omega_1 = 0.5 radMHz$. Polarization ratios for each line were, for $P_I$ and $P_F$, –20:0:20.

An A/E CIDNP multiplet of $2 \times 10^4$ ${}^nP_{eq}$ was used.

Fig.(7.4.4b)

Two simulations in which a deliberately exaggerated nuclear polarization is entered.

${}^{e}T_1 = 2.5\mu s$; ${}^{e}T_2 = 0.8\mu s$; ${}^{n}T_1 = 25.0\mu s$; $\omega_1 = 0.5$radMHz; ${}^{e}P_i = {}^{e}P_f = -20{:}0{:}20$.

$k_2 = 1 \times 10^{9} dm^3 M^{-1} s^{-1}$; $k_x = 1 \times 10^{4} s^{-1}$; ${}^{n}P_i = 1 \times 10^{5}\ {}^{n}P_{eq}$.

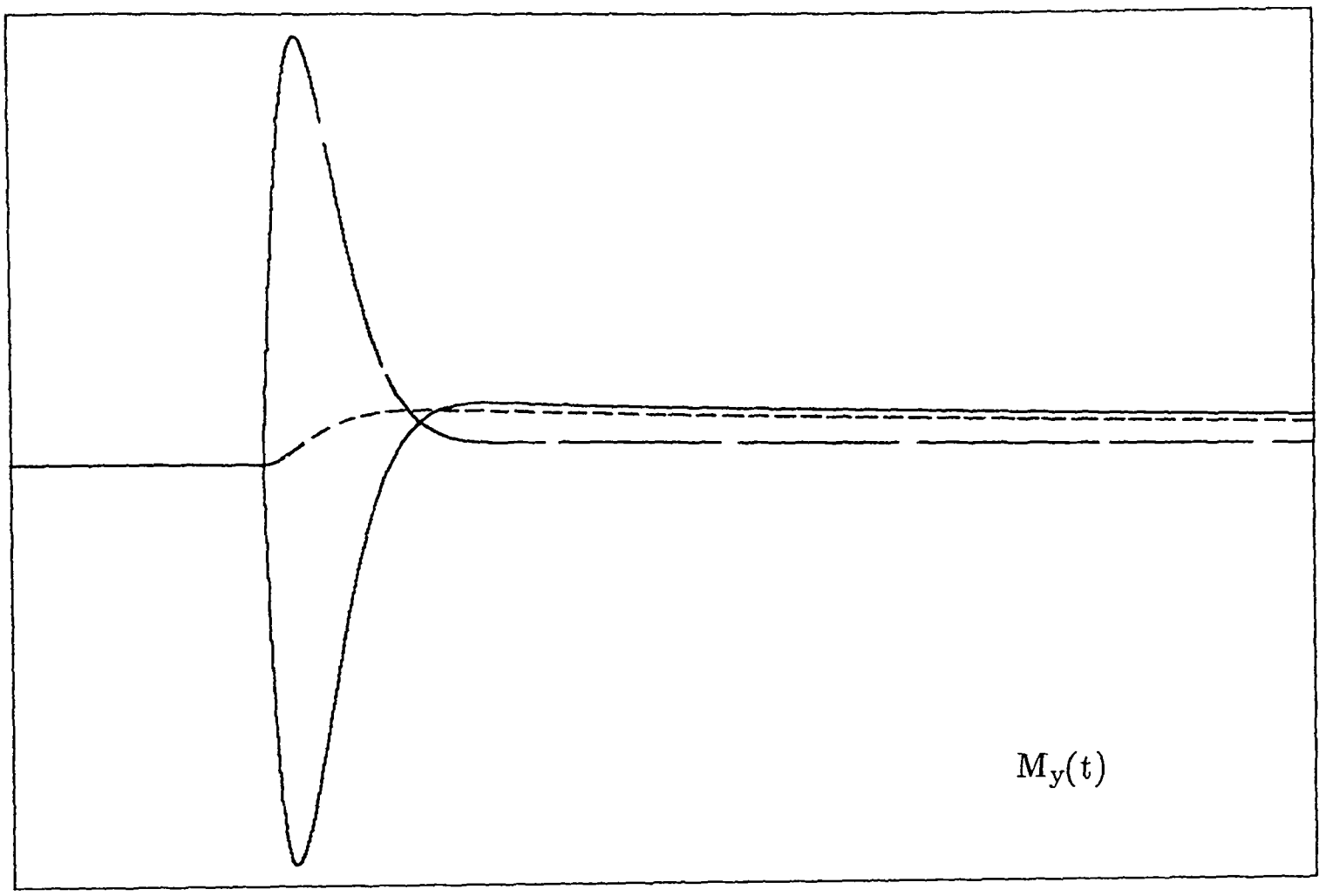


$k_2 = 5 \times 10^{8} dm^3 M^{-1} s^{-1}$; $k_x = 5 \times 10^{4} s^{-1}$; ${}^{n}P_i = 1 \times 10^{5}\ {}^{n}P_{eq}$.

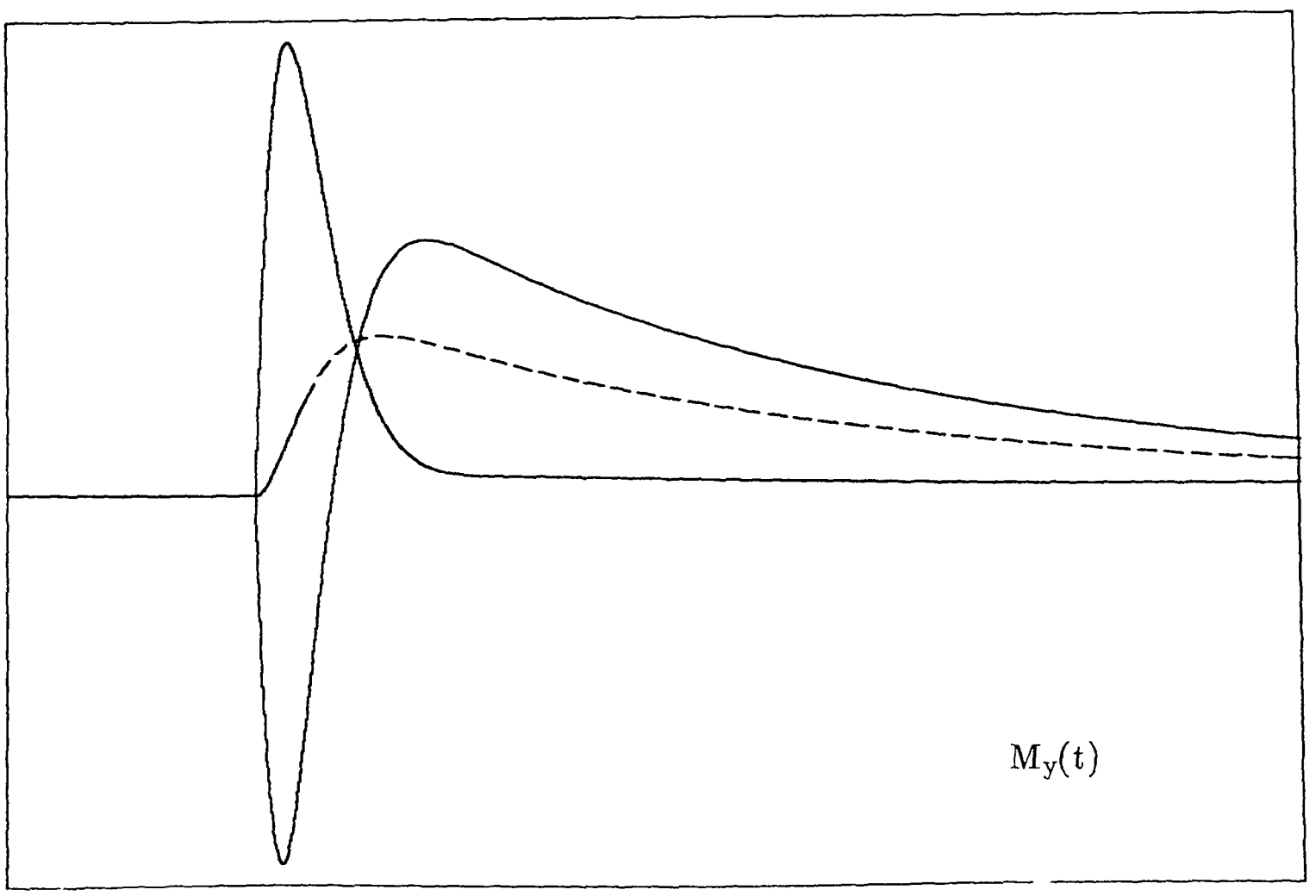

polarization through into the electron spin system which is subject to its own relaxation processes, interaction with the microwave field and F–pair RPM polarization created continuously during the radical lifetime.

The problem with this mechanism is that a vast nuclear polarization is required; the simulations shown in Fig.(7.4.5) indicate that, in order for an A/E phase multiplet to become apparent above the equilibrium electron polarization then a nuclear polarization of more than 10,000 is required. Absolute magnitudes, where they have been measured [61] show that this is ten times larger than observed – and this represents a perfect system, for which a pure and efficient scalar relaxation is the only cross–relaxational process taking place.

However, whilst the CIDNP effect required is large it is not impossibly so, for a theoretical maximum for the polarization of nuclear spins is around $2 \times 10^4$ ${}^{n}P_{eq}$. Instead of trying to look for the Inverse Overhauser effect in an ephemeral radical population, and in an even shorter–lived *e.s.r.* signal it would make more sense to try to measure the result of the Overhauser mechanism on those stable species that are produced upon encounter of escape products. In this case the multiplying effect of $(\gamma_e/\gamma_n)$ works in the experimenter's favour and since what is being observed in this case is a stable species, no complications over unknown and possibly undetected reactions can arise.

The method of detection employed is flash–photolysis *n.m.r.* – equivalent to that described in chapter 2 but operating at higher magnetic field and with a radio–frequency rather than a microwave detection system. A spin–echo technique is favoured: an intense pulse of radio–frequency radiation is applied to the sample at a pre–set delay after the photolysis pulse, which rotates the bulk magnetization vector (this time of a set of resonant nuclei rather than resonant electrons) through 90°; this initially coherent ensemble of spins will diffuse away fron the y–axis mainly under the influence of $T_2$ and

Fig.(7.4.5)

Two further simulations which use more realistic values of CIDNP polarization, ${}^{n}P_i$: ${}^{e}T_1 = 2.5\mu s$; ${}^{e}T_2 = 1.0\mu s$; ${}^{n}T_1 = 25.0\mu s$; $\omega_1 = 0.5$radMHz; $k_2 = 5 \times 10^{8} dm^3 M^{-1} s^{-1}$; $P_i = P_f = -20{:}0{:}+20$; $k_x = 1 \times 10^{5} s^{-1}$; ${}^{n}P_i = 1 \times 10^{4}\ {}^{n}P_{eq}$

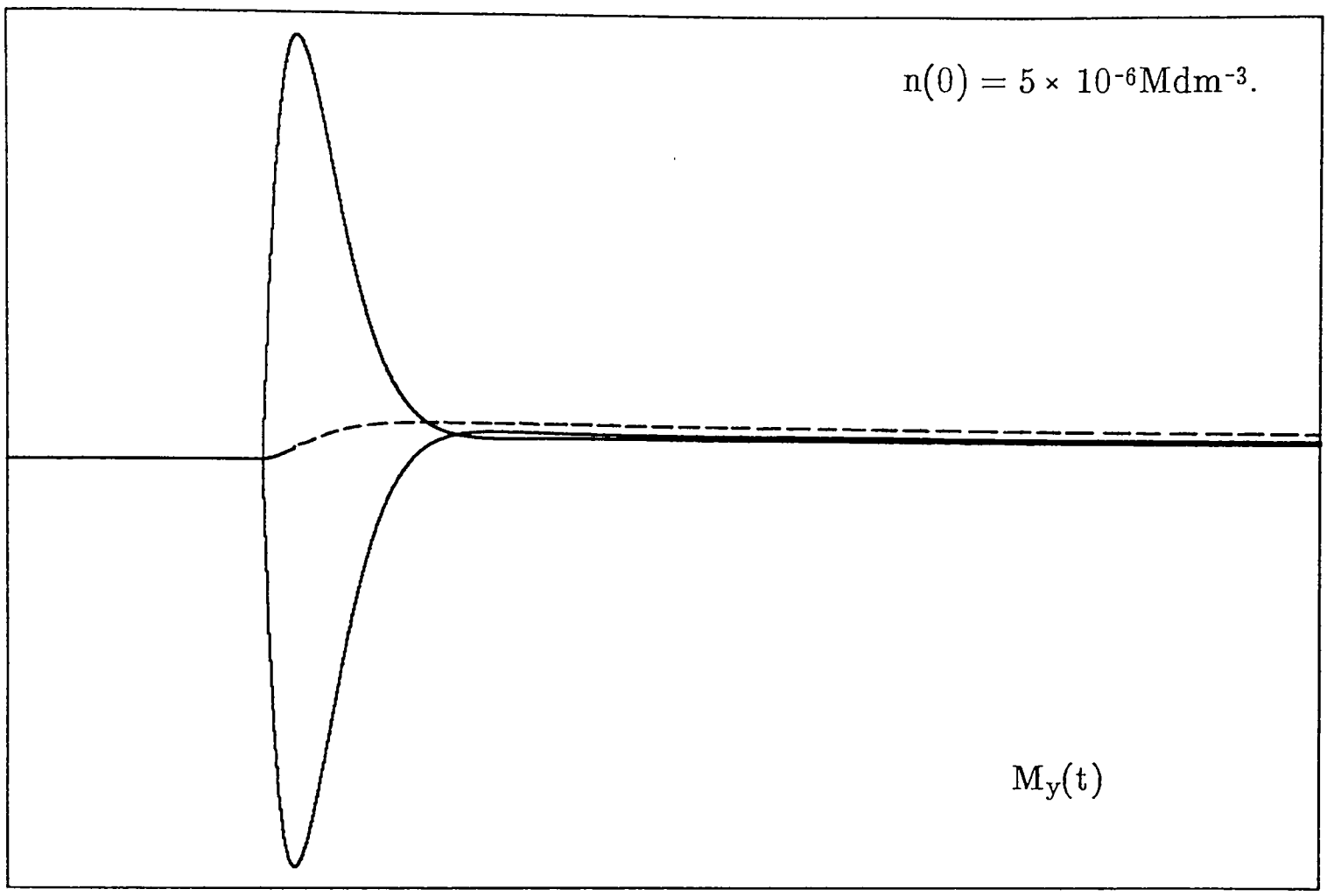


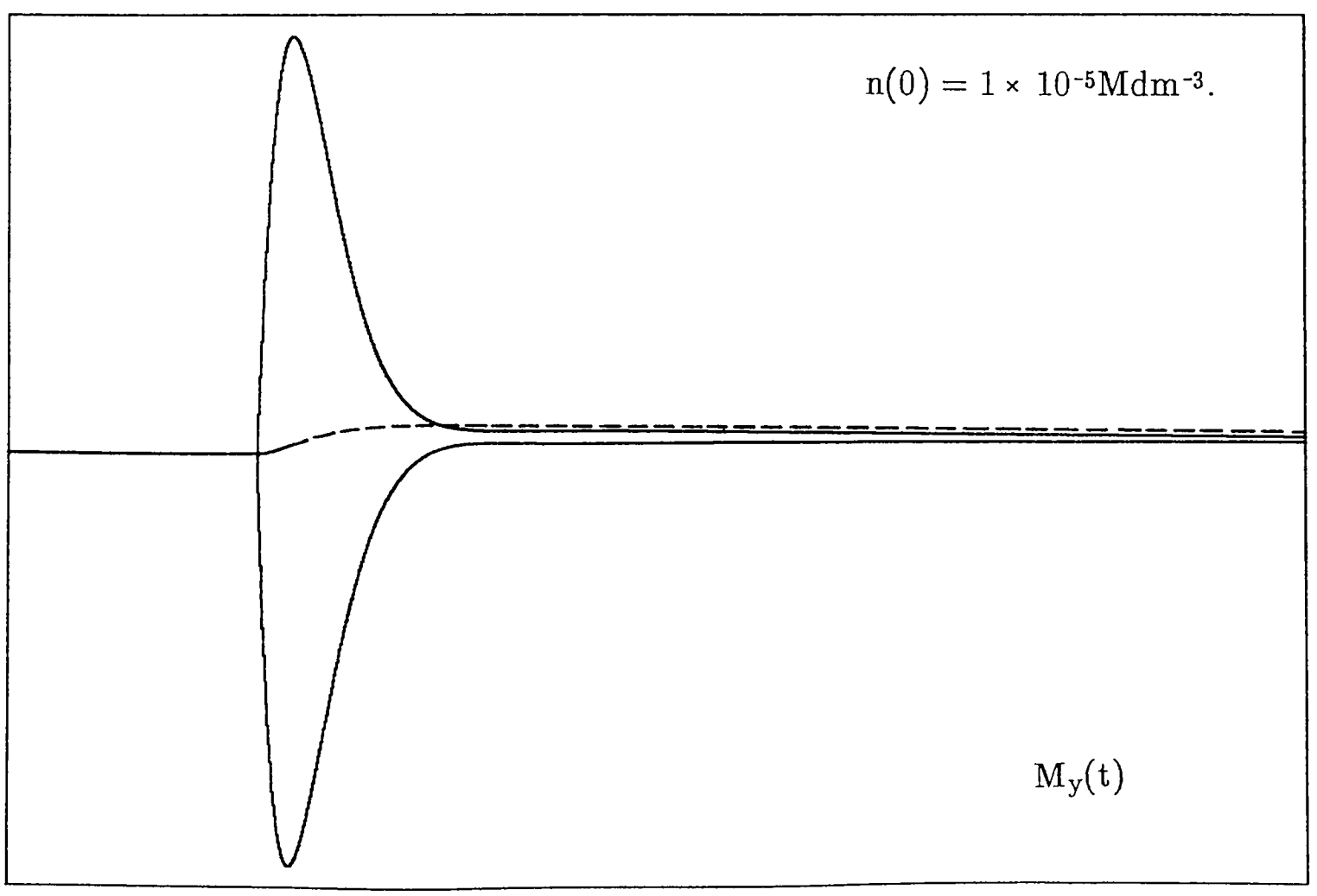

$T_1$ processes but it may be realigned by sequences of further *r.f.* pulses to give an "echo" of the initially coherent y–component of magnitization. *n.m.r.* requires that deuterated solvents be employed for the obvious reason that otherwise the resonances from solvent hydrogen atoms will smother those of the species we wish to observe. This should not worry us for it was shown earlier in this chapter that replacement of protonated by deuterated solvents did not appreciably affect the appearence of a CIDEP spectrum. This study is still in its infancy but the first experiments, kindly communicated by the authors prior to publication [61] look very promising.

In brief, two types of CIDNP polarization are identified, one of which arises from reaction within the geminate cage, the other resulting from reaction of radicals that have escaped this cage. They are predicted to give equal and opposite signs of polarization [58] according to the Kaptein Rules for CIDNP. Observation is over the microsecond timescale, during which nuclear spin states in diamagnetic reaction products are essentially static. The result is that geminate CIDNP is constant over the period of observation whilst that for escape products grows in as the product is formed, and their relative signs of polarization will be opposite for cage (E/A) and escape (A/E) products. In reality the multiplet phase is found to be the same for both products as though escape products are behaving as if they were produced in the cage. Furthermore, a net effect consistent with the transfer of early–time absorptive electron spin polarization to nuclear states has been discerned in escape products. This unexpected E/A phase in the CIDNP *n.m.r.* spectrum cannot apparently be modelled by a pure second order reaction. This is to be expected since cross–relaxation will be taking place *between* encounters so should appear as a first order effect. How, then, could an experiment that categorically separates first and second order events [6] demonstrate that the A/E phase of CIDEP

polarization arises through second order reaction? This is a damning criticism and all that can be said in defence is that cross relaxation may be most effective between pairs of radicals as they encounter but do not react during free diffusion.

(7.4.2) Sensitivity Of The A/E Multiplet To Conditions

With the results of model simulations available to us we can propose various trends in behaviour that we should expect to observe as conditions are varied. Of the many possible influences upon the signal two will have a complicated effect. They have been set down below:

• If we assume that all other parameters are invariant during variation of radical concentration then three regimes may be identified: i) when concentration is low no significant second order reaction takes place and the signal disappears below the noise level before observations at longer times can be made; ii) at high concentrations both F–pair (E/A) and cross–relaxation behaviour (A/E if scalar relaxation dominates) could be detected but the former will greatly outweigh the latter and a net multiplet of E/A would result; iii) at intermediate concentrations the recombinant, pure E/A phase is not as efficient a generator of polarization as the cross–relaxational one, so multiplet phase is overall A/E.

• Temperature and viscosity dependences are more complex still: low temperatures and high viscosities will serve to reduce radical/radical re–encounter and we should therefore expect to see the initial polarization emphasised with respect to F–pair effects, as was shown in the previous chapter; with less F–pair polarization the cross–relaxation phenomenon would be more influential if no substantial change to $T_1$, $\gamma$ and radical population occurs.

The effect of radical concentration is most easily tested by varying the intensity of incident laser radiation. Fig.(7.4.6) displays spectra of the central four lines of the $^{t}$butyl radical produced upon photolysis of di–$^{t}$butyl ketone. Keeping all other conditions constant the laser intensity was varied by attenuation. Over the intensity range available it was not possible to detect any lessening of the rate of inversion as laser power was increased above the minimum level necessary to observe an A/E phase multiplet. This applies over a ten–fold increase in light intensity. This experiment is, for the range of light intensities available to us, unable to distinguish between the hoped–for behaviour and that predicted for normal F–pair polarization.

Figs.(7.4.7) to (7.4.9) give the results of a variation of temperature/viscosity upon the same central four lines. As temperature is raised (and referring back to the previous chapter, the F–/G–pair polarization increases roughly by a factor of ten from 0$^{o}$C to 50$^{o}$C for this system), the A/E phase appears earlier and strengthens. In the last case a comparison of the two central lines reveals that the equilibrium polarization is of the same magnitude as that of the net E/A + A/E polarization. The result is only compatible with our proposed mechanism if the initial polarization decreases in magnitude and relaxes faster at higher temperatures.

(7.4.3) A Second Proposed Solution – The Separation Of "Hot" and "Cold" Radicals.

It is known from other fields [62,45] that the singlet reaction is often an activated process (though this would seem to run counter to the diffusion–controlled rates of reaction of propan–2–olyl radicals alluded to earlier). Thus, for the photolysis of di–$^{t}$butyl phenyl ketone two termination routes exist.

Fig.(7.4.6)

The effect of laser intensity upon the rate of development of an A/E long–time multiplet, for the central four lines of the $^{t}$butyl radical. Each trace was recorded at 39.5 ± 0.2°C and from 100 to 150$\mu$s, over 7.5mT. Laser attenuation is given alongside.

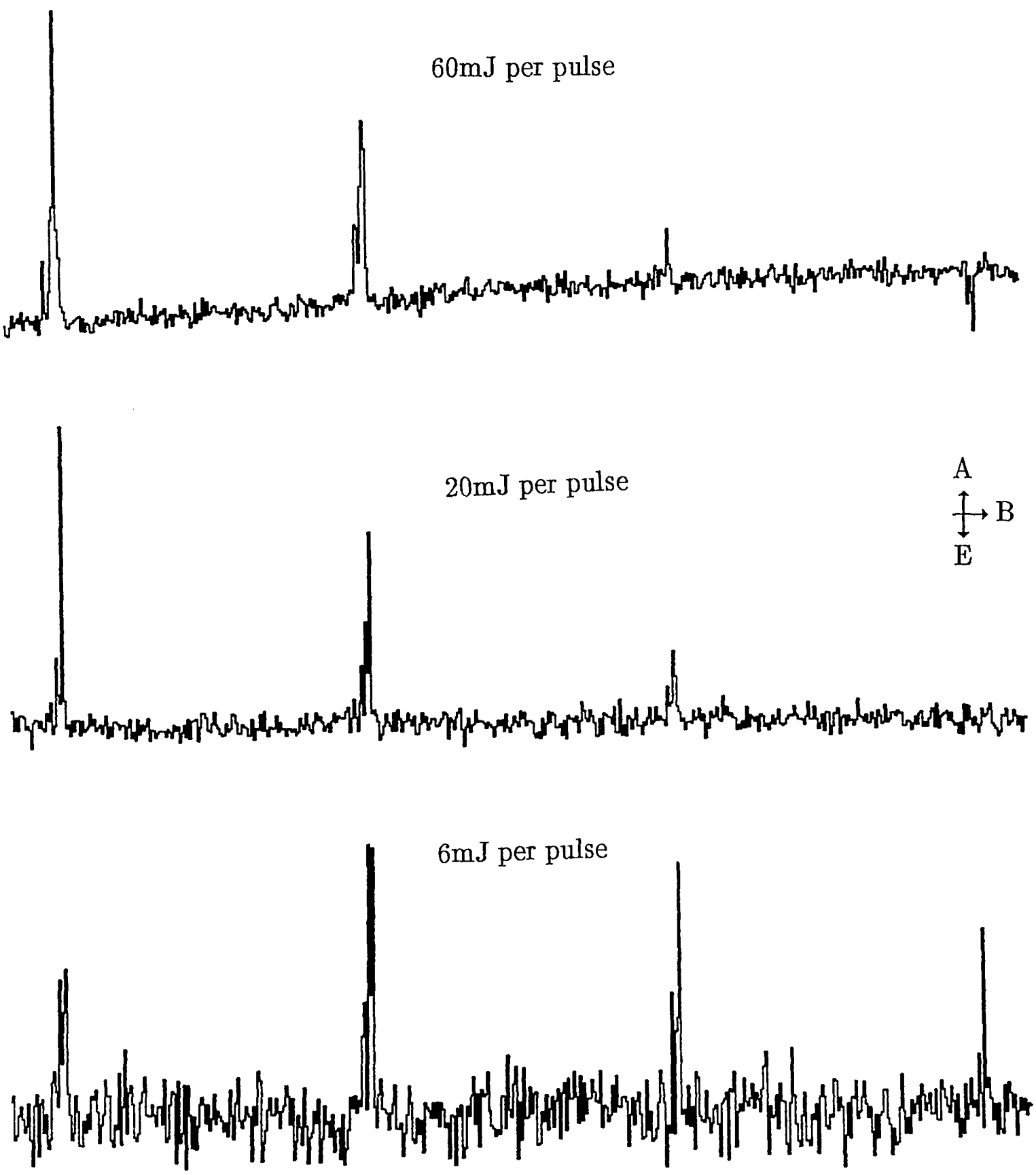

Fig.(7.4.7)

The central four lines of the $^{t}$butyl radical in heavy paraffin, collected at 5 ±0.2°C and recorded over 75mT. Times of integration are given alongside as an indication of the rate of development of the inverted multiplet.

1 to 2$\mu$s

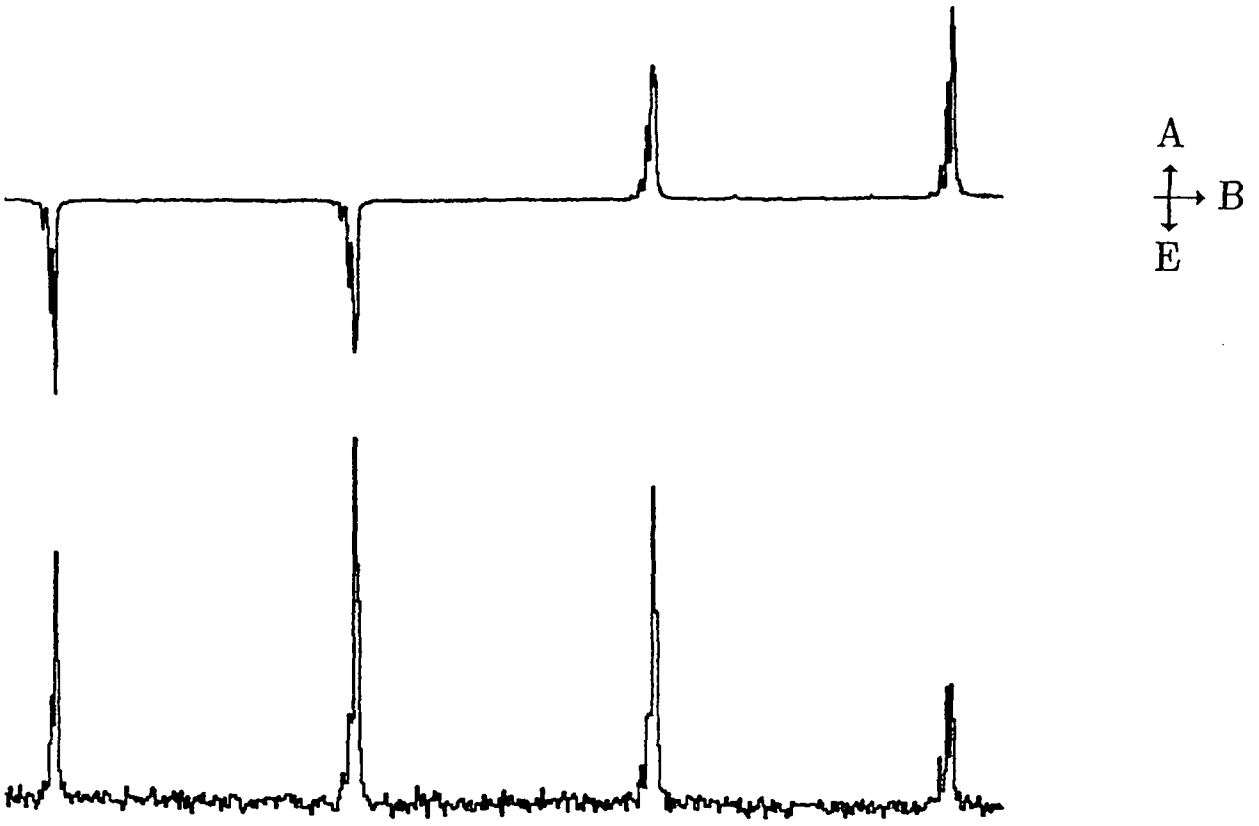


100 to 150$\mu$s

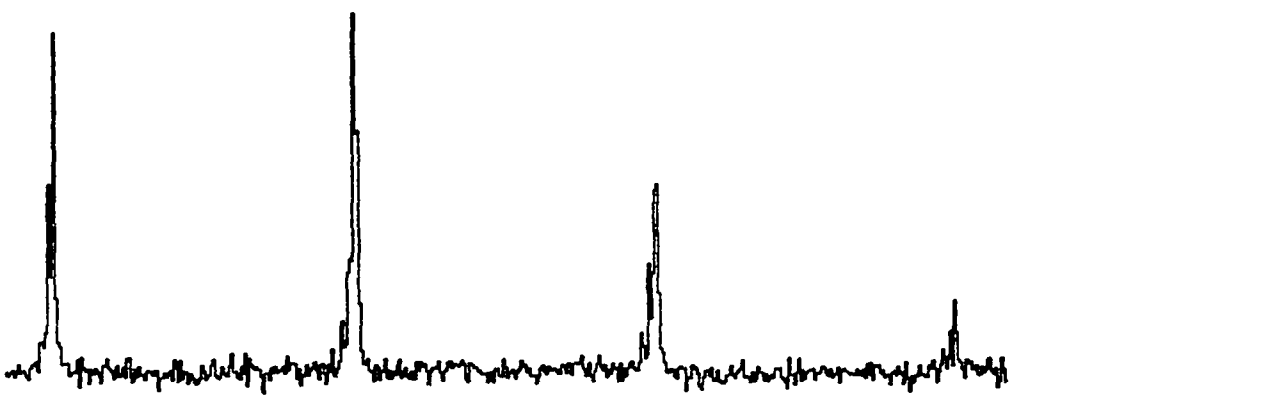

200 to 300$\mu$s

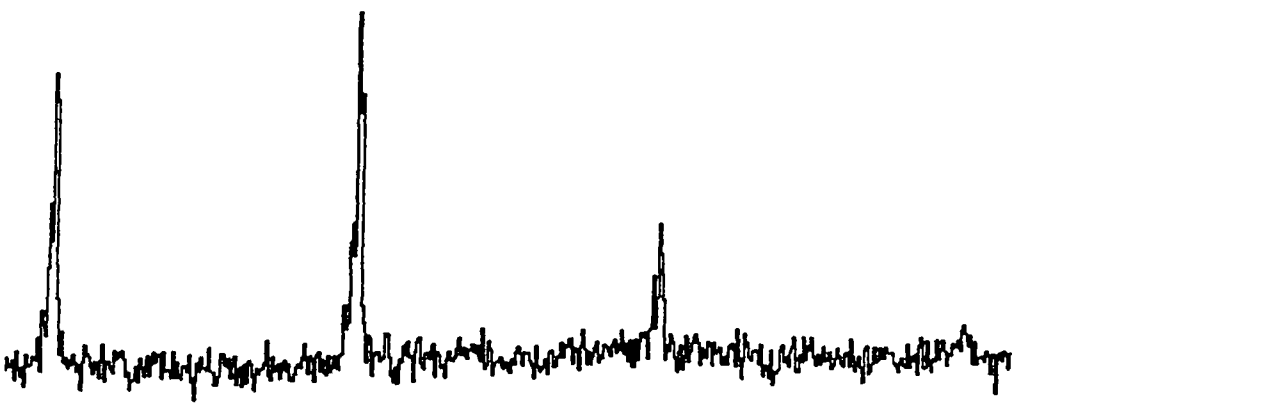

Fig.(7.4.8)

The central four lines of the $^{t}$butyl radical in heavy paraffin, collected at the higher temperature of 27 ±0.2°C and recorded over 75mT. Times of integration are given alongside. Rate of inversion appears to have increased with respect to Fig.(7.4.7).

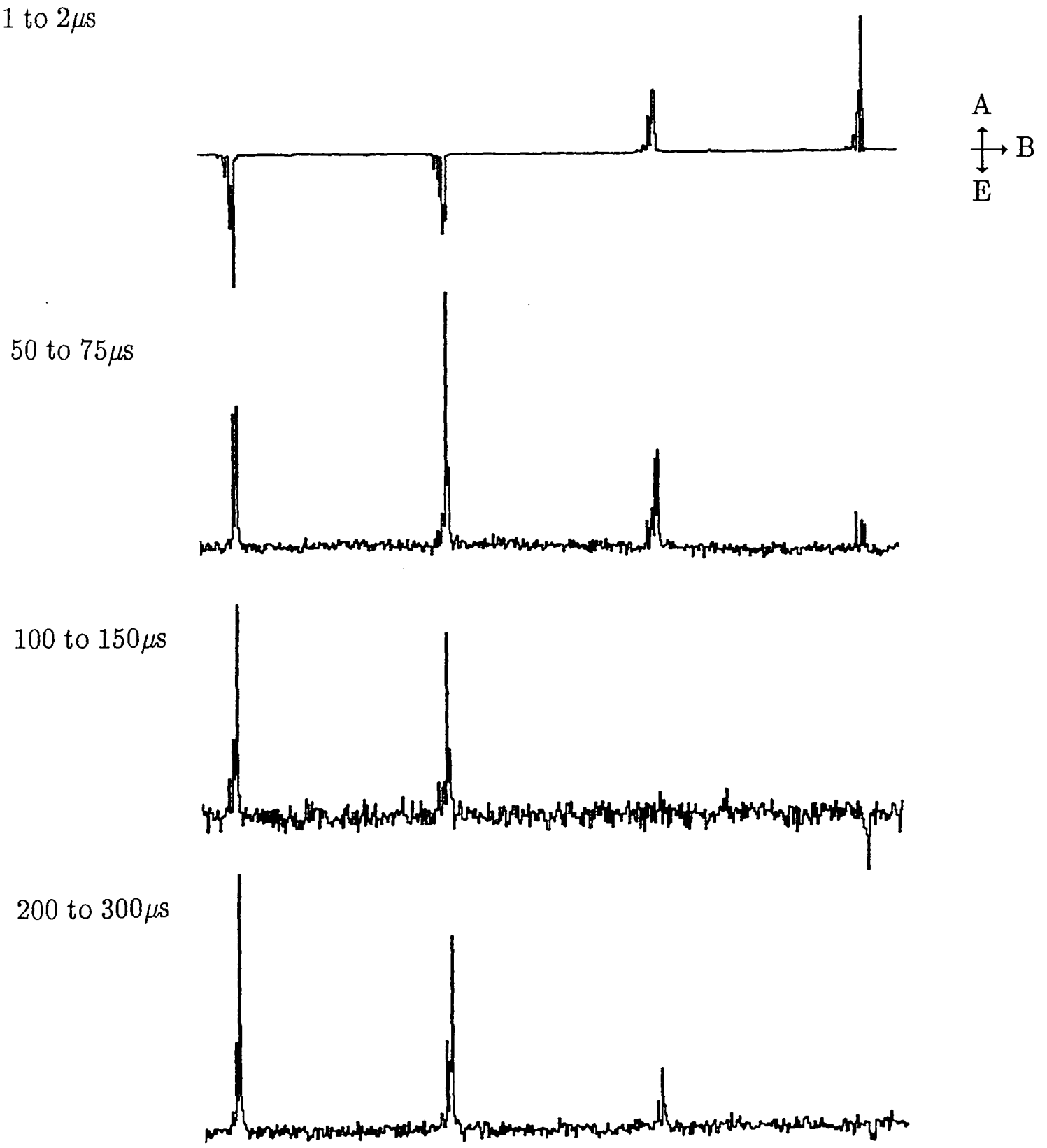

Fig.(7.4.9)

The central four lines of the $^t$butyl radical in heavy paraffin at the relatively high temperature of 39.5 ± 0.2°C and recorded over 75mT. Times of integration are given alongside each spectrum. A clear trend emerges from these three studies, that inversion rate is retarded at lower temperatures.

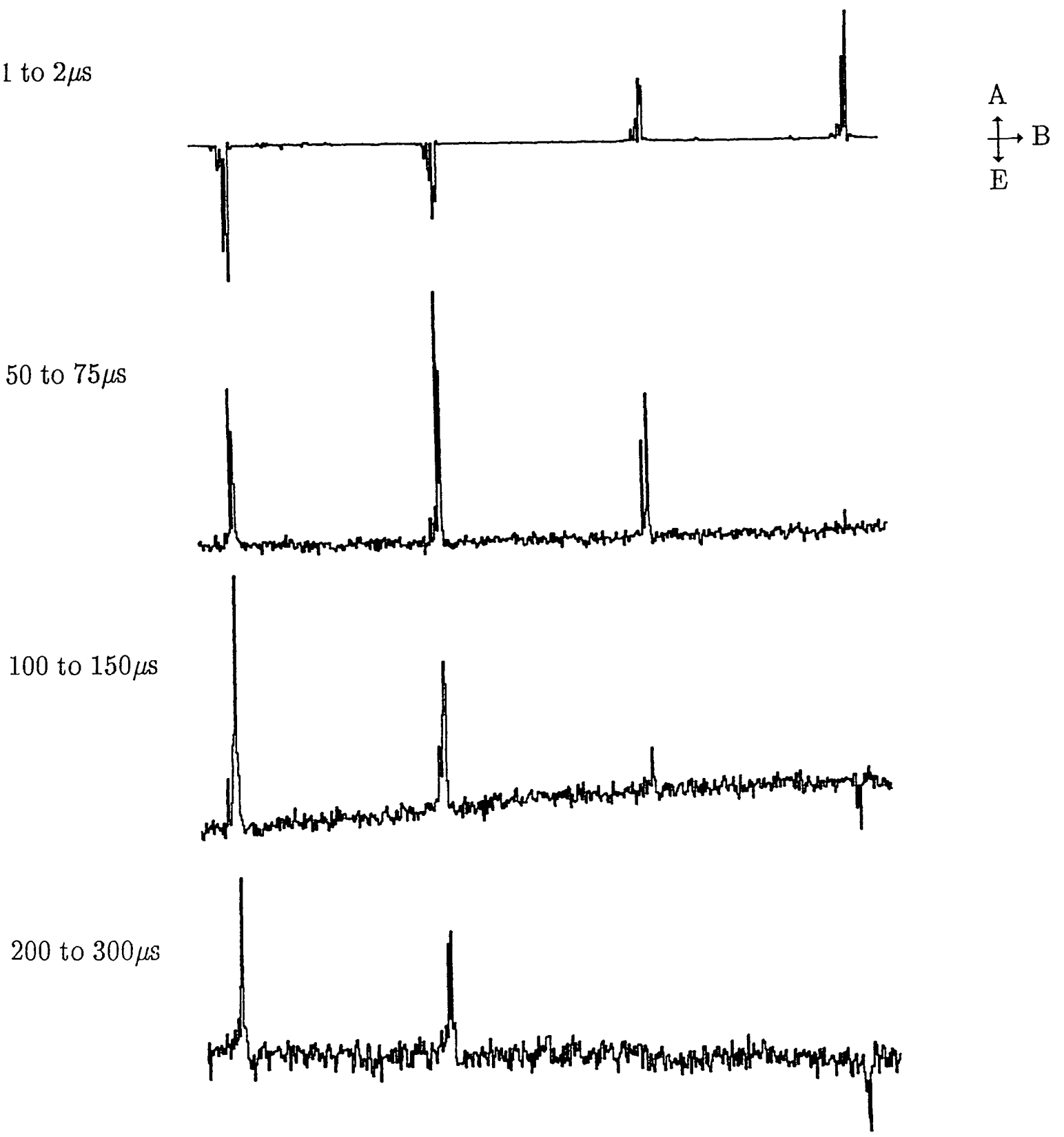

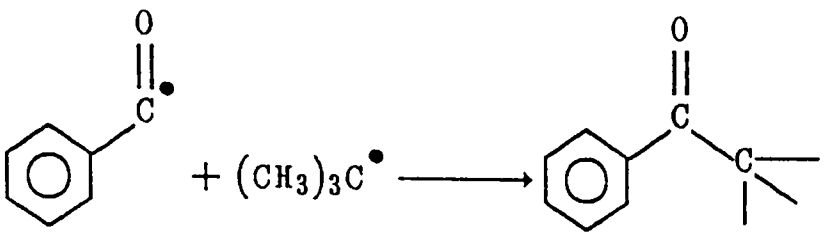

(K)

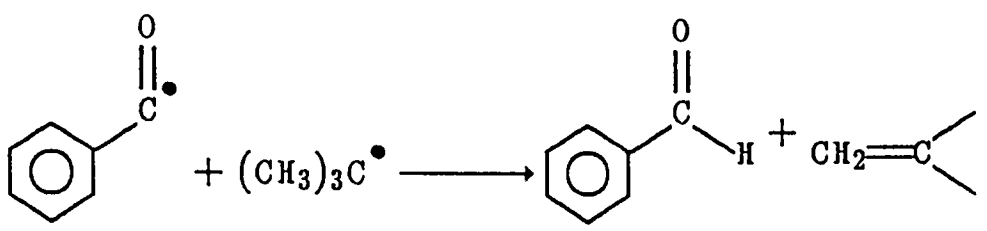

(L)

The former takes place through the singlet state only, whereas the latter may be triplet–mediated. This will be an activated process but it is possible that it would occur preferentially to give the escape products a singlet character. This is quite distinct from the net *singlet character polarization* that would result from limited singlet reactivity but stronger singlet polarization. In effect it means that the radical encounter pair will yield the normal E/A polarization if it has a high energy but for those of a lower energy the phase would be A/E[7].

A measure of the radical energies is simple at long times since the radicals will have attained thermal equilibrium with their surroundings. At shorter times however, not only will the radicals have a high excess energy but the solvent molecules in their vicinity will also be "hot" through relaxation of this energy. A series of temperature studies on the $^{t}$butyl radical from photolysis of di–$^{t}$butyl ketone in heavy paraffin was shown in

---

[7] We might envisage the triplet bi–radical as being more strongly correlated with a singlet groundstate in one triplet sub–level than another. Thus a triplet–selective reaction could produce a net emission at longer times. Some evidence comes from short–chain biradical studies carried out by Doubleday C.E. (*Chem.Phys.Lett.* (1979) 64, 67. (1981) 77, 131. and (1981) 79, 375). In the absence of any knowledge about triplet bi–radical states, however, this will have to remain pure conjecture.

Figs.(7.4.7) to (7.4.9). Referring back to these, the period of crossover does seem to increase as temperature is lowered, which is in broad agreement with a model that proposes activated reaction, as activated singlet reaction will become a less effective pathway. A similar trend has been noted elsewhere [46]. It does not, alas, provide any agreement with the above model.

High laser powers will cause a stronger initial heating of the sample as more energy is absorbed by the solvent and photo–active species. We should expect to see the E/A phase persist for a longer time and, in those systems where A/E polarization may be observed over a range of laser powers, this does seem to be the case [54]. For the propan–2–one/propan–2–ol system, however, the inversion is only seen at high laser powers. This is not inconsistent with the model since, in order to create and observe long time polarization effects we must have a high initial radical concentration: below a critical level, where the bimolecular rate is lower than the relaxation rate, generation of polarization will be slower than the disappearance of the early–time E/A phase multiplet, so no crossover from E/A to A/E will be visible. Provided that the laser discharge is kept above this minimum level then one would expect the crossover time to decrease with increasing laser power. Qualitatively the effect is similar to that for concentration dependence of cross–relaxation.

A further piece of evidence in favour of this scheme is that under no conditions could an inversion of $CH_2^{\bullet}OH$ radical signals be observed. A triplet reaction such as could occur for (L) is not feasible for this radical and the singlet reaction should be less strongly activated, too, as the radical centre is not screened by adjacent methyl groups. Neither have any reports of $^{\bullet}CH_2.CH_2OH$ or $^{\bullet}CH_2CO_2^{\ominus}$ radicals showing A/E phases been published.

(7.5.1) A Conclusion, Such As It Is

If the foregoing is all rather negative then it is worth re–stating the experimental observations and seeing that a great deal has been achieved. A genuine phenomenon has been demonstrated and its occurrence has been limited to tertiary and secondary alkyl radicals and to the photo–decomposition or reduction fragments of ketone photolyses or alcohol H–abstraction products.

It is clear from both problems tackled in this chapter that we still have no definite understanding of all CIDEP phenomena. However, it has proved possible to test and reject ideas and the existence of these anomalies has forced experimenters to re–examine the nature of the detection of transient radicals. Of the two the long–time inversions of phase has proved more amenable to study: along with rejecting two mechanisms, both of which could have caused this inversion and each having important implications for physical understanding of the exchange interaction in solution, singlet reactivity and CIDNP polarization, two tentative resolutions have been proposed. The first of these has been examined and reservations expressed about inconsistencies with both polarization magnitudes and kinetic behaviour. Inversion has been shown to be fairly solvent–independent but its magnitude does appear to be concentration– and system–dependent. A distinction has been made between G– and F–pairs in two of the models but what has been shown is that the real difference must be between radicals observed early on and later in time. The second one does not directly contradict any existing evidence, though with such an arbitrary basis it is hardly likely to!

A separate model has been advanced in which viscosity plays a crucial rôle [50] in generating reversals of phase by modifying encounter and diffusion times. This, too, requires that a division into the "hot" and "cold" radical regimes is made. This is a highly theoretical model but it purports to show how the A/E multiplet could arise in the

ipropyl radical. A look at the off–resonance signal in almost any solvent shows that it takes many microseconds – often as long as several hundred – before the sample cools to the pre–flash level. It seems impossible to go any further with this idea than such observations, alas. Perhaps what these two problems are most indicative of are the complexity and subtlety of the CIDEP phenomenon. If there is an answer to them it is unlikely to be pure and simple. Cetera desunt... .

## REFERENCES – CHAPTER 7


1 Wong S.K, Chiu T.M, Bolton J.R. *J.Phys.Chem.* (1981) 85, 12.

2 Basu S., Grant A.I., McLauchlan K.A. *Chem.Phys.Lett.* (1983) 94, 517.

3 Yamauchi S., Tominaga K., Hirota N. *J.Phys.Chem.* (1986) 90, 2367.

4 McLauchlan K.A., Stevens D.G. *Mol.Phys.* (1987) 60, 1159.

5 Pedersen J.B., Freed J.H. *J.Chem.Phys.* (1975) 62, 1706.

6 Carmichael I., Paul H. *Chem.Phys.Lett.* (1979) 67, 519.

7 McLauchlan K.A., Stevens D.G. *J.Magn.Reson.* (1985) 63, 473.

8 Valyaev V.I., Molin Y.N., Sagdeev R.Z., Hore P.J., McLauchlan K.A. Simpson N.J.K. *Mol.Phys.* (1988) 63, 891.

9 Dalton J.C., Snyder J.J. *J.Am.Chem.Soc.* (1975) 97, 5192.

10 Loutfy R.O., Loutfy R.O. *Can.J.Chem.* (1972) 50, 4052.

11 Tominaga K., Yamauchi S., Hirota N. *J.Phys.Chem.* (1988) 92, 5160.

12 Terazima M., Azumi T. *Chem.Phys.Lett.* (1987) 141, 237.

13 Davidson E.R., Ellenbogen J.C. Langhoff S.R. *J.Chem.Phys.* (1980) 73, 865.

14 Yamauchi S., Tominaga K., Hirota N. *5th. Nodzu Memorial Lectures – Abstracts.* (1985) 24.

15 Buckley C.D., Hore P.J., Hunter D.A., McLauchlan K.A. *Chem.Phys.Lett.* (1987) 135, 307.

16 Shain A.L., Chiang W.T., Sharnoff M. *Chem.Phys.Lett.* (1972) 16, 206.

17 Shain A.L., Sharnoff M. *Chem.Phys.Lett.* (1972) 16, 503.

18 Hayashi H., Nagakura S. *Bull.Chem.Soc.Japan* (1978) 51, 2862.

19 Dellinger B., Hochstrasser R.H., Smith A.B. *J.Am.Chem.Soc.* (1977) 99, 5834.

20 Pasternak R., Wagnière G. *J.Comput.Chem* (1981) 2, 345.

21 Johnston L.J., Scaiano J.C. *J.Am.Chem.Soc.* (1987) 109, 5487.

22 Jent F., Paul H., Fischer H. *Chem.Phys.Lett.* (1988) 146, 315.

23 Livingstone R., Zeldes H. *J.Chem.Phys.* (1966) 44, 1245.

24 Bartels D.M., Lawler R.G., Trifunac A.D. *J.Chem.Phys.* (1985) 83, 2686.

25 Henne A., Fischer H. *J.Am.Chem.Soc.* (1977) 99, 300.

26 Leuschner R., Fischer H. *Chem.Phys.Lett.* (1985) 121, 554.

27 Ledger M.B., Porter G. *J.Chem.Soc. Faraday Trans. I* (1972) 68, 539.

28 Scaiano J.C. *J.Photochem.* (1973/4) 2, 81.

29 Griller D., Ingold K.U. *J.Am.Chem.Soc.* (1974) 96, 630.

30 Paul H., Small R.D., Scaiano J.C. *J.Am.Chem.Soc.* (1978) 100, 4520.

31 Tominaga K., Yamauchi S., Hirota N. *J.Chem.Phys* (1988) 88, 553.

32 McLauchlan K.A., Stevens D.G. *Mol.Phys.* (1987) 60, 1159.

33 Fessenden R.W. *J.Chem.Phys.* (1973) 58, 2489.

34 Paul H. *Chem.Phys* (1979) 40, 265.

35 Paul H., Segaud C. *Intern.J.Chem.Kinet.* (1980) 12, 637.

36 Blank B., Henne A., Laroff G.P., Fischer H.
*Pure & Applied Chem.* (1975) 41, 475.

37 Kivelson D. "*Electron Spin Relaxation In Liquids*"
(Ed. Muus L.T., Atkins P.W.) and references therein (Pub. Plenum N.Y. 1972).

38 Atkins P.W., Kivelson D. *J.Chem.Phys.* (1966) 44, 169.

39 Blättler C., Jent F., Paul H. *Chem.Phys.Lett.* (1990) 166, 375.

40 Steiner U.E., Ulrich T. *Chem.Rev.* (1989) 89, 51.

41 Tominaga K., Yamauchi S., Hirota N. *Chem.Phys.Lett.* (1988) 149, 32.

42 McLauchlan K.A., Stevens D.G. *J.Chem.Phys.* (1987) 87, 4399.

43 Atkins P.W., Dobbs A.J., McLauchlan K.A.
*J.Chem.Soc. Faraday Trans.II.* (1975) 71, 1269.

44 Stevens D.G. *D.Phil.Thesis, Oxford* (1987) Chapter 7.

45 McLauchlan K.A., Frith P.G *J.Chem.Soc.Faraday Trans.II* (1976) 87.

46 Jent F., Paul H. *Chem.Phys.Lett.* (1989) 160, 632.

47 Sessler J.L., Johnson M.R., Lin T.Y. *Tetrahedron* (1989) 45, 4767.

48 Grant A.I., Green N.J.B., Hore P.J., McLauchlan K.A.
*Chem.Phys.Lett.* (1984) 110, 280.

49 Pedersen J.B., Freed J.H. *J.Chem.Phys.* (1973) 59, 2869.

50 Syage J.A. *J.Chem.Phys.* (1987) 87, 1022 ibid 1033/*unpublished work.*

51 Thurnauer M.C., Chiu T.M., Trifunac A.D. *Chem.Phys.Lett.* (1985) 116, 543.

52 Borbat P.P., Milov A.D., Molin Y.N. *Chem.Phys.Lett.* (1989) 164, 330.

53 Jent F., Paul H., McLauchlan K.A., Stevens D.G.
*Chem.Phys.Lett.* (1987) 141, 443.

54 Vollenweider J–K., Fischer H., Hennig J., Leuschner R.
*Chem.Phys.* (1985) 97, 217.

55 Overhauser A.W. *Phys.Rev.* (1953) 92, 411.

56 Adrian F.J. *Chem.Phys.Lett.* (1974) 26, 437.

57 Thomas M.J., Wagner P.J., Manion–Schilling M.L., Roth H.D.
*J.Am.Chem.Soc.* (1977) 99, 3842.

58 Kaptein R. "*Chemically Induced Magnetic Polarization*" (Ed. Muus et al.)
Chapter 1 (Pub. D.Reidel, 1977)

59 Griller D., Ingold K.U., Krusic P.J., Fischer H.
*J.Am.Chem.Soc.* (1978) 100, 6750.

60 Vollenweider J.K., Fischer H. *Chem.Phys.* (1986) 108, 365.

61 Yurkovskaya A.V., Tsentalovich Y.P., Sagdeev R.Z.
*Chem.Phys.Lett.* (1990) in the press.

62 de Kanter F.J.J., Kaptein R. *J.Am.Chem.Soc.* (1982) 104, 4759.

# CHAPTER VIII : A PHOTOCHEMICAL ANALYSIS EMPLOYING CIDEP

# A PHOTOCHEMICAL ANALYSIS EMPLOYING CIDEP

## (8.1.1) An Introduction

In contrast to the previous chapter this one presents a long–standing chemical problem and a simple solution. It is illustrative of the power of flash–photolysis *e.s.r.* and CIDEP as tools for performing mechanistic diagnoses. No attempt is made to analyse the relevant excited states of the chromophore because, for the purpose of this demonstration no knowledge of them is needed: the identification of an emissive signal with an E/A overlying multiplet will prove sufficient evidence to implicate a triplet intermediary, though care will be taken in apportioning different components of a signal to different CIDEP mechanisms. What is given herein is a brief study of an aromatic di–carbonyl system which has given kineticists and organic chemists contradictory results by ordinary analytical techniques.

## (8.2.1) The History Of The oPhthalaldehyde Problem

The first study of the photolytic behaviour of ortho–phthalaldehyde (ortho–carboxy benzaldehyde) was a steady–state photolysis in benzene [1], from which the major product formed was a dimer, structure (I)

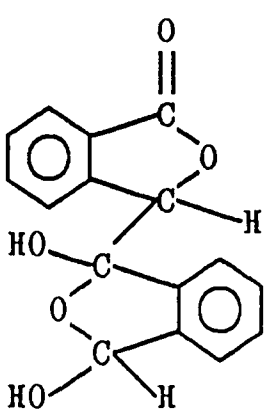


(I)

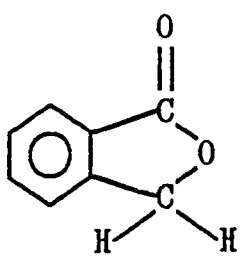


(II)

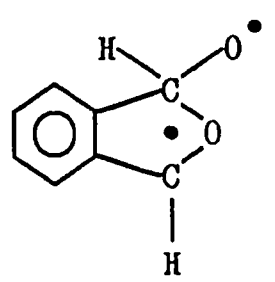


(III)

Later studies [2,3] showed that if the solvent was capable of donating a hydrogen atom or was chlorinated then phthalide (II), formed by a photo–Canizzaro reaction, was the major product, and in accord with this a cyclic biradical was proposed – structure (III).

A subsequent paper [4] suggested that a ketene and carbene route may occur, though little supportive evidence was provided (the observation of a Diels–Alder product with maleic anhydride does not imply that a Diels–Alder reaction has taken place; the ease of free radical addition to maleic anhydride has been demonstrated in chapter 5). Subsequent to this, a kinetic study which attempted numerous triplet–trapping experiments [5] concluded that the reaction, whatever its mechanism, proceeded via a singlet state cyclic enol, in keeping with the proposal of a singlet biradical [6]. The quantum yield of phthalide was found to be approximately one quarter.

The only positive identification of any intermediate species prior to this study[1] was made upon the closely related $^{o}$di–benzoyl benzene, which was found to generate a radical consistent with structure (IV) upon steady–state photolysis (and employing standard *e.s.r.* detection) [7]. Couplings are quoted in milliTesla.

---

1 The first observation of an unusual intermediate in the photolysis of $^{o}$phthalaldehyde was made by J.R.Yousafzai in this laboratory in 1985. Poor quality spectra hampered analysis and his conclusions differ from those given here. His Chemistry "Part II" thesis, Chapter 6, § D and E are useful references for the effects of solvent and pH upon the radicals observed.

(IV)

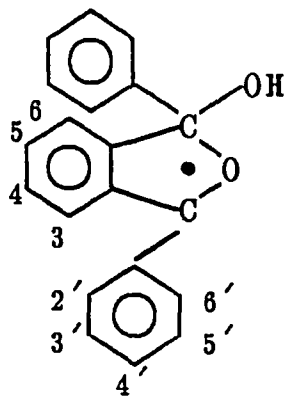

| $A_{4,6}$ | $A_{4,6}$ | $A_{3',5',3,5}$ | $A_{2',6'}$ | $A_{4'}$ |
|---|---|---|---|---|
| 0.028 | 0.118 | 0.235, 0.343 | 0.397 | 0.578 |

(8.2.2) Ortho–phthalaldehyde Ground State And Derived Radicals

Three possible conformers for phthalaldehyde can be identified, which we shall term

ENDO (V)

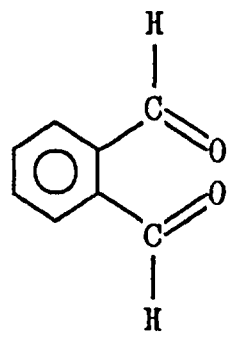

MESO (VI)

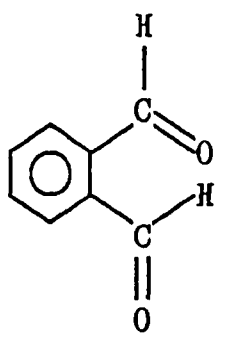

EXO (VII)

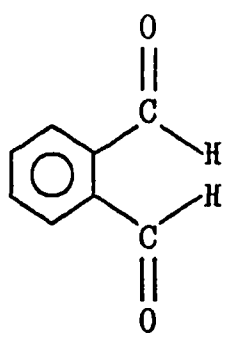

$\pi$–conjugation of carbonyl groups effectively locks them in these three near–planar conformations to such an extent that rotational isomers may be observed by *n.m.r.* [8], the EXO and MESO forms having a lower energy than the ENDO–morph. Molecular orbital calculations confirm that the ENDO form may be discounted at room temperature for °phthalaldehyde, whilst structures VI and VII are separated by about 15kJmol$^{-1}$. Various electrolytic reductions of °phthalaldehyde and related compounds have been carried out and the radical anions studied by steady–state *e.s.r.*, assignment of proton couplings being made by selective deuteration [10]. The results are quoted below for later comparison.

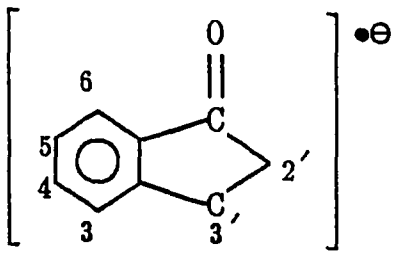

| $A_3$ | $A_4$ | $A_5$ | $A_6$ | $A_{2'}$ | $A_{3'}$ |
|---|---|---|---|---|---|
| 0.016 | 0.692 | 0.147 | 0.569 | 0.160 | 1.300 |

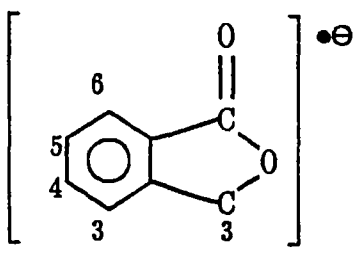

| $A_3$ | $A_4$ | $A_5$ | $A_6$ | $A_{3'}$ |
|---|---|---|---|---|
| 0.031 | 0.779 | 0.137 | 0.566 | 0.625 |

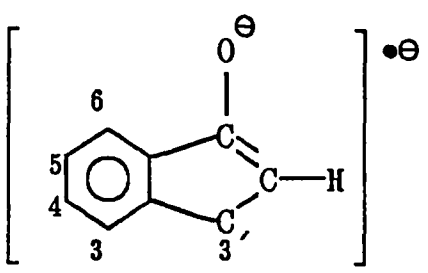

| $A_3$ | $A_4$ | $A_{2'}$ |
|---|---|---|
| 0.016 | 0.250 | 0.077 |

The couplings in the ᵒphthalaldehyde radical anion are harder to establish [11] but the aldehyde proton gives rise to the largest coupling and the MESO conformer is found to predominate, presumably because it is stabilised by an intra–molecular H–bond.

(VIII)

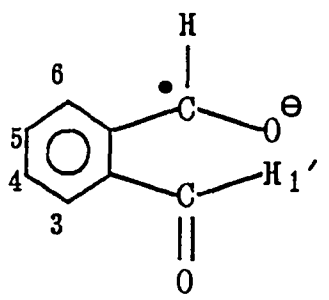

| $A_{3-6}$ | $A_{1'}$ | $A_{\alpha}$ |
|---|---|---|
| 0.049, 0.219, 0.291, 0.372 | 0.000 | 0.462 |

The total spectral spread is thus 1.393mT.

(8.2.3) Objectives And Experiments

Ideally we would wish to isolate all species involved in what is unlikely to be a simple reaction. If kinetic conditions can be chosen so that the rate of H–abstraction

can be kept high or low then we could hope to observe different radical intermediates, provided, as indicated by the variation in product yields with solvent, distinct mechanisms are operating in each case. The solvents chosen for this study were octan–2–ol and hexan–1–ol since both dissolve the photo–active component to a good degree, and are both slow H–donors. In addition, their moderate viscosity enhances any polarization process without slowing rotation of the radical to the extent that its lines are too broad for accurate couplings to be extracted. To a certain extent they, too, will be involved in the initial photo–reduction but they are not sufficiently good H–donors to compete with the two added quenchers, tri–ethyl amine and 2,4,6 tri–$^t$butyl phenol.

The results from two experiments, one of which employs amine as quencher, the other with phenol, are displayed in Fig.(8.2.1) and (8.2.2). Two very clearly different radicals are observed under fast and slow quenching regimes. We may note at once that they are both entirely in emission and this is overlayed by an E/A multiplet, indicative of triplet reactivity: the proposal that reaction occurred via a singlet state was made on the evidence of quenching studies with the bi–pyridinylium ion and with phenols, but from the evidence of these spectra the phenol quencher, at any rate, is too slow to trap the initial triplet, let alone a singlet radical. We are left to speculate that the initial triplet molecule generates a triplet biradical very rapidly. This triplet bi–radical may be less sensitive to phenol quenching than a triplet molecule would be. Amine quenchers are typically a couple of orders of magnitude faster than phenolic ones, since quenching can occur by electron transfer. This would appear reasonable in this case, given the presence of two electron–withdrawing groups on an aromatic nucleus. If the phenol concentration is increased until the solvent is saturated ($>$ 1.5Molar) then both species can be observed simultaneously, the di–$^t$butyl phenoxyl radical appearing as a weak feature, slightly to low–field of the centre of both phthalyl–derived radicals. This can be

Fig.(8.2.1)

A spectrum and simulation of the radical, believed to be (IX), obtained upon photolysing 0.5M °phthalaldehyde in octan–2–ol with 0.5M $Et_3N$ as quencher, recorded over 5mT. Couplings used in this simulation are quoted in the text.

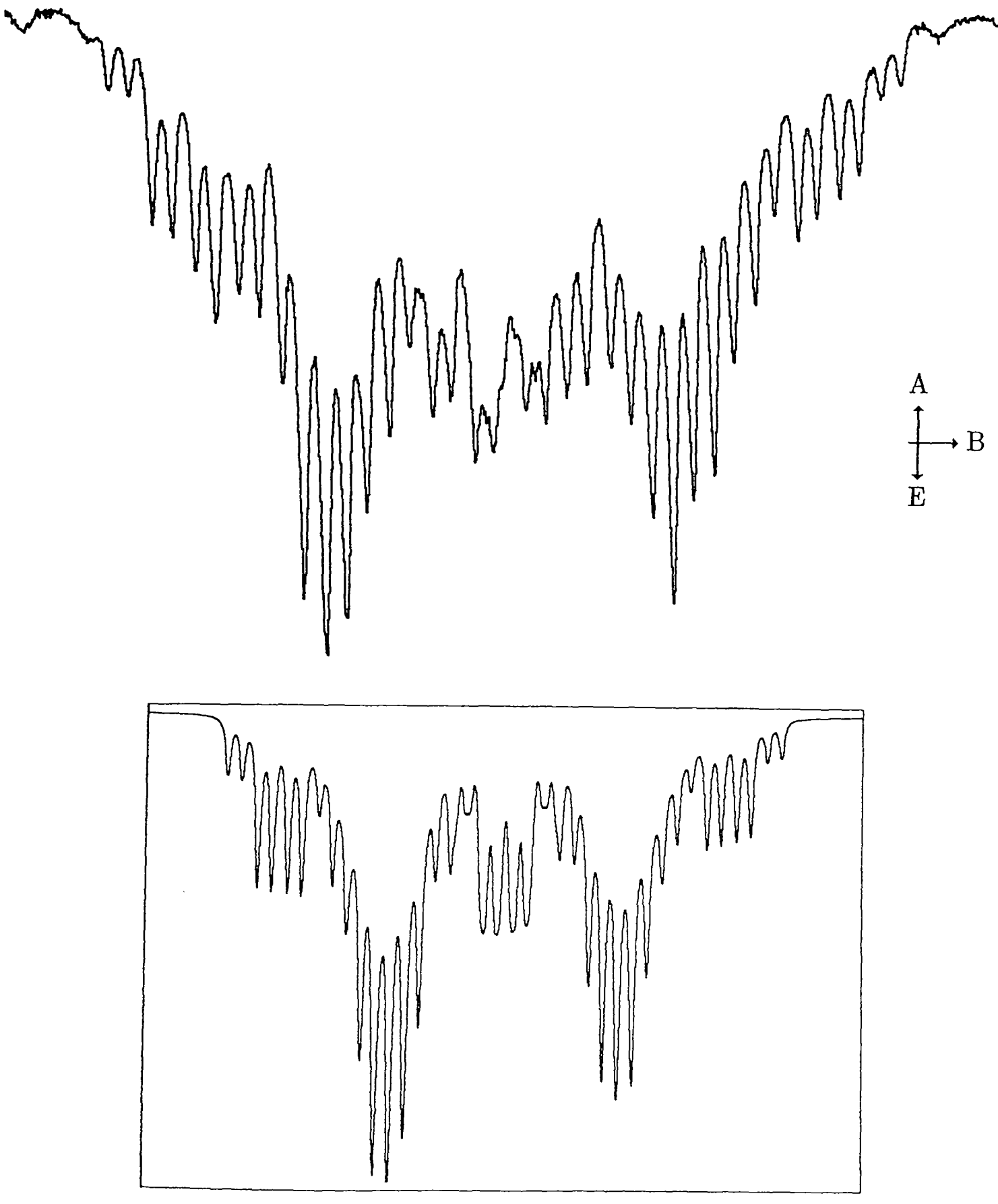

Fig.(8.2.2)

The radical spectrum obtained upon photolysis of 0.5M ophthalaldehyde in octan–2–ol, with 0.1M tri–$^{t}$butyl phenol as quencher (the broad feature slightly to the left of centre is the phenoxyl radical). The proposed structure is (XVI) and couplings used in the simulation are given in the text. Field sweep is over 4mT.

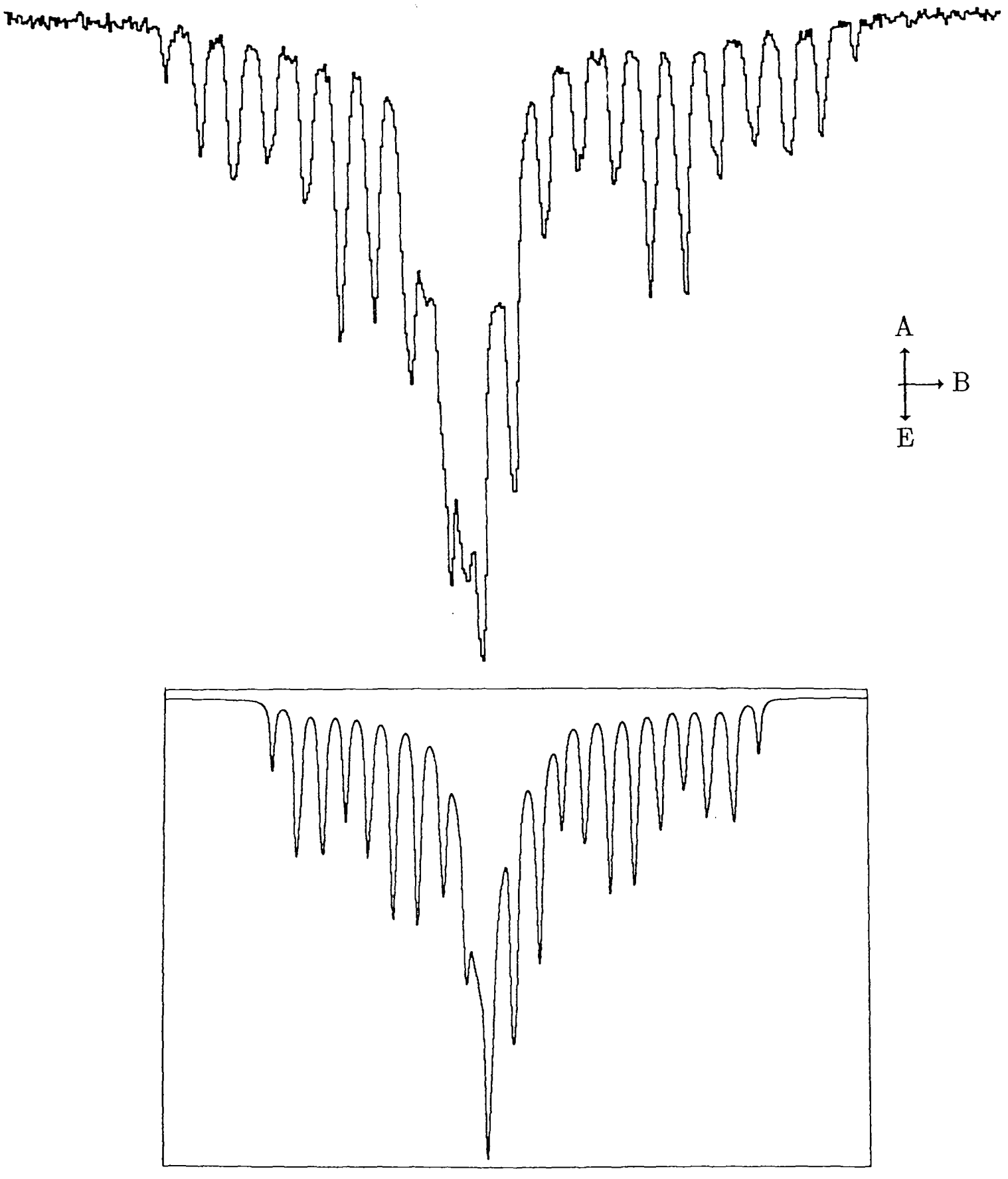

Fig.(8.2.2a)

The simultaneous observation of radicals seen separately in Fig.(8.2.1) and (8.2.2). This result was obtained by increasing the concentration of the quenching phenol until the solvent is saturated.

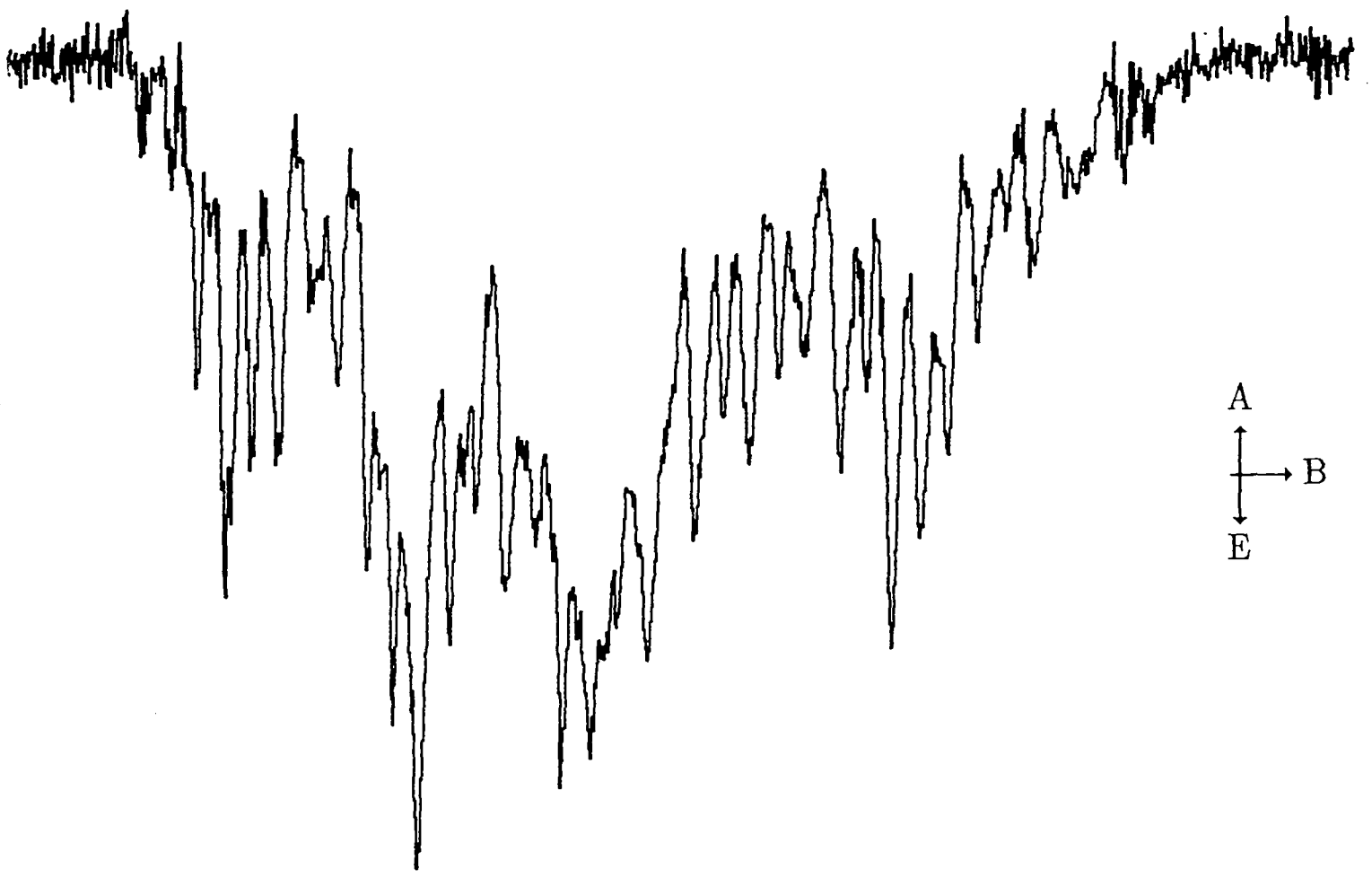

seen in Fig.(8.2.2a). Further, since phthalaldehyde was photolysed at concentrations of around 0.5M then, if we were observing radical anions the degenerate electron exchange process would obliterate the RPM polarization. This polarization, weak though it is, is clearly visible. From this we may assume that we are generating neutral radicals.

Comparison of coupling constants between the species generated by amine quencher and the neutral benzaldehyde radical, also quenched by tri–ethyl amine and showing a strongly emissive TM, suggests that we are dealing with a similar open–chain structure, rather than a close partner to any of the radicals shown in the above table, or an anionic species such as (VIII). We thus assign it a structure (IX), with the couplings used in the simulation included alongside

(IX)

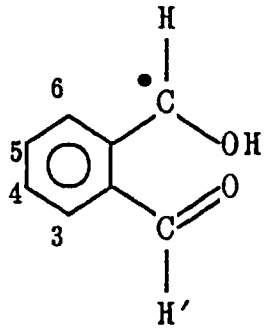


| $A_{3-6}, A_{H'}$ | | | | | $A_{OH}$ | A |
|---|---|---|---|---|---|---|
| 0.165, | 0.169, | 0.177, | 0.529, | 0.676 | 0.081 | 1.285 |

The coupling to the $\alpha$–hydrogen is assigned largely by comparison with the couplings to the $\alpha$–hydrogen in radicals known to be cyclic. For example, in a radical derived from tetrahydrofuran, (X) [12],

(X)

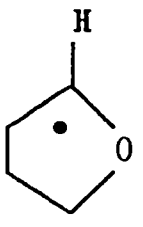


$A_{\alpha_H} = 1.210$ mT.

and the phthalan–derived radical, the spectrum of which is shown in Fig.(8.2.3).

Fig.(8.2.3)

Spectrum of the radical derived from phthalan in the presence of di–$^t$butyl peroxide under photolysis. Couplings used in this simulation are given alongside structure (XI). A $T_2$ of 0.9$\mu$s was found to fit the observed linewidth – longer than for the other radicals examined in this chapter. The broad, unidentified central feature is unlikely to result in an impurity in the phthalan (two separate samples of > 98% purity were screened, the spectrum appearing identical in each), but might be a consequence of using the peroxide as solvent, as well as photo–initiator. It has an apparent centre to low field of the carbon–centred radical, suggestive of an oxygen–centred one – perhaps a peroxyl species.

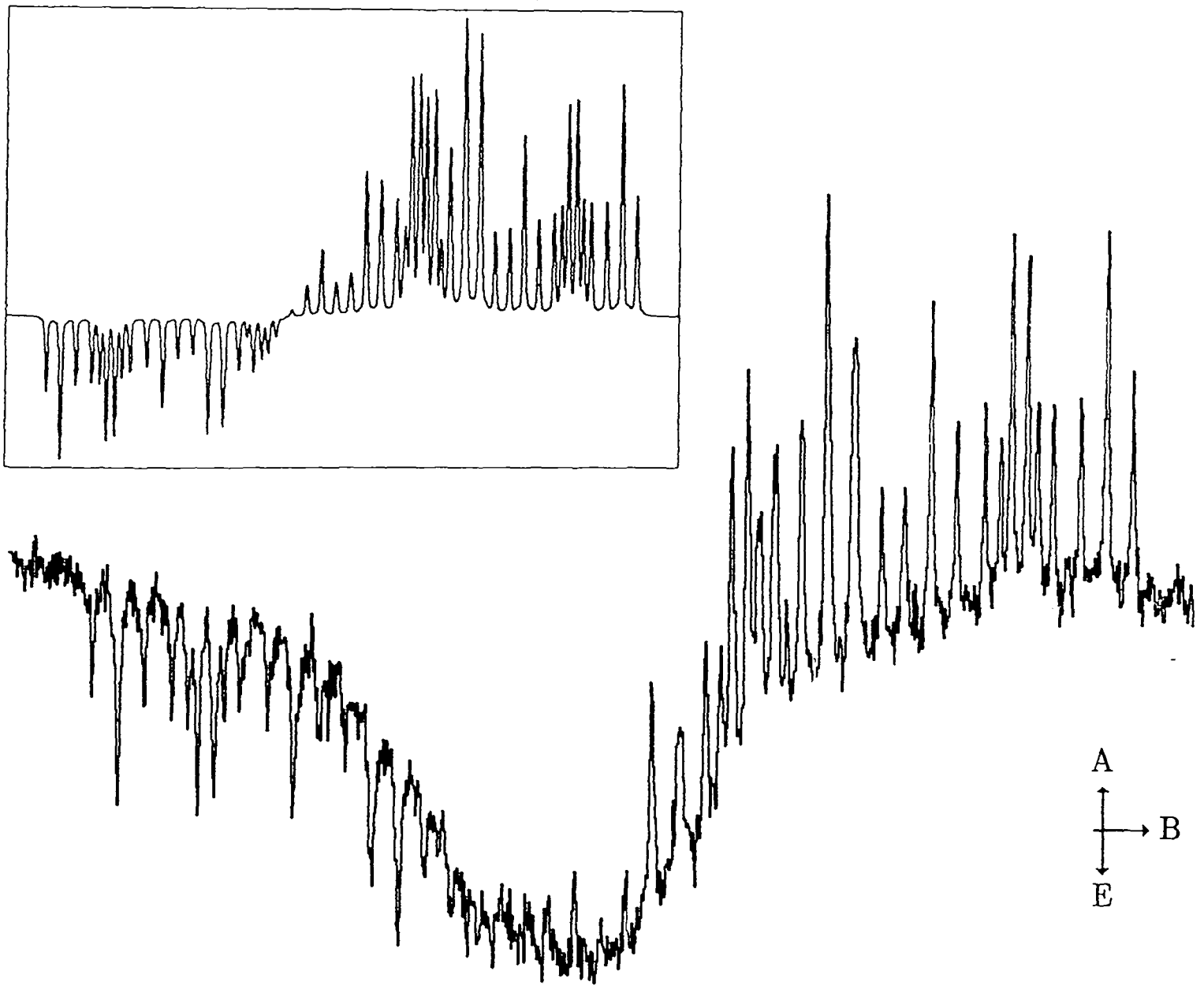

(XI)

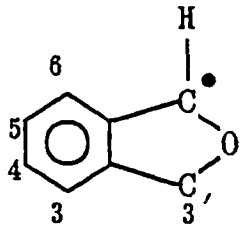


| $A_{3-6}$, $\alpha_H$ | $A_{3'}$ |
|---|---|
| 0.270, 0.320, 0.852, 0.936, 0.961. | 0.088 |

The observed coupling is larger than the largest coupling in the two cyclic species, suggesting that the electron is well localised upon the ketyl carbon and that it is in an orbital with a high s–character. The small couplings to the ring protons corroborate this; non–planarity at the ketyl carbon centre has already been alluded to in previous chapters [13], despite the apparent benefit of delocalisation into the aromatic ring which would result in a lower spin density on, and hence coupling to, the ring protons. This is amply illustrated by (IX) and (XI) since the five–membered ring will enforce a planarity upon the radical centre and enhance spin delocalisation onto the ring. Further confirmation comes from the radicals (XII) and (XIII), prepared again by photolysis in a tri–ethylamine/octan–2–ol mixture (Figs.(8.2.4) and (8.2.5)).

(XII)

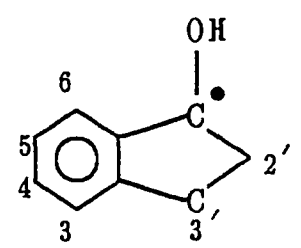


| $A_{2'}$ | $A_{3'}$ | $A_{OH}$ | $A_{3-6}$ |
|---|---|---|---|
| 2.275 | 0.415 | 0.000 | 0.127, 0.166, 0.573, 0.643 |

(XIII)

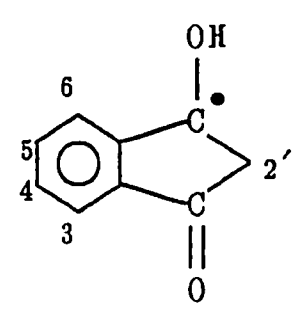


| $A_{3-6}$ | $A_{OH}$ | $A_{2'}$ |
|---|---|---|
| 0.124, 0.160, 0.408, 0.550 | 0.055 | 0.839 |

Fig.(8.2.4)

A spectrum of the indan–1–olyl radical, quenched by tri–ethyl amine and observed at 5–10$\mu$s after creation; by this time the amine radical has largely reacted, facilitating analysis of the indan–1–olyl species. Field sweep is over 4mT. An RPM E/A pattern indicates that the radical is neutral, despite the absence of a measurable OH splitting.

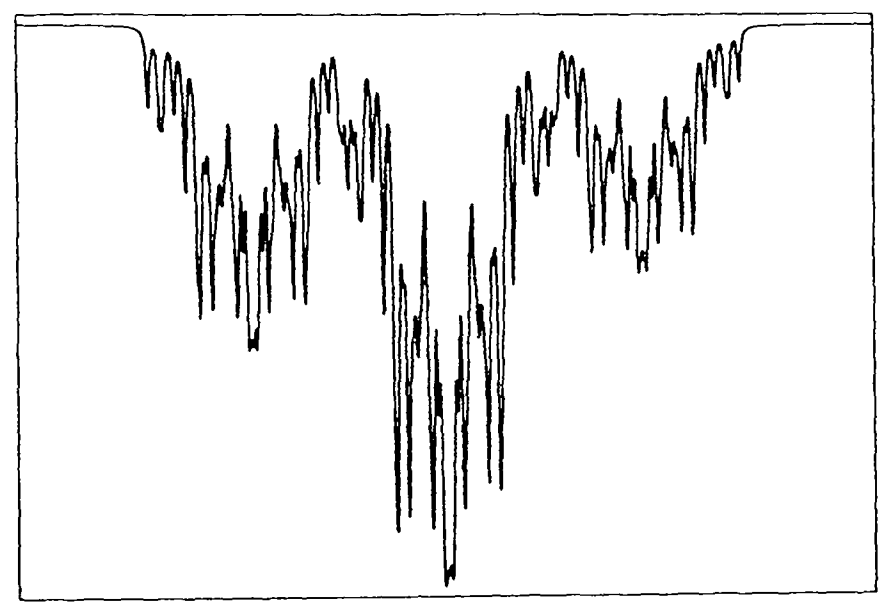

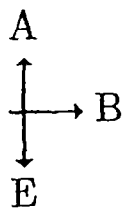


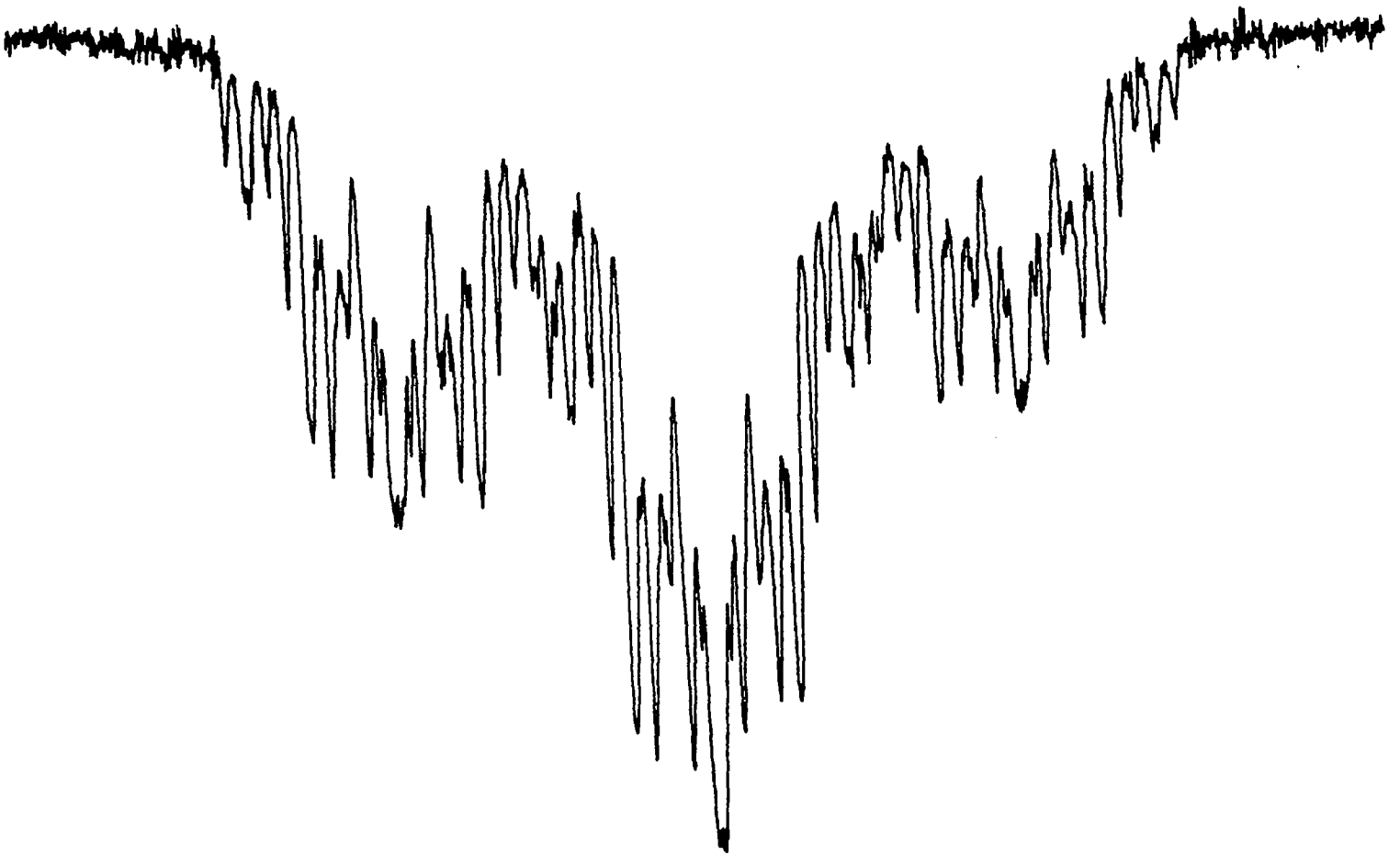

Fig.(8.2.5)

A spectrum of radical (XIII), and a simulation employing the values quoted in the text. Again, the spectrum was recorded in octan–2–ol with 0.1M tri–$^{t}$butyl phenol as quencher – the broad feature to low field. Sweep width is 4mT.

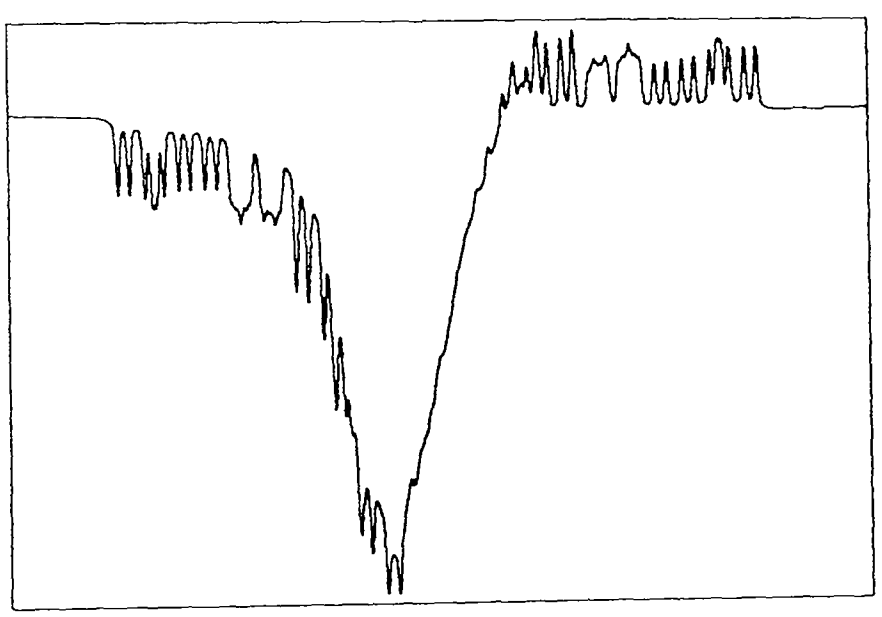

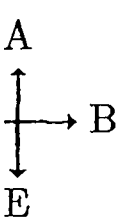


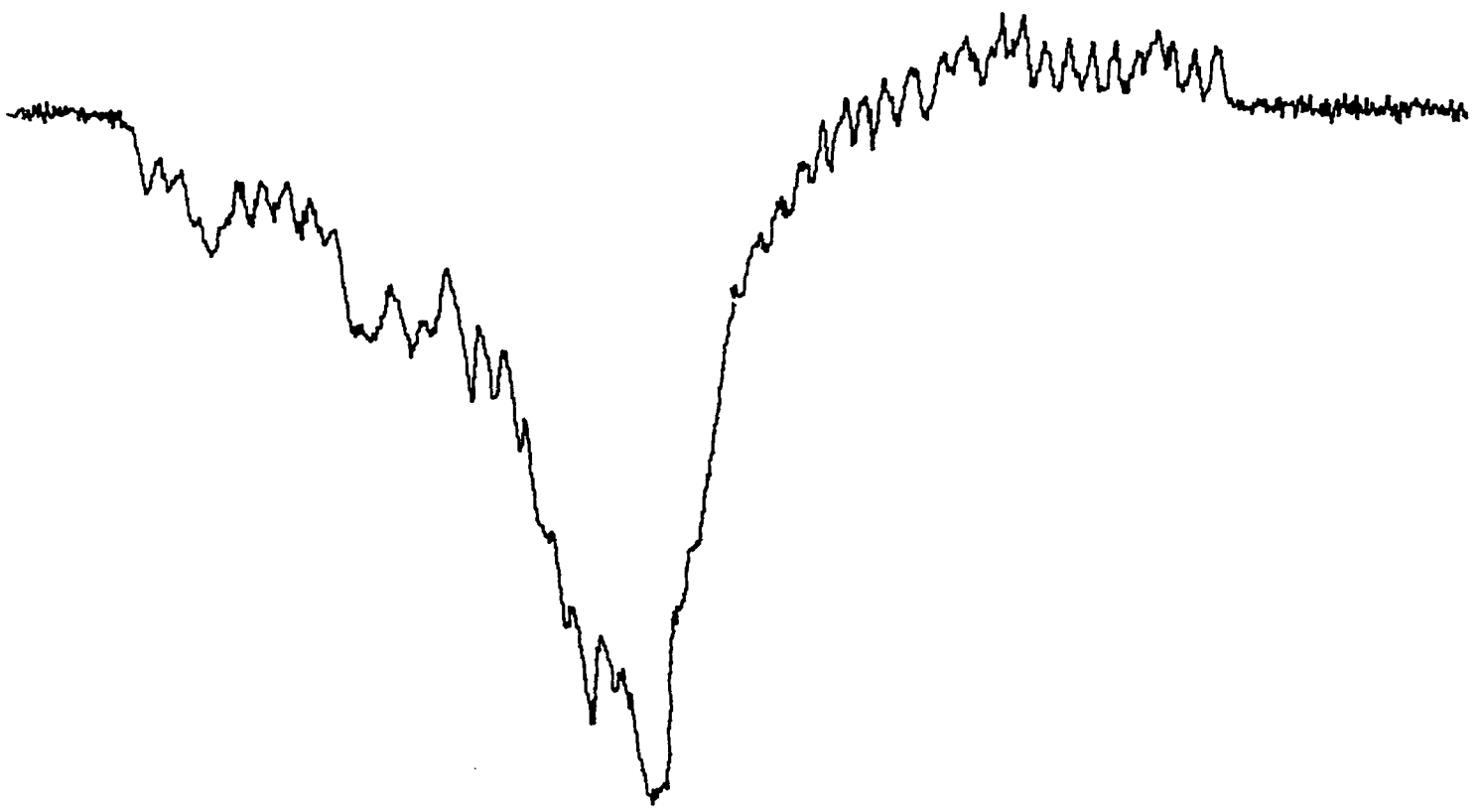

(XIV)

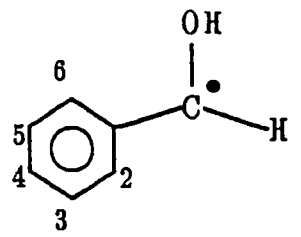

| $A_{\alpha_H}$ | $A_{OH}$ | $A_2$ | $A_3$ | $A_4$ | $A_5$ | $A_6$ | |
|---|---|---|---|---|---|---|---|
| 1.495 | 0.065 | 0.517 | 0.170 | 0.594 | 0.157 | 0.461 | [2] |

(XV)

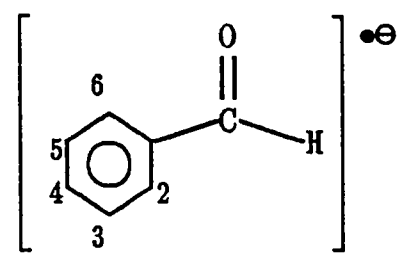

| $A_\alpha$ | $A_2$ | $A_3$ | $A_4$ | $A_5$ | $A_6$ | |
|---|---|---|---|---|---|---|
| 0.851 | 0.469 | 0.131 | 0.648 | 0.075 | 0.339 | [3] |

On the other hand there is a strong resemblance between the values of couplings in the cyclic radicals and those of the radical produced under slow quenching, to which we assign the structure (XVI).

(XVI)

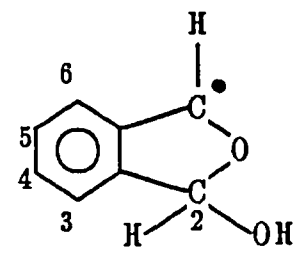

| $A_\alpha$ | $A_{OH}$ | $A_{2-6}$ |
|---|---|---|
| 1.25 | 0.00 | 0.13, 0.14, 0.16, 0.41, 0.70 (± 0.1G). |

The size of the $\alpha$–coupling in our observed radical (XVI) is too large for the corresponding anionic radical but would be smaller than that of the corresponding mono–carbonyl species, as spin density would be apportioned between both moiëties. There are further similarities in sizes of ring couplings of this radical and the proposed open–chain radical (IX) and those of (XIV). However, given that protons on the

---

[2] Recorded in propan–2–ol at 25°C [14].

[3] Recorded in di–methyl formamide at ambient temperature [15].

Fig.(8.2.6)

Simulations of spectra of radicals discussed in the text. All are over a 4mT sweep and a strong, negative TM has been entered for each simulation, as is characteristic of aromatic chromophores. Those simulations of radical anions are given without any RPM contribution, since it is assumed that rapid electron exchange would be taking place.

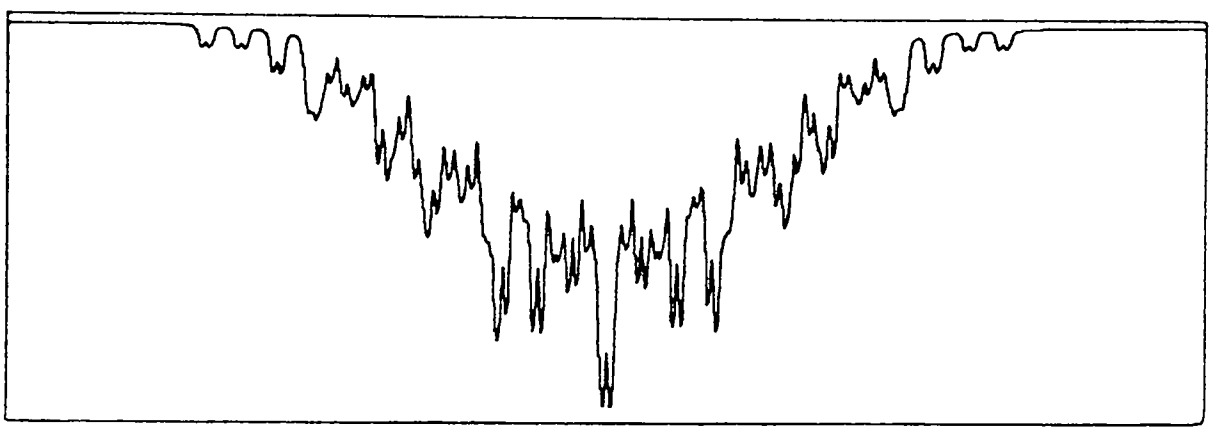

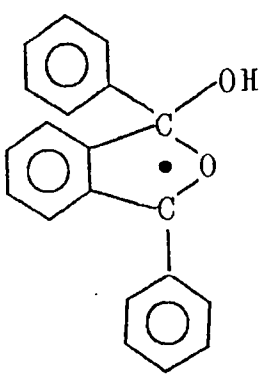


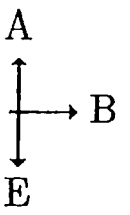


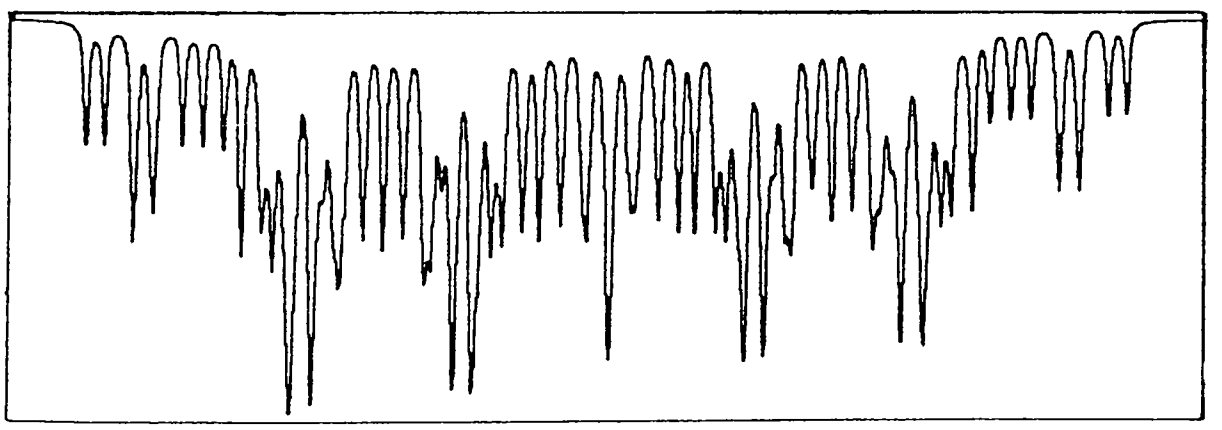

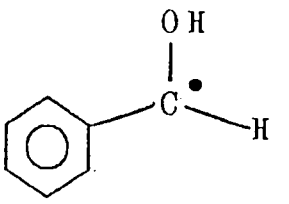

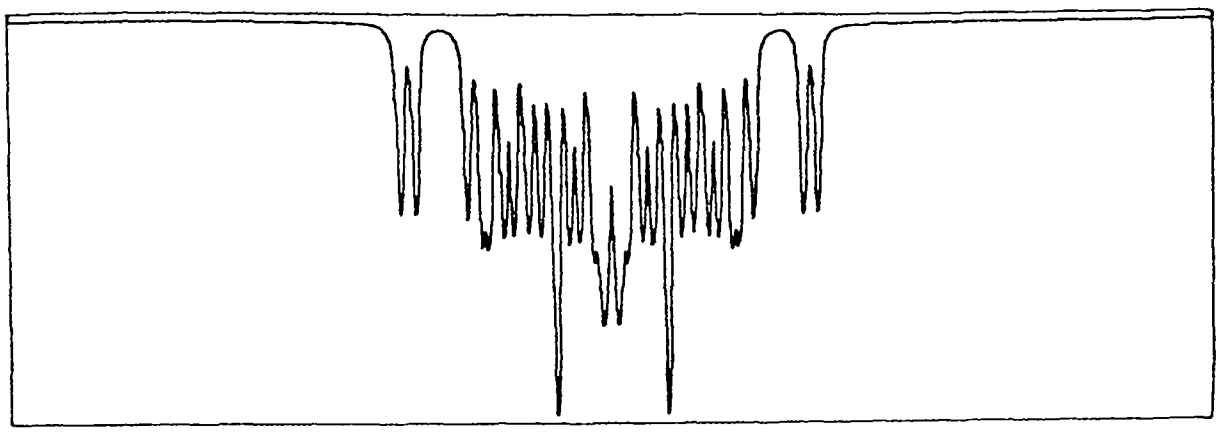

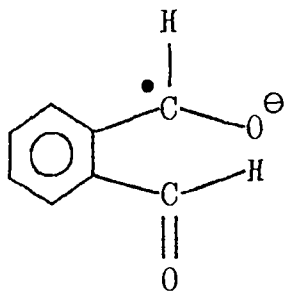
H
C
O
⊖
H
C
O

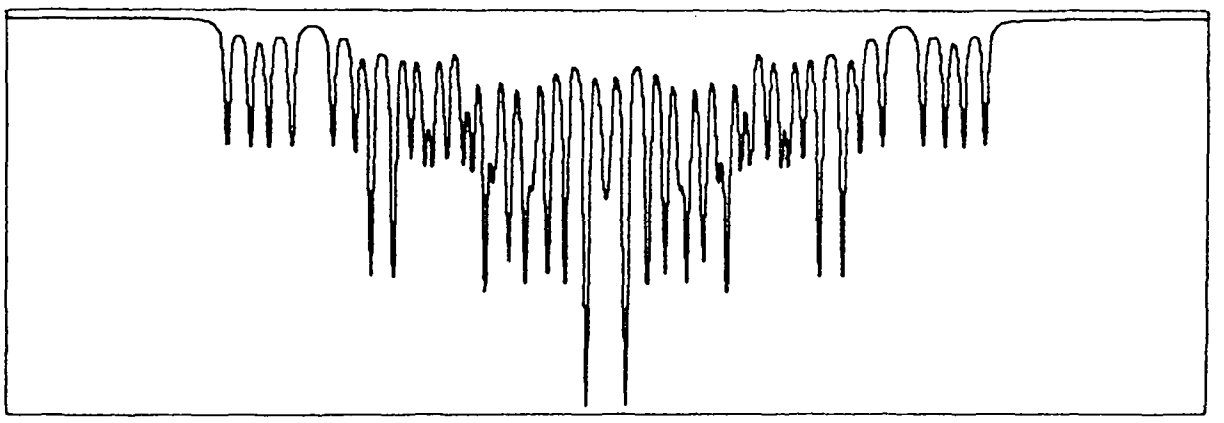

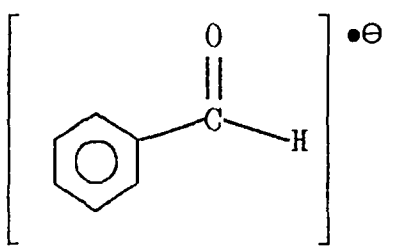
O
C
H
•⊖

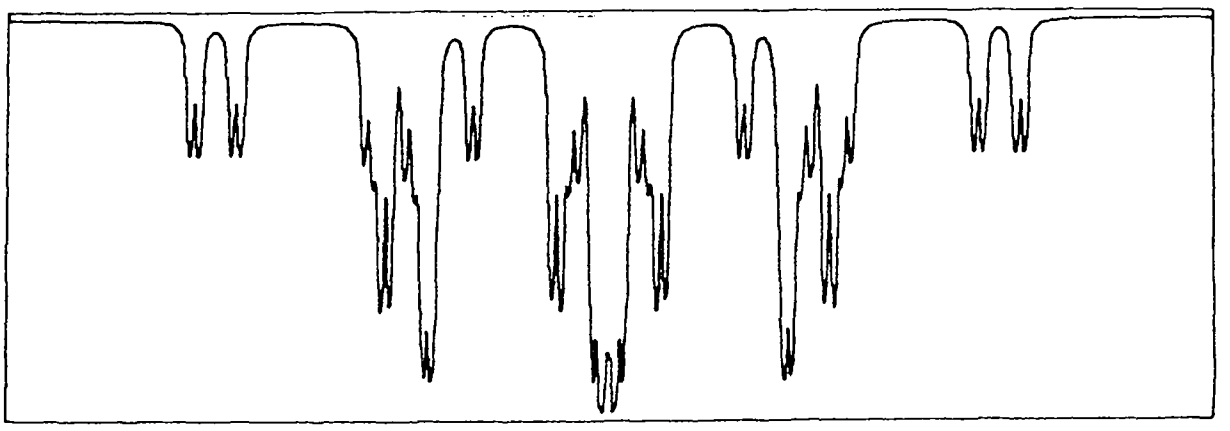

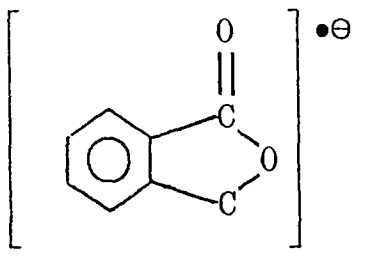
O
C
O
C
•⊖

out–of–plane phenyl group can couple strongly with the electron in this latter case, we cannot draw any lessons from this. Simulations of the spectra of various radicals described in the text are given in Fig.(8.2.6) for ease of comparison.

Ideally we would wish to manufacture (XVI) by a different route in order to confirm its identity. This has not proved easy[4]. Moreover, the quantities of photo–active material required by the flash–photolysis technique made it impractical to deuterate ring positions selectively, to separate out the ring couplings. However, we are currently working in collaboration with Prof. B.C. Gilbert of York University, to attempt a clarification of the problem, ideally by synthesis of the molecules given below. We may then be able to measure the coupling constants for radicals derived therefrom, and especially for those with the radical centre located on the starred carbon atom.

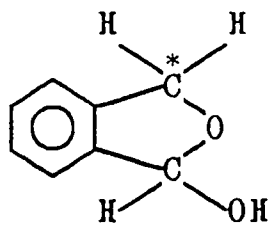


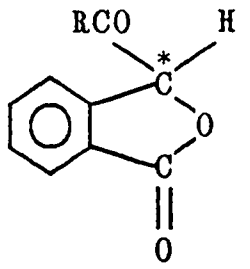


It is interesting to note that the radicals observed at earliest times after the flash show no tendency to interconvert, the spectrum remaining unchanged over twenty microseconds or more. This suggests that the difference in reactivity is intimately bound up with the triplet bi–radical, and that, by changing the quenching medium, we are arresting the intra–molecular reaction pathway.

---

[4] Nor has the creation of a phthalide derived radical: the benzylic H atoms are labile in basic and acidic media and may be substituted by Deuterium easily [10], but they seem utterly immune to free radical attack. Radical creation is also hampered by phthalide's feeble solubility in alcohols or paraffins.

(8.2.4) The Proposed Reaction Scheme

Putting all the observed and inferred facts together, a reaction mechanism consistent with each observation may be constructed:

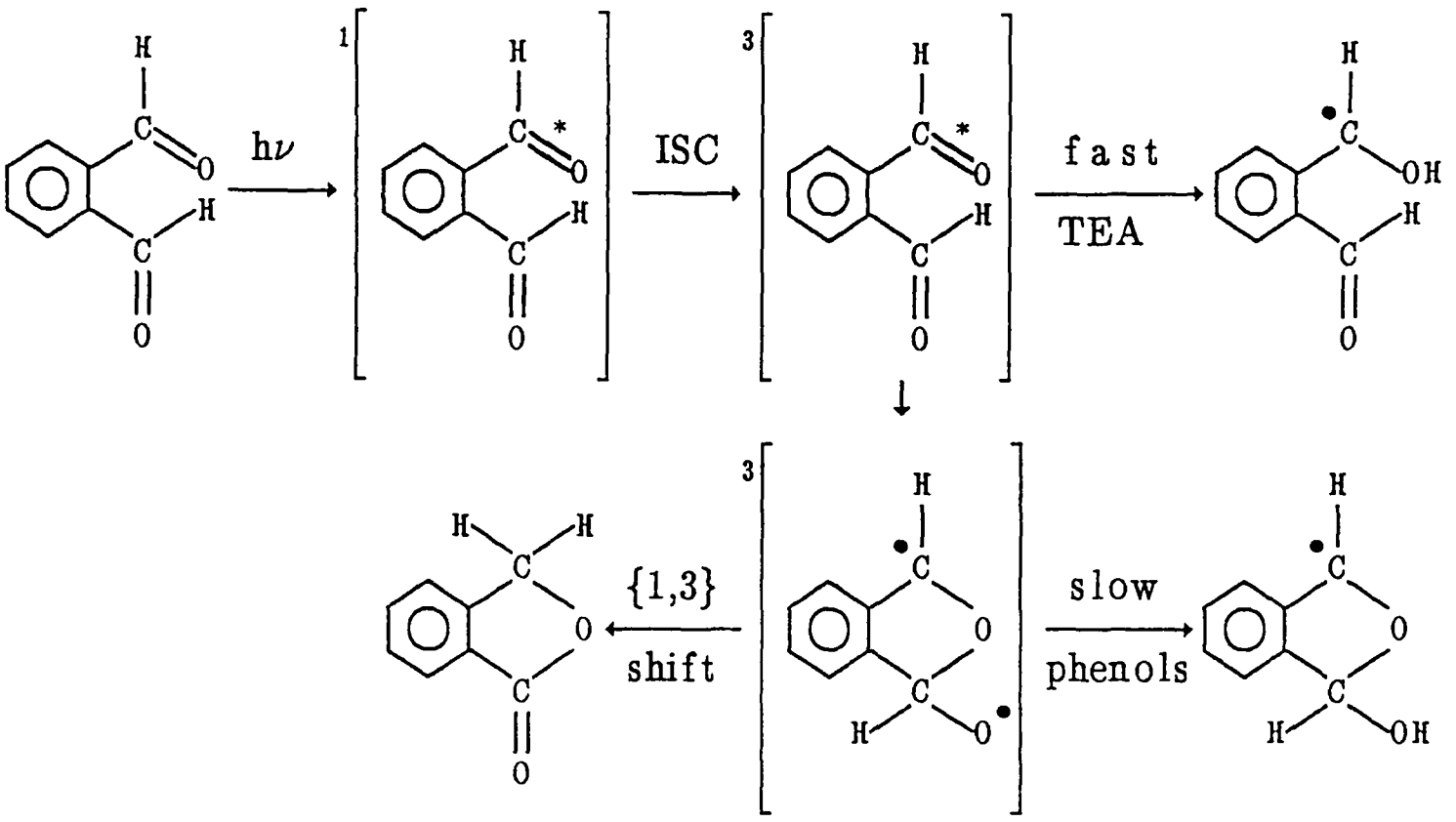


Under slow quenching conditions cyclisation takes place to yield a cyclic triplet species[5] which may, in the presence of H–donating solvents, be quenched to form the cyclic radical observed. Presumably this radical interconverts, by losing and picking up a hydrogen, to phthalide, by a mechanism akin to a {1,3} shift and facilitated by the H–donating or chlorinated solvents. In the absence of such help the triplet biradical would be left to dimerise thus:

---

5 There is plentiful evidence for such bi–radical intermediates in ᵒdi–functional aromatic molecules. See, for example, Hornbeck et al. in *J.Org.Chem.* (1988) 53, 5597. and the references cited therein.

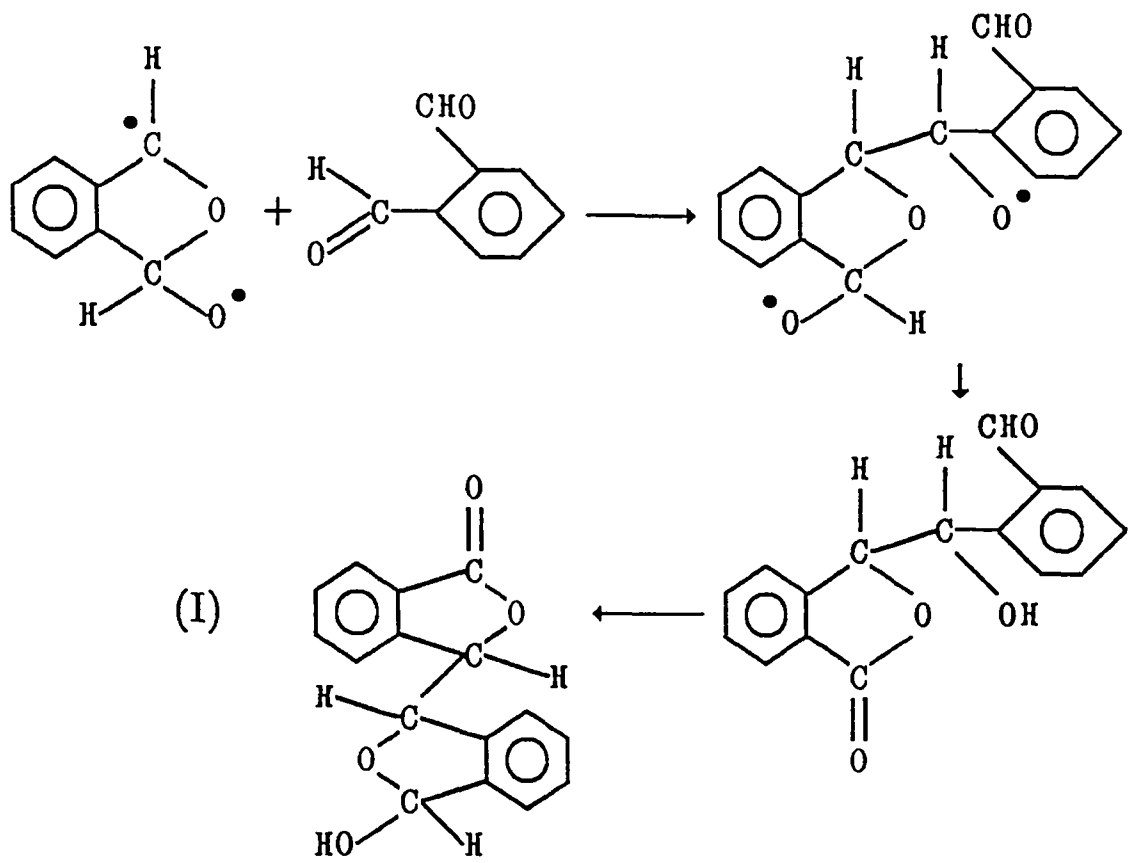

(I)

One piece of evidence that we lack is a product analysis of the really fast quenching reaction. This, however, yields the radical of whose identity we are most certain. To confirm that the nature of the product is kinetically controlled by the quencher, and not controlled by solvent or other effects, 0.5M $^{o}$phthalaldehyde was photolysed in a saturated solution of tri–$^{t}$butyl phenol in octan–2–ol. The two radicals can be seen simultaneously – Fig.(8.2.2a) – under this intermediate quenching regime, demonstrating that the nature of the quencher is irrelevant, provided that quenching can be controlled in this way.

(8.3.1) Observations And A Conclusion.

By administering different quenchers to a molecule photo–excited in the solution phase we have been able to identify two non–equivalent radicals: we assign an open–chain structure to that formed upon quenching at diffusion–controlled rates by

tri–ethyl amine; we assign a closed structure to that obtained by the slower quenching in solvents and with quenchers that do not react under diffusion control [16]. All signals appear wholly in emission, with an E/A multiplet superimposed upon this, which is indicative of triplet and not singlet reactivity.

The mechanism proposed is consistent with all known data on this system and ties in neatly with that obtained on related ones [7,13,14]. Various experiments have been conducted on similar molecules to ascertain values for specific couplings in cyclic and open–chain radicals, although this has only partially confirmed our assignment.

As a final thought and an indication of the care that must be taken in applying observations of polarization to photolytic, mechanistic studies, a biradical has been suggested as an observed intermediate in the photolysis of indan–2–one [16] by the scheme shown below.

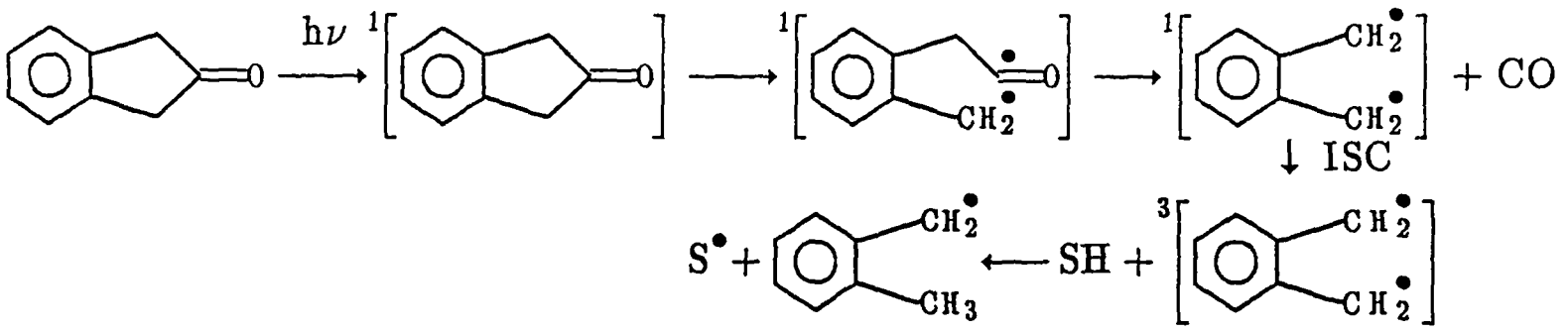


The logic for this scheme came from the observation that the signal is emissively polarised and *that*, according to the rationale, was incompatible with a TM process from an excited triplet state. Indan–2–one, it was argued, would behave like the related ketone cyclopentanone and give, if it gave any, an absorptive TM. A singlet biradical may, on the other hand, produce emission from the ISC since the selection rules for the ISC within such a singlet biradical would be expected to conform with those for aromatic ketones, since the radical centres are now adjacent to the aromatic ring and

not isolated from it by an intervening atom. This has all been stated in ref.[16].

The photolysis of indan–2–one has been carried out in a number of solvents and with various phenolic and amine quenchers, and in most cases a weakly emissive, featureless "hump" (for want of a better word) was noted. This central feature is shown in Fig.(8.3.1). The complete lack of structure suggests either a very rapidly relaxing acyl species (XVII) or a biradical (XVIII).

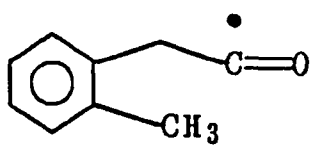


(XVII)

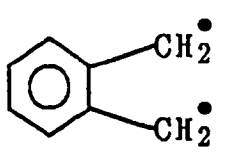


(XVIII)

as suggested originally [17]. When not observed (high amine concentrations) it is possible that it was still present but hidden beneath the counter–radical spectrum.

Creation of an emissive spectrum requires no elaborate photolysis pathway. Instead all that is needed is ST$_-$ mixing, caused by the biradical's inability to separate the electron centres. This has been observed in the spectra of short–chain biradicals [18] – the shorter the chain, the stronger the emission – showing how sensitive ST$_-$ mixing is to constraints on the separation of radical pairs. Our only concern must be with the size of the $J_r$ interaction since if it is too large then the ST$_-$ effect will not be able to take place. Taking typical values of carbon bond lengths from the chemical data manuals gives a typical biradical separation of 0.314nm for the di–benzylic biradical and a maximum separation of 0.468nm for the benzylic/acyl biradical; using a model for the exchange interaction of $J_r = J_0.e^{-\lambda/r}$ and the values estimated in ref.[18] suggests an exchage interaction average for these species of $\approx 5 \times 10^{13}$Hz and $3 \times 10^{9}$Hz respectively[6].

---

[6] Obviously an assumption must be made about the relative separation of the termini of the biradical chain in order to apply such an exchange interaction model.

Fig.(8.3.1)

The central feature in the spectrum produced by photolysis of indan–2–one in octan–2–ol and recorded over 5mT.

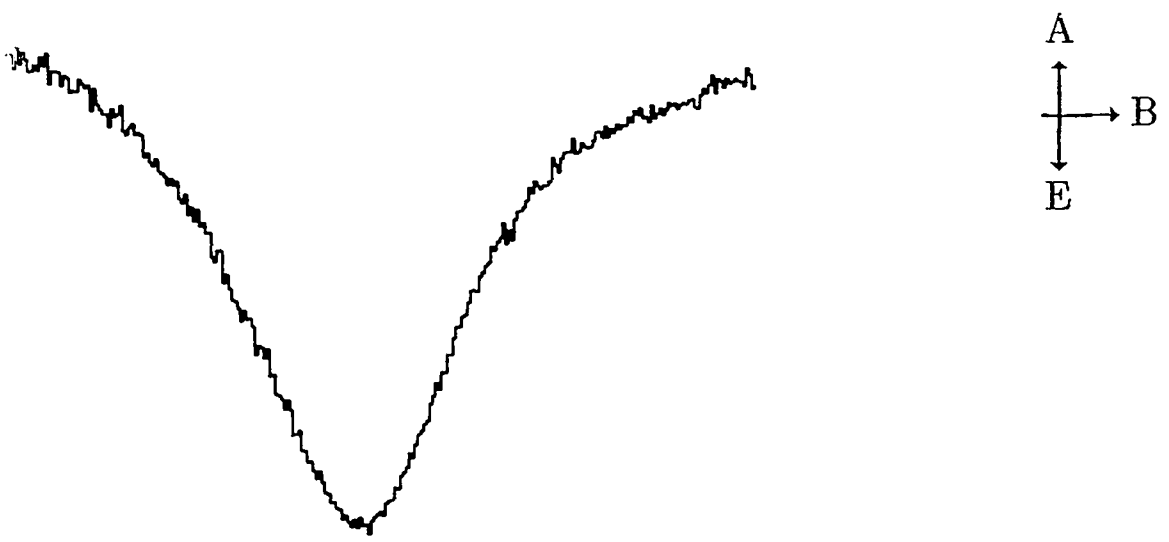


We cannot extract a g–value of sufficient accuracy to confirm that this is an acyl spectrum. However, it is of the same appearance and approximate width as the benzoyl radical spectrum in Fig.(7.3.1).

Upon this evidence the exchange interaction in the former is far too large to allow any ST$_-$ mixing but in the latter it is of a similar size to the Zeeman splitting. Quenching of this biradical at the benzylic carbon would then give a strongly enhanced emissive radical spectrum. We should expect that the exchange in the acyl/benzyl biradical would separate the two chain ends to the maximum extent since it is a repulsive interaction and at this smallish separation it is of the size of kT. The g–value of an acyl radical would be the clinching piece of evidence for this scheme. Alas, the breadth of the signal and a weak but unquantifiable RPM pattern superimposed upon it makes any such evaluation arbitrary. In conclusion, therefore, a simple photolysis mechanism which involves just the $\alpha$–scission of C—CO bond *after* the ISC is entirely consistent with the results from our experiments, though it does not, of course, rule out other possibilities.

---

What was done was to calculate a maximum possible separation and then to halve this, in the best traditions of statistical mechanics. This was repeated for three different biradical chains reported in Ref.[18], to evaluate $J_0$ and $\lambda$.

## REFERENCES – CHAPTER 8


1 Schönberg A., Mustafa A. *J.Am.Chem.Soc.* (1955) 77, 5755.

2 Kagan J. *Tetrahedron Lett.* (1966) 49, 6097.

3 Pappas S.P., Blackwell J.E. *Tetrahedron Lett.* (1968) 29, 3337.

4 Cohen K.F., Pinhey J.T., Smith R.J. *Tetrahedron Lett.* (1968) 46, 4729.

5 Scaiano J.C., Encinas M.V., George M.V. *J.Chem.Soc.Perkin Trans.II* (1980) 724.

6 Harrison D.A., Schwartz R.N., Kagan J. *J.Am.Chem.Soc.* (1970) 92, 5793.

7 Herold B.J., Das Merces M., Marques V., Novais H.M., Steenken S., Hermann H. *Colloq.Intern.C.N.R.S.(278) – Radicaux Libres Organique* (1977) 73, 73.

8 Lunazzi L., Ticca A., Macciantelli D., Spunta G. *J.Chem.Soc. Perkin Trans. II* (1976) 1121.

9 Lumbroso H., Liégeois C., Pappalardo G.C., Librando V. *J.Mol.Structure* (1980) 62, 195.

10 Nelson S.F. *J.Org.Chem.* (1973) 38, 2693.

11 Stone E.W., Maki A.H. *J.Chem.Phys.* (1963) 38, 1999.

12 Gilbert B.C., Trenwith M. *J.Chem.Soc.Perkin Trans.II* (1975) 1083.

13 Dobbs A.J., Gilbert B.C., Norman R.O.C. *J.Chem.Soc.(A)* (1977) 124.

14 Wilson R. *J.Chem.Soc.(B)* (1968) 84.

15 Steinberger N., Fraenkel G.K. *J.Chem.Phys.* (1964) 40, 723.

16 Griller D., Howard J.A., Marriott P.R., Scaiano J.C. *J.Am.Chem.Soc.* (1981) 103, 619.

17 Grant A.I. *D.Phil Thesis, Oxford* (1985) Chapter 3.

18 Closs G.L., Forbes M.D.E. *J.Am.Chem.Soc.* (1987) 109, 6185.

# APPENDICES

# APPENDIX A

## Creation Of A Simulated Spectrum

Any resonance spectrum may be regarded as a convolution of a function containing the frequencies or fields of resonance transitions with a lineshape function, which may include spectrometer response, polarization processes and relaxation, provided the lineshape is not hyperfine–dependent.

We begin by calculating positions of resonance transitions through applying the resonance condition (1.1.3) with, where appropriate, second–order corrections. This will involve inputting radical g–values, coupling constants and the numbers of nuclei creating each coupling. The field/frequency range over which we are operating must also be entered. The result is a stick spectrum corresponding to an equilibrium polarization for that radical. Its TM–polarized equivalent is simply obtained by multiplying the size of each line by the polarization ratio. To calculate the RPM stick spectrum we must draw on the results of chapter 4 and give each line a functional dependence of

$$P_{1,a} \alpha N_{\varrho} \sum_{i} N_i (Q_{ab_i}^{\frac{1}{2}} - aQ_{ab_i}) \qquad (A.1)$$

for radical 1 in a spin state $\varrho$ of degeneracy $N_{\varrho}$. The polarization is a weighted average of all the contributions from radical 2 in spin state $_i$. "a" is normally entered as zero.

Relative contributions from RPM, $ST_0$, $ST_-$ and equilibrium components can now be added together, providing us with a spectrum equivalent to a set of impulses in a field domain $S(\omega)$. We must now clothe this skeleton with a lineshape function, as derived in Chapter 2 and defined by $T_1$, $T_2$, $\omega_1$ and the time period over which we are observing the

radical, $L(\omega)$. In practice it is convenient to separate polarized and unpolarized terms and integrate them into the stick spectrum independently. The final spectrum is given by

$$I(\omega) = \int_{-\infty}^{\infty} S(\omega').L(\omega-\omega')d\omega' = S(\omega) \oplus L(\omega) \qquad (A.2)$$

One may convolute two digitised spectral functions by a Fast Fourier Transform technique[1]. The Convolution Theory states that the convolution of two functions transformed into Fourier space (or Laplace space) is the product of the Fourier (or Laplace) transforms of those two functions. Thus,

$$\mathcal{F}\{L(\omega)\} \rightarrow L(t)\ ;\ \ \mathcal{F}\{S(\omega)\} \rightarrow S(t) \text{ and}$$

$$\mathcal{F}\{S(\omega) \oplus L(\omega)\} = S(t).L(t) \qquad (A.3)$$

However, for our purposes, $S(\omega)$ is mainly a collection of zeroes. As an example, a 1024 point function with a typical stick spectrum of ten lines will be less than 1% non–zero. In these cases direct convolution remains a faster option. This gives a spectrum of 2n points for the convolution of two spectra of n points each. It is necessary to truncate the result by n/2 from each end to return an n–point spectrum. The overall method of simulation is shown below.

---

[1] As explained by S.Brumby *J.Magn.Reson.* (1980) 40, 397.

1st/2nd order perturbation → N–point stick spectrum, $S(\omega)$

$I(\omega)$, 2N–point spectrum ← truncate each end by N/2 ← $S(\omega) \oplus L(\omega)$ ← $S(\omega) + L(\omega)$

Modified Bloch equations → N–point lineshape function, $L(\omega)$

All simulations ignore kinetic decay.

The second problem is the simulation of hyperfine–dependent polarization transfer. This is managed for a doublet primary radical with a single spin–$\frac{1}{2}$ coupling by calculating sub–spectra which correspond to each half of the doublet. Each half is located relative to the other by employing a "virtual g–value", the difference between the two "g–values" corresponding to a splitting equivalent to that of this nucleus in the adduct. The two halves can then be admixed in appropriate proportions, as shown below, the mixing factor in this case reflecting the result of $ST_-$ mixing and $ST_0$ RPM. Pure $ST_0$ polarization of the secondary radical can be calculated separately and added in, to synthesise the true spectrum.

a) A schematic representation of a two–line primary radical spectrum with a net emission superimposed upon an E/A RPM pattern. This corresponds to the spectrum observed for a phosphonyl radical.

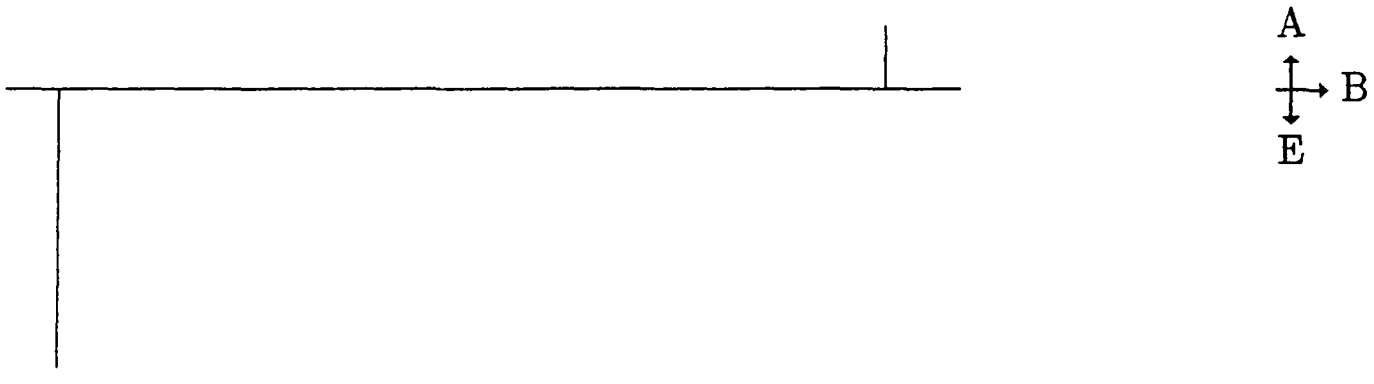


b) A secondary radical derived from this and containing two more couplings would

be simulated by combining the following two sub–spectra, each representing one half of the total adduct spectrum, and separated by the coupling of the nucleus that has remained correlated in initial and final radicals.

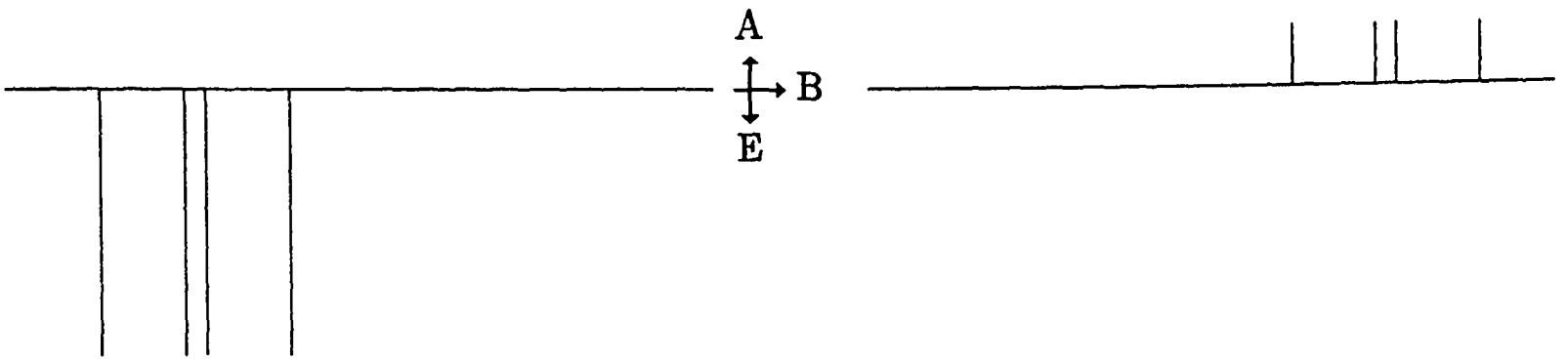


relative hyperfine intensities for each sub–spectrum reflect the relative intensity of the related line in the primary spectrum.

These two elements are combined by addition, the result being shown below on the left. This contrasts with the expected pattern for normal RPM polarization ($ST_0 + ST_-$), which is shown below–right.

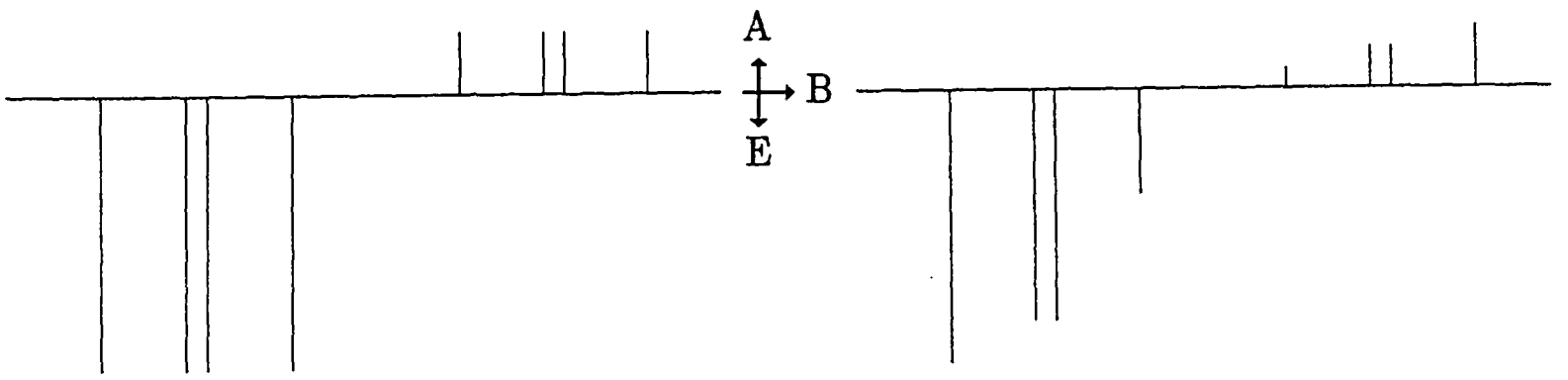

# APPENDIX B

## The Density Matrix And A Rigorous R.P.M. Treatment.

Resonance spectroscopy is a method of probing an ensemble of spins as a physical system, and it may be interpreted by phenomenological equations. This is not quite a rigorous description of the behaviour of the resonance experiment, for individual spins can only be described by statistical pictures. The RPM is a salient example since an electron spin pair cannot, when J(r) is non–negligible, co–exist as a mixture of S and $T_0$ states. For this reason the density matrix description is introduced.

For a time–dependent system $\Psi(t)$, composed of orthonormal functions $c_n\phi_n$, the time–dependence of the system may be transferred to the coefficients of $\phi_n$,

$$|t\rangle = \sum_n c_n(t)|n\rangle \tag{B.1}$$

The expectation value of an operator $\underline{\Omega}(t)$ is given by

$$\langle\underline{\Omega}(t)\rangle = \sum_n\sum_m c_m(t)^*c_n(t)\langle m|\underline{\Omega}(t)|n\rangle = \sum_{m,n}\overline{c_m(t)^*c_n(t)}\langle m|\underline{\Omega}(t)|n\rangle \tag{B.2}$$

the bar indicating that ensemble–averaging has taken place over all states $\phi_n$. The individual products $c_m(t)^*c_n(t)$ may be arranged in a matrix in which the elements

$$\overline{c_m(t)^*c_n(t)} = \langle m|\underline{\rho}(t)|n\rangle = \rho(t)_{nm} \tag{B.3}$$

may be thought of as the consequence of a time–dependent operator $\underline{\rho}(t)$ operating on a static system.

$$\underline{\rho}(t) = N \sum_{ij} |i(t)\rangle \langle j(t)| \tag{B.4}$$

On–diagonal elements of $\underline{\underline{\rho}}(t)$ represent the occupancy of each state comprising $\Psi(t)$; off–diagonal elements give the phase relationship (degree of mixing) between states. Hence,

$$\langle \underline{\Omega}(t) \rangle = \sum_{n} \langle n | \underline{\rho}(t) | n \rangle . \langle n | \underline{\Omega} | n \rangle = Tr\{\underline{\rho}(t).\underline{\Omega}\} \tag{B.5}$$

To calculate $\langle \underline{\Omega}(t) \rangle$ we must find the elements of $\underline{\rho}(t)$. We take (B.1) and the time–dependent Schrödinger equation as a starting point.

$$\mathcal{H}\Psi(t) = i\hbar \frac{\partial \Psi(t)}{\partial t} \tag{B.6}$$

Thus

$$\sum_{n} c_n(t)\, \mathcal{H} |n\rangle = i\hbar \sum_{n} \dot{c}(t)_n |n\rangle \tag{B.7}$$

$$\sum_{n} \langle m | \mathcal{H} | n \rangle . c_n(t) = i\hbar\, \dot{c}(t)_m \tag{B.8}$$

The equation of motion of $\underline{\rho}(t)$ is reflected in the equation of motion of each element of $\underline{\rho}$, $\rho_{ij}(t)$

$$\dot{\rho}_{ij}(t) = \frac{\partial}{\partial t} [c_i(t).c_j(t)^*] = \dot{c}_i(t).c_j(t)^* + c_i(t).\dot{c}_j(t)^*$$

$$\text{or} \quad \dot{\rho}_{ij}(t) = \Big[ (-i/\hbar) \sum_n \langle i | \mathcal{H} | n \rangle . c_n(t) . c_j(t)^* \Big] + c_i(t) . \Big[ (-i/\hbar) \sum_n c_j(t)^* . \langle j | \mathcal{H} | n \rangle \Big]^*$$

$$\dot{\rho}_{ij}(t) = (-i/\hbar)[\ \mathcal{H} . \rho_{ij} - \rho_{ij} . \mathcal{H}\ ] = (-i/\hbar)[\ \mathcal{H}, \rho_{ij}\ ] \qquad \text{(B.9)}$$

Hence, for the whole matrix

$$\dot{\underline{\rho}}(t) = (-i/\hbar)[\ \mathcal{H}, \underline{\rho}(t)\ ] \qquad \text{(B.10)}$$

As shown in chapter 4, it is the development of off–diagonal elements of $\underline{\rho}(t)$ – the re–phasing of $\alpha\beta$ and $\beta\alpha$ relative to one–another that is crucial to the development of RPM polarization[1]. Consider a system defined by just S and $T_0$ states.

$$\underline{\rho} = \begin{pmatrix} \rho_{ss} & \rho_{st} \\ \rho_{ts} & \rho_{tt} \end{pmatrix}; \quad \mathcal{H} = \begin{pmatrix} H_{ss} & H_{st} \\ H_{ts} & H_{tt} \end{pmatrix} = \begin{pmatrix} J_r & Q_{ab} \\ -Q_{ab} & -J_r \end{pmatrix} \qquad \text{(B.11)}$$

The elements of $\underline{\rho}$ are now easily evaluated:

$$\dot{\rho}_{ss} = (iQ_{ab}/\hbar).(\rho_{st} - \rho_{ts}) = -\dot{\rho}_{tt} \qquad \text{(B.12)}$$

$$\dot{\rho}_{st} = (i/\hbar).(Q_{ab}(\rho_{ss} - \rho_{tt}) - 2J_r\rho_{st}) = \dot{\rho}_{ts}^*$$

$$\dot{\rho}_{ts} = (i/\hbar).(Q_{ab}(\rho_{tt} - \rho_{ss}) - 2J_r\rho_{ts}) = \dot{\rho}_{st}^*$$

Combining these terms as was done in creating the vector model of RPM gives

---

1 This has been treated by P.W.Atkins in *Chem.Phys.Lett.* (1979) 66, 403.

$$\dot{\rho}_{tt} - \dot{\rho}_{ss} = (2iQ_{ab}/\hbar).(\rho_{ts} - \rho_{st}) \qquad (B.13)$$

$$\dot{\rho}_{ts} - \dot{\rho}_{st} = (2iQ_{ab}/\hbar).(\rho_{tt} - \rho_{ss}) - (2iJ_r/\hbar).(\rho_{ts} - \rho_{st})$$

$$\dot{\rho}_{ts} + \dot{\rho}_{st} = (-2iJ_r/\hbar).(\rho_{ts} - \rho_{st})$$

Then

$$\ddot{\rho}_{ts} - \ddot{\rho}_{st} = (2iQ_{ab}/\hbar).(\dot{\rho}_{tt} - \dot{\rho}_{ss}) - (2iJ_r/\hbar).(\dot{\rho}_{ts} - \dot{\rho}_{st})$$

$$\ddot{\rho}_{ts} - \ddot{\rho}_{st} = -(4{Q_{ab}}^2/\hbar^2)(\rho_{ts} - \rho_{st}) - (4{J_r}^2/\hbar^2)(\rho_{ts} - \rho_{st})$$

$$\ddot{\rho}_{ts} - \ddot{\rho}_{st} = -[4({Q_{ab}}^2 + {J_r}^2)/\hbar^2].(\rho_{ts} - \rho_{st}) \qquad (B.14)$$

This has a solution of the form $\mathcal{F}$= A.cos(x) + B.sin(x). Setting $\Omega^2 = -({Q_{ab}}^2 + {J_r}^2)/\hbar^2$

$$(\rho_{ts} - \rho_{st}) = A.\cos(2\Omega t) + B.\sin(2\Omega t) \qquad (B.15)$$

The quantity we want is $(\rho_{ts} + \rho_{st})$ so

$$\int_0^t (\dot{\rho}_{ts} + \dot{\rho}_{st})dt = (-2iJ_r/\hbar).\int_0^t (\rho_{ts} + \rho_{st})dt$$

$$(\rho_{ts} + \rho_{st}) = \rho_{ts}(0) + \rho_{st}(0) - (iJ_r/\Omega\hbar)\{A.\sin(2\Omega t) + B[1 - \cos(2\Omega t)]\} \qquad (B.16)$$

This is the density matrix description of polarization. For a system initially in a defined S or $T_0$ state $\rho_{ts}(0) = \rho_{st}(0) = 0$, so A in equation (B.16) must be zero. Therefore, since

$$\dot{\rho}_{ts}(0) - \dot{\rho}_{st}(0) = (2iQ_{ab}/\hbar).(\rho_{tt}(0) - \rho_{ss}(0)) - (2iJ_r/\hbar).(\rho_{ts}(0) - \rho_{st}(0))$$

$$\dot{\rho}_{ts}(0) - \dot{\rho}_{st}(0) = (2iQ_{ab}/\hbar).(\rho_{tt}(0) - \rho_{ss}(0)) = 2\Omega B \qquad \text{(B.17)}$$

where $B = (iQ_{ab}/\hbar\Omega).(\rho_{tt}(0) - \rho_{ss}(0))$

The final solution, then, is

$$(\rho_{ts} + \rho_{st}) = (J_r Q_{ab}/\hbar^2\Omega^2).(\rho_{tt}(0) - \rho_{ss}(0)).(1 - \cos(2\Omega t)) \qquad \text{(B.18)}$$

This corresponds to the solution of the Adrian model used in Chapter 4 if an equivalent two–phase spin evolution is allowed to take place. Lastly, to demonstrate that $(\rho_{ts} + \rho_{st})$ is the observable we wish to determine,

$$Pol_a(t) = (2/\hbar)\langle S_{az}(t)\rangle = (2/\hbar).Tr\{\underline{\rho}(t).S_{az}(t)\}$$

$$Pol_a(t) = \rho_{tt}(S_{az})_{tt} + \rho_{st}(S_{az})_{ts} + \rho_{ts}(S_{az})_{st} + \rho_{ss}(S_{az})_{ss} \qquad \text{(B.19)}$$

$$(S_{az})_{tt} = \tfrac{1}{2}\langle \alpha\beta + \beta\alpha|\, S_{az}\,|\, \alpha\beta + \beta\alpha\rangle = \tfrac{1}{4}\hbar\langle \alpha\beta + \beta\alpha|\, \alpha\beta - \beta\alpha\rangle = 0 = (s_{az})_{ss}$$

By a similar calculation

$$(S_{az})_{st} = (S_{az})_{ts} = \hbar/2$$

Thus $\langle S_{az}\rangle = (\hbar/2).(\rho_{ts} + \rho_{st})$ so $Pol_a(t) = (\rho_{ts} + \rho_{st})$

# APPENDIX C

## The Stochastic Liouville Equation

We start by deriving a basic stochastic equation; that is, an equation which contains a random function, $\mathcal{F}(t)$. Consider a particle acted upon by a fluctuating random force $\mathcal{F}(t)$ such as is caused by molecular buffeting of a radical by surrounding solvent molecules. Acting against its motion is the viscous drag of the solvent which is a function of solvent viscosity $\eta$, $-6\pi\eta a(dr/dt)$ where a is the radical's radius.

$$m.\frac{d^2r}{dt^2} = -6\pi\eta a.\frac{dr}{dt} + \mathcal{F}(t) \qquad (C.1)$$

Multiplying by $(dr/dt)$ and taking a time average gives

$$(m/2).\frac{d^2\langle r^2\rangle}{dt^2} + 3\pi\eta a.\frac{d\langle r^2\rangle}{dt} = m.\frac{d\langle r^2\rangle}{dt} = kT \qquad (C.2)$$

since $m(d\langle r^2\rangle/dt)$ is the mean kinetic energy of the radical and $\langle \mathcal{F}(t)r\rangle = 0$. The solution is

$$\frac{d\langle r^2\rangle}{dt} = (kT/3\pi\eta a) + C.e^{-(6\pi\eta at/m)} \qquad (C.3)$$

This last term becomes insignificant for any period of t greater than about $10^{-8}$s. Ignoring it, therefore, and integrating a second time leaves

$$\langle r^2\rangle - \langle r^0\rangle = (kT/3\pi\eta a)t = 2Dt \qquad (C.4)$$

Thus, provided a long enough period of observation is taken a simple solution results. Each short–time solution represents a different radical trajectory, but we can extract a time–average of all trajectories under the fundamental condition that the random force is not in any way related to the state of the radical; it is implicit in the solution that r and $\mathcal{F}(t)$ are totally independent. Such a case is not appropriate to the modelling of pairs of radicals in solution since spin state will modify diffusion. To state the problem explicitly, a singlet wavefunction, by virtue of its possessing an attractive exchange potential, will be likely to encounter more closely and separate more slowly than an otherwise identical triplet radical pair. Over the short timescale of polarization ($\approx 10^{-8}$s) r and $\mathcal{F}(t)$ will be coupled, therefore, and the only recourse left to us is to take every possible state and trajectory, solve the requisite equation, and add the result to the pile. Mathematically, this is done in the following manner.

The two operators needed to describe the behaviour of a diffusing spin system are a spin Hamiltonian that is spin– and distance–sensitive, $\mathcal{H}(r)$, and a diffusion space, $\Omega_r$. The latter generates a complete set of random variables, r, that describe all possible radical separations; the former is stationary, as no net energy is being put into or taken out of the system, but it has a range of values dependent upon r. In order to combine these two operators into a single equation we note that $\Omega_r$ is Markovian, as defined by the requirement that in the limit $\Delta t \to 0$[1],

$$(1/\Delta t).\int_{r_1}^{r_2} P(r,t+\Delta t)dr = 0 \qquad (C.5)$$

---

[1] This requirement is explained and a general review of construction of stochastic equations is given by Gardiner C.W. in "*Stochastic Methods*" 2nd Edition (Pub. Springer–Verlag Berlin. 1985) Chapter 3.

where P(r.t) is the probability of finding the system in a state r at time t. Since the system is stationary then

$$\Omega_r.P_0(r) = 0 \qquad (C.6)$$

which is a refinement of (C.5). Under such constraints it is possible to combine the density matrix description of the spin system with its spatial diffusion[2].

$$\frac{\partial\rho(r,t)}{\partial t} = -i[\mathscr{H}(r),\rho(r,t)] - \Omega_r.\rho(r,t) \qquad (C.7)$$

where $\rho(r,t)$ is a weighted average of all states available to the radical pair,

$$\int\rho.P(\rho,r,t)dP \qquad (C.9)$$

for a specific value of r and hence a specific value of $\mathscr{H}(r)$.

Equation (C.7) therefore sets up a complete set of spatial terms, characterised by r, each of which will have a particular energy associated with it and a related rate of spatial and spin evolution. The energies that are modulated by this diffusion are the Zeeman, exchange and hyperfine interactions. It is, in essence, still of the form (C.4), however.

A final point is the timescale over which we must simulate radical motion. This will be effectively limited by the time taken for termination of all encounter/re–encounter cycles. The limit is conveniently taken to be that for which

---

[2] As demonstrated by Kubo R. in *Adv.Chem.Phys.* (1969) 15, 101. and applied by Pedersen J.B. and Freed J.H. in *J.Chem.Phys.* (1973) 58, 2746.

$t \to \infty$, for which Laplace transforms can be used to solve (C.7), and boundary conditions must be set upon the spatial diffusion of the radical pair to ensure that an infinite string of re–encounters does not occur.

# APPENDIX D

## The Transfer Problem

We adopt a system in which the termination reactions of the secondary radicals occur so slowly as to be unimportant over the timescale of concern. The equation to be solved is

$$\dot{{}^{s}\underline{M}_{kr}} = {}^{s}\underline{L}^{k}.{}^{s}\underline{M}_{kr}(t) + c{}^{s}\underline{F}(t) + k_1 \sum_{j\,s}{}' {}^{p}\underline{M}_{js}(t) \qquad (D.1)$$

where subscripts $_{kr}$ refer to the $_{k}$th component of the $_{r}$th hyperfine line in the radical observed, and the superscripts $^{s}$ and $^{p}$ refer to secondary and primary species respectively. Thus ${}^{s}\underline{\underline{L}}$ includes ${}^{s}T_2$, ${}^{s}T_1$, ${}^{s}\Delta\omega^{k}$ and the population of the secondary radical ${}^{s}n(t)$. ${}^{s}\underline{F}(t)$ arises from the equilibrium polarization of the secondary radical.

$${}^{s}\underline{F}(t) = \begin{pmatrix} 0 \\ 0 \\ 1 \end{pmatrix}.P_{eq}{}^{s}n(t){}^{s}T_1{}^{-1} \qquad (D.2)$$

The third term in (D.1) includes the transfer of polarization from primary to secondary species, specifically from those c nuclear spin states $_{js}$, that correlate with the $_{kr}$th state in the secondary radical (as indicated by the prime on the summation sign).

(D.1) is commonly solved by a Laplace transform technique; taking Laplace transforms

$$\mathscr{L}\{\dot{{}^{s}\underline{M}_{kr}}\} = {}^{s}\underline{M}_{kr}(0) + s\,\mathscr{L}\{{}^{s}\underline{M}_{kr}\} = s\,\mathscr{L}\{{}^{s}\underline{M}_{kr}\} \qquad (D.3)$$

since ${}^{s}\underline{M}_{kr}(0) = \underline{0}$. Also

$$\mathscr{L}\{{}^{s}\underline{L}^{k}.{}^{s}\underline{M}_{kr}(t) + c{}^{s}\underline{F}(t) + k_1\sum_{j\,s}{}'\,{}^{p}\underline{M}_{js}(t)\} =$$
$$\mathscr{L}\{{}^{s}\underline{L}^{k}.{}^{s}\underline{M}_{kr}(t)\} + c\,\mathscr{L}\{\,{}^{s}\underline{F}(t)\} + k_1\sum_{j\,s}{}'\,\mathscr{L}\{{}^{p}\underline{M}_{js}(t)\} \qquad (D.4)$$

Therefore,

$$(s\underline{1} - {}^{s}\underline{L}^{k})\,\mathscr{L}\{{}^{s}\underline{M}_{kr}(t)\} = c\,\mathscr{L}\{{}^{s}\underline{F}(t)\} + k_1\sum{}'\,\mathscr{L}\{{}^{p}\underline{M}_{js}(t)\} \qquad (D.5)$$

or,

$$\mathscr{L}\{{}^{s}\underline{M}_{kr}(t)\} = \left[c\,\mathscr{L}\{{}^{s}\underline{F}(t)\} + k_1\sum_{j\,s}{}'\,\mathscr{L}\{{}^{p}\underline{M}_{js}(t)\}\right]/(s\underline{1} - {}^{s}\underline{L}^{k}) \qquad (D.6)$$

Taking inverse Laplace transforms gives

$$\mathscr{L}^{-1}\mathscr{L}\{{}^{s}\underline{M}_{kr}(t)\} = \mathscr{L}^{-1}\left\{c\,\mathscr{L}\{{}^{s}\underline{F}(t)\} + k_1\sum_{j\,s}{}'\,\mathscr{L}\{{}^{p}\underline{M}_{js}(t)\}\right\}/(s\underline{1} - {}^{s}\underline{L}^{k}) \qquad (D.7)$$

$${}^{s}\underline{M}_{kr}(t) = \mathscr{L}^{-1}\left\{\left[c\,\mathscr{L}\{{}^{s}F(t)\} + k_1\sum_{j\,s}{}'\,\mathscr{L}\{{}^{p}\underline{M}_{js}(t)\}\right]\right\}/(s\underline{1} - {}^{s}\underline{L}^{k}) \qquad (D.8)$$

By the Convolution theorem

$$\mathscr{L}\left\{\int_0^x f(x-y).g(y)\,dy\right\} = \mathscr{L}\{f(x)\}.\,\mathscr{L}\{g(x)\} \qquad (D.9)$$

ie. $\mathscr{L}^{-1}\,[\,\mathscr{L}\{f(x)\}.\,\mathscr{L}\{g(x)\}] \equiv f(x) \oplus g(x)$, where $\oplus$ signifies that a convolution has taken place. Therefore,

$$\mathscr{L}^{-1}\left[c\,\mathscr{L}\{{}^{s}\underline{F}(t)\} \,/\, (s\underline{1} - {}^{s}\underline{L}^{k})\right] = c\,\mathscr{L}^{-1}\left[\,\mathscr{L}\{{}^{s}\underline{F}(t)\} \,/\, (s\underline{1} - {}^{s}\underline{L}^{k})^{-1}\right]$$

$$= c\,\mathscr{L}^{-1}\left[\mathscr{L}\{{}^{s}\underline{F}(t)\}.\mathscr{L}\{\underline{\Lambda}(t)\}\right] = c\,\mathscr{L}^{-1}\mathscr{L}\{{}^{s}\underline{F}(t)\oplus\underline{\Lambda}(t)\}$$

$$= c\,{}^{s}\underline{F}(t)\oplus\underline{\Lambda}(t) \qquad \text{(D.10)}$$

Similarly for the second term in (D.8) we get

$$k_1\sum_{j\,s}{}' {}^{p}\underline{M}_{js}(t)\oplus{}^{s}\underline{\Lambda}(t) \qquad \text{(D.11)}$$

The complete solution is now

$${}^{s}\underline{M}_{kr} = k_1\sum_{j\,s}{}' {}^{p}\underline{M}_{js}(t)\oplus{}^{s}\underline{\Lambda}(t) + c\,{}^{s}\underline{F}(t)\oplus{}^{s}\underline{\Lambda}(t) \qquad \text{(D.12)}$$

If the ${}_{k}$th line in the secondary radical is well separated from all those in the primary then, since all transverse components of polarization are zero at this point, only the z–component of primary radical polarization can be transferred.

$${}^{p}M_z(t) = \left\{[P_i - P_{eq}].e^{-t/{}^{p}T_1} + P_{eq}\right\}.{}^{p}n(0).e^{-k_1 t} \qquad \text{(D.13)}$$

We can also assume that all lines in the primary radical will have identical time dependence (i.e. we must assume that RPM is negligible or that its effects are equal for lines that connect with those in the secondary species). All subscripts and superscripts may therefore be dropped and replaced by the "correlation weighting" of each line. Thus

$$^{s}M_y(t) = ck_1P_i{}^{p}n(0).{}^{s}\underline{\Lambda}_{yz}(t) \oplus e^{-(k_1 + {}^{p}T_1{}^{-1})t} +$$

$$ck_1P_{eq}{}^{p}n(0).{}^{s}\underline{\Lambda}_{yz}(t) \oplus [e^{-k_1t} - e^{-(k_1 + {}^{p}T_1{}^{-1})t}] +$$

$$cP_{eq}{}^{p}T_1{}^{-1}{}^{p}n(0).{}^{s}\underline{\Lambda}_{yz}(t) \oplus [1 - e^{-k_1t}] \qquad (D.14)$$

For a case of an exactly resonant line ($^{s}\Delta\omega = 0$), $^{s}\underline{\Lambda}_{yz}(t)$ reduces to[1].

$$^{s}\underline{\Lambda}_{yz}(t) = (\omega_1/b).e^{at}.\sin(bt) \qquad (D.15)$$

where $a = -\frac{1}{2}({}^{s}T_1{}^{-1} + {}^{s}T_2{}^{-1})^{-1}$ and $b = [\omega_1{}^2 - \frac{1}{4}({}^{s}T_2{}^{-1} - {}^{s}T_1{}^{-1})^2]^{\frac{1}{2}}$.

A brief interpretation of (D.14) is in order. As noted in its first exposition[2] it represents a convolution of a formation fuction of polarized secondary radicals given by

$$k_1e^{-(k_1 + {}^{p}T_1{}^{-1})t} \qquad (D.16)$$

with the evolution function of such radicals if produced in an initially polarized state, $P_i{}^{p}n(0){}^{s}\Lambda_{yz}(t)$.

When $k_1$ is much slower than all the other parameters then the polarization of the primary radical will have largely relaxed to the equilibrium level by the time substantial reaction has taken place and the net result approximates to a pure equilibrium spectrum for the secondary species. When, however, $k_1$ is much faster than all other processes then formation of the secondary is effectively instantaneous and its magnetization may,

---

[1] This employs expressions for $\Lambda_{yz}$ that were derived by Hore.P.J. and McLauchlan K.A. in *J.Magn.Reson.* (1979) 36, 129.

[2] The problem was defined as laid out above, again by Hore P.J. and McLauchlan K.A. in *Mol.Phys.* (1981) 42, 533. Reference was made to the similarity of the solutions to those for radicals undergoing exchange.

in this limit, be treated as though from a primary species. The evolution of polarization in the secondary radical will be most sensitive to the parameter $(k_1 + {}^{p}T_1^{-1})$ when it is of the same magnitude as $\omega_1$, $T_1^{-1}$ and $T_2^{-1}$.

# APPENDIX E

## Simulation Of Cross–relaxation Of Nuclear Spin Polarization

We begin by taking the now familiar equation

$$\dot{\underline{M}}(t) = \underline{\underline{L}}.\underline{M}(t) + T_1^{-1}n(t)P_{eq}.\begin{pmatrix}0\\0\\1\end{pmatrix} + k_2n(t)^2P_f\begin{pmatrix}0\\0\\1\end{pmatrix} + \dot{n}(t)/n(t)\ .\underline{M}(t) \qquad (E.1)$$

It would make little difference to the time taken to calculate $\underline{M}(t)$ if we omit any of these terms because the bulk of the calculation time is taken up with the evaluation of the essential component $\{\underline{\underline{L}} + \dot{n}(t)/n(t)\}\underline{M}(t)$. In other words, the complete lineshape function is evaluated as though geminate and F– polarization and first order radical scavenging were all taking place as normal. To this is added the following three parameters:

- a nuclear spin relaxation rate, ${}^nT_1$
- a nuclear/electron cross–relaxation rate, $k_x$
- a nuclear spin polarization, included as an initial condition and decaying with time

This latter is modelled as a simple bi–exponential decay from one state to another, according to

$$P_n(t) = P_n(0).e^{-(k_x + {}^nT_1^{-1})t} \qquad (E.2)$$

We deal with each in turn. Values of ${}^nT_1$ in radicals have been estimated from CIDNP

studies by fitting observed polarizations to quantitative theory[1]. A most satisfactory fit is achieved with values of around 100$\mu$s. For inversions in phase by a cross–relaxational mechanism this parameter is found to be fairly unimportant (over a realistic range around this estimate). However, the scalar relaxation rate or, more accurately, the sum of scalar and dipolar rates, cannot exceed ${}^{n}T_1^{-1}$. In all the simulations shown, values of $k_x$ have been chosen that are well under half this value. The magnitude of ${}^{n}P_{CIDNP}$ is more problematical, for although a theoretical maximum of upwards of $2 \times 10^4$ ${}^{n}P_{eq}$ is possible, it is rare to observe even a tenth of this in experiments. For the purpose of simulation it is found to be necessary to use a nuclear polarization of $\leq 10^4$ ${}^{n}P_{eq}$ to cause the high–field line to invert into emission at times after its initial absorption has died away, though lower values can develop a net A/E phase upon an equilibrium signal. A final point about the system chosen is that we require a multiplet CIDNP effect to be converted into a multiplet CIDEP, yet such a CIDNP effect would not be observable in normal *n.m.r.* between such degenerate protons.

The polarization conferred upon an electron spin state will be dependent on the net (scalar – dipolar) cross relaxation rate, the degeneracy of the two states coupled by the cross relaxation, and the nuclear polarization present at the time of transfer:

$$P'_{x\text{-relax}}(t) = ck_x.P_n(t) \qquad (E.3)$$

The prime signifies that this polarization is imparted at a time t, and c is the degeneracy weighting of that state. Since radicals with different nuclear spin states are distinguishable by *e.s.r.* the effect of cross relaxation may be included along with the

---

[1] See, for example, Vollenweider J–K,. Fischer H., Hennig J., Leuschner R. in *Chem.Phys.* (1985) 97, 217.

first order radical–depleting reactions as a pipe through which radical sub–state populations are evened out, rather than as a pure first order scavenging reaction.

This simulation differs from previous ones in that it includes all possible kinetic influences upon the radical pair and manufactures a y–component signal from the system so that direct comparison with experimental data can be made. This distinction becomes important when an early–time polarization subsides; at low microwave powers only a small fraction of this instantaneously generated polarization may be shipped into the y–direction before relaxation, tending to reduce its importance compared to longer–time polarization.

The equation is solved in the following manner:

$$\underline{M}(t+t') = e^{\int_t^{t+t'} \underline{\underline{L}}(t)dt}\left\{ \underline{M}(t') + e^{-\int_t^{t+t'} \underline{\underline{L}}(t)dt} Q(t)\right\} \qquad (E.4)$$

for which $Q(t) = n(t).\left[ \frac{P_{eq}}{T_1} + n(t)k_2P_f + k_xP_{x\text{-relax}} \right]$. The integral between t and $(t + t')$ is evaluated by the trapesium rule.

Simulations are all for a 1:2:1 triplet radical. The operator enters a value for $P_i$ and $P_f$ for the low–field line of x and y. CIDEP polarizations are automatically assigned to the central and high–field lines of 0,0 and –x,–y respectively. It is implicit in this simulation that all lines have identical ${}^eT_1$, ${}^eT_2$, ${}^nT_1$ and offset from resonance.

## ERRATUM

The following errors or omissions remain uncorrected in the text:

p.27 "X–direction" (line 3) should read "x–direction".

p.47 (line 2) "KHz" should stand as "kHz". Similarly for p.51 (line 6).

p.57 "bourne" (penultimate line) should read "borne".

p.70 The normalisation constants in the third, unlabelled equation have been omitted.

p.71 The triplet state in the diagram is the $n\pi^*$ and not the $\pi\pi^*$ state.

p.79 $k_q$ and $k_t$, when used, should be taken as equivalent to $k_r$ (similarly for p.80).

p.157 Simulations have been incorrectly placed; the vertical order should be reversed for correct correspondance with the spectra.

p.165 In equation (C) $CH_3C(=O)H$ should be replaced by $(CH_3)_2CHC(=O)H$.

p.197 In equation (D) the right hand side should be 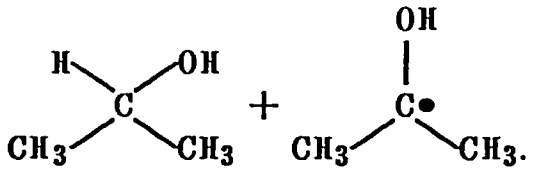

p.223 "$J_r = 10^{-11}s$" (line 9) should read "$J_r = 10^{11}s^{-1}$".

p.228 "$^n1000\ P_{eq}$" (top line) should stand as "$1000^n\ P_{eq}$".

p.243 The second spectrum was recorded from 50 to 75$\mu$s.

p.248 "has" (line 11) should read "have".

In Appendix C equation (C1) should be multiplied through by r, and not **(dr/dt)**.

## ADDENDUM

On p.47 it is asserted that modulated *e.s.r.* would not be able to achieve a really fast time response; it has been pointed out that de Jager and van Wijk obtained 1$\mu$s resolution with 200kHz modulation.

The mechanism depicted on p.273 involves an unlikely attack by a resonance–stabilised C–centred radical upon ground state o–phthalaldehyde, to give an oxygen–centred one. A possible alternative mechanism that avoids this problem is given herewith:

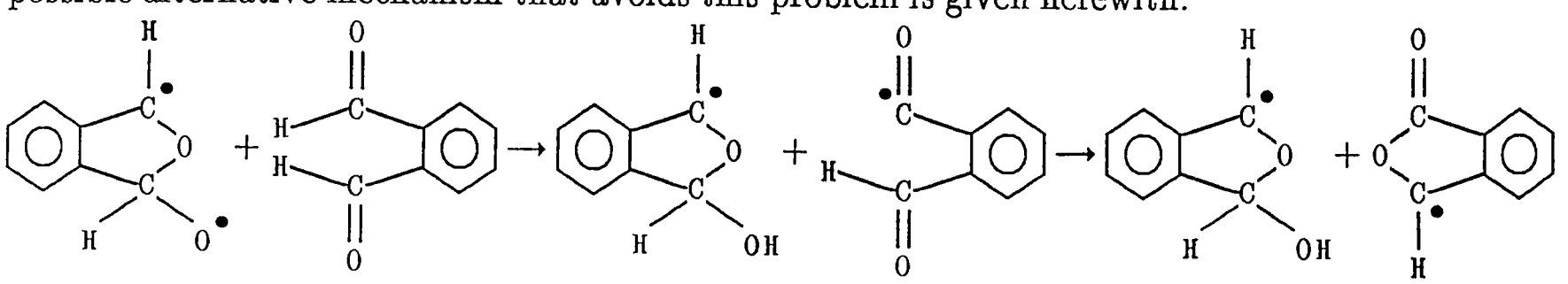

The latter two species react to give the diamagnetic product shown in the originally proposed mechanism. Such an interpretation invokes no such O–centred intermediate, and is consistent in all other respects with the proposal that we are witnessing the initial reaction product of a cyclized triplet biradical.